INFORMATION TO USERS

This manuscript has been reproduced from the microfilm master. UMI films the text directly from the original or copy submitted. Thus, some thesis and dissertation copies are in typewriter face, while others may be from any type of computer printer.

The quality of this reproduction is dependent upon the quality of the copy submitted. Broken or indistinct print, colored or poor quality illustrations and photographs, print bleedthrough, substandard margins, and improper alignment can adversely affect reproduction.

In the unlikely event that the author did not send UMI a complete manuscript and there are missing pages, these will be noted. Also, if unauthorized copyright material had to be removed, a note will indicate the deletion.

Oversize materials (e.g., maps, drawings, charts) are reproduced by sectioning the original, beginning at the upper left-hand corner and continuing from left to right in equal sections with small overlaps. Each original is also photographed in one exposure and is included in reduced form at the back of the book.

Photographs included in the original manuscript have been reproduced xerographically in this copy. Higher quality 6" x 9" black and white photographic prints are available for any photographs or illustrations appearing in this copy for an additional charge. Contact UMI directly to order.

UMI

A Bell & Howell Information Company
300 North Zeeb Road, Ann Arbor MI 48106-1346 USA
313/761-4700 800/521-0600

Phase Behavior of Homopolymer/Diblock Blends

by

Philipp Klaus Janert

A dissertation submitted in partial fulfillment of
the requirements for the degree of

Doctor of Philosophy

University of Washington

1997

Approved by 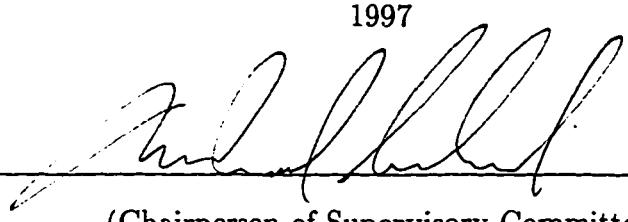

(Chairperson of Supervisory Committee)

Program Authorized
to Offer Degree Department of Physics

Date 05. June 1997

Doctoral Dissertation

In presenting this dissertation in partial fulfillment of the requirements for the Doctoral degree at the University of Washington, I agree that the Library shall make its copies freely available for inspection. I further agree that extensive copying of this dissertation is allowable only for scholarly purposes, consistent with "fair use" as prescribed in the U.S. Copyright Law. Requests for copying or reproduction of this dissertation may be referred to University Microfilms, 1490 Eisenhower Place, P.O. Box 975, Ann Harbor, Michigan 48106, to whom the author has granted "the right to reproduce and sell (a) copies of the manuscript in microform and/or (b) printed copies of the manuscript made from microform."

Signature Ph. Juncker

Date 05. June 1997

University of Washington

Abstract

Phase Behavior of Homopolymer/Diblock Blends

by Philipp Klaus Janert

Chairperson of Supervisory Committee: Prof. Michael Schick

Department of Physics

We study the micro- and macrophase behavior of symmetric AB-diblock copolymers in binary and ternary blends with corresponding homopolymers in mean field theory and for weak to intermediate segregation. We employ the standard Gaussian chain model and numerically solve the mean field equation in Fourier space. Besides homogeneous phases, we consider the following ordered morphologies: sheetlike lamellae, hexagonally arranged cylinders, and spheres on a body-centered-cubic lattice. We consider only symmetric diblocks, but vary the chain length of the homopolymers from 0.1 to 1.5 the length of the copolymer. For the ternary systems, we produce several constant temperature cuts through the Gibbs phase prism. For the binary system, we also study the temperature dependence of the phase diagram. For the symmetric system, in which both homopolymers are of equal length with the diblock, we consider the temperature dependence at all compositions of the ternary mixture. We find the following general trends: homopolymers, longer than the copolymer are expelled from the microstructure and phase separate. Homopolymers comparable to or shorter than the diblock, swell the microstructure, whereas very short homopolymers tend to destroy any ordered phase. For a narrow region in the weak

to intermediate segregation regime, homopolymers comparable in length to the diblock can swell the microstructure indefinitely, leading to a complete unbinding of the ordered phase. The transition from bound to unbound as temperature is varied can be either continuous or first-order. In the latter case, the expected preunbinding line is found as a coexistence region between two different ordered phases with the same symmetry, but of different periodicity. For the symmetric system, in which all chains are of equal length, we find a multicritical Lifshitz point within mean field theory. All these results can be understood in terms of simple brush- and stretching arguments. A comprehensive overview over the statistical theory of flexible chain molecules has been provided, as well as a review over previous experimental and theoretical investigations of self-assembly in block copolymers systems.

TABLE OF CONTENTS

LIST OF FIGURES

ACKNOWLEDGMENTS

First of all, it is a pleasure to thank my advisor Prof. Michael Schick for support, energy and inspiration and for his patience when progress was wanting.

I would like to thank Stephen Colton, Jim Denton and the gang at Wallingford Rod & Foil Fencing Club for encouragement and tolerance.

I acknowledge many pleasant discussions with Dr. Marcus Müller during his stay as Postdoc in 1996.

Sincere thanks go to Chuck Robertson, who was always able to meet my special requests for TA assignments somehow.

My final thoughts go to Angela, who made it all worthwhile again.

GLOSSARY

ADSORPTION: Weak (reversible) attraction of molecules to a surface.

AMPHIPHILE: Molecule with chemically different head and tail groups, *i.e.* surfactant or block copolymer. Amphiphiles tend to assemble at the interface between different phases, to bring both its ends in contact with a favorable environment.

BCC: Abbreviation for body-centered-cubic phase.

BICONTINUOUS PHASE: Self-assembled, ordered or disordered phase, in which two different regions span the entire sample. Examples are the ordered gyroid and the disordered microemulsion phase.

BILAYER: Double layer of amphiphilic molecules or diblock copolymers, shielding the minority component in the core from unfavorable contacts with the environment.

BLEND: Mixture of two or more different polymers without any solvent present, *i.e.* a multicomponent melt.

BLOCK COPOLYMER: Chain molecules made of different monomers, in which the monomers are grouped into block, formed only by identical monomers, *e.g.* a diblock copolymer has the architecture A- ... -A-B- ... -B.

BODY-CENTERED CUBIC PHASE: Self-assembled phase of spherical micelles on the minority component, arranged on a body-centered-cubic lattice.

BRAZOVSKII CLASS: Universality class of continuous transitions, at which the amplitude of a spatially modulated order parameter vanishes continuously at *non-vanishing* wave vector.

BRUSH: Polymers with one end permanently attached to a surface. For sufficiently high grafting density, the polymers are strongly stretched due to the repulsion by the other chains. In this case, the height of the brush is proportional to the index of polymerization, N.

CHAIN LENGTH: Equivalent to index of polymerization, *i.e.* number of monomers per chain. Proportional to the contour length of the chain.

COIL: Configuration of an isolated chain in solution.

COLLAPSED COIL: Equivalent to Globule.

COPOLYMER: Chain molecule, formed by more than one kind of monomer.

CRITICAL END POINT: Critical point, where a line of continuous transitions terminates on a line of first-order transitions.

DNA: Carrier of the genetic information in living cells. Perfectly linear polymer of up to 10^9 repeat units.

DEGENNES-TAUPIN PERSISTENCE LENGTH: Length over which a flexible membrane stays flat on average. The persistence length ξ depends exponentially on temperature and bending modulus κ: $\xi \sim e^{2\pi\beta\kappa}$.

DEGREE OF POLYMERIZATION: Number of monomers per chain.

DIBLOCK (COPOLYMER): Copolymer, consisting of two different kinds of monomers, with the architecture A- ... -A-B- ... -B.

DIMPLING MODE: Fluctuation mode for a lamellar phase of a bilayer, in which the local thickness of the layer varies, while the mid plane of each layer stays flat.

EMULSIFIER: Amphiphile, used to make to normally immiscible fluids miscible.

EXCLUDED VOLUME: Volume per monomer, from which other monomers are excluded by hard core repulsion.

FLORY EXPONENT: The mean end-to-end distance R and the number of segments N in a chain are related by the scaling law: $R \sim N^{\nu}$. For an ideal chain (*i.e.* without excluded volume): $\nu = 1/2$ (Gaussian Exponent). For a chain with excluded volume (*i.e.* a self-avoiding random walk) in three dimensions: $\nu \approx 3/5$ (Flory Exponent).

FLORY PARAMETER χ: Dimensionless interaction parameter, measuring the repulsion between two unlike monomers. For many substances χ is positive and varies inversely proportionally with temperature.

FLORY THEOREM: The Flory Theorem states that in a dens polymer system (*i.e.* a melt or concentrated solution) the excluded volume interaction is screened, so that in a melt or concentrated solution chains behave Gaussian. In particular, the average end-to-end distance scales with the number of monomers per chain N as: $R \sim N^{1/2}$.

FLORY, PAUL J.: 1910– ... ; Nobel prize in Chemistry 1974. Theoretical Polymer Chemist.

FLORY-HUGGINS THEORY: Mean field theory to describe phase separation in polymer solutions and blends.

GAUSSIAN CHAIN: Theoretical chain model visualizing the chain as "beads connected by springs". The distribution function for the end-to-end vector $\mathbf{R}$ of a chain of N segments, each of length a, is $P_N[\mathbf{R}] = (2\pi Na^2/3)^{-3/2} \exp(-\frac{3}{2}\frac{\mathbf{R}^2}{Na^2})$, the root mean square end-to-end distance is $R_0 = aN^{1/2}$. Notice that these expressions hold asymptotically for *any* ideal chain (*i.e.* without excluded volume) for sufficiently large N. Therefore, "Gaussian chain behavior" is equivalent to "no effective excluded volume".

GLOBULE: Configuration of an isolated polymer chain in poor solvent. Its radius R scales with the number of segments N as: $R \sim N^{1/3}$.

GYR: Abbreviation for gyroid phase.

GYROID PHASE: Ordered bicontinuous phase of cubic symmetry (space group $Ia3d$), in which two interpenetrating networks, which are mirror images of one another, of the minority component are embedded in a majority component matrix.

HELFRICH INTERACTION: Steric repulsion in lamellar phases, due to the thermally excited undulations of the layers. The Helfrich interaction energy for two layers of mean separation ℓ behaves as $1/\ell^2$.

HEX: Abbreviation for hexagonal phase.

HEXAGONAL PHASE: Self-assembled phase, formed by cylinders of the minority component, arranged on a hexagonal lattice.

HEXAGONALLY PERFORATED LAMELLAR PHASE: Lamellar phase, in which the minority layers are pierced by channels of the majority component. The holes can either be stacked ABA or ABC.

HOMOPOLYMER: Chain molecule, formed by identical monomers.

HPL: Abbreviation for Hexagonally Perforated Lamellar Phase.

IDEAL CHAIN: Chain without excluded volume interaction. The distribution of the mean end-to-end vector is Gaussian, the root mean square of the end-to-end vector is proportional to the square root of the number of segments in the chain.

KUHN LENGTH: The Kuhn length is defined through: $a_K \stackrel{\text{def}}{=} \langle R^2 \rangle / L$, with mean square end-to-end radius $\langle R^2 \rangle$ and contour length L. The Kuhn length is the length of one statistically independent unit, usually comprising 4–5 chemical repeat units.

L_3 PHASE: Abbreviation for sponge phase.

L_α PHASE: Abbreviation for lamellar phase, used in the context of short-chain amphiphiles.

LAM: Abbreviation for lamellar phase.

LAMELLAR PHASE: Ordered phase of interchanging layers.

LEIBLER POINT: Point of continuous transition from a disordered to an ordered state at non-vanishing wave vector in polymer systems.

LEIBLER TRANSITION: Continuous transition at a Leibler Point. Leibler transitions are of the Brazovskii universality class.

LIFSHITZ POINT: At a Lifshitz point, the amplitude of a spatially modulated order parameter and its wave vector go *simultaneously* continuously to zero.

LINK: Repeat unit in a model chain.

LIPID: Biological surfactant, constituent of the cell membrane.

LIQUID CRYSTAL: Here: system of stiff, rod- or plate-like molecules, that can undergo structural phase transitions as external thermodynamic parameters are varied.

LYOTROPIC PHASE: Self-assembled phase that can undergo structural phase transitions as its composition changes.

MELT: Liquid System of polymers, not containing any solvent. According to the Flory theorem, the excluded volume interactions are screened in a melt and the chains behave ideally on scale much larger than the monomer size.

MESOPHASE: Self-assembled, ordered or disordered phase, with properties intermediate between liquid and solid phases (orientational molecular order, one- or two-dimensional order in a three dimensional material, etc.).

MICELLAR FLUID: Disordered phase of spherical or cylindrical micelles in a homogeneous background.

MICELLE: Well defined isolated self-assembled aggregate. Common are spherical and cylindrical micelles.

MICROEMULSION: Disordered, bicontinuous phase in ternary systems consisting of two different solvents and an amphiphile. A continuous amphiphilic layer separates two regions rich in either of the two solvents. Both solvent regions span the entire sample.

MICROPHASE: Ordered phase of supermolecular aggregates (*e.g.* BCC phase as ordered phase of spherical micelles).

MONODISPERSITY: Situation of vanishing polydispersity.

MONOMER: Chemical repeat unit.

PERSISTENCE LENGTH: Length over which a polymer is flexible. It is defined as the correlation length for intrachain correlations.

OBDD: Abbreviation for ordered bicontinuous double diamond phase.

ORDERED BICONTINUOUS DOUBLE DIAMOND PHASE: Ordered bicontinuous phase of cubic symmetry (space group $Pn3m$). Many samples that were previously alleged to be OBDD have later been identified as gyroid.

POLYAMPHOLYTE: Polymer, carrying both positive and negative charges.

POLYDISPERSITY: Measure of the spread of the chain length distribution in the sample. The polydispersity parameter p is defined as: $p \stackrel{\text{def}}{=} \langle (N - \langle N \rangle)^2 \rangle \, / \, \langle N \rangle^2$. It is possible to achieve $p < 0.01$ in experiments.

POLYELECTROLYTE: Polymer with a fraction f of its links carrying electrical charge q. All charges on the polymer are of the same sign, to establish charge neutrality, polyelectrolytes usually exist in a solution of counterions.

POLYMER: Chain molecule, consisting of a large number of monomers (*i.e.* repeat units), which are linked together with some degree of flexibility in each joint.

POLYMER, LINEAR: Chain molecule without branches, all monomers are linked sequentially.

PREWETTING: Discontinuous jump in the thickness of an adsorbed layer from thin to thick as coexistence is approached.

PROTEIN: Functional units in biological systems. Chemically, proteins are random copolymers.

RADIUS, ROOT MEAN SQUARE: Root mean square of the end-to-end vector in a linear polymer chain.

RADIUS OF GYRATION: Defined through: $R_G \stackrel{\text{def}}{=} \frac{1}{2N} \sum_{n,m}^{N} \langle (\mathbf{R}_n - \mathbf{R}_m)^2 \rangle$, where the sum is over all segments in the chain. Notice that $R_G$is also defined for non-linear chains. For linear chains of segment length a, one finds: $R_G = aN^{1/2}/6$.

SEGMENT: Repeat unit in a model chain.

SEGREGATION: Measure of the effective repulsion between unlike monomers, as measured by the effective interaction parameter χN. Weak segregation regime: $\chi N < 12.0$, strong segregation regime: $\chi N > 50$.

SELF-ASSEMBLY: If the amphiphile concentration in a system is high enough, the amphiphile will *create* additional internal interfaces, at which it can adsorb. These interfaces then self-assemble into various ordered or disordered structures.

SOLUTION: Mixture of a polymer with a solvent of simple molecules.

SOLUTION, CONCENTRATED: Solution, in which the polymer volume fraction approaches one. The excluded volume interaction is screened and the chains behave ideally.

SOLUTION, DILUTE: Polymer solution in which the mean distance between different polymer coils is larger than the coil radius. A dilute solution is essentially a system of isolated chains.

SOLUTION, SEMIDILUTE: Solution in which the polymer coils of radius R overlap, although the solvent concentration is still high. The overlap volume fraction is $\varphi^* \cong a^3 N/R^3 \cong N^{1-3\nu}$ and can be quite small.

SOLVENT: Liquid of small, simple molecules without internal degrees of freedom. Solvents are classified according to their interaction with polymers as good (or athermal), neutral (or Θ) or poor.

SOLVENT, Θ: Same as Neutral Solvent.

SOLVENT, ATHERMAL: Good solvent in the limit of high temperatures. A moderate change in temperature does not change the qualitative behavior of the solvent.

SOLVENT, GOOD: If the polymer segments prefer an environment of solvent molecules over their own kind, the solvent is called good. In good solvents polymers

tend to swell, the root mean-square-radius R scales with the number of segments as $R \sim N^{3/5}$.

SOLVENT, NEUTRAL: If the interactions between the monomers are equal to the interactions with solvent molecules, the solvent is called neutral. The chain behaves Gaussian, the root mean-square-radius R scales with the number of segments as $R \sim N^{1/2}$.

SOLVENT, POOR: If the polymer segments prefer an environment of their own kind over one of solvent molecules, the solvent is called poor. In poor solvents, polymers tend to precipitate (phase separate) from the solvent. The (very few) chains that remain in solution assume a collapsed, globular configuration, the root mean-square-radius R of the globule scales with the number of segments as $R \sim N^{1/3}$.

SPONGE PHASE: Disordered phase in binary amphiphile/solvent systems, in which a continuous amphiphilic bilayer separates two unconnected solvent regions, each of which spans the entire sample.

STRUCTURE FUNCTION: Fourier Transform of the density-density correlation function. For an isolated Gaussian chain of N segments and with mean radius $R_0 = aN^{1/2}$, the structure function is $Ng_D(x)$, where the Debye function is: $g_D(x) = 2(x - \exp(x) + 1)/x^2$, with $x = (q^2R_0^2)/6$.

SURFACTANT: Short chain amphiphile.

SWOLLEN COIL: Configuration of an isolated chain in good solvent. Its size is proportional to N^{ν}, where N is the number of segments in the chain and $nu \approx 3/5$ is the Flory exponent.

THERMOTROPIC PHASE: In the context of liquid crystal systems: ordered phase, which undergoes structural phase transitions as the temperature is varied.

TRIBLOCK (COPOLYMER): Block copolymer with architecture ABA or ABC.

UNDULATION MODE: Fluctuation mode of a lamellar phase or an isolated layer, in which the layers assumes a configuration that is locally not flat, while its thickness is constant throughout.

WETTING: Surface phase transition, in which the thickness of an adsorbed fluid film diverges as external thermodynamic parameters are changed.

WETTING, COMPLETE: Wetting transition, in which the thickness of an adsorbed layer diverges as the bulk coexistence of the wet and dry phases is approached.

WETTING, CRITICAL: Wetting transition, in which the thickness of an adsorbed layer diverges continuously as the temperature is varied, while the system is kept on bulk coexistence.

WETTING, FIRST-ORDER: Wetting transition, in which the thickness of an adsorbed layer diverges discontinuously as the temperature is varied, while the system is kept on bulk coexistence. Adjacent to the first-order wetting transition one finds a prewetting line.

Chapter 1

INTRODUCTION

1.1 What are Polymers?

Polymers are long flexible chain molecules, consisting of many repeat units, or monomers, units, or monomers, linked together into a linear or branched chain. In their technical form, polymers constitute what are known as "plastics" [56]: Styrofoam (polystyrene), shopping bags (polyethylene), tires (mostly polyisoprene), food containers (often polypropylene), but also materials such as adhesives, fibers ("Nylon") or GoreTex (polyurethane). Another very important class of polymers are biological materials [1]: proteins, the main functional elements of cells; DNA and RNA, the carriers of genetic information; and lipids, the prevalent constituent of the cell membrane, are all polymers of different complexity. All these polymers differ in the chemical structure of their monomers and, possibly, in the way the monomers are linked together. Choosing the proper chemical structure to create a material with the desired properties and devising ways to synthesize it are the goals of chemistry, chemical engineering and materials science.

On the other hand, the physicist tries to understand the *generic* behavior of polymers, starting from such properties, common to *all* polymers, as their great length and flexibility. Theoretical predictions based on universal models have been experimentally confirmed on a great variety of *chemically* different, but *structurally* (*i.e.* in regards to length, flexibility, architecture) similar polymers.

The crudest model of a polymer chain is a random walk of N steps, possibly with

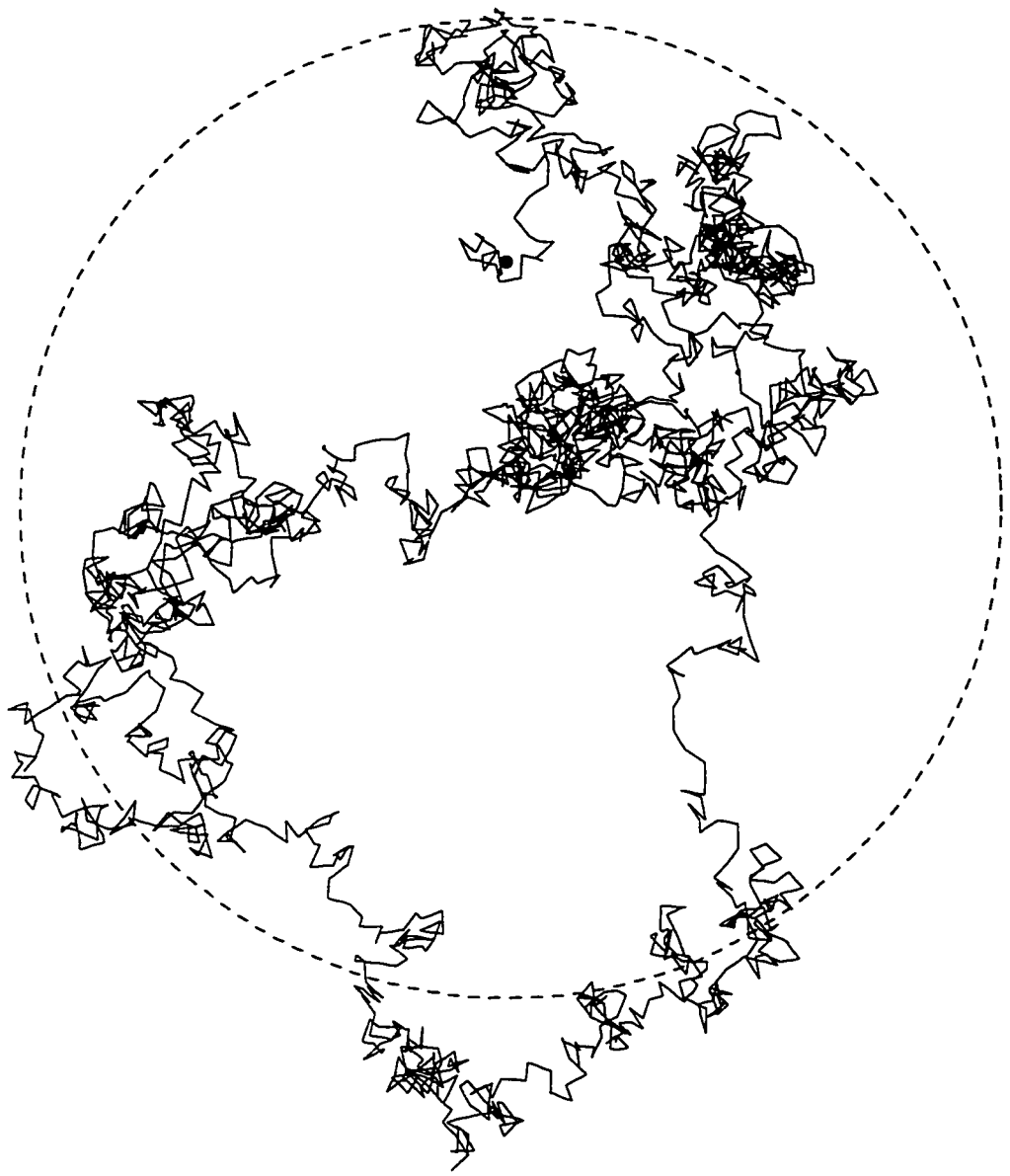

Figure 1.1: Projection of a free random walk of 2400 steps of unit length in 3 dimensions into the $z = 0$-plane. Beginning- and end-points of the walk are shown with dots. The radius of gyration $R_G = \sqrt{N/6}$ is shown with dashes.

some correlations between steps (Figure 1.1). The number of steps can be very large: industrial polymers often contain between 10^4 to 10^6 monomers, the longest linear

polymer known, the DNA, carrier of the genetic information, even up to 10^9 repeat units. For long chains, there will obviously be a large number of possible walks. For sufficiently large N, explicit enumeration of all configurations will be impossible and the treatment of the walk (*i.e.* the polymer) as a *statistical object* will become necessary.

Because of this enormous number of conformations that a long flexible chain can take on, polymers in solution or in the melt belong to the class of "complex fluids", *i.e.* fluids whose constituent molecules possess *internal* degrees of freedom, as compared to simple liquids (*e.g.* liquid argon) [78], whose molecules only possess translational (positional) degrees of freedom. Other complex fluids, besides polymers are (thermotropic) liquid crystals [36], *i.e.* extended, but stiff, rod- or plate-like molecules which can be oriented in space in different ways. Another example is a system of water, oil and a surfactant [67]. Surfactants are amphiphiles, *i.e.* molecules with chemically different parts. Such amphiphiles have, for example, a hydrophilic "head group" and a hydrophobic "tail". In an oil/water mixture, such molecules will try to sit at the oil/water interface, so as to accommodate the preference of each of its ends for a different environment. This is the mechanism by which grease is soluble in water containing dishwashing liquid. In fact, given the opportunity, surfactants will often *create* additional interfaces in a fluid to reduce their frustration in a homogeneous background. Because of their internal degrees of freedom per molecule, complex fluids can overcome the disordering effects of temperature and self-assemble into a partially ordered state.

1.2 What is Self-Assembly?

Molecules with internal degrees of freedom can exist in states intermediate between solid and liquid states. In a perfect crystalline solid, all molecules are arranged in a perfectly periodic array. The correlation length is infinite and scattering by

a crystal gives sharp Bragg peaks. In an isotropic liquid, there is a certain short-range order, which decays exponentially with decay length ξ. The scattering function typically shows a diffuse peak of width $1/\xi$. Intermediate phases can be obtained by imposing orientational order for non-spherical fluid molecules (*e.g.* nematic and cholesteric liquid crystals, or amphiphiles straddling an interface), or by one- or two-dimensional positional order in a three-dimensional fluid phase (columnar or smectic liquid crystals). In accordance with de Gennes [36] we will call these intermediate phases *mesomorphic phases* or mesophases (and retain the expression "liquid crystal" strictly for thermotropic liquid crystals). Specifically, we will be concerned with amphiphilic mesophases.

As mentioned above, amphiphiles can lower their energy by adsorbing to an interface so that both ends of the amphiphilic molecule are placed into their preferred environment. (For the present discussion we will call them "oil" and "water", respectively, keeping in mind however that they may be any two immiscible substances.) For sufficiently high concentration, it is often favorable for the amphiphile to create additional interface, rather than to dissolve randomly. These internal interfaces then assemble into various structures. In Figure 1.2 we show some of the ordered phases that have been observed in experiments. Which of these phases is formed, depends on the architecture of amphiphile and solvent molecules, the composition of the mixture, and temperature.

For lower amphiphile concentration (or higher temperature) disordered, but structured fluid phases, *e.g.* a disordered micellar solution, may be formed when the hexagonal lattice of cylinders or the body-centered-cubic lattice of spheres in Figure 1.2 melts, while still leaving the cylindrical or spherical micelles intact. Another disordered but structured phase is the microemulsion phase, where a disordered array of amphiphilic sheets separates coherent oil- and water-regions. If both oil and water regions span the entire sample, the microemulsion is said to be "bicontinuous" (c.f. Figure 1.2). A remarkable feature of all self-assembled phases, whether ordered or

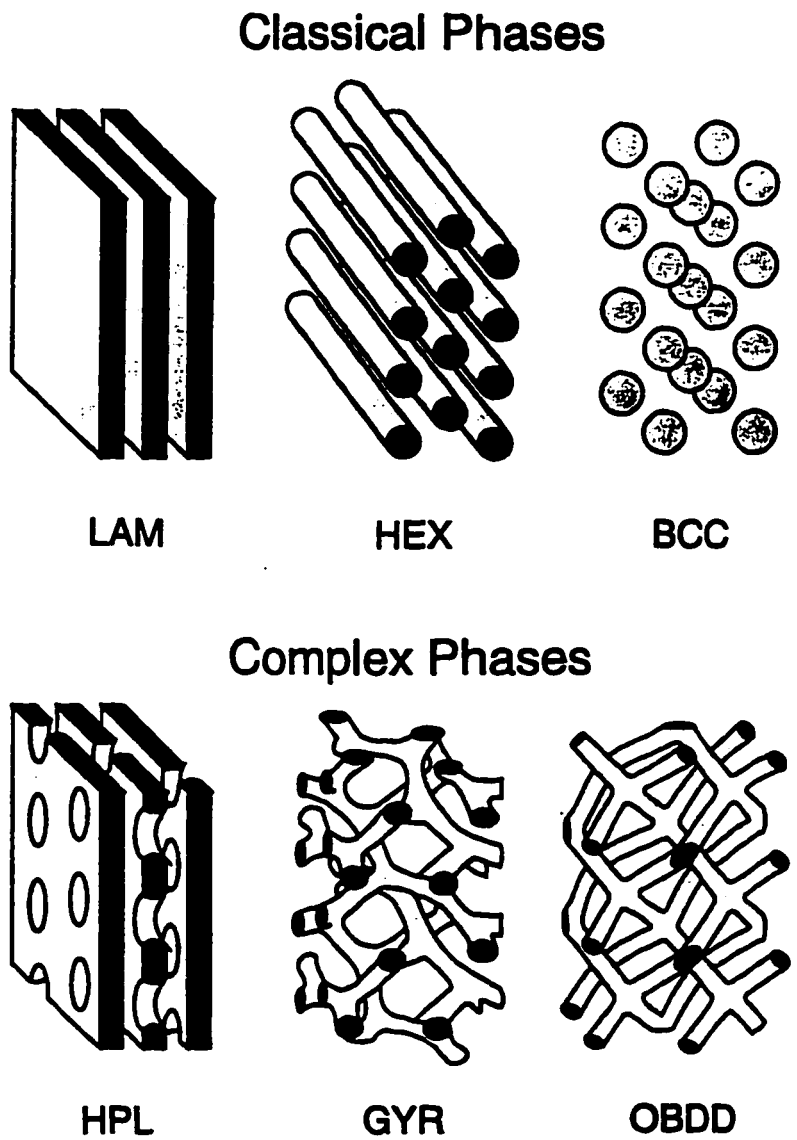

Figure 1.2: Amphiphiles at sufficiently high concentration will often create internal interfaces, which in turn assemble into various ordered structures, depending on temperature, concentration and architecture of the amphiphile. Shown are the most often observed morphologies: sheetlike lamellae (LAM), hexagonally arranged cylinders (HEX), and spheres on a body-centered-cubic lattice (BCC). Also shown are some of the observed or alleged "complex phases": hexagonally perforated lamellae (HPL), the "gyroid" phase (Space group $Ia3d$) (GYR), and the ordered bicontinuous double diamond phase (Space group $Pn3m$) (OBDD). After [152].

disordered, is that they are characterized by an *extensive* amount of internal interface.

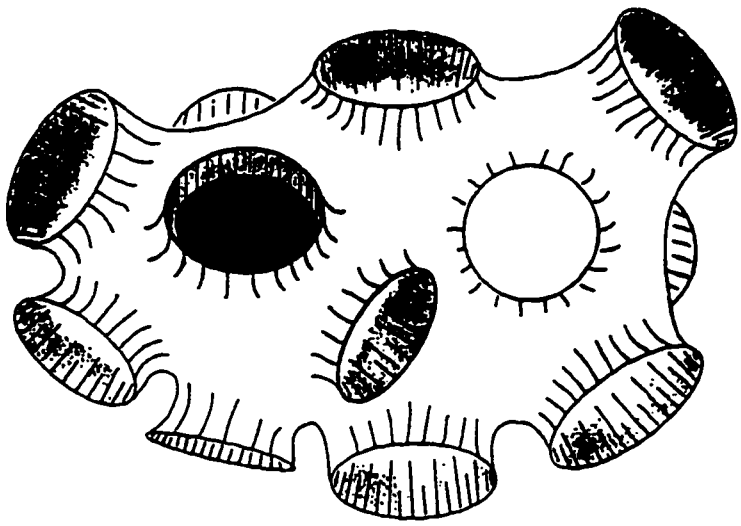

Figure 1.3: Disordered microemulsion phases occur when a coherent amphiphilic layer separates bicontinuous oil- and water-regions. After [85].

Amphiphilic self-assembly may seem like an obscure and rare phenomenon, but it has some common technological uses in soap production and oil recovery. An even more important example is the membrane of living cells, which is a self-assembled bilayer of phospholipids (a certain kind of biological amphiphile) and proteins.

Mesophases in general have a few universal properties: the forces involved are weak and the characteristic energies comparable to the thermal energy k_BT. Defects in the structure will therefore be frequent and the substance as a whole will flow like a (possibly viscous) liquid. The mesophase possesses structure on a molecular or supermolecular length scale, which is much larger than the size of a single molecule (typically 20–500 Å).

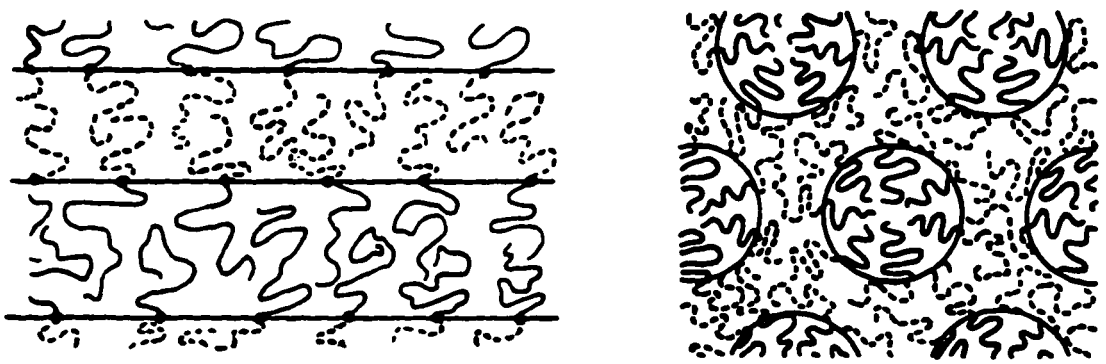

Figure 1.4: Microscopic view of diblock copolymers in lamellar (left) and hexagonal (right) mesophases. After [208].

1.3 Why study Self-Assembly in Polymer Blends?

Block copolymers are chain molecules made out of different "blocks", each of which consists of identical monomers. The simplest block copolymer is the diblock, with architecture A- ... -A-B ... -B. More complicated architectures are possible: ABA- and ABC-triblocks, multiblocks, etc. In general, each A-monomer will prefer a surrounding of other A-monomers to one of B-monomers. Diblock copolymers therefore combine the properties of polymers with those of amphiphiles, and blends of AB-diblocks with the corresponding A- and B-homopolymers are in many respects comparable to mixtures of oil and water with soap (c.f. Figure 1.4).

There are two main reasons why block copolymer systems are so attractive for studying self-assembly: the relevance of the subject on the one hand, and the availability of tools (experimentally and theoretically) on the other, that make such a project feasible.

Since one has reason to expect that the synthesis of novel and chemically different monomers is going to slow down in the future [187], attention is drawn to polymer mixtures and compounds to create new materials with specific properties (such as

flexibility, tensile strength, resistance to heat, etc.). Block copolymers, because of their emulsifying and structuring properties, are an important ingredient.

The latter property in particular, namely the ability to bring about phases with complex order on molecular length scales has some obvious potential applications in the microscopic manufacturing of materials ("nanotechnology"), *e.g.* the formation of capillaries and sieves with holes only a few atomic diameters wide from hexagonal (HEX) or hexagonally perforated (HPL) phases (c.f. Figure 1.2); or the formation of extended, bicontinuous networks (*e.g.* for catalytic converters) from complex phases such as the gyroid (GYR); or the microstructuring of surfaces by bonding an appropriate mesophase to a solid substrate.

On a more scientific level, one tries to understand the fundamental physical mechanism underlying self-assembly. Can one explain the occurrence of ordered phases in complex fluids starting from a first-principles atomistic theory? Why do complex phases, such as the gyroid, form? How can one describe a disordered, but not structureless phase, like a microemulsion?

In blends in particular, there are many interesting additional effects, *e.g.* the possibility of exotic critical phenomena, like Lifshitz and Leibler points, the intricate interplay between micro- and macrophase separation, etc. Given the large parameter space of block copolymeric systems, comprising not only the usual thermodynamic variables, but also the architectural parameters, such as chain length and composition, it is very difficult, if not impossible to develop a coherent picture from experiment alone. A theoretical investigation, mapping out a representative set of parameters, is therefore necessary.

Since the phenomenon of amphiphilic self-assembly is rather universal (the same phases and very similar phase diagrams in terms of temperature and composition have been found for a wide variety of chemically different systems, both for short-chain surfactants, as well as for diblock copolymers), one may hope to be able to arrive at some general conclusions by studying the most convenient and accessible system.

Copolymers provide in many respects an ideal model system to study self-assembly.

On the experimental side, microstructures formed by polymers are easily observed because of the large length ($\approx$ 500 Å) and time (hours to days) scales involved. Most structural phase transitions occur in a fairly convenient temperature range (20–200 °C). Furthermore, since the architecture of polymers can be tailored as desired, one has an additional, systematically tunable parameter at one's disposal. Using deuterium labeling and neutron scattering (c.f. Section 2.2.1.2) one can even obtain precise information about the behavior of any desired monomer of any given chain.

The great theoretical advantage of using polymer melts is that, for most of the parameter space, they are quantitatively well described by rather straightforward mean field theory (Section 3.2). Very intuitively speaking, this can be understood as follows. The local fluctuations are on the scale of the monomers ($\cong$ 10 Å). The ordering phenomena are on the scale of one polymer coil however ($\cong$ 100 Å). Averaged over one chain volume, the local density fluctuations are negligible. Only extremely (often unmeasurably) close to a critical point does the mean field description break down, compelling one to resort to more complicated approaches like liquid-state integral equation theories, renormalization group analysis, etc.

1.4 What is the Purpose of the Present Work?

As the preceding discussion shows, the micro- and macrophase behavior of block copolymer systems provides a rich and fascinating topic in the field of complex fluids, with many interesting and important questions, both scientifical, as well as technological. What is attempted in the present work is to investigate and clarify the phase behavior of *blends* containing a diblock copolymer and one or two corresponding homopolymers.

As compared to the situation in pure diblock copolymer melts, where the phase diagram has been calculated with great accuracy [125, 222, 157, 151] and is found to

be in general agreement with experiments [18, 58, 151], in particular after fluctuation corrections have been taken into account [61, 200, 17, 16], the situation in the technologically particular important case of homopolymer/diblock blends is much less clear. Despite a wealth of experimental work [99, 79, 113, 83, 241, 240, 82, 115, 116, 256, 255, 258, 257, 265, 206, 193, 104, 41], no clear picture of the phase behavior and in particular of the dependence of the phase diagram on architectural parameters has emerged.

It is the aim of this work to present a comprehensive catalogue of reliable phase diagrams for binary and ternary blends, covering the particular interesting weak and intermediate segregation regimes. Calculated phase diagrams for polymer blends undergoing microphase separation should fulfill the following requirements if they are to be useful for further experimental or theoretical work. The particular nature of polymeric liquids must be treated properly, in particular the chain connectivity and the infinite number of chain configurations have to be taken into account. Furthermore, one must allow for ordered phase of arbitrary geometry and for variations in the local monomer density of arbitrary amplitude. Approaches that make additional simplifying assumptions about the structure of the ordered phase (*e.g.* that the lamellar phase is the only occurring ordered morphology [10, 193] or about the amplitude of the local density variations [10] are of limited validity. Finally, the results obtained should be valid in experimentally accessible regions of the parameter space and not only in unphysical (*e.g.* zero temperature) limiting cases [222, 260].

The full self-consistent field theory of the Gaussian chain, formulated in Fourier space (c.f. Chapter 3), fulfills these requirements. The Gaussian chain model [43] is excellent for the *universal* behavior of flexible chains on length scales comparable to the coil size (*i.e.* on the scale that the ordering phenomena take place). The formulation in Fourier space allows for *any* ordered geometry [157, 145] and the mean field treatment is valid for systems composed of long chains in the intermediate and strong segregation regime.

By means of this method, phase diagrams for a variety of binary and ternary blends will be calculated. Emphasis will be put on the chain length ratio $\alpha_A = N_A/N_{AB}$ of homopolymer to diblock chains (where N_κ is the degree of polymerization of component κ) as the parameter, which mainly determines the overall topology of the phase diagram. Since the present work is essentially the first attempt to map out the general phase behavior of homopolymer/diblock blends, we will restrict ourselves for the most part to blends containing symmetric diblocks (with A- and B-blocks of equal length) and consider only the "classical" phases (*i.e.* lamellar, hexagonal and body-centered-cubic), which are well-known to exist in copolymer systems and to fill most of the ordered regions of the phase diagram. For all our results, we try to find intuitive explanations in terms of simple brush, and stretching, arguments.

1.5 Overview

In the first part of the following chapter, we will establish most of the pertinent concepts specific to polymer physics. The treatment will be introductory and straightforward. The main emphasis will be to work out the *scaling behavior* of physical quantities of interest with temperature, concentration and in particular with the chain length. The second part of the chapter is devoted to a discussion of the mathematical properties of the standard ("Gaussian") chain model. In Chapter 3, we will specifically focus on microphase separation phenomena in block copolymeric systems. We will briefly review the main experimental methods and then treat some calculational methods specifically suited for the study of polymeric microphase separation. In Chapter 4, I present and discuss my own research, an investigation of the macro- and microphase behavior of ternary and binary blends of a symmetric diblock copolymer with corresponding A- and B-homopolymers. Finally, the results are summarized in Chapter 5, discussed and compared with other experimental and theoretical investigations.

A glossary of some important terms and concepts, including common abbreviations, from polymer physics and the physics of self-assembly has been provided to avoid repetition and to facilitate comprehension.

I would like to point out that there are some important areas which are not covered in the present work. Since we are interested in the generic physical behavior, no mention is made of the underlying chemistry. Questions of synthesis, characterization, purification etc. will not be addressed. We will only consider linear chains, and ignore all the other architectures that exist: ring and branched polymers as well as polymer networks. The biggest omission concerns the dynamics of flexible chain molecules. Throughout all of this work, we will be *exclusively* concerned with equilibrium statistical mechanics. Consequentially, no attempt has been made to treat transport properties, the approach to equilibrium, or dynamical response.

1.6 Notation

In keeping with the notation used by de Gennes [35], we use the equals sign "=" for *exact* equality, including all numerical factors. If we state only the scaling law, ignoring numerical coefficients, but keeping all dimensional factors, we use the symbol "$\cong$". If we want to stress only the scaling behavior of the left hand side with respect to some particular variable, we use "$\sim$". For approximate equality, *e.g.* after neglecting small terms, we use "$\approx$".

Vectors are signified by boldface upright: $\mathbf{r}$. If no other meaning is obvious from the direct context, β stands for the inverse of the usual product of the Boltzmann constant and absolute temperature: $\beta = 1/k_B T$.

Chapter 2

STATISTICAL THEORY OF CHAIN MOLECULES

2.1 Basic Concepts in the Physics of Chain Molecules

In this chapter, we discuss the most important concepts and results of polymer physics. We will often refer to concepts introduced in this chapter, either to motivate a calculation, or to explain a result.

We progress from the properties of an isolated chain, to systems of many interacting chains, and finally discuss chains under constraints, such as confinement, elongation, etc.

Most of the material in this chapter is covered in the standard monographs [109, 35, 42]. When necessary, more specialized references will be given in the appropriate sections.

2.1.1 Isolated Chains

We begin by studying the statistical properties of a single, isolated chain. This situation has obviously a strongly simplifying "model" character, but its predictions can easily be tested by computer experiments. Furthermore, as we will later see (Section 2.1.2.1), polymers in a dilute solution can often be treated as isolated.

In considering chain models, one major distinction arises immediately: between those models that allow the chain to intersect itself, and those that do not. The former are known as "ideal chain" models, whereas the latter are called "real chains". Because any realistic interatomic or intermolecular interaction potential (Figure 2.4) will include a hard core repulsion, which is dominant at short distances, it might seem

as if ideal chains bear very little resemblance to experimentally accessible scenarios. However, a remarkable result, known as Flory's Theorem (Section 2.1.2.2) asserts that chains in a melt behave as if they were ideal. We will therefore study the properties of ideal chains in some detail in the following three subsections. Then we will turn to real chains and discuss the consequences of the "excluded volume effect" induced by the hard core repulsion.

2.1.1.1 The Freely Jointed Chain Model

Assume a chain, made up of N segments, each of length a, joined together in such a way that each segment can point in any direction with equal probability, independently of any of the other segments. This model is called the "Freely Jointed Chain". Obviously, this chain can take on an enormous number of configurations. Two questions arise: How can we characterize the configuration, short of specifying the positions of all the links explicitly; and what is the probability distribution of the configurations?

The configuration Γ is specified by all the link vectors:

$$\Gamma_N = \{\mathbf{r}_1, \mathbf{r}_2, \ldots, \mathbf{r}_N\}. \tag{2.1}$$

Since all links are statistically independent, the probability for this configuration factors:

$$P[\Gamma_N] = p(\mathbf{r}_1)p(\mathbf{r}_1)\ldots p(\mathbf{r}_N), \tag{2.2}$$

where the (normalized) probability distribution for each link is uniform over the sphere of radius a:

$$p(\mathbf{r}) = \frac{1}{4\pi a^2}\delta\left(|\mathbf{r}| - a\right). \tag{2.3}$$

A convenient way of characterizing a chain conformation on a macroscopic level is by

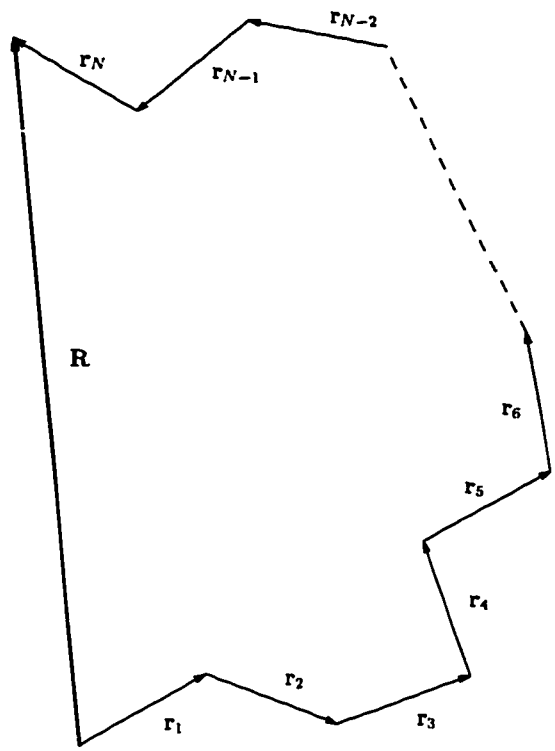

Figure 2.1: Bond vectors $\mathbf{r}_i$ and end-to-end vector $\mathbf{R}$ in a freely jointed chain

its size, as given for example by the length of the end-to-end vector (c.f. Figure 2.1):

$$\mathbf{R} = \sum_{n}^{N} \mathbf{r}_n. \tag{2.4}$$

Since the ensemble average $\langle \mathbf{r}_n \rangle$ of $\mathbf{r}_n$ vanishes for each n, the average end-to-end distance is zero: $\langle \mathbf{R} \rangle = 0$. However, its second moment $\langle \mathbf{R}^2 \rangle$ is non-zero:

$$\begin{aligned} \langle \mathbf{R}^2 \rangle &= \sum_n \sum_m \langle \mathbf{r}_n \cdot \mathbf{r}_m \rangle \\ &= \sum_n \langle \mathbf{r}_n^2 \rangle + \sum_{n \neq m} \langle \mathbf{r}_n \cdot \mathbf{r}_m \rangle \\ &= Na^2. \end{aligned} \tag{2.5}$$

This result follows because $\langle \mathbf{r}_n \cdot \mathbf{r}_m \rangle = 0$ for $n \neq m$, due to the statistical independence of links, and $\langle \mathbf{r}_n^2 \rangle = \int d^3r \frac{\mathbf{r}_n^2}{4\pi a^2} \delta(|\mathbf{r}| - a) = a^2$. Thus, the root mean-square-radius R_0 is given by a power law:

$$R_0 = aN^\nu \quad \text{with} \quad \nu = 1/2. \tag{2.6}$$

We now ask for the probability distribution $P_N(\mathbf{R})$ that a chain of N links has an end-to-end vector $\mathbf{R}$. Given the probability $P[\Gamma_N]$ of each configuration (2.2), we find:

$$P_N(\mathbf{R}) = \int d^3r_1 \ldots d^3r_N \, \delta\Big(\sum_n \mathbf{r}_n - \mathbf{R}\Big) P[\Gamma_N].$$

Using the Fourier representation of the δ-function: $\delta(\mathbf{r}) = \int \frac{d^3k}{(2\pi)^3} e^{i\mathbf{k}\mathbf{r}}$ and equation (2.2), we write this as:

$$P_N(\mathbf{R}) = \int \frac{d^3k}{(2\pi)^3} e^{-i\mathbf{k}\mathbf{R}} \left[\int d^3r \, e^{i\mathbf{k}\mathbf{r}} p(\mathbf{r}) \right]^N. \tag{2.7}$$

The term in brackets can be evaluated in spherical coordinates (note that $\partial_\theta e^{iqr\cos\theta} = -iqr \sin\theta \, e^{iqr\cos\theta}$):

$$\begin{aligned} \int d^3r \, e^{i\mathbf{k}\mathbf{r}} p(\mathbf{r}) &= \frac{1}{4\pi a^2} \int_0^\infty dr \, r^2 \int_0^{2\pi} d\phi \int_0^\pi d\theta \, \sin\theta \, e^{ikr\cos\theta} \delta(r - a) \\ &= \frac{1}{4\pi a^2} \int_0^\infty dr \, r^2 \int_0^{2\pi} d\phi \left[\frac{e^{-ikr} - e^{ikr}}{-ikr} \right] \delta(r - a) \\ &= \frac{\sin ka}{ka}. \end{aligned} \tag{2.8}$$

From equation (2.7) the probability distribution of $\mathbf{R}$ is

$$P_N(\mathbf{R}) = \int \frac{d^3k}{(2\pi)^3} e^{-i\mathbf{k}\mathbf{R}} \left[\frac{\sin ka}{ka} \right]^N. \tag{2.9}$$

Since $\left(\frac{\sin ka}{ka}\right)^N$ is extremely strongly peaked at the origin if N is large, only small values of ka will give relevant contributions. We write: $\left(\frac{\sin ka}{ka}\right)^N = \exp\left(N \log \frac{\sin ka}{ka}\right)$ and expand the logarithm in $ka \ll 1$:

$$\left(\frac{\sin ka}{ka}\right)^N = \exp\left[N \log\left(1 - \frac{k^2a^2}{3!} + \frac{k^4a^4}{5!} + \cdots \right) \right]$$

The integral in equation (2.9) is now Gaussian and we obtain the final result for the probability distribution of the end-to-end vector of the freely jointed chain:

$$P_N(\mathbf{R}) = (2\pi N a^2/3)^{-3/2} \exp\left(-\frac{3\mathbf{R}^2}{2Na^2}\right)\left[1 - \tfrac{3}{20N}\left(5 - \tfrac{10\mathbf{R}^2}{R_0^2} + \tfrac{3\mathbf{R}^4}{R_0^4}\right) + \cdots\right]. \quad (2.10)$$

A few comments are in order here: To leading order, the distribution of the end-to-end vector is Gaussian. This results holds in general and corresponds to the Central Limit Theorem of Statistics [49, 50]: The distribution of a sum of *independent* random variables is Gaussian.

The corrections to Gaussian statistics are very small for the freely jointed chain, being suppressed by a factor of $1/N$. Only for $\mathbf{R}^2 \gg R_0^2$ do they become substantial. However, such configurations have exponentially small probability to occur, so that the leading order term of (2.10) gives a good approximation for all values of $\mathbf{R}$.

The average size R_0 of the chain is far from the contour length of the fully extended chain, the latter being given by

$$L = aN. \quad (2.11)$$

As N becomes very large, the ratio of the two goes to zero:

$$\frac{R_0}{L} = \frac{1}{N^{1/2}} \to 0.$$

The reason for this is that there are far more coiled than extended configurations, so that they dominate the average in equation (2.10).

2.1.1.2 General Properties of Ideal Chain Models

Because all links are independent, the freely jointed chain is a very simple model. In more realistic models, the behavior of any given link will partially be determined by its neighboring links. If, for example, one requires that the angle between two consecutive links is $\theta = const$, while each link can rotate about $\gamma = 0 \ldots 2\pi$ around the preceding one, we obtain the "freely rotating chain" model.

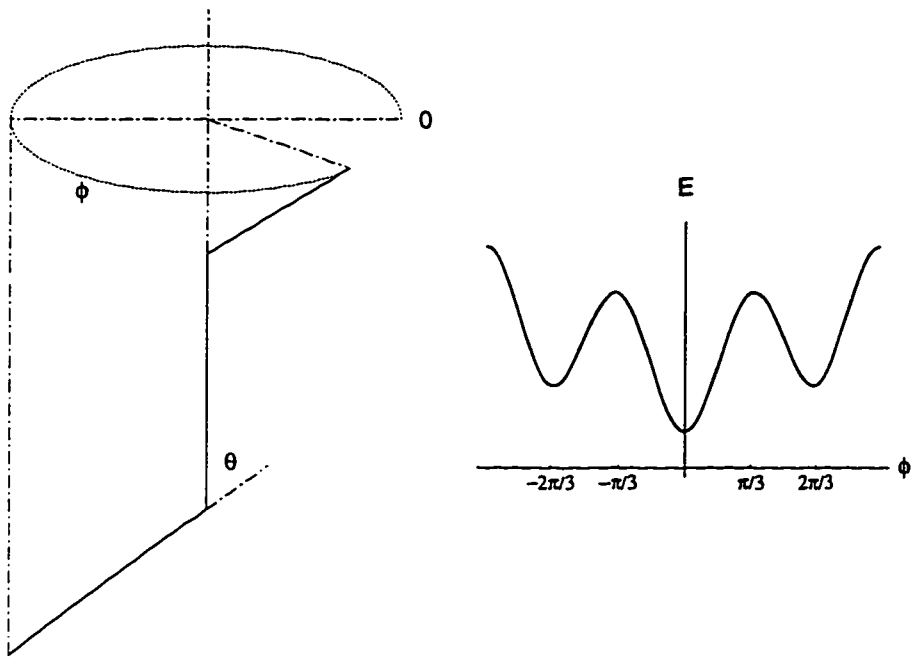

Figure 2.2: Possible configurations of three consecutive chain links (left); and configurational energy E as function of the internal rotational angle ϕ (right). The planar "trans" configuration corresponds to the global minimum at $\phi = 0$, the bend "gauche" configurations to the minima at $\phi = \pm 2\pi/3$.

In real polymers, the rotation about γ is rarely free. Typically, one finds a behavior of the potential energy as shown in Figure 2.2, where ϕ is the angle between the two planes that are spanned by two consecutive bond pairs. As a function of ϕ there is a minimum energy configuration (the "trans" conformation) and two symmetric metastable ("gauche") configurations. For many real polymers the excitation energy for gauche configurations is less than of $k_B T$, so that there will be a significant fraction of links in them. If this interaction between any *three* consecutive links, is taken into account, one arrives at the "rotational isomeric" chain model: one assumes that the chain can only reside in the three discrete states, corresponding to the local minima of the configurational energy, with the probability for each configuration given by the appropriate Boltzmann factor [57].

More complicated models can be invented to describe the interactions that one finds in real polymers. However, as long as the range of the internal interaction extends over any *finite* number of consecutive chain links (or equivalently: as long as correlations die out at least exponentially along the chain), all these models result in the same large scale behavior that one finds for the freely jointed chain, namely a mean-square-radius linear in N and a Gaussian distribution of the end-to-end vector. In particular, the relation (2.6) still holds with the same exponent $\nu = 1/2$; however, the numerical prefactor a has been modified by the internal interaction. To measure the effective step length, one introduces two further lengths: the Kuhn length a_K and the persistence length a_C, besides the bare step length a considered so far. The persistence length a_C is simply the correlation length of interchain correlations: $\langle \mathbf{r}_n \cdot \mathbf{r}_m \rangle \sim \exp(-\frac{|n-m|}{a_C})$. It can be worked out exactly for some simple chain models (c.f. [57]); for a chain characterized by a finite bending energy per unit length, κ, the persistence length is of order $a_C \cong k_B T/\kappa$. For real polymers and for many models, the ratio a_C/a is approximately two.

While the persistence length is defined by the microscopic properties of the model, the Kuhn length a_K is solely determined by experimentally measurable quantities. One of them is $\langle \mathbf{R}^2 \rangle$, which can be obtained from scattering experiments (c.f. Section 2.2.1.2) and the other is the contour length L. The latter is proportional to the total molecular weight (accessible through the osmotic pressure of a solution [56, 40]) and the size of a monomer. The Kuhn length a_K and the effective number of segments $\tilde{N}$ are now determined by the two requirements:

$$\langle \mathbf{R}^2 \rangle = a_K^2 \tilde{N},$$
$$L = a_K \tilde{N}.$$

Eliminating one or the other of the two unknowns, we find:

$$a_K = \frac{\langle \mathbf{R}^2 \rangle}{L}, \tag{2.12a}$$

$$\tilde{N} = \frac{L^2}{\langle \mathbf{R}^2 \rangle}, \tag{2.12b}$$

where now on the right hand side of (2.12a) there are only directly experimentally accessible quantities.

For linear polystyrene, the best studied example of a flexible polymer [204], chains of $10^2 \ldots 10^6$ monomers can easily be synthesized. The Kuhn length is found to be about 15 Å, and one statistical segment consists of 4 to 5 chemical repeat units. In comparison, the longest polymer known, human DNA, carrier of the genetic information, consists of 10^9 base pairs [1]. DNA is a "stiff" molecule, each statistical segment consists of about 150 base pairs and is about 500Å long.

To convince oneself that equation (2.10) holds (to leading order) for any chain model with interactions involving only a finite number n_c of consecutive links, one breaks the chain up into $\tilde{N}$ effective segments $\tilde{\mathbf{r}}_n$, each containing m links. Clearly: $\tilde{N} = N/m$. If $m \gg n_c$, the effective segments become independent, and the same analysis as in section Section 2.1.1.1 can be performed, only that $p(\mathbf{r})$ in (2.7) is now the single link probability distribution for an effective segment $\tilde{\mathbf{r}}$. In equation (2.8) the average has to be taken with respect to this distribution:

$$\begin{aligned} \int d^3r\, e^{i\mathbf{k}\mathbf{r}} p(\mathbf{r}) &= 4\pi \int dr\, r^2 \frac{\sin kr}{kr} p(r) \\ &= \left\langle \frac{\sin kr}{kr} \right\rangle_p, \end{aligned} \tag{2.13}$$

where we have used that $p(\mathbf{r})$ only depends on $|\mathbf{r}|$, since the effective segments are independent by construction. Since we are interested only in the small kr region, we expand the sine:

$$\left\langle \frac{\sin kr}{kr} \right\rangle_p = 1 - \tfrac{1}{3!}\mathrm{k}^2 \left\langle \mathbf{r}^2 \right\rangle_p + \cdots . \tag{2.14}$$

Define an effective step length $a_{\text{eff}}^2 = \langle \mathbf{r}^2 \rangle_p$, and equation (2.9) becomes:

$$\begin{aligned} P_N(\mathbf{R}) &= \int \frac{d^3k}{(2\pi)^3} e^{i\mathbf{k}\mathbf{R}} \left(1 - \tfrac{a_{\text{eff}}^2}{6}\mathbf{k}^2\right)^{\tilde{N}} \\ &\approx \int \frac{d^3k}{(2\pi)^3} e^{i\mathbf{k}\mathbf{R}} e^{-\frac{1}{6}a_{\text{eff}}^2 \tilde{N}\mathbf{k}^2} \\ &= \left(\frac{3}{2\pi a_{\text{eff}}^2 \tilde{N}}\right)^{3/2} \exp\left(-\frac{3\mathbf{R}^2}{2a_{\text{eff}}^2 \tilde{N}}\right) \end{aligned} \tag{2.15}$$

with the same Gaussian behavior as in (2.10).

2.1.1.3 The Gaussian Chain Model

The preceding discussion shows that the distribution of the end-to-end vector depends on the microscopic details of the model only through the effective bond length. If one is only interested in macroscopic properties of the polymer coil, one is therefore free to choose a model that facilitates analytical manipulations as far as possible.

As in the case of the freely jointed chain, we consider a chain of N independent links, but we now relax the constraint (2.3) of fixed bond length. Instead, we assume that the length of each segment is Gauss distributed:

$$p(\mathbf{r}) = g(\mathbf{r}) \stackrel{\text{def}}{=} \left(\frac{3}{2\pi a^2}\right)^{3/2} \exp\left(-\frac{3}{2}\frac{\mathbf{r}^2}{a^2}\right). \tag{2.16}$$

Note that: $\langle \mathbf{r}^2 \rangle = a^2$. The probability of a configuration Γ_N, (2.2) of such a chain is:

$$\begin{aligned} P[\Gamma_N] &= g(\mathbf{r}_1)g(\mathbf{r}_2)\ldots g(\mathbf{r}_N) \\ &= \left[\frac{3}{2\pi a^2}\right]^{3N/2} \exp\left(-\frac{3}{2}\sum_n \frac{\mathbf{r}_n^2}{a^2}\right). \end{aligned} \tag{2.17}$$

This defines a "Gaussian chain". Notice that a Gaussian chain can be envisioned as $N+1$ beads, connected by N springs of spring constant $\frac{3}{a^2}$ and equilibrium length a (Figure 2.3).

Gaussian chains have the important property that the length of each of their subchains is also Gauss distributed. Let $\mathbf{R}_n$ and $\mathbf{R}_m$ be the positions of the "beads"

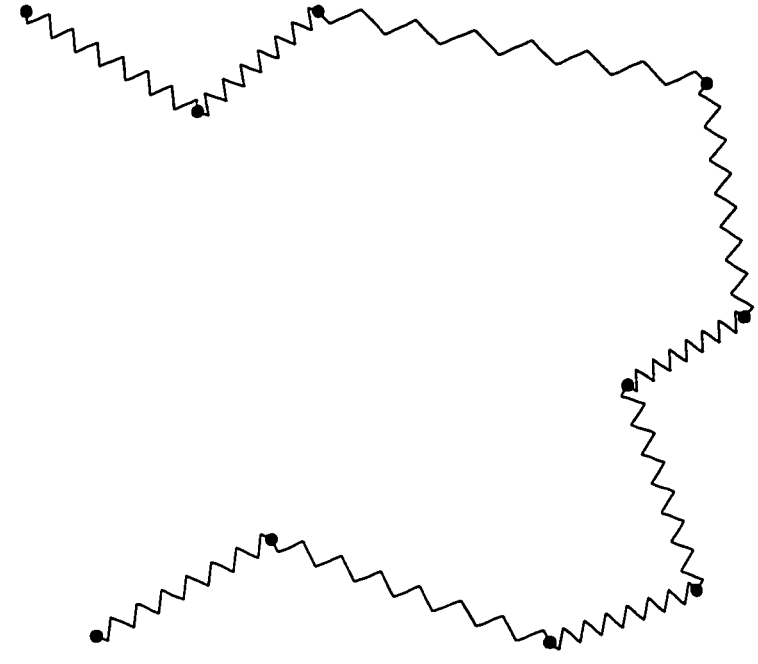

Figure 2.3: Gaussian chain as "beads" connected by "springs".

n and m, respectively, then the probability distribution for the vector $\mathbf{R}_n - \mathbf{R}_m$ is:

$$P_{|n-m|}(\mathbf{R}_n - \mathbf{R}_m) = \left[\frac{3}{2\pi|n-m|a^2}\right]^{3/2} e^{-\frac{3(\mathbf{R}_n-\mathbf{R}_m)^2}{2|n-m|a^2}}. \tag{2.18}$$

Consequentially, the assignment of "beads" is highly arbitrary: to a section of a Gaussian coil with end-to-end vector $\mathbf{R}$, containing N units of length a, we can assign $2N$ units of length $a/\sqrt{2}$ without changing the distribution function for $\mathbf{R}$. If we make the model assumption that we can repeat this process indefinitely, the coil thus obtained is scale invariant.

Let us note that for $n = 0$ and $m = N$, the distribution function of the end-to-end vector $\mathbf{R}$ is:

$$P_N(\mathbf{R}) = \left[2\pi R_0^2/3\right]^{-3/2} e^{-\frac{3}{2}\frac{\mathbf{R}^2}{R_0^2}}. \tag{2.19}$$

From this we obtain the entropy of a Gaussian chain with given radius $\mathbf{R}$:

$$S(\mathbf{R}) = -\frac{3}{2}k_B\left(\frac{\mathbf{R}^2}{R_0^2}\right)^2 + const \tag{2.20}$$

and, using $F = U - TS$, we finally obtain the free energy of a Gaussian chain, and, because of equation (2.15), of *any* ideal chain in three dimensions:

$$\beta F(\mathbf{R}) = \frac{3}{2}\left(\frac{\mathbf{R}}{R_0}\right)^2. \tag{2.21}$$

The Gaussian chain model is readily generalized to a d dimensions. In the general case, one finds $\beta F(\mathbf{R}) = \frac{d}{2}\left(\frac{\mathbf{R}}{R_0}\right)^2$.

One other quantity of interest is the correlation function for segments I and J along the chain. Because of translational invariance the correlation function, *i.e.* the probability that segment J is at $\mathbf{r}$, while I is at the origin, depends only on the spatial distance between the segments:

$$\begin{aligned} G_{IJ}(\mathbf{r}) &= \langle \rho_I(0)\rho_J(\mathbf{r})\rangle \\ &= P_{|I-J|}(\mathbf{r}) \\ &= \exp\left(-\frac{3}{2}\frac{\mathbf{r}^2}{|I-J|a^2}\right), \end{aligned} \tag{2.22}$$

where $\rho_I(\mathbf{r}) = \delta(\mathbf{r}-\mathbf{r}_I)$ is the local segment density. The Fourier Transform of $G_{IJ}(\mathbf{r})$ is:

$$\begin{aligned} S_{IJ}(\mathbf{q}) &= \int d^3r\, e^{-i\mathbf{q}\mathbf{r}} G_{IJ}(\mathbf{r}) \\ &= \exp\left(-\frac{q^2a^2}{6}|I-J|\right). \end{aligned} \tag{2.23}$$

Often one is interested in the correlation between *any* two segments, being separated by $\mathbf{r}$. This leads to the structure factor of an isolated chain:

$$\begin{aligned} S(\mathbf{q}) &= \frac{1}{N}\sum_{I,J} S_{IJ}(\mathbf{q}) \\ &= \frac{1}{N}\int_0^N dn \int_0^N dm \exp\left(-\frac{q^2a^2}{6}|n-m|\right) \end{aligned}$$

(the replacement of the discrete sums by integrals is permissible for $N \gg 1$)

$$= N g_D(x) \qquad \text{where } x = \frac{Nq^2a^2}{6} = \frac{1}{6}q^2R_0^2 \tag{2.24a}$$

and

$$g_D(x) = \frac{2(x + e^{-x} - 1)}{x^2} \tag{2.24b}$$

is the Debye function. It can be approximated by

$$g_D(x) \approx \frac{N}{1 + x^2/2}$$

to within 15% over the entire region of q.

We will study Gaussian chains in more detail in Section 2.2.

2.1.1.4 Real Chains

Up to this point, we considered chains free from interactions except for those due to chain connectivity. For any realistic chain model however, one will have an interaction potential between any two segments like that shown in Figure 2.4, consisting of a short-range repulsion and a (weak) long range attraction. In general, the bare interaction potential is modified by the presence of a medium, *e.g.* a solvent, into which the chain is placed. Since we will mostly be concerned with the interactions between the links themselves, we will not include the effect of the solvent explicitly, and only consider the effective segment-segment potential, with the tacit understanding that it includes the possible interactions with the background.

One approach to include the interaction is to assume that the free energy of the polymer separates: into an ideal part F_{id}, describing an ideal chain, free of interactions, but including the effects of chain connectivity, and an interaction part, F_{int}:

$$F = F_{\text{id}} + F_{\text{int}} \tag{2.25}$$

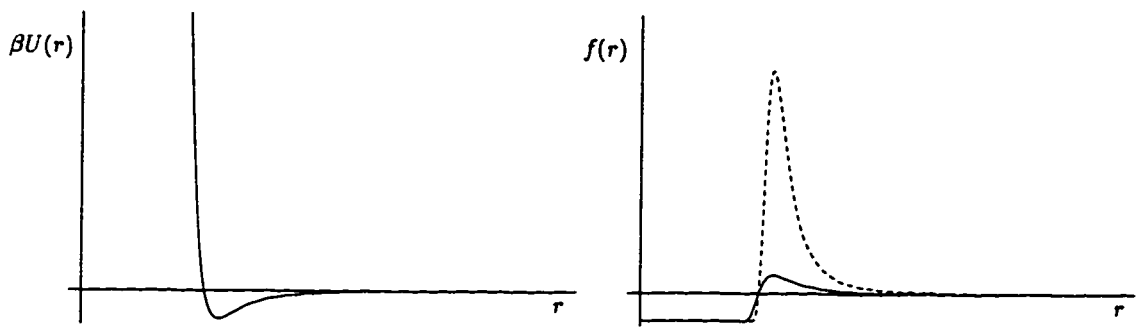

Figure 2.4: Typical dimensionless interaction potential $\beta U(r)$ (left); Mayer function $f(r) = \exp(-\beta U(r)) - 1$ for the potential plotted on the left for two different values of β (right). The dashed curve corresponds to lower temperatures (greater β).

Since we assume that all the effects of the chain connectivity have been included through $F_{\rm id}$, $F_{\rm int}$ need only describe a system of disconnected links, interacting via their pairwise potential. Since the density of links in the volume occupied by the polymer coil is low (being proportional to $N/R_0^3 \sim N^{-1/2}$ for a Gaussian coil), we can assume for $F_{\rm int}$ an expansion in powers of the link density:

$$\beta F_{\rm int} = V\left[B\left(\frac{N}{R^3}\right) + C\left(\frac{N}{R^3}\right)^2 + \cdots\right], \tag{2.26}$$

where $B, C, \ldots$ are the virial coefficients and R is the radius of the coil. They can be found from the interaction potential $U(\mathbf{r})$ [78]. For B we have:

$$B = -\frac{1}{2}\int d^3r\, \exp\left(-\beta U(\mathbf{r})\right) - 1. \tag{2.27}$$

Note that we only consider interaction potentials that fall off fast enough at large distances for the integral in (2.27) to converge. This includes for example attraction between links due to van-der-Waals interactions, but not the Coulomb potential. Chains with charged links (polyampholytes and polyelectrolytes) are a special case, that will not be considered here (c.f. [13] for a recent review). We will come back to the study of interacting chains in general in Section 2.1.2.

For the moment, we will ignore the attractive part of the potential. We then have a chain with no other interactions than those due to chain connectivity, and those arising from the hard-core repulsion. The fact that now the chain cannot intersect itself strongly reduces the number of possible configurations, as compared to the case of ideal chains considered so far. While the configurations of ideal chains correspond to free random walks, the conformations of chains with excluded volume are *self-avoiding* random walks. One expects that the size of a coil that cannot intersect itself will be greater than one that could. In particular, we expect the exponent ν in equation (2.6) to be modified. An extremely simple, though surprisingly effective way to calculate the value of ν for the chain with excluded volume was devised by Flory in 1949 [55]. We present it here for the case of arbitrary dimensionality d. Consider a chain of unknown radius R and internal monomer concentration

$$c \cong \frac{N}{R^d}. \tag{2.28}$$

The free energy due to the internal repulsive hard-core interaction takes the following form:

$$\begin{aligned} \beta F_{\text{int}} &= Nvc \\ &= v\frac{N^2}{R^d}, \end{aligned} \tag{2.29}$$

since there are N segments, each with probability c of colliding with each other. The "excluded-volume parameter" v is essentially the second virial coefficient (c.f. equation (2.27)) and has the dimension of a volume. The chain connectivity is included through equation (2.21):

$$\begin{aligned} \beta F_{\text{id}} &\cong \frac{R^2}{R_0^2} \\ &\cong \frac{R^2}{a^2 N}. \end{aligned} \tag{2.30}$$

The radius R_F of the coil is the one that minimizes

$$\begin{aligned} \beta F &= \beta F_{\text{id}} + \beta F_{\text{int}} \\ &\cong \frac{R^2}{a^2 N} + v\frac{N^2}{R^d}. \end{aligned} \tag{2.31}$$

Omitting numerical factors, we find:

$$R_F^{d+2} \cong v a^2 N^3$$

or

$$R_F \sim N^{\nu} \qquad \text{with} \quad \nu = \frac{3}{d+2} \tag{2.32a}$$

in particular:

$$R_F \sim N^{3/5} \qquad \text{in 3 dimensions.} \tag{2.32b}$$

This result is surprisingly accurate at all dimensions. For $d = 1$ it gives the obviously correct value $\nu = 1$ and for $d = 2$ and $d = 3$ it is within one percent of the best theoretical and experimental results.

Note also that for $d = 4$, Flory's formula yields the ideal chain exponent $\nu = 1/2$. Intuitively, this can be understood by evaluating the repulsive free energy F_{int} at the equilibrium extension R_F. One finds: $F_{\text{int}} \sim N^{2-3d/(2+d)}$. For $d \geq 4$, the exponent becomes negative, so that the internal repulsion scales away as N becomes large. However, the elastic free energy F_{id} is not affected by the dimensionality of space, so we are left with an ideal chain.

Two comments are in order: The Flory calculation as presented above benefits from an almost miraculous cancelation of errors: the repulsion is grossly overstated by neglecting the chain connectivity, and so is the elastic free energy, since it should depend on R/R_F instead on R/R_0. Attempts to systematize the calculation of ν often failed because they improved on one, but not the other of the contributions to equation (2.31). In particular, any attempt to improve on (2.31) based on a mean

field approach failed, since the density of links inside a coil is strongly fluctuating in space, and not well described by an average field.

A perturbation calculation, based on a Mayer cluster expansion has been performed [188]. The effective expansion parameter is the probability for binary collision in the chain, $z \cong vN/R_0^3 \cong BN^{1/2}/a^3$, where B is the second virial coefficient (2.27). Notice that z is small only in the immediate vicinity fo the Θ-temperature, where B vanishes. However, resummation techniques [123], can be applied to obtain an accurate value for the exponent ν even for non-zero B.

Monte Carlo simulations are difficult, since the asymptotic scaling limit is only reached for very large N, and the statistics of the simulation show a strong dependency on the details of the model, in particular for lattice simulations [164, 5]. Off-lattice calculations are also possible, *e.g.* for the freely rotating chain model, but with excluded volume [53, 54].

Renormalization group methods (both real space and ε-expansion), which are clearly appropriate for this system of interacting, strongly fluctuating particles, have also been applied to the excluded volume problem [40, 63]. The most recent results for ν in three dimensions are:

$\nu = 0.588 \pm 0.001$	experiment [204],
$\nu = 0.588 \pm 0.001$	theory [188],
$\nu = 0.581 \pm 0.009$	simulation [53].

2.1.2 Many Chain Systems

Up to this point, we have only considered the statistical mechanics of isolated chains. We now turn to systems of polymers at finite concentration. If the chains are in a medium made up of small molecules (*i.e.* molecules without internal degrees of freedom), we speak of a polymer solution. If the polymers are densely packed, without any solvent present, the system is called a melt.

In the following sections, we will always assume that all chains in the system have the same number of links. Such a system is called "monodisperse". Polymer samples in experiments will always have some distribution of chain lengths. A measure of the width of this distribution is its variance p, defined through:

$$p = \frac{\langle (N - \langle N \rangle)^2 \rangle}{\langle N \rangle^2}.$$

Samples of polydispersity $p < 0.01$ can nowadays be obtained through living cationic polymerization, followed by size-exclusion chromatography [40].

2.1.2.1 Solutions

Polymer solutions are characterized by their polymer concentration as dilute, semidilute and concentrated. In the dilute case, the concentration of polymer coils is so low that on average the polymer coils do not overlap. We smoothly cross over to the semidilute regime at the concentration $c^* \cong \frac{N}{R^3} \sim N^{1-3\nu}$. We see that the overlap concentration can be quite small (corresponding to a polymer volume fraction $\varphi = 0.01 \ldots 0.0001$), no matter if we use the Flory exponent $\nu = 3/5$ or the ideal chain exponent $\nu = 1/2$. In the semidilute regime, we have strongly overlapping coils, although the total polymer concentrations is still low. The semidilute regime is specific to polymer solutions and has no correspondence in solutions of simple molecules. When the polymer concentration approaches 1, we enter the concentrated regime, and finally, when there is no solvent present, the melt state.

Solvents are classified as good, neutral (or "Θ") and poor, depending on their interactions with the polymer segments and independent of the polymer concentration. When the polymer segments on average prefer contacts with the solvent over contacts with their own kind, the solvent is called good. In a good solvent, the chains will swell, compared to the ideal chain size, to avoid unfavorable segment-segment collisions. In the opposite case of a poor solvent, the monomers prefer each other over the solvent and the chains collapse unto themselves and eventually phase separate from

the solvent. The crossover region, where these effects cancel, is called the Θ-region and the solvent is called a neutral or Θ-solvent. In many cases, a rise in temperature is enough to bring about a change in solvent characteristic from poor to good. For simplicity we will assume this henceforth.

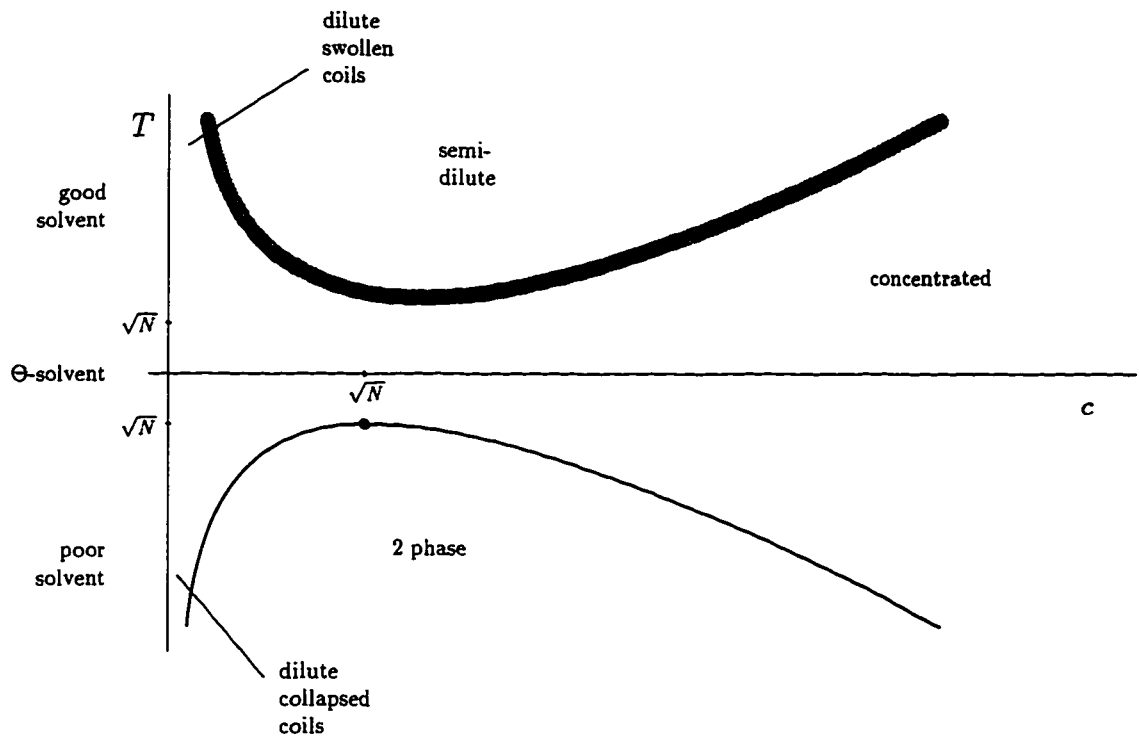

Figure 2.5: Schematic phase diagram for solutions of flexible polymers in temperature T versus polymer concentration c. Note the phase separation in poor solvents and the crossover *region* (indicated by the grey band) into the semidilute regime in good solvents.

The most general phase diagram of polymer solutions is therefore given in terms of the polymer concentration c and temperature (Figure 2.5. It will prove useful to introduce the dimensionless parameter $\tau = \frac{T-\Theta}{\Theta}$, measuring the deviation from the Θ-temperature. A positive τ corresponds to a good, a negative τ to a poor solvent.

This section is organized as follows: First we discuss dilute solutions in good, neutral and poor solvents (left hand side of Figure 2.5), thus concluding the discussion

of Section 2.1.1.4 of isolated, real (*i.e.* interacting) chains. Then we turn to semidilute and concentrated solutions under good solvent conditions (upper half of the right hand side in Figure 2.5). Our main interest will be to find the scaling forms for the crossover concentrations and to develop some semi-intuitive understanding of the behavior of strongly overlapping chains. Finally, we discuss the case of poor solvents (bottom half of Figure 2.5). The most notable effect here is the phase separation of a solution into a polymer-rich and a solvent-rich phase.

Dilute Solutions. As stated above, in a dilute solution the coils are so far separated from each other, that they can be treated as isolated. We therefore will now conclude our discussion of isolated real chains, that we started in Section 2.1.1.4. We assume a free energy of the form:

$$F = F_{\text{id}} + F_{\text{int}}$$

as given in equation (2.25). We have already seen, that F_{id} contains the entropic penalty for stretching the chain. We will generalize slightly and include the effect of compressing a chain. Anticipating a result we will derive in Section 2.1.3.3, we can write the loss of entropy, that a chain suffers when compressed to size R, as $\left(\frac{R_0}{R}\right)^2$, so that the configurational part of the free energy becomes:

$$\beta F_{\text{id}} \cong \left(\frac{R}{R_0}\right)^2 + \left(\frac{R_0}{R}\right)^2, \tag{2.33}$$

where the first and second term are applicable for $R \gg R_0$ and $R \ll R_0$, respectively.

For the interaction term, we make use of the virial expansion (2.26), truncated to the first two terms:

$$\beta F_{\text{int}} = N\left[B\left(\frac{N}{R^3}\right) + C\left(\frac{N}{R^3}\right)^2\right]. \tag{2.34}$$

The third virial coefficient C, describing the effect of simultaneous collisions of three particles is generally positive, while the value of B changes with temperature: for

large values of T, the attractive part of the interaction potential can be neglected and the integral in equation (2.27) is dominated by the repulsive part, so that B is positive, for low temperatures the mutual attraction is significant and B is negative. The temperature at which B vanishes is called the Boyle temperature in the statistical mechanics of simple fluids and defines the Θ-temperature in polymer physics. Close to $T = \Theta$, B will vary linearly with τ:

$$B = v\tau. \tag{2.35}$$

For high T, the value of B approaches a constant, independent of T. One therefore refers to a very good solvent also as an "athermal" solvent.

The total free energy (2.25) with (2.33) and (2.34) has the following form:

$$\beta F(\zeta) \cong \zeta^2 + \zeta^{-2} + N^{1/2}\left(\frac{B(T)}{a^3}\right)\zeta^{-3} + \left(\frac{C}{a^6}\right)\zeta^{-6}, \tag{2.36}$$

where we have introduced the dimensionless swelling parameter $\zeta = \left(\frac{R}{R_0}\right)$. The equilibrium size of the chain, depending on T (through B) is given by the minimum of $\beta F(\zeta)$ with respect to ζ:

$$\zeta^5 - \zeta \doteq \tfrac{3}{2}N^{1/2}\frac{B}{a^3} + 3\frac{C}{a^6}\zeta^{-3}. \tag{2.37}$$

In the case of repulsive interactions ($B > 0$), the chain swells ($\zeta \gg 1$) and the second terms on both sides of equation (2.37) can be neglected. We obtain:

$$\zeta = \left(N^{1/2}\frac{B}{a^3}\right)^{1/5}$$

or

$$R \sim \tau^{1/5}N^{3/5}. \tag{2.38}$$

Notice that we recover the Flory exponent $\nu = 3/5$, correct for a strongly swollen coil.

In the opposite case of strong compression ($\zeta \ll 1$), both terms on the left hand side of (2.37) can be neglected and we obtain:

$$\zeta^{-3} \cong N^{1/2}\frac{a^3 B}{C}$$

or

$$R \sim (-\tau)^{-1/3} N^{1/3}. \tag{2.39}$$

In other words, a chain with partially attractive links ($B < 0$) collapses into a dense globule. Notice that the density of links in such a globule is of order unity, since $c = N/\mathbf{R}^3 \sim 1$, according to (2.39). In particular, the density inside the globule is independent of N. This is to be compared with the extremely low density inside a swollen coil $c \sim N^{-4/5}$ or inside a Gaussian coil $c \sim N^{-1/2}$. Consequentially, inside a globule the monomer density does not fluctuate strongly; instead, the inside of a globule can be treated as a polymer melt (c.f. Section 2.1.2.2).

Finally, the chains behave ideally (*i.e.* $\zeta \approx 1$) if

$$B \cong -N^{-1/2}\frac{C}{a^3}$$

or

$$|\tau| \sim N^{-1/2}. \tag{2.40}$$

In a small, but finite region around the Θ-point, the chains behave as if they were Gaussian. This is in contrast to gases or solutions at the Boyle point, which, at finite concentration, do not behave according to the ideal gas law. The reason is that in a gas or solution, triple and higher order interactions are appreciable, while inside a polymer coil the probability for the occurrence of a simultaneous collision of three segments is vanishingly small: the probability for a collision of p segments is proportional to Nc^{p-1}, where c is the density of links in a Gaussian coil: $c \cong N/R_0^3 \sim N^{-1/2}$. In

other words, we find the collision probability to be proportional to $N^{(3-p)/2}$, *i.e.* of order $N^{1/2}$ for binary, but only of order 1 for ternary interactions.

So far, we considered the interactions inside an isolated coil. If two coils come close enough to overlap, so that a fraction f of the monomers of one coil penetrates into the other, we have from equation (2.34) a repulsive interaction energy

$$F_{\text{int}} = fN \cdot B\left(\frac{N}{R^3}\right) \sim N^{2-3\nu},$$

which is very large for large N. Therefore, coils in a dilute solution in good or neutral solvent, act as hard, impenetrable spheres.

Semidilute Solutions in Good Solvents. We now turn to our discussion of semidilute solutions in good solvents. In a semidilute solution, the coils overlap strongly, but the total solvent concentration is still high. The onset of this regime is the monomer concentration c^*, when separate coils first come into contact. Obviously:

$$\begin{aligned} c^* &\cong \frac{N}{R_F^3} \\ &\sim N^{-4/5} \end{aligned} \tag{2.41}$$

with $R_F = aN^\nu$ being the Flory radius and $\nu = 3/5$ for good solvents. Note that this overlap concentration can be very small. For a typical value of $N = 10^4$, we expect the volume fraction $\varphi = a^3 c$ at the overlap threshold to be $\varphi^* \approx 10^{-3}$.

Since the chains overlap, they form a transient network of mesh size ξ, Figure 2.6. We can estimate the scaling behavior of the mesh size by noting that:

1. at $c = c^* : \xi \cong R_F$

2. for $c \gg c^*$, ξ depends only on c, but not on N, since the mesh size is much smaller than the coil size.

We can therefore assume a scaling form:

$$\xi \cong R_F \left(\frac{c}{c^*}\right)^m \quad \text{with } m = -3/4 \tag{2.42}$$

the exponent being fixed by requirement 2. We see that the mesh size decreases rapidly, as the polymer concentration is raised.

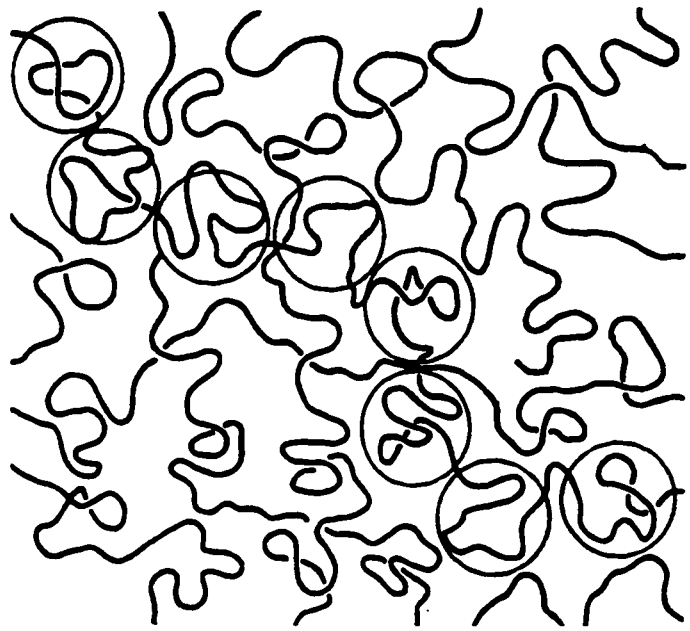

Figure 2.6: Schematic drawing of the transient network formed in a semidilute solution. For one particular chain the blobs of size ξ are shown. After [109].

If we consider a single chain in a semidilute solution, we can regard it as a string of "blobs" of size ξ. Inside each blob, the chain does not interact with other chains, only with itself. Therefore, the number of monomers per blob g, is given by the law of swollen coils:

$$\xi = a g^{\nu} \tag{2.43}$$

or

$$g = \left(\frac{\xi}{a}\right)^{5/3} \tag{2.44}$$

with equation (2.42) we see that:

$$c \cong \frac{g}{\xi^3}, \tag{2.45}$$

i.e. the blobs are densely packed. If we take the blobs as basic unit, we see that the semidilute solution is a dense melt of chains consisting of N/g links, each link of size ξ. Using Flory's Theorem, that the excluded volume interaction is screened out in a melt (c.f. Section 2.1.2.2) so that chains behave ideally, we can evaluate the size of the chain of blobs:

$$\begin{aligned} R^2 &= \frac{N}{g}\xi^2 \\ &\cong N a^2 \varphi^{-1/4}. \end{aligned} \tag{2.46}$$

We see that the chains shrink as the concentration increases, because the excluded volume interaction is increasingly screened.

Finally, we evaluate the scaling behavior of the cross over region from the semidilute to the dilute and the concentrated regime, respectively. We pass into the dilute regime at the overlap concentration $c^* \cong N/R_F^3$. Using equation (2.38) we find:

$$\tau \sim c^{5/3} \quad \text{dilute - semidilute.} \tag{2.47}$$

We can estimate the onset of the concentrated regime by requiring that the size of the chain in the semidilute solution (2.46) scales like the size of the chain in the melt: $R^2 \sim N$. Using equation (2.38) again, we find:

$$\tau \sim c \quad \text{semidilute - concentrated.} \tag{2.48}$$

Phase Separation in Poor Solvents. In poor solvents, the polymer chains have a tendency to phase separate from the solvent (to precipitate) to reduce the number of unfavorable contacts with the solvent.

To derive an expression for the free energy of the system which incorporates this behavior, we assume a lattice with spacing a, such that each lattice site is occupied either by a solvent molecule or a chain monomer. The volume fraction of monomer is then $\varphi = ca^3$. The entropy per site (in a mean field way) is then:

$$S(\varphi) = \frac{\varphi}{N}\log\frac{\varphi}{N} + (1-\varphi)\log(1-\varphi) + S_{\text{internal}}. \tag{2.49}$$

The first two terms are the translational entropy of the chains and the solvent molecules, respectively, while the last term represents the entropy associated with the internal degrees of freedom of the chains. Since every N monomers are linked together, they cannot choose their positions independently: only an entire chain counts as an independent particle. The density of independent particles, and, consequentially, the translational entropy of polymers, is therefore reduced by a factor $1/N$.

The interaction energy per site U, has three contributions:

$$U = \epsilon_{pp}\varphi^2 + 2\epsilon_{sp}\varphi(1-\varphi) + \epsilon_{ss}(1-\varphi)^2, \tag{2.50}$$

measuring the contribution from monomer-monomer, monomer-solvent and solvent-solvent contacts. The total free energy per site is the $F = U - TS$, with U and S given by (2.50) and (2.49), respectively. However, to study phase separation, etc., we are only interested in the part of F that is different in different phases. This is the free energy of mixing (per site), defined by:

$$\begin{aligned}\beta F_{\text{mix}} &= \beta\left[F(\varphi) - \varphi F(1) - (1-\varphi)F(0)\right] \\ &= \frac{\varphi}{N}\log\varphi + (1-\varphi)\log(1-\varphi) + \chi\varphi(1-\varphi),\end{aligned} \tag{2.51}$$

with the dimensionless Flory-Huggins parameter χ, measuring the strength of the interaction:

$$\chi = \epsilon/k_BT = \tfrac{1}{2}\left[\epsilon_{pp} + \epsilon_{ss} + \epsilon_{sp}\right]/k_BT. \tag{2.52}$$

Notice that all terms independent of φ, and terms linear in φ have dropped out, including the terms depending on the internal degrees of freedom of the chains.

The Flory-Huggins parameter is generally positive. If the only interactions present are van-der-Waals forces, the interaction energy between any two particles is proportional to the product of their respective polarizibilities: $\epsilon_{\kappa\kappa'} \sim \alpha_\kappa\alpha_{\kappa'}$ and $\chi \sim (\alpha_\kappa - \alpha_{\kappa'})^2$. This result shows that, quite generally, unlike particles have a tendency to repel each other.

As written down so far, χ varies inversely proportionally with temperature. However, besides van-der-Waals interactions there are other forces present, *e.g.* steric hindrances. If, for example, monomer and solvent molecules are of different size, a solvent particle will not fit well into a space vacated by a monomer. This leads to an additional entropic repulsion (so-called "non-local entropy of mixing"). Often, the form:

$$\chi = \frac{A}{T} + B$$

is used to fit experimental data, with B arising from an entropic contribution (c.f. Figure 3.1).

For low polymer concentration, we can replace the second term in equation (2.51) by its virial expansion:

$$\beta F_{\text{mix}} = \frac{\varphi}{N} \log \varphi + \left(\frac{1}{2} - \chi \right) \varphi^2 + \frac{1}{6} \varphi^3 + \cdots . \tag{2.53}$$

(A linear term dropped out, as before.) We see that χ is related to the second virial coefficient:

$$\begin{aligned} B\tau &= 1/2 - \chi \\ &= \frac{T - 2\epsilon}{T}, \end{aligned}$$

in particular, the Θ-point, where the second virial coefficient vanishes, corresponds to $\chi = 1/2$.

If the effective repulsion between solvent and polymer particles exceeds a critical value, the system can lower its free energy by splitting up into two different phases. The phase boundaries can be found by equating the exchange chemical potential: $\mu = \frac{\partial V F_{\text{mix}}}{\partial N} = a^3 \frac{\partial F_{\text{mix}}}{\partial \varphi}$ and the pressure: $-p = \frac{\partial V F_{\text{mix}}}{\partial V} = F_{\text{mix}}$ of both phases. The polymer concentrations in the coexisting phases are fully specified by the two conditions of phase equilibrium. Notice that in the present case of constant particle density equating the pressure amounts to equating the free energy density.

The critical point is the extremum of the spinodal, defined by:

$$\frac{\partial^2 F}{\partial \varphi^2} = \frac{1}{N\varphi} + \frac{1}{1-\varphi} \doteq 0.$$

We find the position of the critical point in mean field theory to be:

$$\varphi_C = \frac{1}{1+\sqrt{N}} \approx N^{-1/2} \tag{2.54a}$$

$$\chi_C - \chi_\Theta = \frac{1}{\sqrt{N}} + \frac{1}{2N} \approx N^{-1/2}. \tag{2.54b}$$

Phase separation occurs close to the Θ-temperature, and for very low polymer concentration. (Compare equation (2.54), applicable for poor solvent conditions, with equations (2.41) and (2.40) for the crossover from a dilute solution in neutral solvent to a semidilute solution in good solvent.) As seen before, the chains in the solvent phase assume collapsed globule configurations. Intuitively, the reason for the low miscibility of polymers can be understood as follows: for each k_BT in translational entropy that we gain by bringing a chain from the polymer rich to the solvent phase, we pay on the order of Nk_BT in enthalpy, due to the increased number of polymer-solvent contacts. This is in contrast to solutions of simple molecules, where for each k_BT of entropy gain, we only pay on the order of one k_BT in enthalpy.

2.1.2.2 Melts and Blends

A liquid polymer system without any solvent present is called a melt, if there is only kind of polymer present, otherwise a blend. Such dense polymer systems have two remarkable properties. Firstly, chains in a melt behave as if they were ideal, *i.e.* the excluded volume interaction is screened by the presence of the other chains. This is the contents of the so-called "Flory Theorem". Secondly, critical fluctuations in blends are strongly suppressed (by a negative power or N, the exponent depending on the kind of critical point), making mean field theory quantitatively correct for blends, even very close to a critical point.

A polymer melt is characterized by small overall density fluctuations. At length scales greater than the *monomer* size, the local density profile is nearly constant throughout the sample. An experimental consequence is the necessity to label some of the chains or some part of every chain, in order to obtain sufficient intensity in elastic scattering experiments at length scales comparable to the chain size (*i.e.* for $qa \ll 1$). The perturbation caused by heavy atoms inserted into the chain as markers for X-ray scattering are often prohibitively strong in a homogeneous polymer melt, so one usually resorts to deuterium-labeling, where some of the hydrogen atoms are replaced by deuterium. Since hydrogen and deuterium nuclei have very different scattering lengths for low energy neutrons (of energy $E = 0.1 \ldots 0.001$ eV, corresponding to wavelength of 1–10 Å), but are almost identical in their chemical properties, neutron scattering is the preferred experimental technique to study the structure and correlation effects in polymer systems.

The homogeneity of the monomer density furnishes a first, trivial proof of the Flory Theorem. As we have seen in equation (2.29), the excluded volume interaction is strongest where the monomer density is highest. In a weakly fluctuating polymer melt, where the monomer density is constant throughout, there is therefore no net force tending to swell each chain [55].

Another way of describing the same effect considers the local environment of a given chain link. If the chain were isolated, the probability for the test link to collide with another chain link would be spatially varying and greater towards the center of mass of the coil. In the melt case, the test link is densely surrounded by other links. Since all links are identical, it has no way of distinguishing which of the surrounding links belong to different chains and which do not. Consequentially, it experiences no net force in any direction. A more formal proof has been given by Edwards [45].

Polymer blends combine the properties of melts (see above) with the ones of poor solvents (c.f. Section 2.1.2.1). The entropy of mixing is reduced by a factor of $1/N$; equivalently, transferring one chain of monomers of type A to a phase consisting

mostly of chains of type B is penalized by an enthalpy cost on the order of χN. The appropriate generalization of the Flory-Huggins expression for the free energy density to the case of a binary blend of chains of type A with index of polymerization N_A and chains of type B with index of polymerization N_B is:

$$\beta F = \frac{\varphi_A}{N_A} \log \varphi_A + \frac{\varphi_B}{N_B} \log \varphi_B + \chi \varphi_A \varphi_B. \tag{2.55}$$

Making use of the incompressibility constraint $\varphi_A + \varphi_B = 1$ and multiplying through by $N = N_A$, we obtain:

$$\beta N F = \varphi \log \varphi + \alpha(1-\varphi) \log(1-\varphi) + \chi N \varphi (1-\varphi), \tag{2.56}$$

with $\varphi = \varphi_A$ and $\alpha = N_A/N_B$. We see that the effective interaction parameter is χN, not χ. Proceeding as in Section 2.1.2.1, we can find the maximum value of χN, for which the chains are miscible. It corresponds to the critical point:

$$\chi_C N = \frac{1}{2}(1+\sqrt{\alpha})^2, \tag{2.57a}$$

$$\varphi_C = \frac{1}{1+\sqrt{\alpha}}, \tag{2.57b}$$

where φ_C is the critical concentration. An important reference point is the critical point of a symmetric system ($N_A = N_B$, $\alpha = 1$):

$$\chi_C N = 2,$$

$$\varphi_C = 0.5.$$

If $N_B = 1$, equations (2.55) reduces to the result for a polymer solution in poor solvent. For $N_A \geq N_B$, φ is small and we can expand equation (2.55) in a virial series:

$$\beta F = \frac{\varphi}{N_A} \log \varphi + \left(\frac{1}{2N_B} - \chi \right) \varphi^2 + \cdots \tag{2.59}$$

Consider now a blend of two polymers of identical monomers (so that χ vanishes), but of different length. For $N_A = N_B$, we recover the melt condition, and all chains

behave ideally. For $N_B \to 1$ however, we expect the A-chains to swell, since the single monomers provide a good (in fact athermal) solvent. The length N_B at which the system crosses over between these two regimes is found from equation (2.37): we see that the product $N_A^{1/2}B$, where B is the second virial coefficient, has to be of order unity or less for the excluded volume interaction to become negligible. In the present case, $B = 1/2N_B$, so that the crossover occurs at:

$$N_A \cong N_B^2. \tag{2.60}$$

For $N_B < \sqrt{N_A}$ the longer chains swell, for $N_B > \sqrt{N_A}$, all chains are ideal [203].

In simple fluids, a mean field description is imvalid close to a critical point, because large scale density fluctuations become important. For melts of long polymer chains, the critical region is small, becoming narrower as the chains are made longer.

We will now estimate the size of the critical region with the help of a Ginzburg criterion [32, 106]. According to this, mean field theory fails to be valid when the fluctuations $\Delta\varphi^2$ of the order parameter, averaged over one "correlation volume" ξ^3 are greater than the magnitude of the square of the order parameter. The appropriate order parameter for the demixing transition is the concentration difference between the two coexisting phases: $\delta\varphi = \varphi_1 - \varphi_2$.

Close to the critical point the compositions of the coexisting phases are given by $\varphi_{1,2} = \varphi_C \pm \delta\varphi$ (from a Landau expansion of (2.55) around φ_C) and we can obtain $\delta\varphi$ by equating the chemical potentials: $\frac{\partial F}{\partial\varphi}|_{\varphi_C+\delta\varphi} \doteq \frac{\partial F}{\partial\varphi}|_{\varphi_C-\delta\varphi}$. Using (2.57), noting that (2.57a) is equivalent to $T_C \cong N_A/(1+\sqrt{\alpha})^2)$, one finds:

$$\delta\varphi^2 = \frac{\Delta T}{T_C}\frac{\sqrt{\alpha}}{(1+\sqrt{\alpha})^2}, \tag{2.61}$$

where $\Delta T = T_C - T$.

Now we consider the fluctuations. Let $g_{AA}(\mathbf{r}) = \left\langle \varphi_A(0)\varphi_A(\mathbf{r}) - \langle\varphi_A\rangle^2 \right\rangle$ be the A-monomer correlation function, and $S_{AA}(\mathbf{q})$ its Fourier transform. Then the mean value of the fluctuations is: $\langle\Delta\varphi^2\rangle = S_{AA}(0)/\xi^3$ (Fluctuation-Correlation Theorem,

[19]). For a pure melt of Gaussian chains we already know the form of $S^0_{AA}(\mathbf{q})$: it is proportional to the Debye function $\varphi_A N_A g_D\,(q^2a^2N_A/6)$ (2.24), where the factor φ_A of the A-monomer density gives the probability of encountering an A-monomer in the blend. The interactions modify the bare correlation functions, which can be calculated in linear response theory [31]. According to this, the perturbation $\delta\varphi_A(\mathbf{r})$, due to a weak perturbing external field $U_A(\mathbf{r}')$ is:

$$\delta\varphi_A(\mathbf{r}) = -\beta \int d^3r\, G_{AA}(\mathbf{r}-\mathbf{r}')U_A(\mathbf{r}') \tag{2.62}$$

or in Fourier Space:

$$\delta\varphi_A(\mathbf{q}) = -\beta S^0_{AA}(\mathbf{q})U_A(\mathbf{q}). \tag{2.63}$$

The presence of the B-monomers, and the overall incompressibility constraint $\delta\varphi_A(\mathbf{r})+\delta\varphi_B(\mathbf{r}) = 0$ contribute two further fields acting on the A-chains (and similarly for the B-chains):

$$-\delta\varphi_A = \beta S^0_{AA}\left[U_A + V + \chi\delta\varphi_B\right], \tag{2.64a}$$

$$-\delta\varphi_B = \beta S^0_{BB}\left[U_B + V + \chi\delta\varphi_A\right]. \tag{2.64b}$$

Using the incompressibility constraint to eliminate V, we find:

$$-\delta\varphi_A = \beta\left[\frac{1}{S^0_{AA}} + \frac{1}{S^0_{BB}} - 2\chi\right]^{-1} U_A - \beta\left[\frac{1}{S^0_{AA}} + \frac{1}{S^0_{BB}} - 2\chi\right]^{-1} U_B,$$

where the coefficients of U_A and U_B respectively are the response functions S_{AA} and S_{AB} for the interacting system. Expanding the Debye function for small $\mathbf{q}$ (since close to T_C the correlation length is large), we find:

$$S_{AA}(\mathbf{q}) = \left[\frac{(1+\sqrt{\alpha})^2}{\sqrt{\alpha}}q^2 + \frac{\Delta T}{T_C}\frac{(1+\sqrt{\alpha})^2}{N_A}\right]^{-1}.$$

If we assume an Örnstein-Zernicke form for the correlation function $S(q) \sim (q^2 + 1/\xi^2)^{-1}$, we find:

$$S_{AA}(0) = \frac{T_C}{\Delta T}\frac{N_A}{(1+\sqrt{\alpha})^2} \qquad \xi = \left(\frac{T_C}{\Delta T}\frac{N_A}{\sqrt{\alpha}}\right)^{1/2}. \tag{2.65}$$

Finally,

$$\langle \Delta\varphi^2 \rangle = \frac{S_{AA}(0)}{\xi^3} = \left(\frac{\Delta T}{T_C}\right)^{1/2} \frac{\sqrt{\alpha}^{3/2}}{\sqrt{N_A}(1+\sqrt{\alpha})^2}, \tag{2.66}$$

and the critical region, where mean field theory fails, is now given by:

$$\frac{\langle \Delta\varphi^2 \rangle}{\delta\varphi^2} > 1,$$

i.e.

$$\frac{\Delta T}{T_C} < \frac{\sqrt{\alpha}}{N_A} = \frac{1}{\sqrt{N_A N_B}}. \tag{2.67}$$

We will now compare the size of the critical region ΔT with the size of the Θ-region $(\Theta - T)$, where the chains are ideal. If $\Delta T \gg \Theta - T$, fluctuations are important and mean field theory fails. Assume $\alpha > 1$. From equation (2.59) we find $\chi_\Theta \sim 1/\Theta = 1/2N_B$ and $\Theta - T_C = \Theta \frac{\sqrt{\alpha}}{(1+\sqrt{\alpha})^2}$ and finally:

$$\frac{\Delta T}{\Theta - T_C} = \frac{T_C}{\Theta} \frac{(1+\sqrt{\alpha})^2}{N_A} \approx \frac{\alpha}{N_A} = \frac{1}{N_B}. \tag{2.68}$$

The size of the critical region is small and mean field theory is valid if the length of the *shorter* of the chains is still much greater than one. In the case that the length of the shorter one approaches one (becoming more "solvent"-like), $\frac{\Delta T}{\Theta - T_C} \to 1$ and the size of the critical region is large.

2.1.3 Constrained Chains

So far, we only considered chains which were unconstrained, except for possible interactions with themselves of with each other. However, many technologically and theoretically interesting situations involve polymers that are under some sort of external constraint. We discuss three particularly important examples: chains elongated by an external force; chains with one end permanently attached to a wall (this will turn out to be a special case of the stretched chain problem); and polymers which are compressed from their equilibrium configuration.

Besides the references listed at the beginning of the chapter, a remarkably comprehensive reference for the present section is [52]. Useful are also [72, 73].

2.1.3.1 Stretched Chains

Imagine an ideal chain stretched by applying weak forces $\mathbf{f}$ and $-\mathbf{f}$ at both ends. At equilibrium, these forces are counterbalanced by the elastic response of the chain:

$$\begin{aligned} f &= \frac{\partial F}{\partial R} \\ &= 3k_BT\frac{R}{R_0^2} = 3k_BT\frac{R}{La}, \end{aligned} \tag{2.69}$$

where F is the free energy of a Gaussian chain (2.21), so that the extension of the chain is:

$$R_{\rm el} = \frac{1}{3}\beta f R_0^2. \tag{2.70}$$

Note that this linear response of the chain (Hooke's Law) is only valid as long as $R_{\rm el} \ll L$, *i.e.* if $af \ll k_BT$: the chain is far from a fully extended conformation. The proportionality of the elongation to temperature reflects the entropic origin of the elastic response.

Consider now the same forces applied to a real chain. The expected elongation R, compared to the unperturbed radius R_F can only depend on the unperturbed size, the force f and temperature. We form the dimensionless variable R_F/ξ, where the length ξ is defined through: $\xi f = k_BT$. So:

$$\frac{R}{R_F} \cong \varphi\left(\frac{R_F}{\xi}\right) = \varphi(\beta f R_F). \tag{2.71}$$

We try to find the asymptotic behavior of φ. In the limit of weak forces, $\beta f R_F \ll 1$, we expect a linear response to f: $\varphi(x \to 0) \sim x$, or:

$$R \cong R_F^2 \beta f \qquad \text{for } fR_F \ll k_BT. \tag{2.72}$$

In the opposite case of large extension, the chain breaks up into a stretched chain of blobs, inside of which the chain is essentially unperturbed by the external force. In order to achieve this, the blob size ξ has to be chosen such that the characteristic energy ξf per blob is less than the thermal energy. The number of links g per blob is then given by requiring $\beta f \xi = \beta f a g^{\nu}$ to be of order unity: $g = (\beta f a)^{-1/\nu}$, where ν is the Flory exponent $\nu = 3/5$. Since the chain as a whole is an extended chain of N/g blobs, we find in the limit of strong forces:

$$\begin{aligned} R &\cong \xi \frac{N}{g} \\ &\cong N a (\beta f a)^{2/3} \qquad \text{for } f a \ll k_B T. \end{aligned} \tag{2.73}$$

A real chain has an elastic response which is linear at small extensions, then smoothly crosses over to a nonlinear behavior. Again, these considerations are only valid when $\frac{R}{R_F} \ll 1$, *i.e.* the chain is not fully extended.

For the freely jointed chain model, the problem is equivalent to a noninteracting Heisenberg magnet in an external field and can thus be solved exactly. Consider the change in energy when the size of the chain changes by $\Delta \mathbf{R}$, due to the applied forces:

$$\begin{aligned} \Delta E &= \Delta \mathbf{R} \cdot \mathbf{f} \\ &= \sum_i^N \Delta \mathbf{r}_i \cdot \mathbf{f} \\ &= a|f| \sum_i^N \cos\theta_i, \end{aligned} \tag{2.74}$$

where $\Delta \mathbf{r}_i$ is the change in each link vector. Note that the length of each link is fixed, so $\mathbf{f}$ acts like an orienting field on each segment of the chain. The angles θ_i measure the deviation of each link from the direction of $\mathbf{f}$. The partition function

can be calculated exactly in this case:

$$Z = \int \prod_i^N d\phi_i \, \sin\theta_i \, d\theta_i \, \exp\left(-\beta a f \sum_i^N \cos\theta_i\right)$$
$$= 4\pi \left[\frac{\sinh \beta h}{\beta h}\right]^N \qquad \text{with } h = af. \tag{2.75}$$

The mean radius $R(f)$ is now the response with respect to the applied force:

$$R = k_B T \frac{\partial}{\partial f} \log Z$$
$$= Na \left[\coth \beta h - \frac{1}{\beta h}\right]$$
$$\approx Na \frac{af}{3k_B T} = \frac{R_0^2 f}{3k_B T} \qquad \text{for } \beta h \ll 1, \tag{2.76}$$

in agreement with the result (2.70), obtained from the Gaussian free energy.

2.1.3.2 Brushes and Grafts

One conceptually and technologically very important example involving constrained chains consists of chains permanently attached with one end to a surface, thus forming a "polymer brush" (c.f. Figure 2.7). Note that the grafting surface need not be a hard wall, but may also be an internal interface between two immiscible solvent phases. An amphiphilic polymer, consisting of two chemically different blocks, each preferring one of the two solvents, will straddle the interface so as to maximize the number of favorable monomer-solvent contacts. Each block of the copolymer then extends into its preferred solvent, thus forming a brush on the interface (c.f. Figure 2.7). Note that the interface does not need to be flat (Figure 1.4).

For simplicity, we will consider only brushes in contact with a Θ-solvent, such that $R_0 \cong aN^{1/2}$ for the unconstrained chain. Despite this, the chains in the brush may be strongly extended, due to the repulsion by neighboring chains. A simple estimate for the brush height h can be found from the following free energy per chain:

$$\beta F \cong \frac{h^2}{2R_0^2} + vN\varphi, \tag{2.77}$$

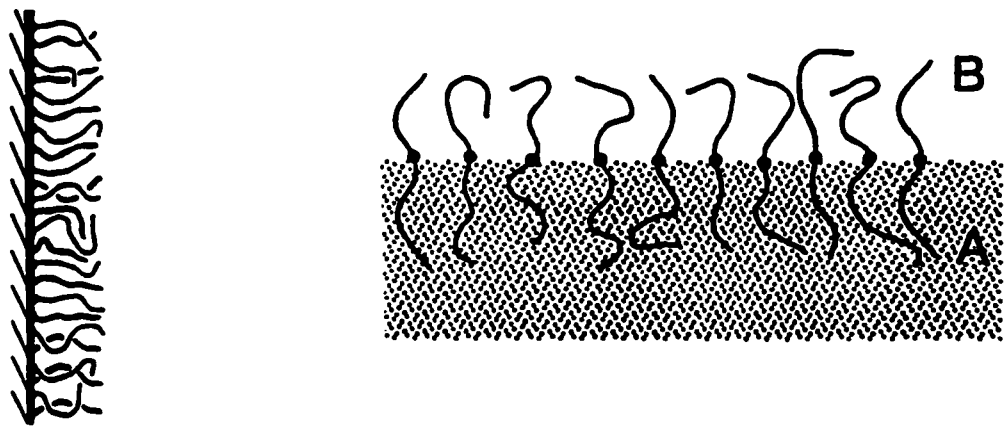

Figure 2.7: Brush formed by polymers grafted to a hard wall (left); and by diblocks straddling an interface between coexisting phases (right).

valid when the grafting density σ exceeds the overlap threshold $\sigma^* \cong 1/R_0^2 = 1/(a^2N)$. The first term is the the familiar stretching entropy in one dimension (c.f. equation (2.21)), the second term gives the interaction of the N monomers of the test chain with the mean field of the other chains. Here, v is the excluded volume parameter, corresponding to the volume occupied by one monomer, and $\varphi = \frac{N\sigma}{h}$ is the assumed constant monomer density inside the brush. Minimizing equation (2.77) with respect to h, we find:

$$h \sim N\sigma^{1/3}. \tag{2.78}$$

We see that h is proportional to N, *i.e.* the chains in a brush are very strongly stretched, and that the height of the brush increases with σ, the grafting density.

However, it is not correct to assume that all chains in the brush are evenly stretched. This configuration, which leads to a step-function density profile of the brush (the so-called Alexander-de Gennes model), was later shown to be unstable. In the following, we will discuss the "parabolic brush" [172, 175], a simple self-consistent mean field treatment, that qualitatively agrees with experiments and more refined self-consistent field calculations.

We consider a free energy per chain similar to the one in equation (2.77), but now we allow for non-uniform, spatially varying extension of the chain:

$$\beta F = \int dt \left(\frac{\partial \mathbf{r}}{\partial t}\right)^2 + U\left[\mathbf{r}(t)\right]. \tag{2.79}$$

We have replaced the discrete sum over segments by the continuous variable t. The potential $U = v\varphi$, which has to be found self-consistently, is proportional to the local monomer density and a functional of the chain configuration $\mathbf{r}(t)$.

Written in this form, the free energy per chain resembles the classical action of a particle moving in a potential, with "time" corresponding to the monomer index along the chain and the chain configuration $\mathbf{r}(t)$ being the "trajectory" of the particle.

We already know from the the simple Alexander-de Gennes model, that the chains are very strongly stretched (2.78). In this regime, the number of configurations available to the chains is strongly reduced, in other words, the chain fluctuates weakly about the most probable path. The latter is the one that minimizes "the action" (2.79). Minimization with respect to $\mathbf{r}(t)$ leads to the Euler-Lagrange equation:

$$\frac{\partial^2 \mathbf{r}}{\partial t^2} = -\nabla U \qquad\qquad U(\mathbf{r}) = -v\varphi(\mathbf{r}) \tag{2.80}$$

subject to the boundary conditions:

$$\mathbf{r}(t = N) = 0,$$
$$\left.\frac{\partial \mathbf{r}}{\partial t}\right|_{t=0} = 0.$$

The first of the boundary conditions is the requirement that the chains are anchored to the wall, while the second assumes that no tension is applied to the free end. This assumption is obviously correct for the free end of an isolated chain; in a dense brush however, it can be shown that the surrounding chains exert a net force on the last segment [190]. This force vanishes when the brush height becomes much larger than R_0. In the language of classical mechanics, the particle starts at rest at time $t = 0$. Note that we have not specified where in the brush the free end is located; in general,

free ends will be found throughout the brush. The additional entropy associated with this distribution of end points is ignored in (2.79).

We assume that the density profile varies only in the direction normal to the wall, so that we can replace $\mathbf{r}$ by z.

Now we make use of the fixed length of the chains: each chain has to terminate at the wall after exactly N steps, *i.e.* the particle starting at rest at any position $\mathbf{r}(0)$ has to reach $\mathbf{r} = 0$ at time $t = N$. The unique potential that fulfills this equal time constraint is the harmonic oscillator potential, so that we can write in full generality:

$$\begin{aligned} -U(z) &= v\varphi(z) \\ &= A - Bz^2. \end{aligned} \tag{2.81}$$

The constant B can be found from the equal time constraint: N corresponds to one quarter of a period of the harmonic oscillator, so $\sqrt{2B} = \omega = \frac{\pi/2}{N}$, *i.e.*

$$B = \frac{\pi^2}{8N^2}. \tag{2.82}$$

Finally, the constant A is found from the requirement that the total number of monomers in the brush is equal to N:

$$\begin{aligned} N\sigma &= \int_0^h dz\, \varphi(z) \\ &= Ah - \frac{B}{3}z^3, \end{aligned} \tag{2.83}$$

which leads to:

$$A = \frac{N\sigma}{h} + \frac{B}{3}h^2. \tag{2.84}$$

The last adjustable quantity is the brush height h. Since the density φ cannot be negative, h is fixed at that point, where $\varphi = (A - Bz^2)/v$ with (2.84) and (2.82) first becomes negative. This leads to an equilibrium brush height:

$$h = \left(\frac{12}{\pi^2}\right)^{1/3} (\sigma v)^{1/3} N, \tag{2.85}$$

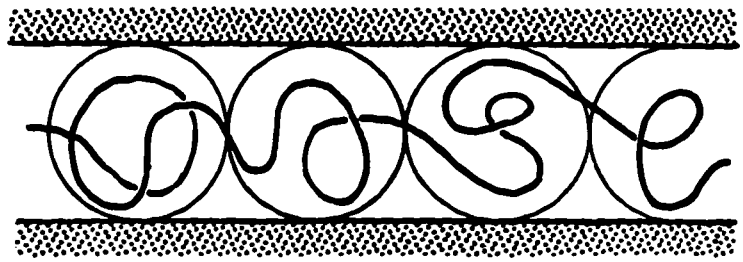

Figure 2.8: A chain trapped in a tube of diameter D. Several of the confinement blobs of diameter D are shown. After [109]).

and to a density profile:

$$\varphi(z) = \left(\frac{B}{v}\right)\left(h^2 - z^2\right). \tag{2.86}$$

Notice that the brush profile goes to zero continuously at $z = h$ (in contrast to the Alexander-de Gennes brush), but that $z = h$ also marks a sharp cutoff of the density profile. This last feature of the parabolic brush is slightly unrealistic. Calculated density profiles have a small "foot" extending to $z > h$ and approaching $\varphi = 0$ asymptotically [198, 170]. With respect to other measurable quantities, like the scaling behavior with σ and N [52, 174, 73], the density profiles obtained from this simple approximation agree well with more refined self-consistent calculations [52, 198].

The above approximation has been extended to polydiperse brushes [173], and to curved interfaces [8, 253, 134]. The latter system allows the determination of the bending moduli of copolymer decorated interfaces in immiscible blends [171].

2.1.3.3 Confinement

We would like to estimate the free energy of a chain that has been compressed, so that its size is smaller than its equilibrium size. This corresponds to a chain that has been placed in a narrow slit or capillary. The loss in configurational entropy that the chain suffers when enclosed in a cavity of size D, much larger than a single monomer,

but smaller than the equilibrium size of the chain aN^{ν}, can be estimated as follows: On length scales smaller than D, the chain is insensitive to the presence of the walls, *i.e.* it forms "blobs", inside of which it performs unperturbed random walks. The maximum size of these walks is on the order of the size of the cavity, D. The number of chain segments g per blob is found from:

$$D \cong a g^{\nu}, \tag{2.87}$$

and the number of blobs that the chain breaks up into is:

$$\frac{N}{g} = N \left(\frac{a}{D}\right)^{1/\nu}. \tag{2.88}$$

Within each blob the chain collides approximately once with the walls. Each reflection from the wall removes one degree of freedom of the chain, *i.e.* it costs on the order of $k_B T$ in entropy. Therefore, the loss in entropy due to confinement is:

$$\beta S_{\text{conf}} \cong -N \left(\frac{a}{D}\right)^{1/\nu}, \tag{2.89}$$

where $\nu = 3/5$ for real and $\nu = 1/2$ for ideal chains. In the latter case, we find in particular:

$$\beta F_{\text{conf}} \cong \left(\frac{R_0}{D}\right)^2 \qquad \text{for ideal chains.} \tag{2.90}$$

2.2 *Mathematical Aspects of the Statistics of Flexible Chain Molecules*

In the present section, we will study some of the properties of Gaussian chains (Section 2.1.1.3) in more detail. After considering the uniqueness of the characteristic length scale R_0 of the coil and the principles of its determination in elastic light scattering experiments, we introduce the standard model of flexible polymer chains and its formulation in terms of path integrals.

2.2.1 Structure of a Gaussian Coil

2.2.1.1 Structural Characterization of Gaussian Coils

The size of a coil is characterized by the unique length scale $aN^{1/2}$. Once the number of steps has been fixed, any measure of the average size of a coil is found from this relation by a renormalization of the steplength a. To illustrate this, let us calculate several different measures of the coil size, *e.g.* the moments of the square of the end-to-end vector $\mathbf{R}^2$:

$$\left\langle (\mathbf{R}^2)^n \right\rangle = \int d^3R\, \mathbf{R}^{2n} P_N(\mathbf{R}) = (a^2N)\left[\frac{(2n+1)!!}{3^n}\right]. \tag{2.91}$$

We see that any characteristic end-to-end distance $R^2 \cong \langle (\mathbf{R}^2)^n \rangle^{1/n}$ is proportional to a^2N, irrespective of the order of the moment, n. Another important measure of the coil size is the mean radius of gyration, R_G, which can be directly measured in elastic light scattering experiments (c.f. Section 2.2.1.2). The radius of gyration is defined by:

$$R_G^2 = \frac{1}{N}\sum_{n=1}^{N} \left\langle (\mathbf{R}_n - \mathbf{R}_{cm})^2 \right\rangle, \tag{2.92}$$

where

$$\mathbf{R}_{cm} = \frac{1}{N}\sum_{m=1}^{N} \mathbf{R}_m. \tag{2.93}$$

is the position of the center-or-mass of the chain. Equation (2.92) can be rewritten as:

$$\begin{aligned} R_G^2 &= \frac{1}{N}\sum_{n=1}^{N}\left\langle \mathbf{R}_n^2 - 2\mathbf{R}_n \frac{1}{N}\sum_{m=1}^{N}\mathbf{R}_m + \frac{1}{N^2}\sum_{m,l=1}^{N}\mathbf{R}_m\mathbf{R}_l \right\rangle \\ &= \left\langle \frac{1}{N}\sum_n \mathbf{R}_n^2 - \frac{2}{N^2}\sum_n \mathbf{R}_n \sum_m \mathbf{R}_m \right\rangle \\ &= \frac{1}{2N^2}\sum_{n,m}\left\langle (\mathbf{R}_n - \mathbf{R}_{cm})^2 \right\rangle. \end{aligned} \tag{2.94}$$

Notice that the radius of gyration is also uniquely defined for a branched or ring-polymer, in contrast to the end-to-end vector. For a linear Gaussian chain, equation (2.94) is easily evaluated by replacing the sums by integrals:

$$\begin{aligned} R_G^2 &= \frac{1}{2}\sum_{n,m}\langle(\mathbf{R}_n - \mathbf{R}_{\rm cm})^2\rangle \\ &= \frac{1}{2}\int_0^N dn \int_0^N dm\,|n-m|a^2 \\ &= \frac{a^2}{2}\int_0^N dn \int_0^n dm\,(n-m) - \int_n^N dm\,(n-m) \\ &= \frac{Na^2}{6}. \end{aligned} \tag{2.95}$$

i.e. $R_G = R_0/\sqrt{6}$ for linear chains.

It must be noted however that the fluctuations in the coil size are of the same order as the size itself:

$$\frac{\langle(\mathbf{R}^2 - \langle\mathbf{R}^2\rangle)^2\rangle}{\langle\mathbf{R}^2\rangle^2} = \frac{\langle\mathbf{R}^4\rangle - \langle\mathbf{R}^2\rangle^2}{\langle\mathbf{R}^2\rangle^2} = \frac{2}{3}, \tag{2.96}$$

i.e. the Gaussian coil is a strongly fluctuating object.

Inside each coil, the average density of links is $N/R_0^3 \sim N^{-1/2}$ and so goes to zero for long chains. Locally, however, the link density may deviate strongly from the average density. We see in particular, that a description of a coil as ball of radius R_0 with mean density N/R_0^3 is not a good description of the tenuous structure of an ideal polymer.

2.2.1.2 Scattering-, Structure- and Correlation-Functions

In the prototypical elastic light scattering experiment [27], an incoming particle with momentum $\hbar\mathbf{k}$ in the plane wave state $|\mathbf{k}\rangle$ interacts with the potential U of a scattering center in the target and leaves in the final state $|\mathbf{k}'\rangle$. We assume that the potential is sufficiently weak that only single scattering events contribute appreciably. The transition rate from initial to final state is, by Fermi's Golden rule, proportional to

the matrix element:

$$\langle \mathbf{k}' | U | \mathbf{k} \rangle = \int d^3x \, e^{-i\mathbf{k}\mathbf{x}} U(\mathbf{x}) e^{i\mathbf{k}'\mathbf{x}}. \tag{2.97}$$

For multiple scattering centers, we write the potential as a sum over the contributions from each center:

$$U(\mathbf{x}) = \sum_i U_i(\mathbf{x} - \mathbf{x}_i), \tag{2.98}$$

where $\mathbf{x}_i$ is the position of the i^{th} scattering center. The matrix element now becomes:

$$\begin{aligned}
\langle \mathbf{k}' | U | \mathbf{k} \rangle &= \sum_i \int d^3x \, e^{-i\mathbf{k}\mathbf{x}} U_i(\mathbf{x} - \mathbf{x}_i) e^{i\mathbf{k}'\mathbf{x}} \\
&= \sum_i \int d^3r_i \, e^{-i\mathbf{k}(\mathbf{r}_i + \mathbf{x}_i)} U_i(\mathbf{r}_i) e^{i\mathbf{k}'(\mathbf{r}_i + \mathbf{x}_i)} \qquad \mathbf{r}_i = \mathbf{x} - \mathbf{x}_i \\
&= \sum_i \left[\int d^3r_i e^{-i\mathbf{q}\mathbf{r}_i} U_i(\mathbf{r}_i) \right] e^{-i\mathbf{q}\mathbf{x}_i} \qquad \mathbf{q} = \mathbf{k} - \mathbf{k}' \\
&= \sum_i U_i(\mathbf{q}) e^{-i\mathbf{q}\mathbf{x}_i},
\end{aligned} \tag{2.99}$$

where $U_i(\mathbf{q})$ is the form factor, containing the information about the scattering potential. The intensity of scattered radiation from a given configuration is proportional to the differential cross section, which in turn is proportional to the square of the matrix element:

$$|\langle \mathbf{k}' | U | \mathbf{k} \rangle|^2 = \sum_{i,j} U_i(\mathbf{q}) U_j^*(\mathbf{q}) e^{-i(\mathbf{x}_i - \mathbf{x}_j)\mathbf{q}}. \tag{2.100}$$

Measuring the intensity over a finite time interval amounts to sampling an average of the possible configurations of the system. If all the scattering centers are identical the measured intensity is:

$$|U_i(\mathbf{q})|^2 \cdot I(\mathbf{q}) = |U_i(\mathbf{q})|^2 \left\langle \sum_{i,j} e^{-i(\mathbf{x}_i - \mathbf{x}_j)\mathbf{q}} \right\rangle, \tag{2.101}$$

where $I(\mathbf{q})$ is the *structure function*, containing all the information about the positions of the scattering centers in the sample. If correlations in the positions of the scattering

centers extend only over a finite distance, only terms with $\mathbf{x}_i \approx \mathbf{x}_j$ do not average to zero and the structure function is proportional to the number of particles N. If we divide by N to obtain an intensive quantity, we obtain the *structure factor*:

$$S(\mathbf{q}) = \frac{1}{N} I(\mathbf{q}). \tag{2.102}$$

Note that the structure function is the Fourier transform of the density-density autocorrelation function:

$$\begin{aligned}
\sum_{i,j} \left\langle e^{i\mathbf{q}(\mathbf{x}_i - \mathbf{x}_j)} \right\rangle &= \sum_{i,j} \left\langle e^{i\mathbf{q}\mathbf{x}_i} e^{-i\mathbf{q}\mathbf{x}_j} \right\rangle \\
&= \int d^3x\, d^3y \sum_{i,j} \left\langle e^{i\mathbf{q}\mathbf{x}_i} \delta(\mathbf{x} - \mathbf{x}_i) e^{-i\mathbf{q}\mathbf{x}_j} \delta(\mathbf{y} - \mathbf{x}_j) \right\rangle \\
&= \int d^3x\, d^3y\, e^{i\mathbf{q}(\mathbf{x}-\mathbf{y})} \sum_{i,j} \left\langle \delta(\mathbf{x} - \mathbf{x}_i) \delta(\mathbf{y} - \mathbf{x}_j) \right\rangle \\
&= \int d^3r\, d^3y\, e^{i\mathbf{q}\mathbf{r}} \sum_{i,j} \left\langle \delta(\mathbf{r} + \mathbf{y} - \mathbf{x}_i) \delta(\mathbf{y} - \mathbf{x}_j) \right\rangle \\
&= \sum_{i,j} \int d^3r\, e^{i\mathbf{q}\mathbf{r}} \left\langle \delta(\mathbf{r} + \mathbf{x}_j - \mathbf{x}_i) \right\rangle ,
\end{aligned} \tag{2.103}$$

and we made use of the homogeneity of the system when writing $\mathbf{r} = \mathbf{x} - \mathbf{y}$. From equation (2.24) we know that the structure factor is $N g_D(x)$, where the Debye function is $g_D(x) = 2(x + e^{-x} - 1)/x^2$ with $x = \mathbf{q}^2 R_0^2/6 = (qR_G)^2$. In this way, scattering experiments on disordered phases give direct information about the radius of gyration.

2.2.2 The Standard Model: Continuum Limit for the Gaussian Chain

In Section 2.1.1.2 we have seen that any ideal chain has a Gaussian distribution of chain properties an scales much larger than the monomer size. Consequentially, in Section 2.1.1.3, we introduced the Gaussian model, *i.e.* "beads" connected by "springs", which on scales comparable to the coil size, is equivalent to more realistic chain models.

In the present section, we will study the "Standard Model" for flexible polymers, which is obtained by assuming that the Gaussian distribution (2.18) holds for *any*

two points on the chain and taking the continuum limit. For any experimentally studied polymer, the equivalent Gaussian chain can be constructed by appropriately adjusting the Kuhn length and number of monomers. It should be kept in mind that results based on the standard model will be valid on length scales comparable to or greater than the coil size, but will be erroneous on the scale of the Kuhn length.

The chains obtained by taking the continuum limit in (2.18) are free random walks with variable step length and root-mean-square displacement a at each step. The Gaussian standard model can therefore be described by the Wiener Integral [108, 214] developed for Brownian motion. This path integral description is a very useful starting point for further analytical developments. In particular, we will be able to exploit the close connection between Brownian motion and diffusion to derive a description of polymer chains in terms of a diffusive partial differential equation in Section 2.2.2.1. In the following section, we will consider the solutions to this differential equation in the limit of infinitely long chains. Very useful references for the present section are the monographs [214, 252, 205] and the reviews [62, 251, 44].

2.2.2.1 Path Integral representation for the Gaussian Chain

Consider a Gaussian chain of N links in the configuration Γ_N (2.1):

$$\Gamma_N = \{\mathbf{x}_0, \mathbf{x}_1, \ldots, \mathbf{x}_N\}, \tag{2.104}$$

where the $\mathbf{x}_i = \mathbf{x}(t_i)$ are the positions of the "beads". Here we have introduced a continuous measure t of the position along the chain, such that $t_0 = 0$, $t_N = N$ and $t_i - t_{i-1} = \epsilon = 1/N$. Let the chain be subject to an external field $w_i = w(\mathbf{x}(t_i))\epsilon = \beta U(\mathbf{x}_i)\epsilon$. This field does not have to be a "real" physical (*e.g.* electric, magnetic etc.) field, but may also be an "effective" field due to the interactions with other monomers or with an adsorbing or repelling surface, etc. It will be useful to set $w_0 = 0$.

The probability for the chain to be in the particular configuration Γ_N is:

$$P[\Gamma_N] = e^{-w_N} g(\mathbf{x}_N, \mathbf{x}_{N-1})\, e^{-w_{N-1}} \ldots e^{-w_2} g(\mathbf{x}_2, \mathbf{x}_1)\, e^{-w_1} g(\mathbf{x}_1, \mathbf{x}_0). \tag{2.105}$$

where

$$g(\mathbf{x}_i, \mathbf{x}_{i-1}) = \left[2\pi a^2 \epsilon/3\right]^{-1} \exp\left(-\frac{3(\mathbf{x}_i - \mathbf{x}_{i-1})^2}{2\epsilon a^2}\right) \tag{2.106}$$

is the Gauss distribution for a single link and e^{-w_i} is the Boltzmann factor due to the interaction with the external field. The configurational part or the single chain partition function is obtained by integrating over all coordinates, *i.e.* summing over all possible configurations:

$$Q = \int d^3x_0 \ldots d^3x_N \, e^{-w_N} g(\mathbf{x}_N, \mathbf{x}_{N-1}) \, e^{-w_{N-1}} \ldots e^{-w_2} g(\mathbf{x}_2, \mathbf{x}_1) \, e^{-w_1} g(\mathbf{x}_1, \mathbf{x}_0) \, . \tag{2.107}$$

Also useful are the constrained partition functions for chains with one or both ends held fixed:

$$G_N(\mathbf{x}_N) = G(\mathbf{x}_N, N; \mathbf{x}_0, 0) = \int d^3x_1 \ldots d^3x_{N-1} \prod_{i=1}^{N-1} \left[e^{-w_i} g(\mathbf{x}_i, \mathbf{x}_{i-1})\right], \tag{2.108}$$

i.e. the (unnormalized) probability to have the last segment at $\mathbf{x}_N$, given that the first segment is at $\mathbf{x}_0$, and

$$q(\mathbf{x}, N) = \int d^3x_0 \ldots d^3x_{N-1} \prod_{i=1}^{N-1} \left[e^{-w_i} g(\mathbf{x}_i, \mathbf{x}_{i-1})\right], \tag{2.109}$$

The unconditional probability for a chain to terminate at $\mathbf{x}_N$.

The function $G(\mathbf{x}_N, N; \mathbf{x}_0, 0)$ is called the Green's function (see below for the justification of this name) or the Single Chain Propagator. Obviously, $q(\mathbf{x}, t)$ and Q can be obtained from the Green's function by integrating out one or both of the endpoints.

Obviously, we can obtain the Green's function $G_{N+1}(\mathbf{x}_{N+1})$ for a chain of $N+1$ links from the Green's function $G_N(\mathbf{x}_N)$ of a chain of N links:

$$G_{N+1}(\mathbf{x}_{N+1}) = \int d^3x_N \, e^{-w(\mathbf{x}_{N+1})} g(\mathbf{x}_{N+1}, \mathbf{x}_N) \, G_N(\mathbf{x}_N). \tag{2.110}$$

Equation (2.110) is an expression of the Markov property of ideal chains: each new step depends only on the immediately preceding one. In probability theory, this equation is known as the Chapman-Kolmogorov equation [50].

We will now rewrite equation (2.107) for the partition function by using the explicit expression for $g(\mathbf{x},\mathbf{y})$:

$$\begin{aligned} Q &= \left[\frac{3}{2\pi\epsilon a^2}\right]^{3(N+1)/2} \int d^3x_0 \ldots d^3x_N \exp\left(-\sum_{i=1}^{N}\left[\frac{3}{2a^2}\frac{(\mathbf{x}_i-\mathbf{x}_{i-1})^2}{\epsilon} + w(\mathbf{x}_i)\epsilon\right]\right) \\ &= \left[\frac{3}{2\pi\epsilon a^2}\right]^{3(N+1)/2} \\ &\qquad \int d^3x_0 \ldots d^3x_N \exp\left(-\epsilon\sum_{i=1}^{N}\left[\frac{3}{2a^2}\left(\frac{\mathbf{x}_i-\mathbf{x}_{i-1}}{\epsilon}\right)^2 + w(\mathbf{x}_i)\right]\right). \end{aligned} \tag{2.111}$$

We now take the continuum limit $N \to \infty$, $\epsilon \to 0$, $N\epsilon = const$ in the above expression and obtain:

$$Q = \mathcal{N}\int \mathcal{D}\mathbf{r}(\cdot)\, e^{-\int dt\, \frac{3}{2a^2}\left(\frac{\partial \mathbf{r}}{\partial t}\right)^2 + w[\mathbf{x}(t)]}, \tag{2.112}$$

where $\mathcal{N}$ is a normalization constant. This is the path integral representation of the partition function for an Gaussian polymer chain in an external field.

This equation expresses a sum over all possible conformations of the chain as integral over all continuous space curves (of a certain average size), weighted by the appropriate probability. The factor weight factor

$$\exp\left[-\int dt\, \left(\frac{\partial r}{\partial t}\right)^2\right] \tag{2.113}$$

in equation (2.112) is the "Wiener measure", and provides a mathematically rigorous measure in the space of continuous curves [108, 214]. A well-known property of the so defined Wiener integral (2.112) is that almost all the paths contributing to Q are nowhere differentiable. The main use of (2.112) for polymer physics lies in its intuitive appeal and flexibility with regard to formal manipulation. We will *always* regard an

expression like (2.112) as an abbreviation for the discrete expression (2.107). If in doubt, we introduce a discrete set of points $\{t_i | i = 0, \ldots, N\}$ along the chain, perform our calculation on this and take the continuum limit in the end.

Before we continue, it should be pointed out that equation (2.107)-(2.112) are only the configurational parts of the single chain partition function, a kinetic term $\lambda_T^{-3} = \left[\hbar/\sqrt{2\pi k_B T m}\right]^{-3} = \int \frac{d^3p}{h^3} e^{-\beta \frac{p^2}{2m}}$ per bead has been omitted. Here m is the mass per bead, *i.e.* if M is the mass of the entire chain, $m = M/(N+1)$. In practical calculations, the kinetic part is never evaluated, but is lumped into the normalization constant $\mathcal{N}$ in (2.112), which cancels for all physical quantities, but serves to make the partition function dimensionless.

For the Green's function $G_N(\mathbf{x})$ the corresponding path integral representation is:

$$G(\mathbf{x}_N, N; \mathbf{x}_0, 0) = \int_{\mathbf{x}_0}^{\mathbf{x}_N} \mathcal{D}\mathbf{r}(\cdot)\, e^{-\int dt \, \frac{3}{2a^2}\dot{\mathbf{r}}^2 + w[\mathbf{r}]}. \tag{2.114}$$

This expression is (except for a factor of i in the exponent) equivalent to the path integral for the one-dimensional quantum mechanical propagator ("kernel" in [51]). We will now derive the partial differential equation for $G_N(\mathbf{x}_N)$ corresponding to the Schrödinger equation in Quantum Mechanics.

Consider the Chapman-Kolmogorov equation (2.110) for two points which are separated by an infinitesimal distance $\epsilon = t_{N+1} - t_N$:

$$\begin{aligned} G(\mathbf{y}, N+\epsilon; \mathbf{x}_0, 0) &= \int d^3x \, e^{-w(\mathbf{y})} g(\mathbf{y}, \mathbf{x}) G(\mathbf{x}, N; \mathbf{x}_0, 0) \\ &= \left[\frac{3}{2\pi a^2 \epsilon}\right]^{3/2} \int d^3x \, e^{-\frac{3}{2a^2}\frac{(\mathbf{y}-\mathbf{x})^2}{\epsilon} - w(\mathbf{y})\epsilon} G(\mathbf{x}, N; \mathbf{x}_0, 0). \end{aligned} \tag{2.115}$$

We see that only conformations with $(\mathbf{y}-\mathbf{x})^2 \approx \epsilon$ will contribute significantly to the integral, others being suppressed by the Gaussian factor. We introduce $\boldsymbol{\eta} = \mathbf{x} - \mathbf{y}$ and expect $\boldsymbol{\eta}$ to be of order $\sqrt{\epsilon}$. Expanding G up to order ϵ (*i.e.* up to second order in $\boldsymbol{\eta}$) we obtain (c.f. [214] for a careful discussion of the choice of position at which

to evaluate w):

$$G_N(\mathbf{y}) + \epsilon\frac{\partial G_N(\mathbf{y})}{\partial t} + \cdots = \left[\frac{3}{2\pi a^2\epsilon}\right]^{3/2} e^{-\epsilon w(\mathbf{y})} \int d^3\eta\, e^{-\frac{3}{2a^2}\frac{\eta^2}{\epsilon}} \left[G_N(\mathbf{y}) + \boldsymbol{\eta}\nabla G_N(\mathbf{y}) + \frac{\boldsymbol{\eta}^2}{2}\nabla^2 G_N(\mathbf{y}) + \cdots\right] \tag{2.116}$$

We can rewrite $e^{-\epsilon w(\mathbf{y})} \approx 1 - \epsilon w(\mathbf{y})$, neglecting terms of order ϵ^2:

$$G_N(\mathbf{y}) + \epsilon\frac{\partial G_N(\mathbf{y})}{\partial t} = \left[\frac{3}{2\pi a^2\epsilon}\right]^{3/2} [1 - \epsilon w(\mathbf{y})] \int d^3\eta\, e^{-\frac{3}{2a^2}\frac{\eta^2}{\epsilon}} \left[G_N(\mathbf{y}) + \boldsymbol{\eta}\nabla G_N(\mathbf{y}) + \frac{\boldsymbol{\eta}^2}{2}\nabla^2 G_N(\mathbf{y})\right] \tag{2.117}$$

Performing the Gaussian integrals and noticing that the term linear in $\boldsymbol{\eta}$ vanishes because of symmetry, we find:

$$G_N(\mathbf{y}) + \epsilon\frac{\partial G_N(\mathbf{y})}{\partial t} = [1 - \epsilon w(\mathbf{y})] \left[G_N(\mathbf{y}) + \frac{1}{4}\frac{2a^2\epsilon}{3}\nabla^2 G_N(\mathbf{y})\right]$$

and finally (again omitting a term of order ϵ^2):

$$\frac{\partial}{\partial t}G_N(\mathbf{y}) = \frac{a^2}{6}\nabla^2 G_N(\mathbf{y}) - w(\mathbf{y})G_N(\mathbf{y}). \tag{2.118}$$

This is the diffusion equation corresponding to the path integral (2.114). The function $G_N(\mathbf{x})$ is subject to the boundary conditions that $G_N(\mathbf{x}) = 0$ for $N < 0$ and that for a chain of length $N = 0$, the start- and end-point have to be the same: $G(\mathbf{x}, 0; \mathbf{y}, 0) = \delta(\mathbf{x} - \mathbf{y})$. Consequentially, G_N is the Green's function for the diffusion equation (2.118). Once the Green's function is known, every statistical quantity of the Gaussian chain can be evaluated.

Chapter 3

MICROPHASE SEPARATION IN COPOLYMER SYSTEMS

3.1 Experimental Studies of Copolymer Systems

Consider a system containing an AB-diblock copolymer, *i.e.* a chain molecule consisting of two blocks, each consisting of only one kind of monomer. At sufficiently high temperatures, this system will assume a disordered state. As the temperature is lowered, the repulsion between unlike monomers outweighs the entropic tendency to disorder, and the system can lower its free energy by phase separating. Because the two blocks are linked together, a macrophase separation into macroscopic A- and B-rich regions is impossible, and the system instead undergoes a microphase separation, forming regions on the order of the coil size, rich in A- or B-monomers (c.f. Figure 1.4). These regions themselves may be ordered (c.f. Figure 1.2) or disordered (c.f. Figure 1.3). In this chapter, we will discuss experimental and theoretical methods specifically designed to treat this microphase separation transition in block copolymer systems.

In the present section, we describe some typical experimental methods and give an overview of available experimental results for microphase separation in melts containing block copolymers, as well as references to related topics. In the following section, we describe the full self-consistent field method used in this work in detail, including its numerical implementation. Then we discuss some other mean field theories, which are valid in certain limiting cases. We conclude this chapter with a discussion of the effects that thermal fluctuations have on the mesophase behavior in copolymer melts

and describe calculations that include them.

Experimental samples are usually prepared by dissolving a certain amount of polymer in a good solvent for both A- and B-monomers (*e.g.* toluene for polystyrene and polyisoprene). The solvent is then slowly evaporated and the sample annealed for several hours or days at the desired temperature (between 20 °C and 200 °C), then rapidly quenched in liquid nitrogen, so that the polymer undergoes a glass transition. Once quenched, the microphases are metastable at room temperature [70].

In choosing a particular polymeric substance for experimental studies, one is mainly guided by the desire to eliminate non-universal features as far as possible. One therefore seeks polymers that form flexible chains, have monomers of comparable size, can be obtained with low polydispersity, are chemically stable under experimental conditions, and are free of branching points. The combination of polystyrene and polyisoprene has been experimentalists first choice over many years (c.f. Figure 3.1), but other combinations are also popular [215].

The structure of the ordered phase can be found from small angle neutron or X-ray scattering, using radiation with a wavelength of a few Å. Because the energies involved in the self-assembly of polymers are small and equilibration times for entangled chain molecules are very long, diffraction peaks of order 5 or higher can only be seen after extremely long annealing times (up to several weeks [71]). One therefore uses transmission electron microscopy to verify the structure of an ordered phase: ultrathin sections, less than a micrometer thick, are cut out and subjected to Osmium tetroxide vapor, which selectively stains the polyisoprene monomers. One can obtain electron micrographs with a resolution of 50 Å or better.

For complex morphologies, both methods can lead one astray: what is now considered the gyroid phase (space group $Ia3d$) was over years misidentified and thought to be OBDD (space group $Pn3m$). After mean field theory predicted the gyroid phase to be the stable one [157], a careful experimental reexamination [71] showed that the symmetry had been misidentified as OBDD, and was indeed gyroid.

	Name	Structure	Monomer Volume (Å^3)	Density (g/cm^3)	χ with PS (T in Kelvin)
PS	Polystyrene "Styrofoam"	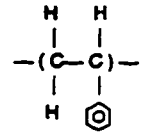	179	0.969[a]	
PI	Polyisoprene "Rubber"	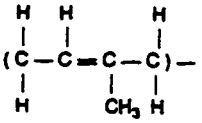	136	0.913[b]	$7.9 \cdot 10^{-2} + \frac{17.6K}{T}$
PBD	Polybutadiene	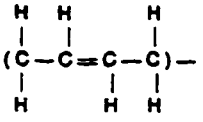	111	0.900[b]	$-1.57 \cdot 10^{-2} + \frac{18.7K}{T}$
PMMA	Polymethyl-methacrylate	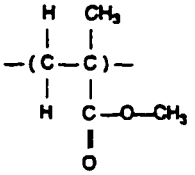	149	1.13[a]	$1.29 \cdot 10^{-2} + \frac{1.96K}{T}$

[a] at $T = 403K$
[b] at $T = 298K$

Figure 3.1: Structure and properties of some polymers often used in experiments on copolymeric self-assembly. The best studied system is PS-PI, but experiments on PS-PBD and PS-PMMA are also common. The last column gives the observed temperature behavior of the Flory-Huggins parameter χ of the respective monomer with Polystyrene (c.f. Section 2.1.2). Information compiled after [140].

To determine the location of phase boundaries, rheological measurements on unquenched samples prove especially useful: a sample, a few millimeters thick, is sheared at a constant rate between 0.01 Hz and 100 Hz, while the temperature is slowly changed. A sharp change in the measured mechanical response indicates a transition to a different morphology.

One general difficulty with experiments on microphase separation in copolymers concerns the possibility of metastable phases, in particular close to the glass transi-

tion. The equilibration times for chains of high molecular weight can be extremely long, in particular for transitions between complex phases. Over the years [18, 76, 75] observations of HPL phases between the lamellar and the hexagonal phase at intermediate segregation have been reported. This phase is now considered [69] to be only a metastable state (in accord with self-consistent field calculations).

Diblock copolymers have a peak in the structure function (Section 2.2.1.2) at non-zero wavevector even in the disordered state [31, 35]. Information about the structure function is again obtained by small angle scattering techniques [204, 180], where the interest now lies in particular with the position and height of the peak, the latter being infinite at a continuous transition. In reality, both quantities are affected by fluctuations and cannot be obtained from mean field theory, but are well predicted by fluctuation calculations [12, 17, 16] or integral equation theories [220, 219, 221].

Experiments on diblock copolymers date back at least to the 1970s [99]. Early work was often directed at *blends* containing a block copolymer, with the motivation to study the emulsifying properties on block copolymers. Nowadays, random- (instead of block-) copolymers are deemed more appropriate for this purpose [100, 254, 7, 111, 64, 28], and the interest in block copolymeric systems today focuses specifically on their microphase behavior.

For the *pure* diblock, the phase diagram has been mapped out in recent years [18, 151, 158], and emphasis is again put on blends. Blends of two AB-diblocks, of different length or architecture have attracted a great deal of interest, both experimentally [84, 81, 114, 160, 262, 234], as well as theoretically [144, 148, 226, 228].

Experiments on binary AB/A systems, comprising a diblock and a corresponding homopolymer, are relatively numerous [113, 83, 241, 240, 82, 115, 116, 256, 255, 258, 257, 265, 206, 193, 104, 41], as compared to ternary AB/A/B blends [99, 79, 240, 137]. Also, ABA triblocks and their blends [77, 112] have attracted some interest, as have systems containing more than two different monomers, *e.g.* AB/C blends [80] or ABC triblocks [178, 177, 179, 6, 65, 189, 263].

Very recently, work has begun on aqueous solutions of water soluble block copolymers [139, 259, 183, 238, 85, 2, 182] (especially on polypropylene oxide and polyethylene oxide), thus providing a bridge between long chain copolymers and short chain surfactants [67]. Bicontinuous microemulsions, previously known only in short chain surfactant mixtures, have been observed in systems of water soluble polymers [85], and very recently also in purely polymeric blends [105, 15].

Further related work on block copolymers, concerns their behavior at interfaces between coexisting bulk fluid phases [126, 127, 231, 22, 23, 97, 30, 29] or near hard walls [59, 176, 246]. Very interesting also is the behavior of block copolymers in confined geometries, *e.g.* in thin films [244, 245, 247, 52] or in narrow slits [118, 229, 233, 117, 68, 147]. Related to the last problem is the study of polymers confined into self-assembled microphases [202, 192, 132] and work on polymer decorated self-assembled layers [141, 96, 249, 89].

3.2 Self-Consistent field method for the Gaussian chain

In this section, we present some theoretical tools, specifically suited for the investigation of microphase separation in copolymer blends. First, we consider a variation of the self-consistent field method [92, 93, 94, 194] for the Gaussian model of flexible chains (Section 2.2.2) in the grand canonical ensemble [146, 102] and discuss its implementation in Fourier space [157, 145]. We then discuss some alternative approaches that hold in specific limiting cases. Finally, we turn our attention to calculations beyond the mean field level.

3.2.1 Self-Consistent Field Method in the Grand Canonical Ensemble

We consider a ternary blend of A and B homopolymer, of polymerization indices $\alpha_A N$ and $\alpha_B N$ respectively, and AB diblock of index N of which a fraction f is A monomer. We employ the Gaussian model of flexible polymer chains, and work in the

grand canonical ensemble in which the number n_κ of chains of type $\kappa = A,\ B,\ AB$ is not fixed [146]. The configurational part of the partition function is

$$\mathcal{Z} \propto \sum_{n_A}^{\infty}\sum_{n_B}^{\infty}\sum_{n_{AB}}^{\infty} \frac{z_0^{n_{AB}}(z_A z_0)^{n_A}(z_B z_0)^{n_B}}{n_{AB}!n_A!n_B!} \int \prod_{i=1}^{n_A} \tilde{\mathcal{D}}\mathbf{r}_{A,i} \prod_{j=1}^{n_B} \tilde{\mathcal{D}}\mathbf{r}_{B,j} \prod_{k=1}^{n_{AB}} \tilde{\mathcal{D}}\mathbf{r}_{AB,k} \times \exp\left[-\frac{\chi}{v}\int d^3r\, \hat{\varphi}_A(\mathbf{r})\hat{\varphi}_B(\mathbf{r})\right], \quad (3.1)$$

where v is the volume occupied by each monomer, $z_\kappa = \exp(\beta\mu_\kappa)$, $\beta = 1/k_BT$, and μ_κ is the chemical potential of component κ to within an additive constant z_0. Tildes indicate that the functional integrals are weighted by the Wiener measure $P[\mathbf{r};0,1]$ for diblocks and $P[\mathbf{r};0,\alpha_A]$, $P[\mathbf{r};0,\alpha_B]$ for the homopolymers (2.113), with

$$P[\mathbf{r};0,s_0] \propto \exp\left(-\frac{3}{2Na^2}\int_0^{s_0} dt \left|\frac{d\mathbf{r}}{dt}\right|^2\right), \quad (3.2)$$

where a is the statistical segment length taken to be the same for both monomers, and we have reparametrized the polymer chain by a continuous index $t \to t/N$, as compared to the convention of Section 2.2.2. To simplify formulae below, we shall set $z_0 = Nv$.

Information about the configurations of the chains is contained in the local, dimensionless, densities:

$$\hat{\varphi}_A(\mathbf{r}) = \hat{\varphi}_A(\mathbf{r},\{r_{A,i}\},\{r_{AB,k}\}) = Nv\sum_i^{n_A}\int_0^{\alpha_A} dt\,\delta(\mathbf{r}-\mathbf{r}_{A,i}(t)) + Nv\sum_k^{n_{AB}}\int_0^{f} dt\,\delta(\mathbf{r}-\mathbf{r}_{AB,k}(t)). \quad (3.3a)$$

$$\hat{\varphi}_B(\mathbf{r}) = \hat{\varphi}_B(\mathbf{r},\{r_{B,i}\},\{r_{AB,k}\}) = Nv\sum_i^{n_B}\int_0^{\alpha_B} dt\,\delta(\mathbf{r}-\mathbf{r}_{B,i}(t)) + Nv\sum_k^{n_{AB}}\int_f^{1} dt\,\delta(\mathbf{r}-\mathbf{r}_{AB,k}(t)). \quad (3.3b)$$

We include a hard core repulsion between monomers by requiring the melt to be incompressible, so that only such configurations are allowed, that do not contain two monomers occupying the same position in space. As a consequence, there are only two independent chemical potentials, and we set that of the copolymer to zero.

We introduce the following linear combinations of the local densities:

$$\hat{\varphi}_{\pm} = \frac{\hat{\varphi}_A \pm \hat{\varphi}_B}{2}, \tag{3.4}$$

so that the the integral in (3.1) becomes:

$$\int \prod_{i=1}^{n_A} \tilde{\mathcal{D}}\mathbf{r}_{A,i} \prod_{j=1}^{n_B} \tilde{\mathcal{D}}\mathbf{r}_{B,j} \prod_{k=1}^{n_{AB}} \tilde{\mathcal{D}}\mathbf{r}_{AB,k} \exp\left[-\frac{\chi}{v}\int d^3r\ (\hat{\varphi}_+(\mathbf{r})^2 - \hat{\varphi}_-(\mathbf{r})^2)\right]. \tag{3.5}$$

Despite its appearance, this integral is not Gaussian, since it is the positions of the chains, not the $\hat{\varphi}$ that are integrated over. The difficulty in evaluating (3.5) is that the local densities couple directly to each other. To make the integral more tractable, we make use of the identity:

$$e^{b^2/4a} = \sqrt{\frac{a}{\pi}}\int dx\, e^{-ax^2+bx} \tag{3.6}$$

("uncompleting the square") so that (3.5) now becomes:

$$\frac{-1}{4\pi\chi}\int \prod_{i=1}^{n_A} \tilde{\mathcal{D}}\mathbf{r}_{A,i} \prod_{j=1}^{n_B} \tilde{\mathcal{D}}\mathbf{r}_{B,j} \prod_{k=1}^{n_{AB}} \tilde{\mathcal{D}}\mathbf{r}_{AB,k} \cdot \mathcal{D}W_+\mathcal{D}W_- \times \exp\left[-\frac{1}{v}\int d^3r \frac{1}{4\chi}(W_+^2 - W_-^2) + W_+\hat{\varphi}_+ + W_-\hat{\varphi}_-\right]. \tag{3.7a}$$

If we want to write this in terms of the physical quantities $\hat{\varphi}_A$ and $\hat{\varphi}_B$, we introduce conjugate fields through: $W_{\pm} = W_A \pm W_B$:

$$\frac{2}{4\pi\chi}\int \prod_{i=1}^{n_A} \tilde{\mathcal{D}}\mathbf{r}_{A,i} \prod_{j=1}^{n_B} \tilde{\mathcal{D}}\mathbf{r}_{B,j} \prod_{k=1}^{n_{AB}} \tilde{\mathcal{D}}\mathbf{r}_{AB,k} \cdot \mathcal{D}W_A\mathcal{D}W_B \times \exp\left[-\frac{1}{v}\int d^3r \frac{W_AW_B}{\chi} + W_A\hat{\varphi}_A + W_B\hat{\varphi}_B\right]. \tag{3.7b}$$

Notice that in going from $W_{\pm}$ to W_A, W_B, we have picked up a constant factor from the Jacobian. The integrals in (3.7) are still constrained to such configurations that the chains do not overlap.

It is useful to make use of the identity (3.6) once more and to write (3.7a):

$$\frac{-1}{4\pi^2}\int\prod_{i=1}^{n_A}\tilde{\mathcal{D}}\mathbf{r}_{A,i}\prod_{j=1}^{n_B}\tilde{\mathcal{D}}\mathbf{r}_{B,j}\prod_{k=1}^{n_{AB}}\tilde{\mathcal{D}}\mathbf{r}_{AB,k}\cdot\mathcal{D}W_+\mathcal{D}W_-\mathcal{D}\Phi_+\mathcal{D}\Phi_-$$
$$\times\exp\left[-\frac{1}{v}\int d^3r\,-\chi\left(\Phi_+^2-\Phi_-^2\right)+W_+\Phi_++W_-\Phi_-+W_+\hat{\varphi}_++W_-\hat{\varphi}_-\right], \quad (3.8a)$$

or, in physical meaningful variables:

$$\frac{1}{4\pi^2}\int\prod_{i=1}^{n_A}\tilde{\mathcal{D}}\mathbf{r}_{A,i}\prod_{j=1}^{n_B}\tilde{\mathcal{D}}\mathbf{r}_{B,j}\prod_{k=1}^{n_{AB}}\tilde{\mathcal{D}}\mathbf{r}_{AB,k}\cdot\mathcal{D}W_A\mathcal{D}W_B\mathcal{D}\Phi_A\mathcal{D}\Phi_B$$
$$\times\exp\left[-\frac{1}{v}\int d^3r\,W_A\Phi_A+W_B\Phi_B-\chi\Phi_A\Phi_B+W_A\hat{\varphi}_A+W_B\hat{\varphi}_B\right]. \quad (3.8b)$$

The local densities $\hat{\varphi}_A$ and $\hat{\varphi}_B$, which depend explicitly on the chain conformations, now do not couple *directly* to each other, but instead to the fluctuating fields W_A and W_B. We can now perform the sums over n_κ, and, using $\sum_n \frac{x^n}{n!}=\exp(x)$, we obtain for the partition function (3.1):

$$\mathcal{Z}\propto\int\mathcal{D}\Phi_A\mathcal{D}\Phi_B\mathcal{D}W_A\mathcal{D}W_B\,\exp(-\beta F[\Phi_A,\Phi_B,W_A,W_B]), \quad (3.9)$$

where the free energy functional is:

$$-Nv\beta F[\Phi_A,\Phi_B,W_A,W_B]=z_AQ_A[W_A]+z_BQ_B[W_B]+Q_{AB}[W_A,W_B]+$$
$$\int d^3r\,[\Phi_A(\mathbf{r})W_A(\mathbf{r})+\Phi_B(\mathbf{r})W_B(\mathbf{r})-\chi N\Phi_A(\mathbf{r})\Phi_B(\mathbf{r})], \quad (3.10)$$

and a factor $1/N$ has been absorbed into the definition of the fields W_A, W_B.

The Q_κ are the partition functions of *single* polymers in external fields W_A and/or W_B. These single polymer partition functions can be obtained from $Q_\kappa=\int d^3r\,q_\kappa(\mathbf{r},\alpha_\kappa)$, $\kappa=A,B$, and $Q_{AB}=\int d^3r\,q_{AB}(\mathbf{r},1)$, where the end-segment distribu-

tion functions are

$$q_\kappa(\mathbf{r}, s_0) = \int \mathcal{D}\mathbf{r}(\cdot)_\kappa P[\mathbf{r}_\kappa; 0, s_0]\, \delta\left(\mathbf{r} - \mathbf{r}_\kappa(s_0)\right) \exp\left(-\frac{1}{v}\int d^3r\, W_\kappa \hat{\varphi}_\kappa\right) \qquad \kappa = A, B \tag{3.11a}$$

$$q(\mathbf{r}, s_0) = \int \mathcal{D}\mathbf{r}(\cdot)_{AB} P[\mathbf{r}_{AB}; 0, s_0]\, \delta(\mathbf{r} - \mathbf{r}_{AB}(s_0)) \exp\left(-\frac{1}{v}\int d^3r\, [W_A\hat{\varphi}_A + W_B\hat{\varphi}_B]\right) \tag{3.11b}$$

$$q^\dagger(\mathbf{r}, s_0) = \int \mathcal{D}\mathbf{r}(\cdot)_{AB} P[\mathbf{r}_{AB}; 1, s_0]\, \delta(\mathbf{r} - \mathbf{r}_{AB}(s_0)) \exp\left(-\frac{1}{v}\int d^3r\, [W_A\hat{\varphi}_A + W_B\hat{\varphi}_B]\right) \tag{3.11c}$$

Because the two ends of the diblock are distinct, we have introduced $q^\dagger_{AB}(\mathbf{r}, t)$, which is defined similarly to $q_{AB}(\mathbf{r}, t)$, except that the functional integral is taken from s_0 to 1. Since the polymers are modeled as Gaussian chains, these distributions satisfy the diffusion equations:

$$\frac{\partial q}{\partial t} = \begin{cases} \frac{Na^2}{6}\nabla^2 q - W_A q & t < f, \\ \frac{Na^2}{6}\nabla^2 q - W_B q & t > f, \end{cases} \tag{3.12a}$$

$$-\frac{\partial q^\dagger}{\partial t} = \begin{cases} \frac{Na^2}{6}\nabla^2 q^\dagger - W_A q^\dagger & t < f, \\ \frac{Na^2}{6}\nabla^2 q^\dagger - W_B q^\dagger & t > f, \end{cases} \tag{3.12b}$$

for the diblock and

$$\frac{\partial q_\kappa}{\partial t} = \frac{Na^2}{6}\nabla^2 q_\kappa - W_\kappa q_\kappa \qquad \kappa = A, B \tag{3.12c}$$

for the homopolymers, respectively. The initial conditions are $q_\kappa(\mathbf{r}, 0) = 1$ for all components.

In place of calculating the exact free energy, the self-consistent field theory approximates it by the value of the free energy functional $F(\Phi_A, \Phi_B, W_A, W_B)$ obtained by extremizing it under the incompressibility constraint, which is incorporated by means of a Lagrange multiplier ξ, so that we can now drop the constraint on the configurations that no two monomers overlap. The densities and fields which extremize

the free energy, and which we denote by φ_A, φ_B, w_A and w_B are solutions of the variational equations:

$$\varphi_A = z_A \frac{\mathcal{D}Q_A[w_A]}{\mathcal{D}w_A} + \frac{\mathcal{D}Q_{AB}[w_A, w_B]}{\mathcal{D}w_A}, \tag{3.13a}$$

$$\varphi_B = z_B \frac{\mathcal{D}Q_B[w_B]}{\mathcal{D}w_B} + \frac{\mathcal{D}Q_{AB}[w_A, w_B]}{\mathcal{D}w_B}, \tag{3.13b}$$

$$w_A = \chi N \varphi_A + \xi, \tag{3.13c}$$

$$w_B = \chi N \varphi_B + \xi, \tag{3.13d}$$

$$1 = \varphi_A + \varphi_B. \tag{3.13e}$$

From equations (3.13) and the definition of the single polymer partition functions Q_κ it is seen that φ_A is the ensemble average of $\hat{\varphi}_A$, and similarly for φ_B. They can be written in terms of the end-segment distribution functions as

$$\varphi_A(\mathbf{r}) = z_A \int_0^{\alpha_A} dt\, q_A(\mathbf{r}, t)\, q_A(\mathbf{r}, \alpha_A - t) + \int_0^f dt\, q_{AB}(\mathbf{r}, t)\, q^\dagger_{AB}(\mathbf{r}, t), \tag{3.14a}$$

$$\varphi_B(\mathbf{r}) = z_B \int_0^{\alpha_B} dt\, q_B(\mathbf{r}, t)\, q_B(\mathbf{r}, \alpha_B - t) + \int_f^1 dt\, q_{AB}(\mathbf{r}, t)\, q^\dagger_{AB}(\mathbf{r}, t). \tag{3.14b}$$

3.2.2 Implementation of the Self-Consistent Field Method in Fourier Space

To find the density profiles and the free energy of an ordered phase, we have to solve the mean field equations (3.13) together with the relations (3.14) and the diffusion equations (3.12). Since we are interested in ordered solutions of (3.13) with well defined symmetry, we expand any function of position $g(\mathbf{x})$ in a complete set of orthonormal basis functions $\{f_i(\mathbf{x})\}$ which possess the required symmetry [157]:

$$g(\mathbf{x}) = \sum_i^\infty g_i f_i(\mathbf{x}). \tag{3.15}$$

In practical calculations, this sum is truncated after a finite number of terms. The number of basis functions retained determines the accuracy of the solution. The maximum number that we can handle computationally is fifty. The basis functions

$f_i(\mathbf{x})$ having the required symmetry obey the following condition:

$$f_n(\mathbf{x}) = f_n(R_j\mathbf{x}), \tag{3.16}$$

where R_j is a symmetry operation that transforms one position $\mathbf{x}$ in the unit cell into an equivalent one. The index j runs over all equivalent positions, *i.e.* over all elements of the group. Since we are considering a case of periodic symmetry, f must be periodic and can be written as $\exp(i\mathbf{kx})$. The following f fulfills the requirement (3.16):

$$f_n(\mathbf{x}) = \sum_j e^{i\mathbf{k}_n R_j \mathbf{x}}, \tag{3.17}$$

because $f_n(R_k\mathbf{x}) = \sum_j e^{i\mathbf{k}_n R_j R_k \mathbf{x}} = \sum_l e^{i\mathbf{k}_n R_l \mathbf{x}} = f_n(\mathbf{x})$, where we have made use of the group property in the second step. This is equivalent to:

$$f_n(\mathbf{x}) = \sum_j e^{i(R_j^{-1}\mathbf{k}_n)\mathbf{x}}. \tag{3.18}$$

The wavevector $\mathbf{k}_n$ is element of the Brillouin zone, *i.e.*

$$\mathbf{k}_n = \frac{2\pi}{D}\begin{pmatrix} n_1 \\ n_2 \\ n_3 \end{pmatrix}, \qquad \text{where } n_1, n_2, n_3 \in \mathbb{Z} \tag{3.19}$$

and the sum in (3.18) is taken over the entire star of $\mathbf{k}_n$. To include *all* vectors in the Brillouin Zone in the expansion, it is therefore sufficient to restrict $\{n_1, n_2, n_3\}$ to $\mathbb{N}_0$, so that the expansion is over all independent stars. Note that if $\mathbf{k}_n$ is on a symmetry position, some of the terms in (3.18) may be equal to one another.

To proceed further, we introduce dimensionless coordinates: $\mathbf{x} \rightarrow \mathbf{x}/D$, where D is the single length scale in the problem, the dimension of the unit cell. The Laplacian in the diffusion equation transforms accordingly: $\nabla^2 \rightarrow \frac{1}{D^2}\nabla^2$ and all integrals over the unit cell do not depend on D anymore. In particular, the volume V of the unit cell equals one.

We use (3.15) in equations (3.12)–(3.14) and project the coefficients out by operating with $\int_V d^3x\, f_k(\mathbf{x})$ and find (summation over repeated indices is implied):

$$\varphi_{Ak} = \int_0^f dt\, q_i(t)\Gamma_{ijk}q_j^\dagger(t) + z_A \int_0^{\alpha_A} dt\, q_{Ai}(t)\Gamma_{ijk}q_{Aj}(\alpha_A - t), \tag{3.20a}$$

$$\varphi_{Bk} = \int_f^1 dt\, q_i(t)\Gamma_{ijk}q_j^\dagger(t) + z_B \int_0^{\alpha_B} dt\, q_{Bi}(t)\Gamma_{ijk}q_{Bj}(\alpha_B - t), \tag{3.20b}$$

$$\delta_{k1} = \varphi_{Ak} + \varphi_{Bk}, \tag{3.20c}$$

$$w_{Ak} - w_{Bk} = \chi N(\varphi_{Bk} - \varphi_{Ak}), \tag{3.20d}$$

$$2\xi_k = w_{Ak} + w_{Bk} + \chi N\delta_{k1}, \tag{3.20e}$$

where

$$\Gamma_{ijk} = \int_V dx\, f_i(\mathbf{x})f_j(\mathbf{x})f_k(\mathbf{x}) \tag{3.21}$$

is a dimensionless tensor.

Since the functions $f_k(\mathbf{x})$ are eigenfunctions of the Laplacian, the diffusion equations (3.12) become:

$$\frac{\partial}{\partial t}q_{Ak}(t) = A_{kj}q_{Aj}(t), \tag{3.22a}$$

$$\frac{\partial}{\partial t}q_{Bk}(t) = B_{kj}q_{Bj}(t), \tag{3.22b}$$

$$\frac{\partial}{\partial t}q_k(t) = \begin{cases} A_{kj}q_j(t) & \text{if } t < f, \\ B_{kj}q_j(t) & \text{if } t > f, \end{cases} \tag{3.22c}$$

$$-\frac{\partial}{\partial t}q_k^\dagger(t) = \begin{cases} A_{kj}q_j^\dagger(t) & \text{if } t < f, \\ B_{kj}q_j^\dagger(t) & \text{if } t > f, \end{cases} \tag{3.22d}$$

where the matrices A and B are:

$$A_{ij} = -\frac{Na^2}{6D^2}\lambda_i - w_{Ak}\Gamma_{ijk}, \tag{3.23a}$$

$$B_{ij} = -\frac{Na^2}{6D^2}\lambda_i - w_{Bk}\Gamma_{ijk}. \tag{3.23b}$$

What has been achieved is that the set of equations (3.13) for the *functions* $\varphi_A(\mathbf{x})$ etc. at *all* $\mathbf{x}$ has been transformed into a *discrete* set of equations in the *coefficients*. The partial differential equations (3.12) have similarly been transformed into sets of linear, first-order *ordinary* differential equations. Their solutions take the following form:

$$q_{Ak}(t) = T_{A,k1}(t), \tag{3.24a}$$

$$q_{Bk}(t) = T_{B,k1}(t), \tag{3.24b}$$

$$q_k(t) = \begin{cases} T_{A,k1}(t) & \text{if } t < f, \\ T_{B,kj}(t-f)T_{A,j1}(f) & \text{if } t > f, \end{cases} \tag{3.24c}$$

$$q_k^\dagger(t) = \begin{cases} T_{A,kj}(f-t)T_{B,j1}(1-f) & \text{if } t < f, \\ T_{B,k1}(1-t) & \text{if } t > f, \end{cases} \tag{3.24d}$$

where the matrices $T_A(t) = \exp(At)$ and $T_B(t) = \exp(Bt)$ transfer q a distance t along an A- or B-portion of a chain, respectively.

Equations (3.24) are evaluated by diagonalization: Let U and V be the matrices of eigenvectors of A and B, respectively. Since A and B are real and symmetric, U and V are orthogonal, *i.e.* $U_{ij}^{-1} = U_{ji}$. We can now perform the integrals in (3.20) explicitly. Consider the first term in (3.20a) (*i.e.* the contribution to the total A-monomer density from the A-block of the copolymer):

$$\int_0^f dt\, q_i(t)\Gamma_{ijk}q_j^\dagger(t) = \int_0^f dt\, T_{A,i1}(t)\Gamma_{ij}^k T_{A,jl}(f-t)T_{B,l1}(1-f) \tag{3.25}$$

Note that in general $T_{ij} = U_{ip}^{-1}\sigma_{pq}U_{qj}$, where σ_{pq} is the diagonal matrix of eigenvalues of T.

We first evaluate $q_i(t)$:

$$\begin{aligned} q_i(t) &= T_{A,i1}(t) \\ &= U_{ip}e^{\alpha_p t}U_{pi}^{-1} \end{aligned}$$

Here, $e^{\alpha_p t}$ is the element σ_{pp} in the diagonal matrix σ formed by the exponentials of the eigenvalues α_p of A times the scalar parameter t.

$$\begin{aligned} &= U_{ip}U_{1p}e^{\alpha_p t} \\ &= c_{ip}e^{\alpha_p t} \qquad\qquad c_{ip} = U_{ip}U_{1p} \end{aligned}$$

Now we evaluate $q_j^\dagger(t)$ (with β_n being the eigenvalues of B):

$$\begin{aligned} q_j^\dagger(t) &= T_{A,jl}(f-t)T_{B,l1}(1-f) \\ &= U_{jm}e^{\alpha_m(f-t)}U_{ml}^{-1}V_{ln}e^{\beta_n(1-f)}V_{n1}^{-1} \\ &= U_{jm}U_{lm}e^{\alpha_m(f-t)}V_{ln}V_{1n}e^{\beta_n(1-f)} \\ &= U_{jm}U_{lm}e^{\alpha_m(f-t)}d_l \qquad\qquad d_l = \sum_n V_{ln}V_{1n}e^{\beta_n(1-f)} \\ &= c_{jm}^\dagger e^{\alpha_m(f-t)} \qquad\qquad c_{jm}^\dagger = U_{jm}\sum_l U_{lm}d_l. \end{aligned}$$

In terms of c and $c^\dagger$ expression (3.25) is:

$$c_{ip}\Gamma_{ij}^k c_{jm}^\dagger \int_0^f dt\, e^{\alpha_m f}e^{(\alpha_p-\alpha_m)t}. \tag{3.26}$$

The integral evaluates to $E_{pm} = \frac{e^{\alpha_p f}-e^{\alpha_m f}}{\alpha_p-\alpha_m}$ if $\alpha_p \neq \beta_m$ and to $E_{pm} = fe^{\alpha_m f}$ otherwise. Now, expression (3.26) can be evaluated by three consecutive matrix multiplications, *i.e.* the integration of the diffusion equation (3.12c) has been reduced to a sequence of successive algebraic operations.

Given a set of Fourier coefficients for the fields w_{Ak}, w_{Bk}, the self-consistent equations (3.20) can be evaluated by the procedure outlined above. The equations are then solved, either by a multidimensional Newton-Raphson method [201] or by the multidimensional secant method due to Broyden [39]. It is found that the latter is faster by about a factor of 5.

Once the solutions of the self-consistent equations are known, we can evaluate the free energy, which in Fourier space takes the final form:

$$-Nv\beta F = q_1(1) + z_A q_{A1}(\alpha_A) + z_B q_{B1}(\alpha_B) + \frac{1}{2}(w_{A1}+w_{B1}-\chi N) + \chi N\sum_k \varphi_{Ak}\varphi_{Bk}$$

Finally, the free energy is minimized with respect to the length scale D of the ordered structure, appearing explicitly in (3.23). By comparing the value of the free energy for different phases, one constructs the phase diagram. In addition to the disordered (DIS) phases, we are interested in the general behavior of the lyotropic ones. We consider only the simple, "classical" ones: lamellar (LAM), cylinders arranged in a hexagonal lattice (HEX), and spheres in a body-centered-cubic lattice (BCC) Figure 1.2. It is known that most of the other phases which could arise, such as the gyroid and the hexagonally perforated lamellar phase [70, 216, 18, 82, 258, 76, 75], would be located in a narrow region between the lamellar and cylindrical phases.

Density profiles of strongly swollen phases are far from sinusoidal and require a large number of basis functions to be represented well. However we find that the value of the free energy is relatively insensitive to the number of terms kept. Additionally we find that for strongly swollen phases, the minimum of the free energy as a function of D is extremely broad, so that phases with very different length scales and compositions are nearly equal in free energy. Since the composition of a phase is calculated with far less accuracy than its free energy, we draw the boundaries of strongly swollen phases with dashed lines in all figures.

3.3 Other Mean Field Theories

3.3.1 Weak Segregation Limit

Leibler's weak segregation theory is an example of a Landau Theory, *i.e.* the free energy is expanded in powers of the order parameter. A good order parameter to describe the microphase separation transition is *e.g.* :

$$\psi(\mathbf{r}) = \varphi_A(\mathbf{r}) - \langle \varphi_A \rangle \,, \tag{3.27}$$

the deviation of the local A-monomer density from its ensemble (or sample) average. The free energy in powers of the order parameter ψ corresponds to the "effective

potential" in field theory parlance and the coefficients correspond to the "vertex functions", *i.e.* they can be obtained from the order parameter correlation functions of the interacting theory [122, 3]. The correlation functions are now obtained from the single chain correlation functions (Section 2.1.1.3) under the assumption that the Gaussian behavior of the chains in the melt does persist even when the interaction χ between A- and B-monomers is switched on. The free energy thus has the following form:

$$\beta(F - F_{\text{hom}}) = \frac{1}{2}\sum_{\mathbf{q}} \Gamma_2(\mathbf{q})\psi(\mathbf{q})\psi(-\mathbf{q}) + \frac{1}{3!}\sum_{\substack{\mathbf{q}_1,\mathbf{q}_2,\mathbf{q}_3 \\ \mathbf{q}_1+\mathbf{q}_2+\mathbf{q}_3=0}} \Gamma_3(\mathbf{q}_1,\mathbf{q}_2,\mathbf{q}_3)\psi(\mathbf{q}_1)\psi(\mathbf{q}_2)\psi(\mathbf{q}_3) + \frac{1}{4!}\sum_{\substack{\mathbf{q}_1,\mathbf{q}_2,\mathbf{q}_3,\mathbf{q}_4 \\ \mathbf{q}_1+\mathbf{q}_2+\mathbf{q}_3+\mathbf{q}_4=0}} \Gamma_4(\mathbf{q}_1,\mathbf{q}_2,\mathbf{q}_3,\mathbf{q}_4)\psi(\mathbf{q}_1)\psi(\mathbf{q}_2)\psi(\mathbf{q}_3)\psi(\mathbf{q}_4), \tag{3.28}$$

where the Γ_k are the $\mathbf{q}$-dependent vertex functions.

The structure factor $S(\mathbf{q}) = 1/\Gamma_2(\mathbf{q})$ has the asymptotic behavior:

$$S(\mathbf{q}) = \begin{cases} \frac{2}{3}Nf^2(1-f)^2(qR_G)^2 & qR_G \ll 1 \\ 2Nf(1-f)/(qR_G)^2 & qR_G \gg 1 \end{cases} \tag{3.29}$$

and close to the order/disorder-transition it is strongly peaked at a particular value q^* of $\mathbf{q}$. Consequentially, all modulation modes of the order parameter with $|\mathbf{q}| \neq q^*$ are strongly suppressed. The sums in (3.28) can therefore be restricted to $\mathbf{q}$ of length q^*.

Be evaluating the free energy (3.28) for different symmetries (*i.e.* restricting the set of $\mathbf{q}$ in (3.28) to vectors of the reciprocal lattice of the desired space group), Leibler constructed a mean field phase diagram for the pure diblock copolymer, which is very similar to the phase diagram obtained from the full self-consistent field theory (Figure 4.1). For $\chi N > 10.495$, ordered phases appear, of lamellar symmetry for roughly symmetric diblocks, of hexagonal, and body-centered-cubic symmetry for more asymmetric ones. For the case of unbroken symmetry (*i.e.* a copolymer with blocks of equal

length), the transition is continuous, first-order otherwise. The continuous transition at the critical point ("Leibler's point"):

$$\chi N = 10.495 \tag{3.30a}$$

$$f = 0.5 \tag{3.30b}$$

is peculiar in that the order parameter has diverging fluctuations on a whole sphere $|\mathbf{q}| = q^*$ and not, as is usual, at a single point $\mathbf{q} = 0$. Leibler's critical point is therefore in the Brazovskii universality class [20].

Close to the critical point, where the order parameter is small, the results of the weak segregation approximation agree exactly with those of the self-consistent field theory (Section 3.2), as would be expected for a Landau theory.

Leibler's weak segregation theory is of great importance because it provides a microscopic Landau free energy, and therefore allows further systematic analytical treatment. Several workers [142, 74, 38, 159, 37, 107] extended Leibler's original treatment to include higher harmonics of the dominant wave vector. Others investigated the structure and repeat distance of the ordered phases for diblocks [195] and ABC-triblocks [189, 263], or the behavior of copolymers at interfaces [126, 154] or hard walls [59]. Since the weak segregation theory provides an analytical expression for the correlation functions and the structure factor, it has been applied to study the structures of microemulsions in polymer blends [91, 21, 105]. Furthermore, the q-dependent expression for the free energy (3.28) has been the starting point for one of the most influential fluctuation calculations [61] (see below).

3.3.2 Strong Segregation Limit

Semenov's strong stretching approximation [222] assumes that the repulsion between unlike monomers is so strong that each microdomain consists purely of A- or B-monomers. The junction point of the A- and B-blocks in the copolymer are consequentially confined to the infinitely narrow interface, and the blocks form dense

brushes on either side of the interface. Because the brushes are dense, the blocks are stretched strongly away from the interface (c.f. Section 2.1.3.2). Under these assumptions, the number of configurations available to each polymer is strongly reduced and it is possible to replace the sum over all configurations in the partition function by the most probable one. In other words, the free energy

$$\beta F = \int dt \left(\frac{\partial \mathbf{r}}{\partial t}\right)^2 + U\left[\mathbf{r}(t)\right] \tag{3.31}$$

(c.f. equation (2.79)), consisting of an entropic stretching and an enthalpic interaction part is minimized with respect to the trajectory $\mathbf{r}(t)$ under the constraints of local incompressibility ($\int dt \left(\frac{\partial \mathbf{r}}{\partial t}\right)^{-1} = 1$) and inextensibility of the chain ($\int dt \left(\frac{\partial \mathbf{r}}{\partial t}\right) = N$), for the desired symmetry.

The results of the strong stretching approximation agree qualitatively with the self-consistent field theory in the limit $\chi N \to \infty$, but not quantitatively. This failure of the strong stretching theory has been explained by Matsen and Bates [149, 152] through a detailed comparison of the different contributions to the free energy in the strong segregation and in the self-consistent theory. The free energy (3.31) contains only the configurational entropy and the enthalpic cost of the interface. Both of these are well approximated by the strong stretching theory. However, the assumption that all junction points lie at the interface turns out to be too restrictive. Even for very strong segregation, the junctions have some freedom of movement, giving rise to both a translational entropy of the junction point, as well as to an enthalpic contribution from increased number of AB-contacts, since now the microdomains do not consists *purely* of A- or B-monomers. The strong stretching approximation misses out on both these effects. However, as a non-perturbative approach that applies in the limit strong segregation *and* allows analytical treatment, it has been enormously influential [175]. Besides the original treatment of the pure diblock [222] it has been applied to complex phases [133, 196, 197], to blends [224, 260], triblocks [264, 143] and surfaces [223, 225, 244, 246, 247].

3.3.3 Variations

Besides the continuum formulation of the self-consistent field theory described in Section 3.2, there exist variations of the same self-consistent theory on a lattice [52, 210, 211]. These calculations agree well with those of the continuum theory, but are essentially restricted to situations, in which the density profiles vary in one dimension only, *e.g.* planar interfaces [210, 231, 229], flat brushes [52] or cylindrical or spherical micelles [230, 124]. It also has been applied to lamellar phases [232, 156].

A very interesting variant of the self-consistent field theory, which does not assume Gaussian chains, is the one of Gelbart, Ben-Shaul and Szleifer [239, 24, 25, 26]. Instead of obtaining the single chain partition functions (3.11) and densities (3.13a)–(3.13b) from the diffusion equation (3.12), the fields are obtained by randomly sampling a representative subset of all possible chain configurations. The advantage of this method is that it can be applied to chains of arbitrary architecture, for example to chains containing a rigid section [186]. Specifically, the dependence of the phase diagram on details of the architecture (*e.g.* the position along the chain of a double bond etc.) can be worked out [184].

Whether in the lattice or in the continuum formulation, these approaches yield a correct, self-consistent description of the ordered microphases, with the mean field approximation being the only approximation made, besides those inherent in the model adopted (the sampling approach gives considerable freedom even on this point). Several calculations have been reported that include additional approximations, some of them of questionable validity. Several authors [10, 11], solved the self-consistent field theory for homopolymer/diblock blends, but restricted their attention to the first harmonic of the lamellar phase, *i.e.* assumed cosine-shaped density profiles. As the complete treatment [102] and Chapter 4 shows, other geometries besides the lamellar one are very important and occupy large portions of the phase diagram. Similar assumptions about the shape of the density profile have also been included

into variations of Leibler's weak segregation theory [165, 131].

The assumption of infinite chain length in (3.12) allows one to ignore the variation of the end-segment distribution functions (3.11) with t, the position along the chain. In the so-called narrow interface approximation [86], the chain connectivity of the diblock is ignored, and the interfaces between microdomains are treated as if they were interfaces between immiscible homopolymer bulk phases. Papers employing this approximation continue to appear [199].

3.4 Fluctuation Corrections

Several approaches have been developed to estimate the effect of fluctuations on the microphase behavior in copolymer melts.

The most influential has been Fredrickson's and Helfand's [61] study of fluctuations close to Leibler's critical point (Section 3.3.1). Their starting point is the assumption that the expression (3.28), in particular the expressions for the vertex functions Γ_i, are the correct form of the microscopic Hamiltonian of the polymeric system. Leibler's identification of this Hamiltonian, evaluated for the average order parameter ψ, then amounts to the mean field approximation of $e^{-\beta F} = \mathrm{Tr}\, e^{-\beta H}$. Furthermore, because $1/\Gamma_2(\mathbf{q})$ is strongly peaked at $|\mathbf{q}| = q^*$, Leibler disregarded wavevectors of different magnitude. Fredrickson and Helfand, following Brazovskii [20], went a step further by expanding Γ_2 to second order about the maximum, so that the Hamiltonian now becomes:

$$H = \frac{v}{2}\int \frac{d^3q}{(2\pi)^3}\,(\tau + (q-q^*))^2\,\psi(\mathbf{q})\psi(-\mathbf{q}) + \frac{\mu}{3!}\int \frac{d^3q_1}{(2\pi)^3}\frac{d^3q_2}{(2\pi)^3}\frac{d^3q_3}{(2\pi)^3}\,\delta(\mathbf{q}_1+\mathbf{q}_2+\mathbf{q}_3)\psi(\mathbf{q}_1)\psi(\mathbf{q}_2)\psi(\mathbf{q}_3) + \frac{\mu}{3!}\int \frac{d^3q_1}{(2\pi)^3}\frac{d^3q_2}{(2\pi)^3}\frac{d^3q_3}{(2\pi)^3}\frac{d^3q_4}{(2\pi)^3}\,\delta(\mathbf{q}_1+\mathbf{q}_2+\mathbf{q}_3+\mathbf{q}_4)\psi(\mathbf{q}_1)\psi(\mathbf{q}_2)\psi(\mathbf{q}_3)\psi(\mathbf{q}_4), \quad (3.32)$$

where $\tau = (\chi_s N - \chi N)$ is the distance from the mean field spinodal $\chi_s N$. We follow the original treatment [61], which ignored the angle dependence of the cubic and

quartic coefficients. In later studies [12], the full expression for the vertex functions has been incorporated into the theory.

The vertex functions are now recalculated from the modified Hamiltonian (3.32), and the q-dependence is integrated out. In this way, a free energy functional is obtained, formally equal to the mean field free energy (3.28), but the coefficients have been modified by the fluctuations. In particular, one finds that the fourth order coefficient becomes negative *outside* the spinodal, *i.e.* where the second order coefficient is positive. Fluctuations therefore induce a first-order transition, in place of the continuous transition found in mean field theory. The discontinuity of the order parameter at the transition is proportional to $N^{-1/6}$ and vanishes for $N \to \infty$. The order/disorder transition is shifted away from its mean field location to higher values of χN (*i.e.* to lower temperatures) by an amount proportional to $N^{-1/3}$. Another effect correctly predicted by this theory is the shift in the position and the height of the peak of the structure function [17, 16].

The overall effect on the phase diagram (Figure 4.1) of inclusion of fluctuations through the method due to Fredrickson and Helfand is that the region of stability of the ordered phases is cut off almost horizontally, at some value of χN greater than, but close to, Leibler's critical point. In particular, "windows" of transitions open up, from the lamellar and hexagonal [61] and the gyroid [200] phase directly to the homogeneous state, in accord with experiments [18, 158].

We can summarize the results of the Brazovskii-Fredrickson-Helfand theory by stressing the following three points:

1. The inclusion of fluctuations drives the order/disorder transition for the symmetric diblock first order.

2. The chain length N is a third scaling field in the full theory, besides the two fields χN and f, present also on the mean field level.

3. The shift in the transition temperature and the discontinuity of the order parameter across the transition are proportional to negative powers of N and vanish as $N \to \infty$: mean field theory becomes exact for infinitely long chains.

Similar results have been obtained in a very different approach, based on liquid state integral equation theories for polymeric fluids [220, 219, 221], and also through a field theoretic diagrammatic expansion of (3.1) [235].

Because the Fredrickson-Helfand theory provides an analytic expression for a fluctuation corrected thermodynamic potential, it has been applied to study a variety of effects, *e.g.* the kinetics of nucleation of lamellar phases form the disordered state [60, 90], the elastic response of an ordered lamellar (smectic) phase [4] and the effects of surface induced ordering of copolymer melts next to hard walls [176].

So far, we only considered fluctuations around the disordered phase close to the order/disorder transition. Very recently, a series of studies [261, 227, 120] investigated small amplitude fluctuations around the *ordered* state in terms of Gaussian fluctuations around the exact mean field solution. The authors were able to calculate the most unstable (*i.e.* the most easily thermally excited) modes for the lamellar, hexagonal and body-centered-cubic phases. The anisotropic scattering functions obtained are in agreement with experiments [216].

Computer simulations of polymer melts, finally, are possible but very difficult because of the enormous time scales necessary to equilibrate dense systems of long chains. Recently two studies of homopolymer/diblock blends appeared [121, 185] that compute phase diagrams including ordered phases. We will refer to them in Chapter 4 in comparison with our mean field results.

Chapter 4

INVESTIGATION OF THE MICROPHASE BEHAVIOR IN HOMOPOLYMER/DIBLOCK BLENDS

sectionIntroduction

Systems containing block copolymers are interesting due to their ability to cause ordered phases of various symmetries to form spontaneously [158]. Besides being of both fundamental and applied interest in their own right, polymer mixtures provide systems which are well-characterized, both experimentally and theoretically, with which to study the phenomenon of self-assembly, a phenomenon also displayed by lipids and short-chain surfactants.

The behavior of a melt of pure AB-diblock is rather well understood [125, 151]. At sufficiently small values of the effective interaction parameter χN, where χ is the dimensionless incompatibility between unlike segments, and N is the number of statistical segments per chain, the melt is disordered. As χN is increased, either by lowering the temperature or by increasing the chain length, the incompatibility causes the system to order. Because of the connectivity of the blocks, there can be no macroscopic phase separation into two phases of like components. Instead, the melt undergoes a microphase separation characterized by extensive amounts of internal interface which separate coherent regions of A monomer from B. The copolymer chains straddle the interfaces forming a "brush" on either side. The symmetry of the ordered phase is determined by the architecture of the diblock, that is, the fraction f of it which is comprised of A monomer. In an almost symmetric diblock, the cost to stretch either block is nearly the same, with the consequence that the system forms

the flat interfaces of lamellar phases. However if one of the blocks is sufficiently longer than the other, a curved interface is formed, with the longer block on the outside. This allows the longer block to increase its configurational entropy which more than compensates for the cost of stretching of the shorter block on the inside of the curved interface (c.f. Figure 4.1).

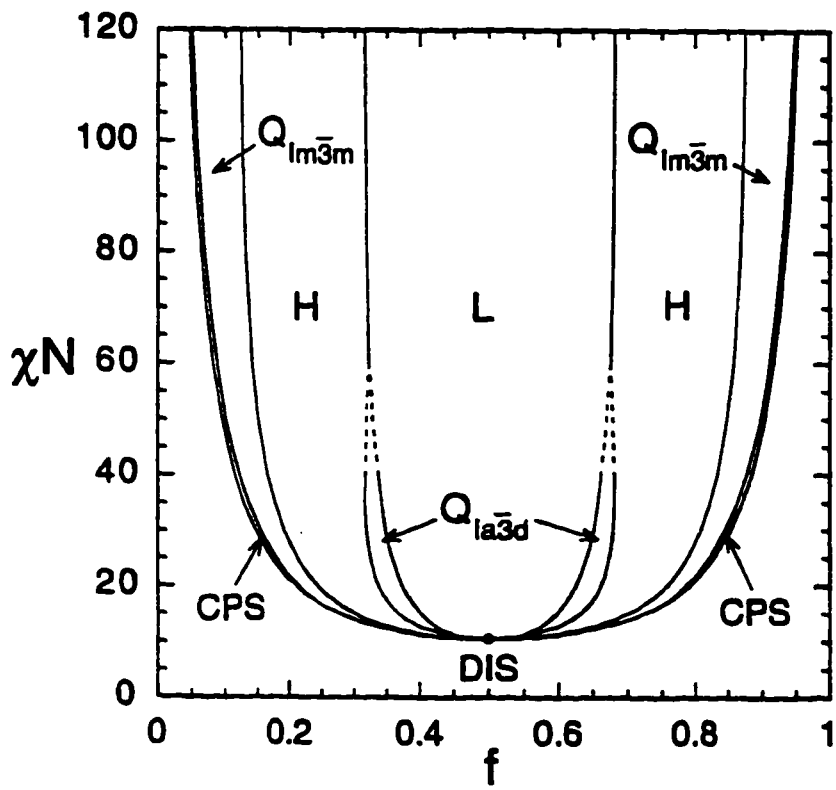

Figure 4.1: Phase diagram for the pure diblock copolymer in the effective interaction parameter χN versus fraction f of A-monomers in the chain. Note that χN varies inversely proportionally with temperature. The lamellar phase is denoted L, the hexagonal phase H, and the body-centered-cubic phase by Q_{Im3m} and the gyroid phase by Q_{Ia3d}. Notice that for intermediate to strong segregation there is a narrow region of close packed spheres (hexagonally close packed of face-centered-cubic), denoted CPS, between the body-centered-cubic and the disordered phase. The dashes indicate extrapolated phase boundaries that could not be calculated exactly. After [151].

Our understanding of blends containing diblock copolymer is far less complete,

although much progress has been made recently [146, 145, 224, 260]. The simplest system consists of an AB-diblock blended with A-homopolymer, of chain lengths N and N_A, respectively. The fact that this system is now a true two-component mixture permits two behaviors absent in the pure diblock case. On the one hand, the blend can phase separate into two distinct bulk phases, each of which can be microstructured. On the other, the microstructure can be swollen by added homopolymer. In the extreme case, this swelling can proceed indefinitely so that the period of the microstructure grows without limit. This leads to the complete unbinding of the ordered phase [145, 130, 101]. These additional behaviors take place in the enlarged parameter space of the binary blend which comprises not only the polymerization index N and fraction f of the diblock, but also the volume fraction φ of the homopolymer and its chain length $N_A = \alpha_A N$. The topology of the phase diagram is largely determined by the parameter α_A.

As noted above, the spontaneous curvature of a copolymer layer is determined by the composition parameter f. The ability of A homopolymer chains to enter a diblock layer is determined by the relative chain lengths, i.e. by α_A. This ability has been studied in systems of polymers grafted at one end to a surface and immersed in a homopolymer melt. It was found [33] that homopolymers longer than the chains in the brush are expelled from it ("dry" brush), while those which are shorter swell the brush ("wet" brush). This argument was later extended to several other situations; to brushes formed by diblocks assembled at an internal flat interface between coexisting bulk phases of immiscible homopolymers, to the curved interfaces of copolymer micelles [127, 128], and to the phase behavior of binary homopolymer/diblock blends in the strong segregation limit [224].

As the preceding discussion shows, the phase behavior of *blends* containing block copolymer is determined by many competing mechanisms. In general it is not possible to determine even the overall topology of the phase diagram without performing detailed calculations. Our aim is to provide a comprehensive catalogue of possible phase

diagrams of binary and ternary blends containing and AB-diblock and corresponding A- and B-homopolymers at all compositions and for the particularly interesting weak to strong segregation regime. Special emphasis is put on working out the dependence of the phase behavior on the chain length ratio α, but for the most part we will restrict ourselves to symmetric diblock copolymers (*i.e.* $f = 0.5$). Since we are mainly interested in the overall topology of the phase diagram, we restrict ourselves to the three "classical" phase: flat sheetlike lamellae (LAM), hexagonally arranged cylinders (HEX), and spheres on a body-centered-cubic lattice (BCC). The existence of these phases not only in polymer systems, but also in surfactant and lipid mixtures, is well established, as well as the fact that they occupy most of the ordered region of the phase diagram. Complex phases (c.f. Figure 1.2) are usually found only in a narrow region between the lamellar and the hexagonal phase at intermediate segregation [151].

In Section 4.1 we will discuss ternary blends, containing both A- and B-homopolymer in addition to the diblock at one particular value of the effective interaction parameter χN. In the following section (Section 4.2), we will describe the specially intricate phase diagram of the "symmetric system", comprising an AB-diblock and A- and B-homopolymers, all three components having the *same* degree of polymerization. Finally, in Section 4.3, we study the temperature dependence of the phase diagram in binary blends containing one homopolymer besides the diblock.

4.1 *Influence of Relative Chain Lengths in the Ternary System*[1]

4.1.1 Introduction

In the present section we will study the phase behavior of ternary blends containing both A- and B-homopolymers, as well as a diblock copolymer. Our motivation is threefold: First, the microphase separation behavior of ternary blends has received

[1] The material of this section has been published in *Macromolecules*, **30**, 1, 137–144 (1997)

little experimental attention [99, 79, 240, 137, 14]. Theoretical studies have concentrated either on the interfacial activity of diblock copolymers between coexisting bulk phases [97, 248], or on the phase diagram of disordered, homogeneous phases [21, 91]. The only theoretical study [10] focusing specifically on the microphase behavior of ternary blends was severely restricted by approximations made in addition to that of the mean-field theory. In particular the restriction to the lamellar phase as the only ordered structure, and its description by a single Fourier component caused some crucial features to be missed *e.g.* the complete unbinding. Thus our primary goal is to elucidate the general phase behavior of these important systems, particularly with regard to the lyotropic phases.

The parameter space of the ternary system AB, A,B is rather large as there are two independent chain length ratios, and two independently variable volume fractions, in addition to f and χN. The dependence of the phase behavior on these parameters is not obvious, and determining it experimentally is not practical. Thus our second goal is to produce a representative catalogue of typical phase diagrams, and to give physically motivated interpretations of them that permit the extension of our results to related systems.

Lastly it is of interest to make possible the comparison of ternary homopolymer, diblock melts with water, oil, and surfactant systems for which an enormous number of experimental phase diagrams has been assembled [46, 243]. The apparently universal character of self-assembly as manifested in the often observed sequence of lamellar to hexagonal to body-centered-cubic to disordered phases with increasing dilution of the amphiphile leads one to expect that information about short-chain amphiphiles can be gained from the study of polymers. The latter are far more easily described theoretically than the former. Of course with the synthesis of long chain surfactants [139, 259, 183, 238, 85, 2, 182], the distinction between the two systems is becoming increasingly artificial.

4.1.2 Results and Discussion

As explained above, the parameter space of the general three component system is too large to be mapped out completely. We restrict ourselves therefore to one value of the interaction parameter, $\chi N = 11.0$ and, with one exception shown in Figure 4.12, to a symmetric diblock, $f = 0.5$. This way we retain the feature characteristic of ternary blends, namely the competition between the two homopolymers, in general of unequal length, to swell the brush formed by the diblock at the internal interface. We elucidate this behavior by systematically varying $\alpha_A = N_A/N$ and $\alpha_B = N_B/N$. We discuss the influence of changing f and χN in Figure 4.12 and further below.

We employ the Gaussian chain model (Section 2.2.2) in Fourier space (Section 3.2.2). We solve the self-consistent equations (3.20) numerically to obtain the phase diagrams shown in Figure 4.2 through Figure 4.12. We present constant temperature cuts through the three component phase prism for eleven different systems of a diblock copolymer and corresponding homopolymers.

The diagrams in Figure 4.2 through Figure 4.11 are divided into two sequences. In Figure 4.2 through Figure 4.7, the A homopolymer is shorter than the diblock and its relative length is kept fixed at $\alpha_A = 0.3$, while that of the B homopolymer varies from $\alpha_B = 1.2$ to $\alpha_B = 0.1$. In the second sequence, Figure 4.8 through Figure 4.11, the B homopolymer is longer than the diblock and of fixed length $\alpha_B = 1.5$, while that of the A homopolymer varies from $\alpha_A = 1.5$ to 0.5.

We now discuss each phase diagram in turn. In Figure 4.2, we show the constant temperature phase diagram of a system with $\alpha_A = 0.3$ and $\alpha_B = 1.2$, in other words, the diblock is slightly shorter than the B homopolymer, while it is about three times as long as the A homopolymer. Regions of phase coexistence between an ordered and a disordered phase dominate the phase diagram. The B homopolymer is, for the most part, expelled from the microstructure formed by the diblock and is found in a uniform, disordered phase of large B homopolymer, and very small A

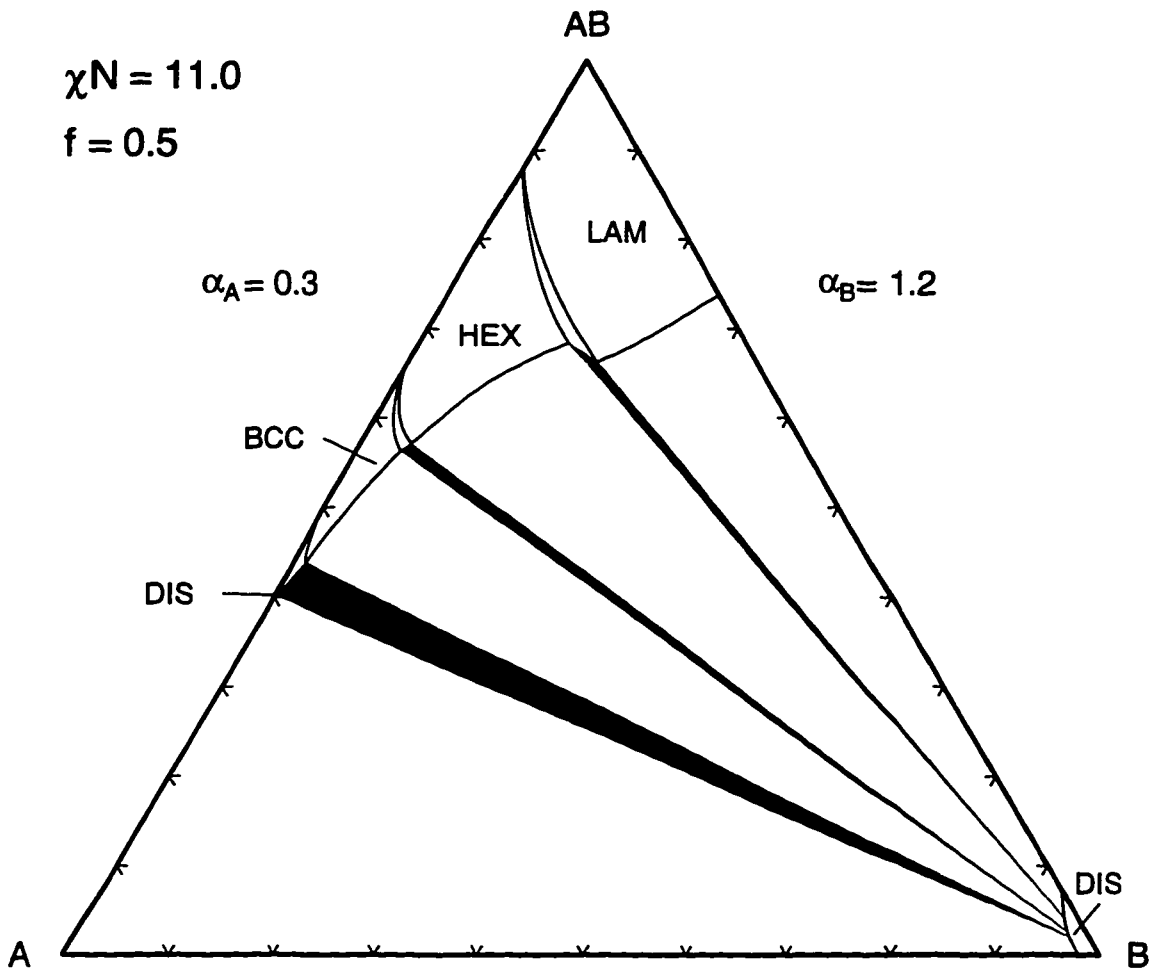

Figure 4.2: Constant temperature phase diagram of the ternary system of a symmetric AB-diblock copolymer of length N with an A homopolymer of length $\alpha_A = 0.3N$ and a B homopolymer of length $\alpha_B = 1.2N$. The value of the effective incompatibility parameter χN is 11.0. LAM denotes a lamellar phase, HEX hexagonally arranged cylinders, BCC spheres on a body centered cubic lattice and DIS homogeneous phases. Regions of three phase coexistence are shaded, biphasic regions are unlabeled. Phase boundaries of strongly swollen phases, that could not be located exactly, are shown with dashed lines. Note the almost B-free disordered phase on the left hand side.

homopolymer content, and which coexists with the diblock-rich, ordered phases. The volume fraction of B homopolymer in the ordered phases does not exceed 0.25.

This result can be understood as follows. If the large B homopolymer is added to

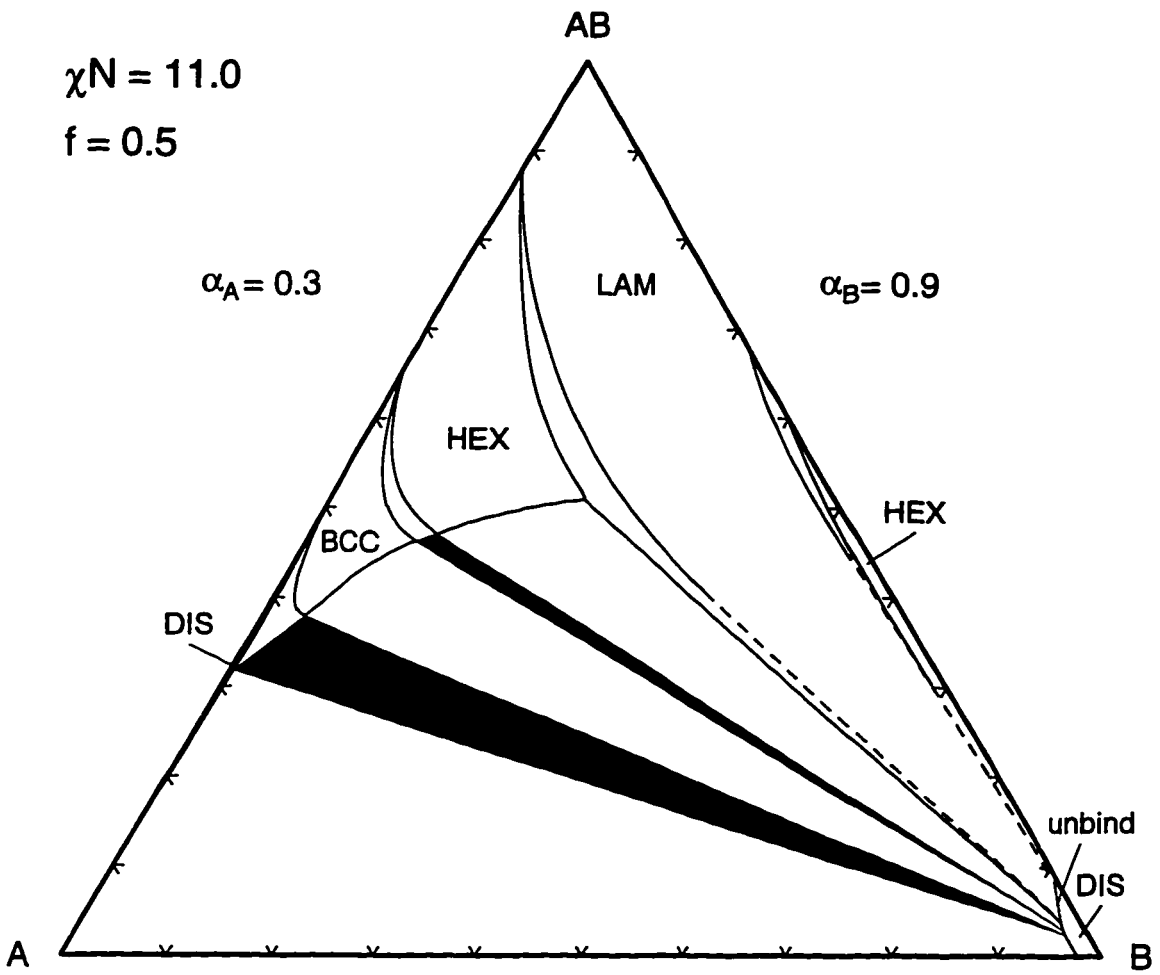

Figure 4.3: Phase diagram for a symmetric AB-diblock of length N with an A homopolymer of length $\alpha_A = 0.3N$ and a B homopolymer of length $\alpha_B = 0.9N$. The notation is that of figreffig:short1. Note the unbinding transition of the lamellar and hexagonal phases into the B-rich disordered phase.

an ordered microphase, it would preferentially assemble in the domains formed mainly by B segments of the diblock so as to reduce the number of unfavorable A, B contacts. However, since the size of those regions is comparable to the mean radius of gyration of the B block, it is smaller than the size of the undisturbed B homopolymer. Therefore, were a B homopolymer to enter the microphase, it would have to be compressed. The loss of configurational entropy entailed by such an arrangement is large, whereas the

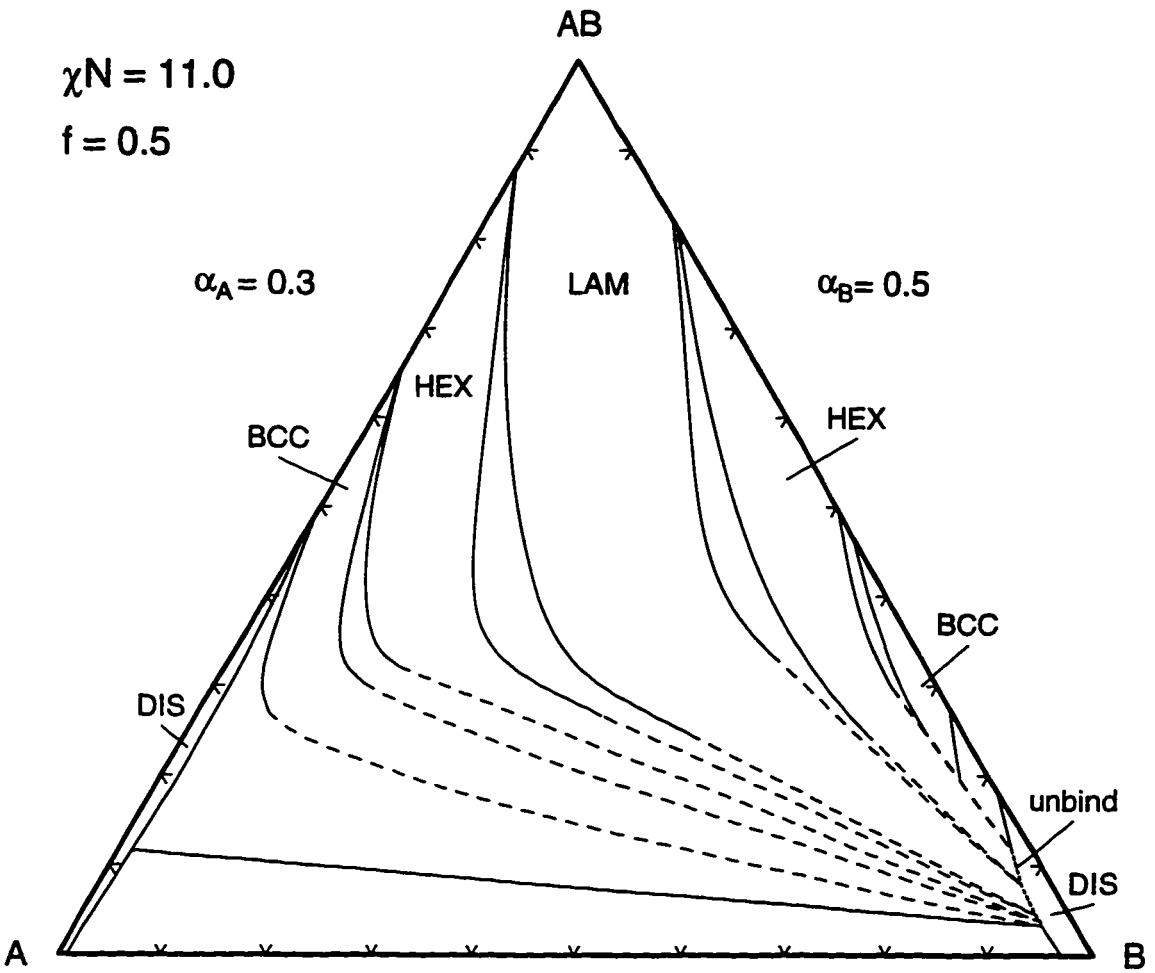

Figure 4.4: Phase diagram for a symmetric AB-diblock of length N with an A homopolymer of length $\alpha_A = 0.3N$ and a B homopolymer of length $\alpha_B = 0.5N$. The notation is that of Figure 4.2. Note the unbinding of strongly swollen ordered phases.

loss of entropy of mixing and of translation is small because of the larger size of the homopolymer. On the other hand, the B homopolymers, because of their relatively large length, lose little translational entropy by demixing form the diblock copolymer. The net effect is that the B homopolymer separates from the microstructure. For the same reasons, cylindrical and spherical domains accommodate less B homopolymer than does the lamellar phase.

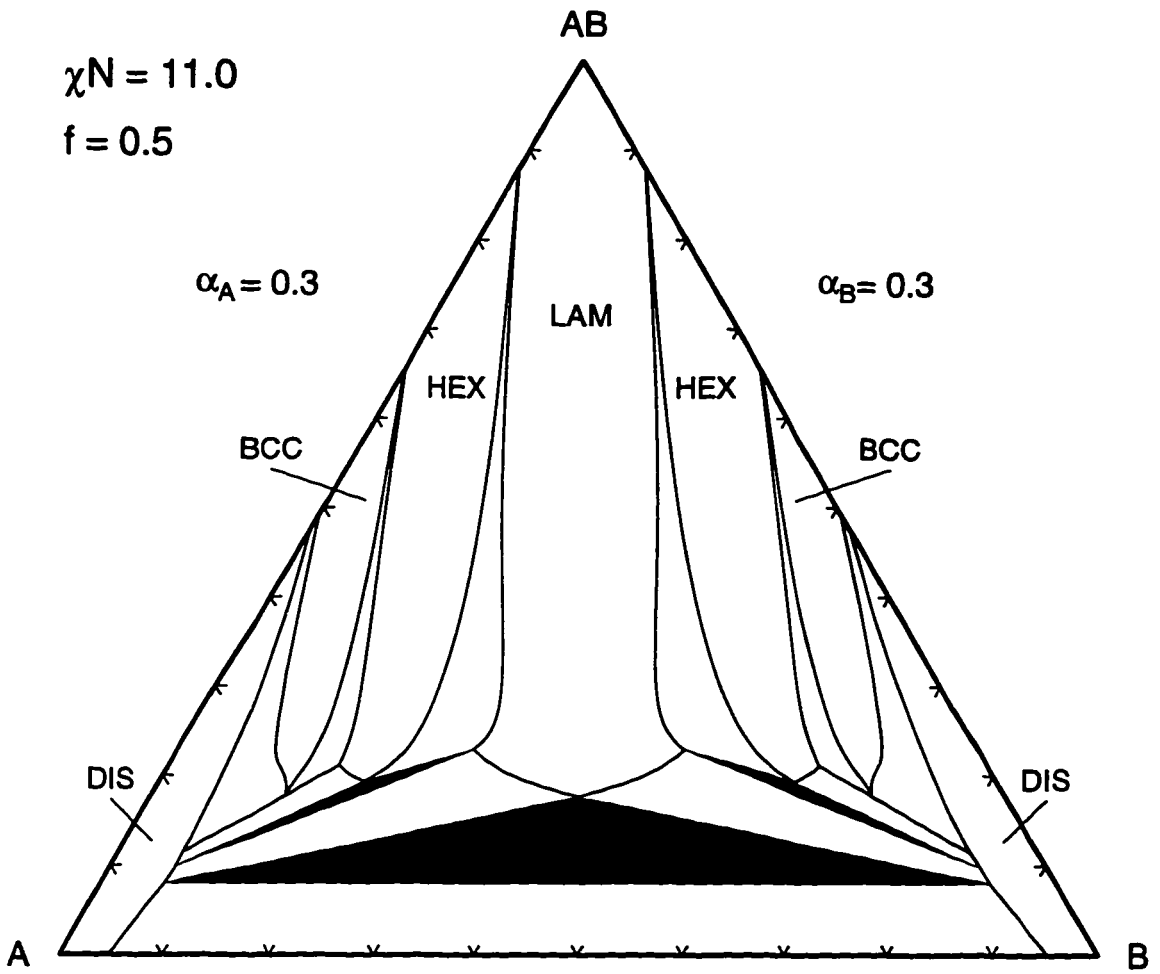

Figure 4.5: Phase diagram for a symmetric AB-diblock of length N with an A homopolymer of length $\alpha_A = 0.3N$ and a B homopolymer of length $\alpha_B = 0.3N$. The notation is that of Figure 4.2. Note that the phase boundaries of the BCC phase for copolymer volume fraction smaller than 0.2 may be affected by truncation error (c.f. text).

In contrast, the A homopolymers, being considerably shorter than the A block of the copolymer, are able to penetrate into the brush. In order to make room for the A homopolymers and to avoid stretching the A block of the copolymer, the layer of diblock bends with the convex side toward the A homopolymers. This "wedge" effect of short homopolymers gives rise to a non-vanishing preferred curvature of the

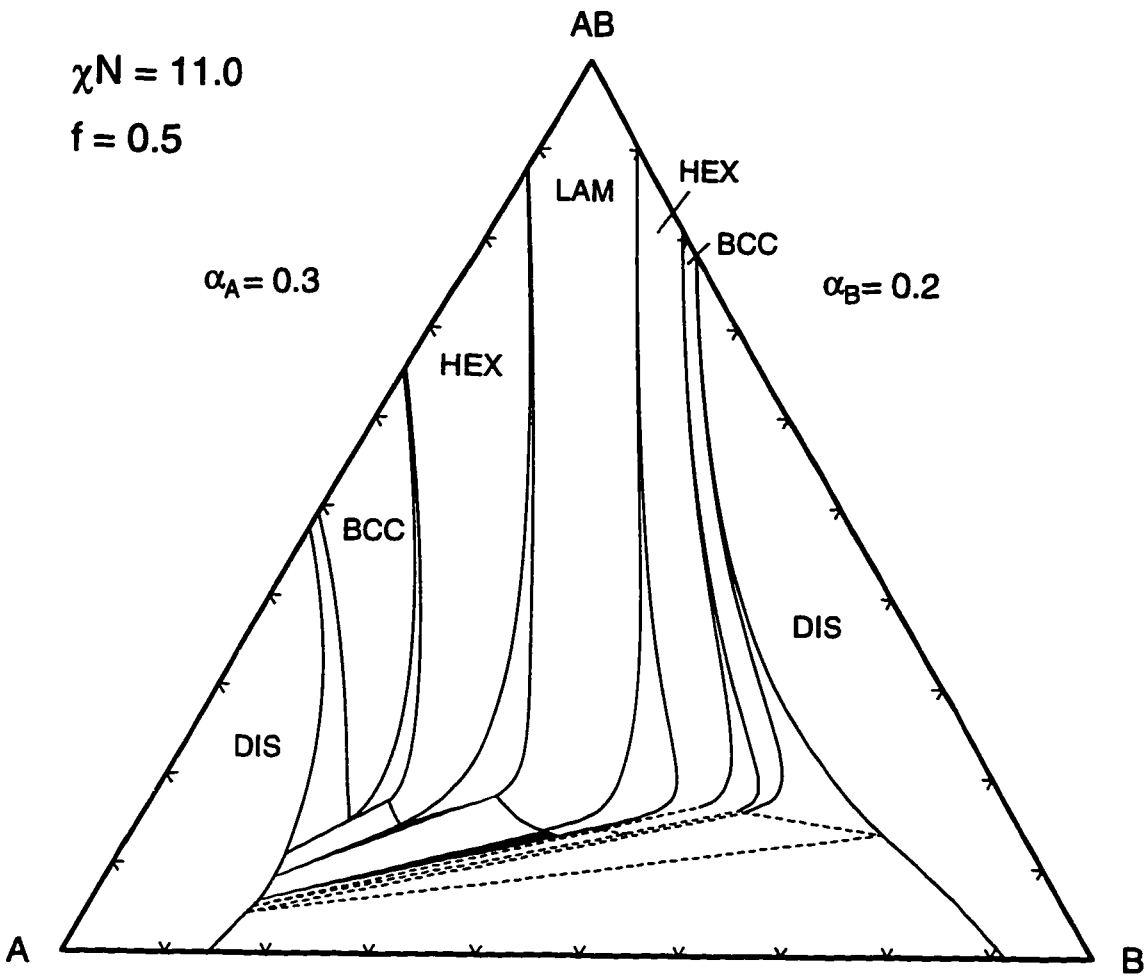

Figure 4.6: Phase diagram for a symmetric AB-diblock of length N with an A homopolymer of length $\alpha_A = 0.3N$ and a B homopolymer of length $\alpha_B = 0.2N$. The notation is that of Figure 4.2. Note the high copolymer concentration at the order/disorder transition on the right hand side.

copolymer layer, even for symmetric diblocks. On the binary AB, A side, it brings about the ubiquitous sequence of first-order transitions towards phases with greater mean curvature of their internal interfaces: lamellar to cylindrical to body-centered-cubic. In addition to this wedge effect, the short homopolymer is able to reduce the stretching energy of the diblock chains in additional ways that favor this sequence of phases. Due to their relatively large translational entropy, the short A homopolymer

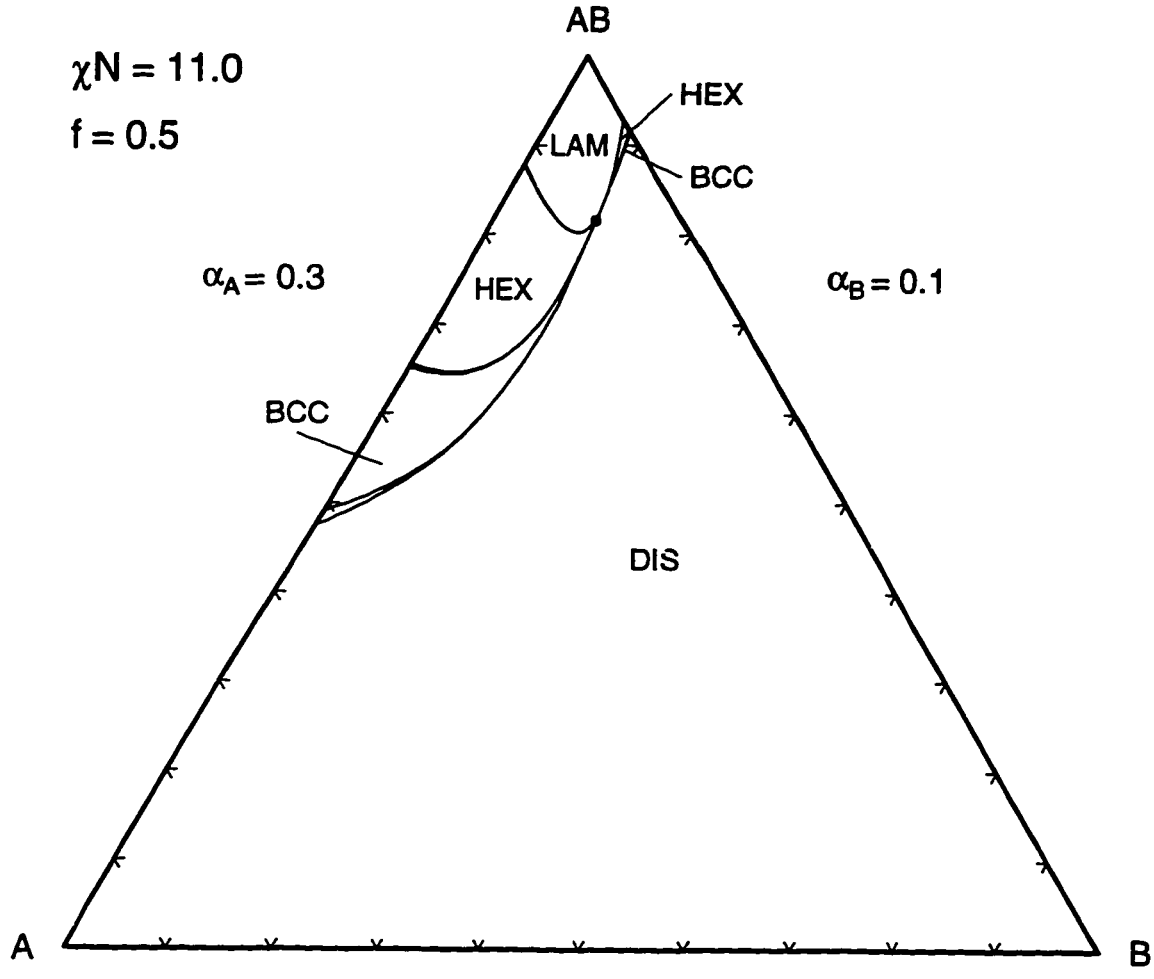

Figure 4.7: Phase diagram for a symmetric AB-diblock of length N with an A homopolymer of length $\alpha_A = 0.3N$ and a B homopolymer of length $\alpha_B = 0.1N$. The notation is that of Figure 4.2. The stability region of the B-rich BCC phase is too small to be resolved on the scale of this graph. The dot denotes Leibler's critical point. Note that the DIS/DIS demixing transition takes place at $\chi N = 12.44$ for this system.

chains enter the cores of cylindrical and spherical structures thus relieving some of the stretching of the B block. However this also increases the number of unfavorable A, B contacts. They also enter the interstices between cylindrical and spherical structures thus relieving the stresses induced by the inability of these units to fill space.

In the system shown in Figure 4.3, the B homopolymer is now shorter than the diblock, but comparable to it, $\alpha_B = 0.9$. This leads to entirely different behavior on the AB, B binary side of the phase diagram. The B homopolymer is no longer expelled from the microstructure as it is not larger than the B-rich regions of the pure diblock phase.In fact, the B domains of the lamellar phase accommodate any amount of B homopolymer which leads to a complete unbinding of the lamellar phase as the fraction of B homopolymer is increased. The complete unbinding is a continuous transition, as the wavevector, characterizing the lamellar phase vanishes without a jump. In this limit, the free energy density and the composition of the lamellar phase become equal to those of the disordered phase with the same chemical potential. This results from the fact that the slabs between lamellae become identical in composition to the disordered phase, and the lamellae, whose number per unit length vanishes, do not contribute an extensive term to the free energy. There is also a narrow region of A cylinders in a B-matrix, brought about by the wedge effect of the B homopolymers. The cylinders also unbind into the disordered phase on the B-rich side of the phase diagram.

On the A-rich side of the phase diagram where B blocks are in the center of cylinders and spheres, B homopolymer cannot swell the B blocks without changing the curvature of the internal interfaces, and this is prevented by the wedge effect of the short A homopolymer. As a result, the phase boundaries of A-rich BCC and HEX phases change little from Figure 4.2 to Figure 4.3, in contrast to the major change in the lamellar phase boundary.

In the system shown in Figure 4.4, the B homopolymer are now sufficiently short, $\alpha_B = 0.5$, to penetrate and swell the B block of the copolymer. Therefore the entire sequence of first-order transitions from lamellar to cylindrical to body-centered-cubic appears on the B-rich as well as the A-rich side. As the homopolymers are of comparable length, the lamellar phase, in which the "wedge" effects of both homopolymer are balanced, occupies a large region of the phase diagram. Only when the lamel-

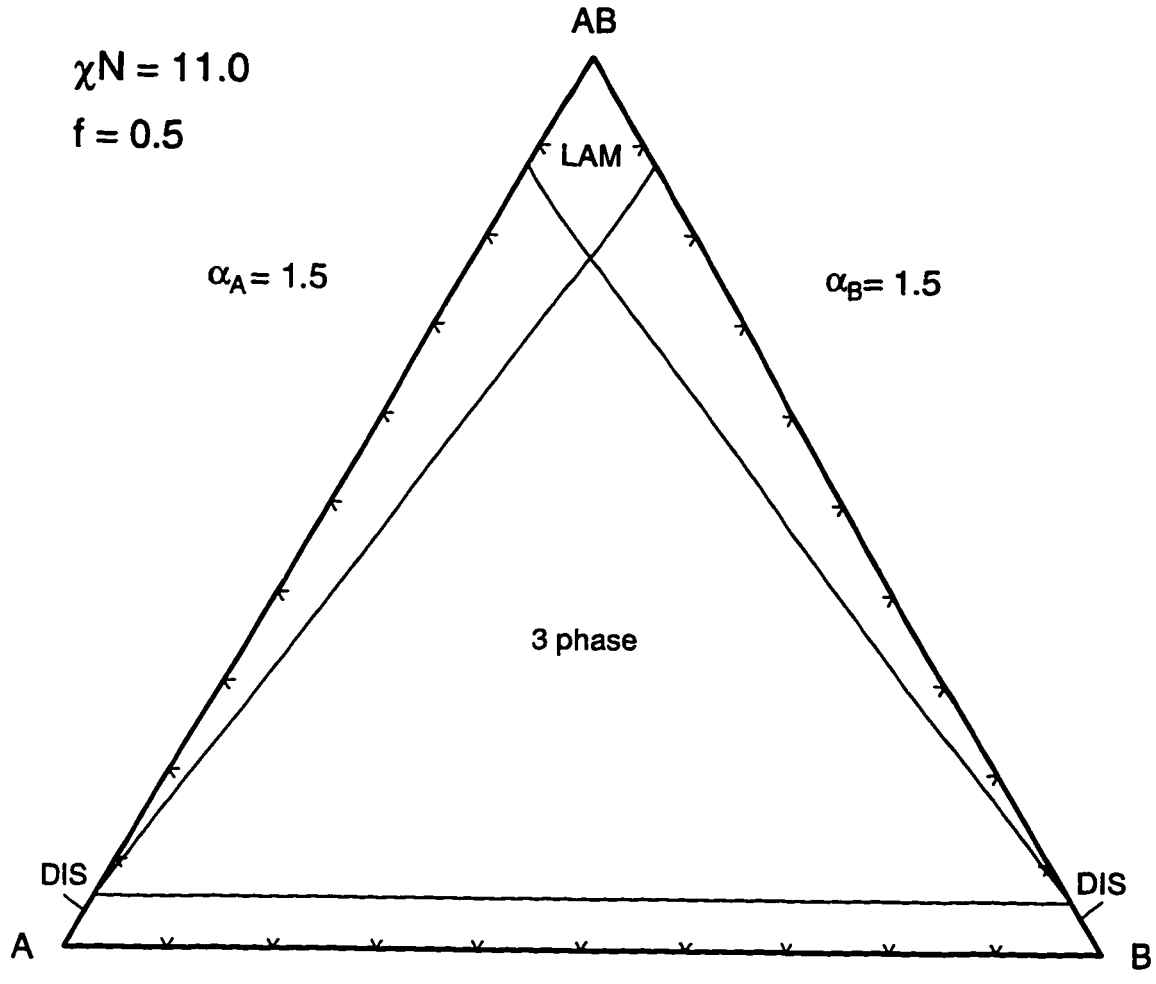

Figure 4.8: Phase diagram for a symmetric AB-diblock of length N with an A homopolymer of length $\alpha_A = 1.5N$ and a B homopolymer of length $\alpha_B = 1.5N$. The notation is that of Figure 4.2. Note the large region of three- phase coexistence between the lamellar and the A- and B-rich disordered phases.

lae are well separated does the different ability of A and B homopolymer to swell the respective brushes becomes apparent, and a larger fraction of the longer B homopolymer is necessary to balance the shorter A homopolymer. In contrast to the situation in Figure 4.3 where the B homopolymers were too long to be incorporated into the cores of the cylindrical and body-centered-cubic structures on the A-rich side of the diagram, the B homopolymers are now short enough to enter the cylindrical

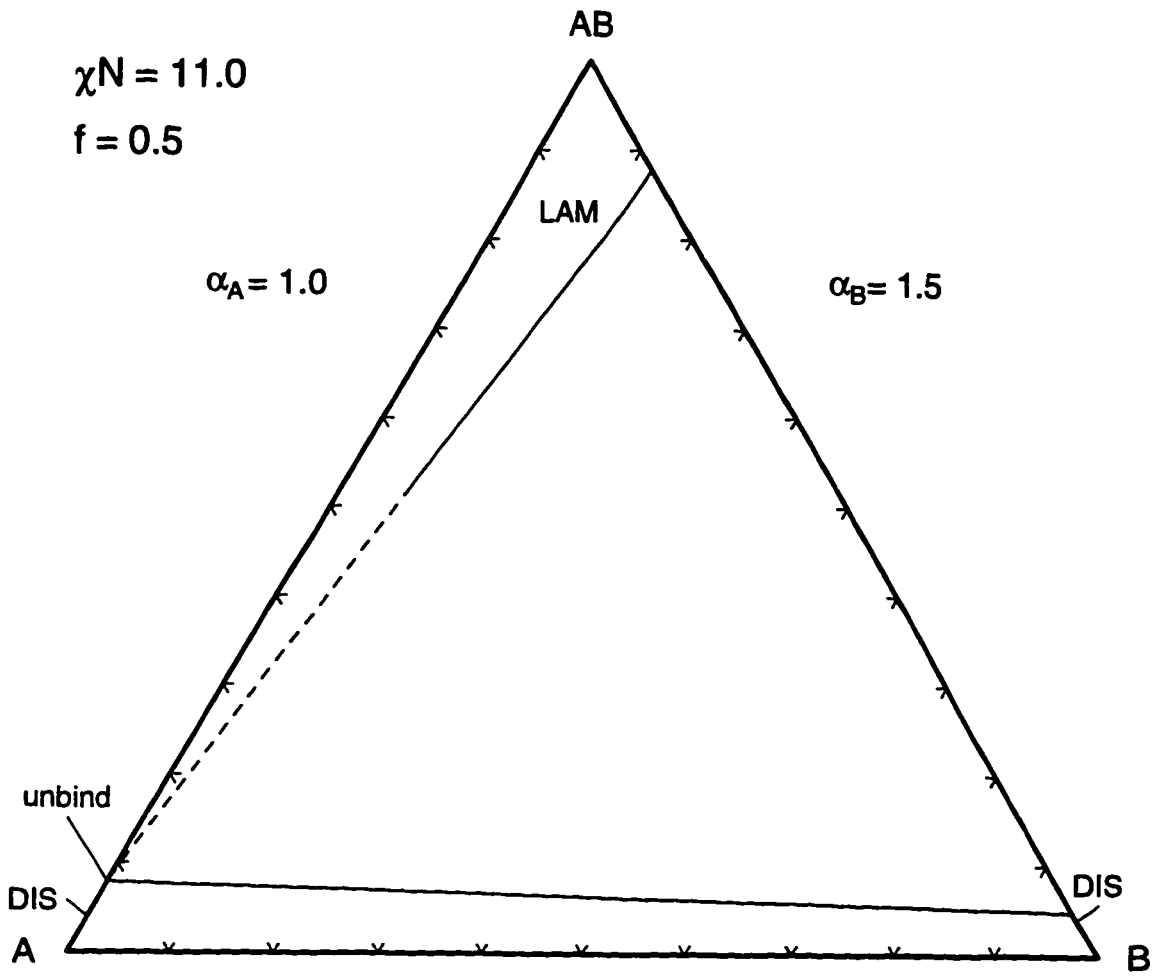

Figure 4.9: Phase diagram for a symmetric AB-diblock of length N with an A homopolymer of length $\alpha_A = 1.0N$ and a B homopolymer of length $\alpha_B = 1.5N$. The notation is that of Figure 4.2. The lamellar phase unbinds into the almost B-free disordered phase on the left hand side.

or spherical structures and relieve some of the stretching energy of the diblock layer.

The two homopolymers are of equal size in the system of Figure 4.5 with $\alpha_A = \alpha_B = 0.3$. A noteworthy feature is that while the ordered phases cannot be swollen very much on the binary sides of the diagram, even a small amount of the third component permits the structures to swell considerably. The reason is that on the A-rich side, for example, when A homopolymers enter the B cores to relieve stress,

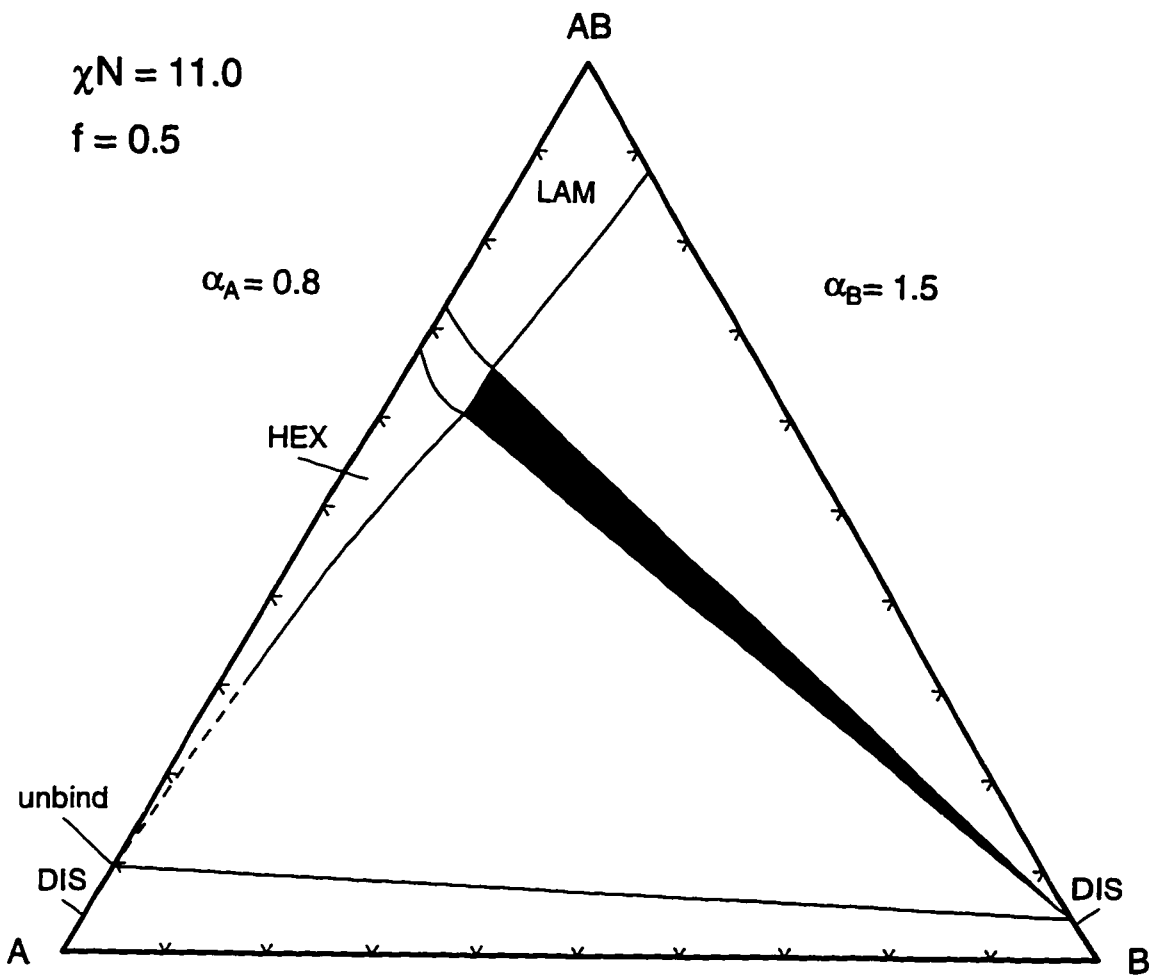

Figure 4.10: Phase diagram for a symmetric AB-diblock of length N with an A homopolymer of length $\alpha_A = 0.8N$ and a B homopolymer of length $\alpha_B = 1.5N$. The notation is that of Figure 4.10. Note the unbinding of the hexagonal phase on the left hand side.

they also increase the number of unfavorable contacts. However the addition of B homopolymer relieves the stress equally well without the enthalpic penalty. Note also the absence of any unbinding transition. The homopolymers are now so short that the increase in translational entropy on forming a disordered phase outweighs the cost of increased A, B contacts in such a phase.

We see the same trend continue in Figure 4.5 and Figure 4.6. In Figure 4.5 the

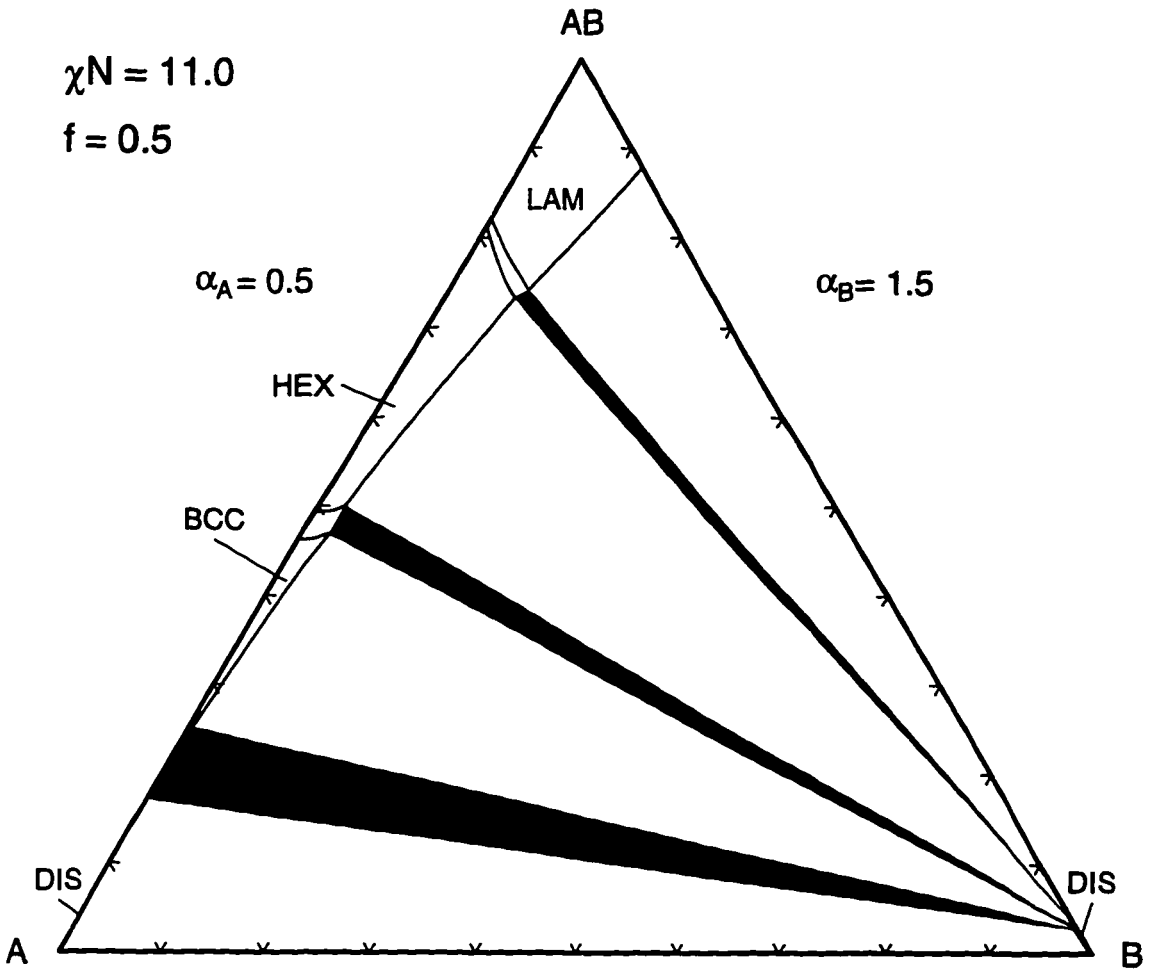

Figure 4.11: Phase diagram for a symmetric AB-diblock of length N with an A homopolymer of length $\alpha_A = 1.5N$ and a B homopolymer of length $\alpha_B = 0.5N$. The notation is that of Figure 4.2. The unbinding transition is preempted by a first-order transition.

B homopolymer chains are now quite short, $\alpha_B = 0.2$, and less than the value of 0.25 noted [21] to mark the onset of a disordering effect of added homopolymer. In accordance with this observation, the ordered phases on the B-rich side of the phase diagram can support no greater a volume fraction of B homopolymer than $\phi_B = 0.21$, a small value compared with that on the A-rich side of $\phi_A = 0.54$ for only slightly longer chains. Note that as in Figure 4.6 for well separated lamellae, a larger number

of longer chains are needed to balance the smaller chains. Otherwise a transition to a cylindrical and then to a body-centered-cubic phase will occur with the longer homopolymer chains on the inside. This is again due to the stronger wedge effect of the shorter chains. Remarkably this transition occurs for systems of Figure 4.4 and Figure 4.6 at roughly the same lamellar spacing ($D \approx 2.5 \ldots 3.0 R_0$), although the diblock volume fraction is rather different.

In Figure 4.7, the last of this sequence, the length of the B homopolymer is only a tenth that of the diblock. Therefore its disordering effect is very strong. The B homopolymer volume fraction in the ordered phases does not exceed 0.15. Note that the coexistence region at the bottom of the phase diagram has vanished; for the given chain lengths, the homopolymers are miscible for $\chi N \leq 12.44$. Also note the continuous transition from the disordered to the lamellar state. This critical point is similar to the point $f = 0.5$, $\chi N = 10.49$ first described by Leibler [125] for the pure diblock melt. It is characterized by a continuously vanishing amplitude of the spatial modulation with a non-zero wavevector.

We now turn to the second sequence, Figure 4.8 through Figure 4.11, in which a B homopolymer, longer than the diblock ($\alpha_B = 1.5$), is blended with A homopolymer chains of equal or shorter length. All diagrams are dominated by large coexistence regions between ordered phases, containing less than 0.13 volume fraction of B homopolymer, and an almost pure B-rich disordered phase. On the left hand side, shorter A homopolymers bring about ordered phases, characterized by more strongly curved internal interfaces, due to the increasing wedge effect of such short homopolymers.

All our results thus far have been obtained for a symmetric diblock and one value of the incompatibility parameter. We now try to extend our findings to moderately asymmetric diblocks and to different temperatures. In Figure 4.12 we have one example of a system containing an asymmetric diblock, $f = 0.54$, blended with two homopolymers of equal degree of polymerization, $\alpha_A = \alpha_B = 1.0$. The resulting

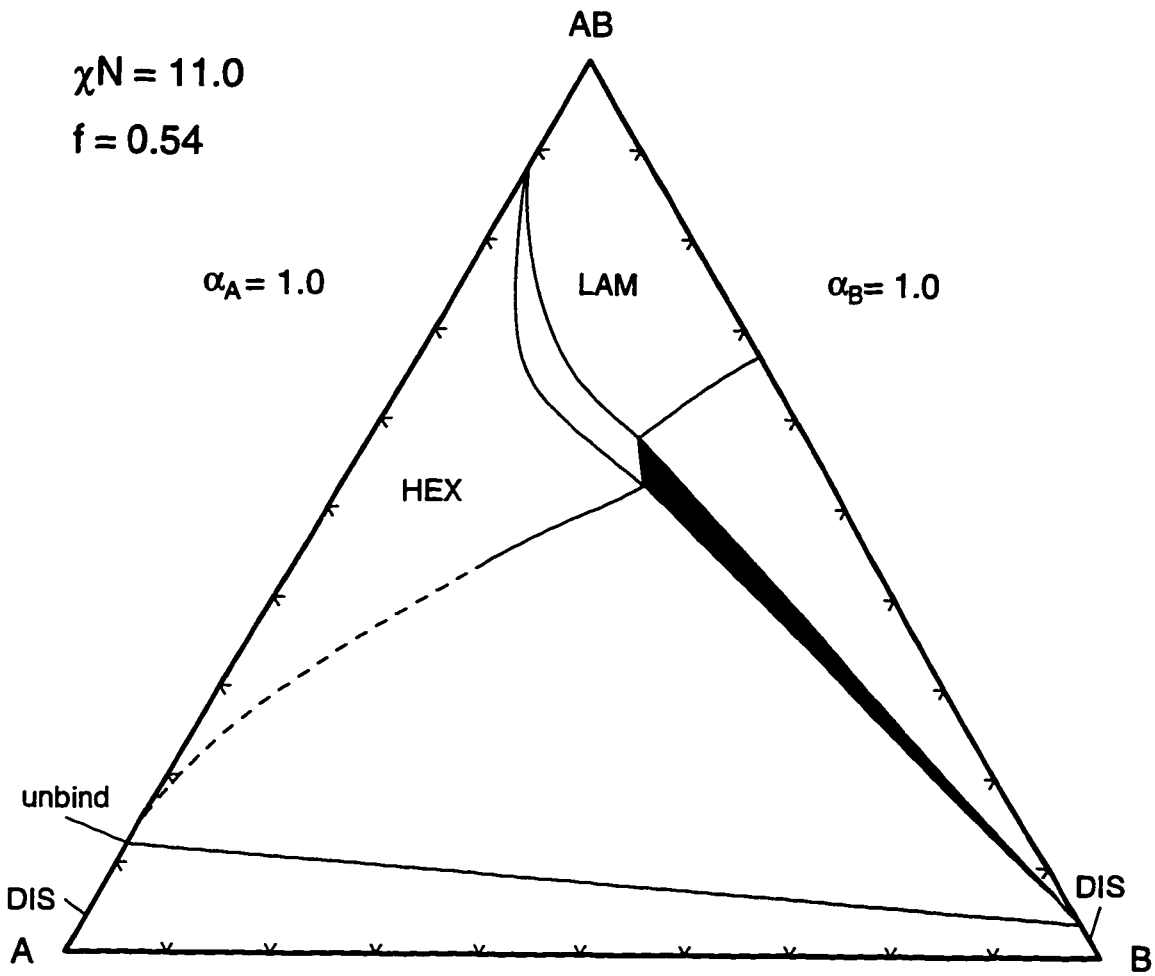

Figure 4.12: Phase diagram for an asymmetric AB-diblock of N segments, $0.54N$ of which are of type A, blended with corresponding homopolymers with the same number of segments. The notation is that of Figure 4.2. Note the similarity of this diagram with Figure 4.10.

phase diagram is topologically identical to the one in Figure 4.10. Both are characterized by internal interfaces that have a moderate tendency to curve towards the B-side. In the system in Figure 4.10, this is brought about by the wedge effect of the homopolymers of unequal length. In that of Figure 4.12 the diblock layer itself is asymmetric and therefore has a spontaneous curvature. This result and others like it lead us to believe that increasing f and decreasing α_A/α_B have comparable effects

on the overall structure of the phase diagram, at least for roughly symmetric diblock copolymers.

When attempting to extrapolate our results to other temperatures, one can be guided by the following observations. Larger values of χN favor more-strongly segregated configurations. Consequentially the size of two-phase regions grows with χN. In particular, unbinding transitions may be completely preempted by first-order transitions for values of χN larger than some threshold [101]. On the other hand, at smaller values of χN, one finds more-weakly segregated structures of larger periodicity, and a trend towards unbinding of swollen phases. The stability region of ordered phases shrinks as χN decreases. Additional homopolymer with values of α between 0.3 and 1.0, is able to induce microphase ordering, such that blends may be ordered even if the pure diblock melt is not, and ternary mixtures may be ordered even if the binary blend is not.

Our calculations do not include the effect of fluctuations. Although composition fluctuations are in general strongly suppressed in polymer melts, they are of importance close to a critical point, such as that in Figure 4.7, and will drive the system to a weakly discontinuous transition [61]. However, for most of the parameter space considered here, defects in the spatial ordering will be important. Electron micrographs [99, 104] of homopolymer-swollen, ordered, microphases reveal a fair degree of disorder, *e.g.* large amplitude undulations of lamellar phases. This agrees with our result that for strongly swollen microphases, the minimum of the free energy as a function of the repeat distance becomes extremely shallow. It is likely that the system can lower its free energy by making a first-order transition to disordered micellar or bicontinuous phases as suggested in [145]. Such disordered phases which still contain much structure are not described well by mean-field theory. The occurrence of such a first-order transition, preempting the unbinding transition, would be in accord with the experimental situation in highly swollen amphiphilic systems [85].

4.1.3 Summary

We summarize our main results for the phase behavior of approximately symmetric diblock copolymers, blended with corresponding homopolymers of varying length.

(1.) Homopolymers longer than the diblock ($\alpha > 1$) are expelled from the ordered phases. This is due to the loss of configurational entropy that they would suffer were they confined to the microstructure. Large regions of coexistence, between an ordered phase and a disordered one which contains most of the homopolymer, are formed.

(2.) Homopolymers shorter than the diblock enter the brush formed by it, leading to phases characterized by increasing mean curvature of the internal interfaces.

(3.) Homopolymers that are slightly shorter or comparable to the diblock ($0.5 \leq \alpha \leq 1.0$) can swell the microphase indefinitely, leading to a complete unbinding transition within mean field theory. We expect thermal fluctuations to destroy a strongly swollen phase and bring about a weak, first-order transition to a disordered phase.

(4.) Short homopolymers ($0.25 \leq \alpha \leq 0.5$) swell the microstructure, but because of the substantial entropy they gain upon distributing themselves randomly, they cause the unbinding to be preempted by discontinuous transitions. As homopolymers of this length enter cylindrical and spherical structures and relieve stress incurred on the inside of the copolymer layer, they have an ordering effect on the ternary blend.

(5.) Very short homopolymers ($\alpha \leq 0.25$) tend to disorder any microphase, since their gain in translational entropy outweighs the enthalpic penalty due to the increased number of A, B contacts.

(6.) For f close to 0.5 and α not very different from 1, increasing f and decreasing α_A/α_B have comparable effects on the overall shape of the phase diagram.

4.1.4 Conclusions

We have considered the phase behavior of ternary blends of symmetric and almost symmetric AB-diblock copolymers with corresponding A- and B-homopolymers at all compositions. We find that, depending mainly on the relative chain lengths and the architecture of the diblock, a variety of different behaviors may be observed. Most of these can be explained by "wet" brush/"dry" brush pictures [127, 128] and stretching arguments [224]. Our results compare favorably with experimental studies of polymer systems with roughly symmetric diblocks and comparable chain lengths [99, 14, 137]. Systems with one long and one shorter homopolymer (c.f. Figure 4.2, Figure 4.10, Figure 4.11 produce phase diagrams similar to the ones of water/oil/surfactant-mixtures (*e.g.* c.f. Figures 37, 38 in [46]). Larson [121] has modeled the amphiphile in such mixtures by a very short AB diblock copolymer, and the oil and water by single A and B monomers. The model has been studied by extensive Monte Carlo simulations. It is interesting to observe that with $\alpha_A = \alpha_B = 0.25$, the phase diagram obtained [121] with a symmetric diblock is very similar to our Figure 4.5 with $\alpha_A = \alpha_B = 0.3$ even though Larson considers extremely short chains of N equal to eight. Furthermore the large extent to which the ordered phases are swollen by homopolymer is comparable in Larson's model to that which we find. This indicates that the disordering effect of fluctuations, present in the simulations but not in our self-consistent field treatment, may not be as great as one would expect. In this connection, it would be desirable to include micellar phases into the mean-field phase diagram, and to examine the effect of such structured, yet disordered, phases on the stability of the lyotropic ones.

4.2 *Microphase Unbinding in the Symmetric System*[2]

4.2.1 Introduction

The system of symmetric AB-diblock copolymer and A- and B-homopolymer, all of the same index of polymerization, is perhaps the simplest ternary polymer blend which undergoes microphase separation. Until recently, little attempt had been made to determine what ordered phases it displays, or to map out its full phase diagram. Earlier work on this system focused on the phase coexistence of disordered phases only [21, 91], or on the interfacial activity of the diblock assembled between coexisting unstructured bulk phases [126, 154, 250]. However, a recent Monte Carlo study [185] obtained a cut through the full phase diagram along the isopleth, i.e. at equal concentrations of A- and B-homopolymer. In addition to the homogeneous phases, the diagram includes a disordered, but structured, microemulsion and a lamellar phase, but no phases possessing hexagonal or cubic symmetry. It is the point of the present section to show that within mean-field theory, the phase diagram has an unexpectedly rich structure. Although ordered phases of higher symmetry are unstable in mean-field theory just as in the simulations, three different lamellar phases exist, one being symmetric, and two asymmetric. The symmetric one consists of roughly equidistant copolymer monolayers, separating A- and B-rich regions. For lower overall copolymer concentration, this phase becomes unstable with respect to the formation of two coexisting phases of diblock *bilayers* in a homopolymer background. The asymmetric lamellar phases undergo complete unbinding transitions as homopolymer is added, but the symmetric one does not.

In a complete unbinding transition [169, 191, 136], added homopolymer swells the lamellae, and the wavelength of the lamellar phase diverges. In this limit, the system undergoes a transition to the disordered phase. At larger values of the incom-

[2] The material of this section has been accepted for publication in *Macromolecules*

patibility, the swelling does not increase without limit. Instead a lamellar phase of finite wavelength coexists with the disordered phase. This change of behavior with changing incompatibility can either be continuous [130], or first-order [135]. In the latter case, a preunbinding line is expected, analogous to the prewetting line which accompanies a first-order wetting transition [212]. Matsen demonstrated [145] within mean-field theory that a complete unbinding occurs in the binary AB/A system at small incompatibility, while at sufficiently large incompatibility it does not. It was later shown that the transition between these regimes is first-order, and the preunbinding line, at which two lamellar phases of different wavelength coexist, was located [101].

In this paper we shall see that the complete unbinding transition of the lamellar phase of AB bilayers in majority A homopolymer remains when their cores are slightly swollen by minority B homopolymer. However when a sufficiently large concentration of the latter is added, it forms the majority component of an asymmetric lamellar phase with minority A within the cores. The two asymmetric lamellar phases coexist. Near the isopleth, a symmetric lamellar phase exists only at sufficiently large diblock concentrations. As the amount of diblock is reduced, this phase becomes unstable to the two asymmetric lamellar phases before it can unbind. Only these asymmetrically swollen lamellar phases eventually undergo complete unbinding. This result is in accord with experimental observations [236] that ordered lamellar phases of bilayers in very asymmetric mixtures extend to much lower concentrations of diblock than do lamellar phases of monolayers in symmetric systems. These observations were very recently explained within the context of a phenomenological curvature model which also included the effect of van-der-Waals interactions and of thermal fluctuations in the lamellar phase [218]. Our microscopic calculation indicates that the relative stability of bilayer lamellar phases as compared to monolayer ones persists even when van-der-Waals interactions and fluctuations are negligible.

4.2.2 Phase Diagrams

4.2.2.1 Binary Blend

We employ the Gaussian chain model to describe the ternary mixture of symmetric AB-diblock blended with A- and B-homopolymers. All components have the same index of polymerization. We work in the grand canonical ensemble [146, 102] and Section 3.2 and solve the mean-field equations in Fourier space [157] and Section 3.2.2. In addition to lamellar phases, we examine solutions of hexagonal symmetry, but do not consider hexagonally perforated lamellar or cubic structures. The phase diagram of the binary AB/A limit of the ternary system is shown in Figure 4.13. At strong segregation the lamellar phase (labeled L) can only be swollen to a certain degree by additional homopolymer before phase separation occurs to an almost pure homopolymer phase (denoted A). However, for values of χN less than $\chi_U N = 11.766$, the lamellar phase can be swollen indefinitely. At the unbinding line, indicated by dashes in Figure 4.13, the separation between the lamellar sheets diverges, *i.e.* the wavenumber characterizing the lamellar phase vanishes continuously, while the Fourier coefficients of the copolymer density profile remain non-zero. The unbinding transition at $\chi_U N$ from bound to unbound lamellae along the lamellar/disordered phase boundary is a first-order one, with a preunbinding line which extends to a critical point at $\chi_{pu} N = 11.344$ [101]. Along the preunbinding line, two lamellar phases coexist, one of densely packed layers (L) and the other of layers strongly swollen by A-homopolymer (L_A). In the strongly swollen L_A-phase, copolymer rich bilayers (with the B-blocks on the inside) are separated from each other by homopolymer-rich regions similar in composition to the A-phase at the unbinding line.

The line of complete unbinding transitions extends to the Lifshitz critical point at $\chi_L N = 8.0$ [21]. There it meets a line of continuous transitions from the disordered phase to a lamellar phase of non-zero wavenumber. These transitions are similar to

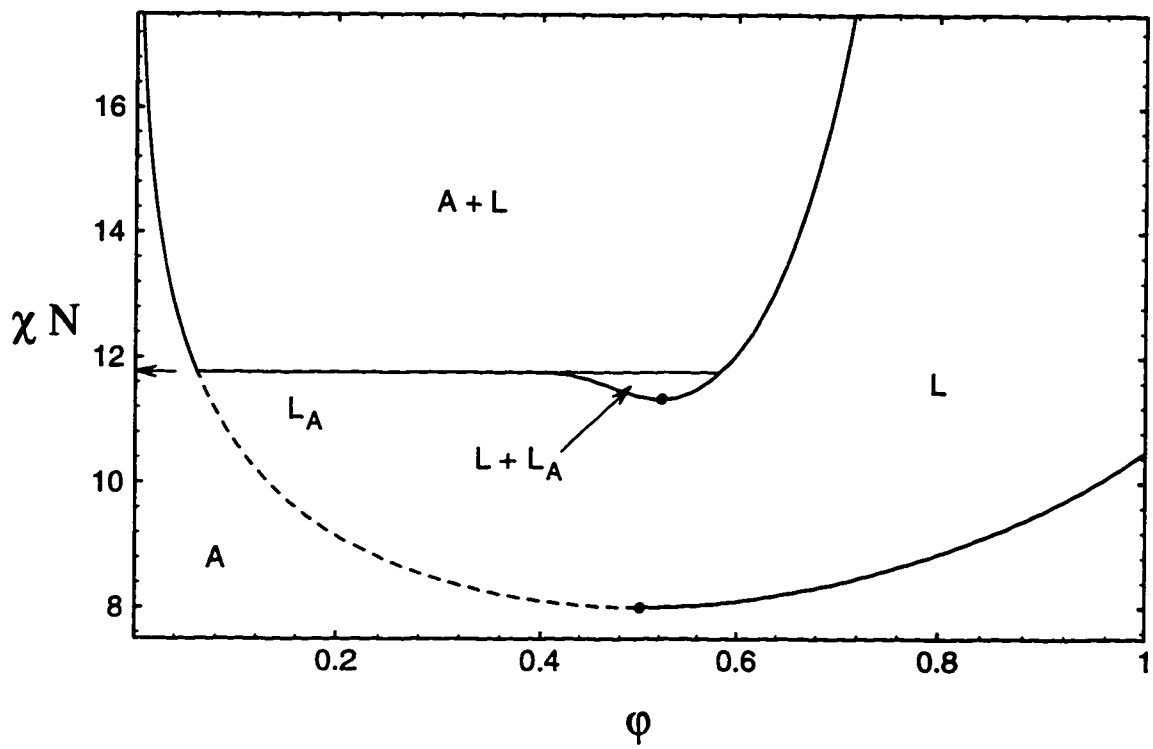

Figure 4.13: Calculated phase diagram for the binary homopolymer/diblock system. The incompatibility parameter χN is shown versus the copolymer volume fraction ϕ. The disordered homopolymer phase is denoted A, the dense lamellar phase L, and the swollen bilayer phase L_A. The preunbinding critical point and the Lifshitz point are shown with dots. The unbinding line is dashed, while Leibler's line of continuous transitions is shown solid. The arrow indicates the location of the first-order unbinding transition, $\chi_U N$.

those described by Leibler [125], in that the amplitude of all Fourier coefficients of the copolymer density profile vanish continuously. Only at the Lifshitz point do both the Fourier amplitudes and the wavenumber of the lamellar phase vanish simultaneously.

That the order/disorder transition is continuous for high copolymer concentration can be seen as follows: The order parameter which becomes critical at the order/disorder transition is the difference between the local density difference of A- and B-monomers and the average value of this difference. We let $\langle \ldots \rangle$ denote thermal

averages, and subscripts HA, CA, and A denote A-homopolymer, A-copolymer and total A-monomer density, respectively. Then the local order parameter is:

$$\eta = [\varphi_A - \langle\varphi_A\rangle] - [\varphi_B - \langle\varphi_B\rangle]$$
$$= [(\varphi_{HA} - \langle\varphi_{HA}\rangle) + (\varphi_{CA} - f\langle\varphi_C\rangle)] - [(\varphi_{HB} - \langle\varphi_{HB}\rangle) + (\varphi_{CB} - (1-f)\langle\varphi_C\rangle)] .$$

For $f = 1/2$ this order parameter is odd under interchange of the *labels* A and B, indicating the absence of any odd power of η from the Landau expansion of the free energy, suggesting that the transition is second order for all compositions, in agreement with numerical results.

4.2.2.2 Balanced Ternary Blend

The behavior found on the isopleth, i.e. for equal amounts of A- and B-homopolymer in the system, is shown in Figure 4.14. For large values of χN (i.e. for $\chi N \geq \chi^* N = 11.222$), the lamellar phase can only be swollen to a certain extent before additional homopolymer phase separates from the microstructure. Since the homopolymers are immiscible for values of χN greater than 2.0, a three-phase region is formed at which the symmetric lamellar phase coexists with the A-rich and B-rich disordered phases. For values of χN less than $\chi^* N$, there is no phase coexistence between the ordered and the disordered phases anymore. However, the two-phase coexistence of the $A + B$ disordered phases now extends across the unbinding line into the lamellar region: the formation of sheet-like micelles (bilayers) does not make the prevalently A- or B-rich phases miscible. Instead, for sufficiently low copolymer concentration, phase separation into two lamellar phases ($L_A + L_B$) occurs. The three-phase region between the symmetric lamellar phase and the A- and B-rich ordered, asymmetric lamellar phases persists for $\chi^* N > \chi N > \chi_T N$. This three-phase coexistence region ends at a tricritical point at $\chi_T N = 10.627$. For χN less than this, the two asymmetric lamellar phases merge along a line of critical points at which they form the symmetric lamellar phase. We have numerical difficulties in following this consolute line, but

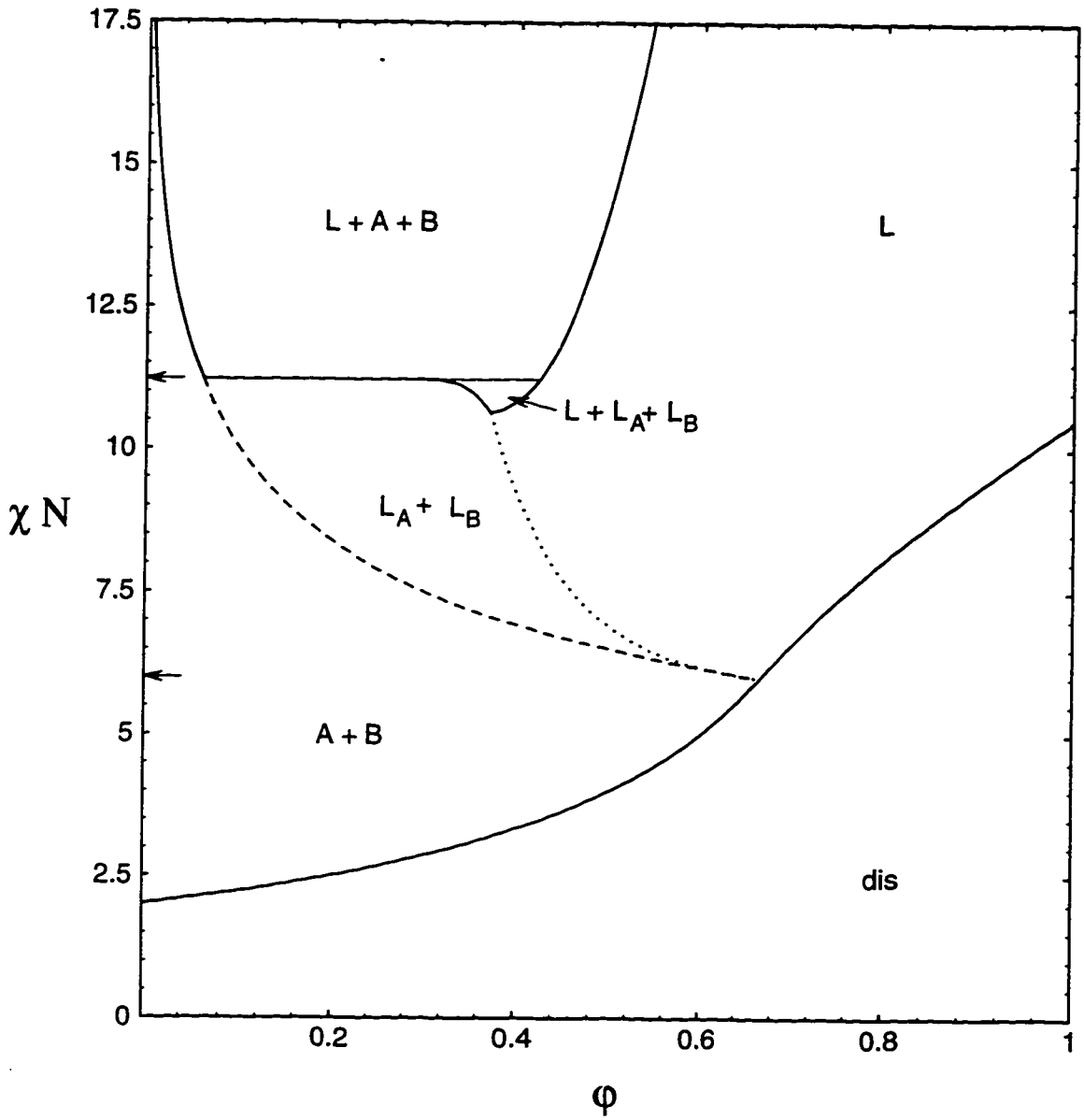

Figure 4.14: Calculated phase diagram for the balanced system, containing equal amount of A- and B-homopolymer. The notation is the same as that of 4.13. The one-phase disordered region is denoted "dis". The consolute line of the asymmetric bilayer phases L_A and L_B, shown dotted, is schematic. The arrows indicate the locations of the unbinding transition, $\chi^* N$ and of the multicritical Lifshitz point, $\chi_M N$.

it is reasonable to presume that it extends to the Lifshitz multicritical point[21, 91] at $\chi_M N = 6.0$. At this point the following critical lines meet: the above-mentioned consolute line of lamellar phases; the consolute line of disordered phases; two lines of Lifshitz points which originate on the binary side [21] and which separate the sheets of Leibler transitions from the sheets of complete unbinding transitions; two lines of critical-end points at which the sheets of complete unbinding transitions intersect the first-order sheet separating A-rich and B-rich phases.

4.2.2.3 Full Ternary Phase Diagrams

We can now construct the full ternary phase diagrams at all values of χN. To clarify the behavior, we present a sequence of schematic drawings (not to scale) in Figure 4.15, whereas the results of the numerical computation are given in Figure 4.16 through Figure 4.18.

At large incompatibilities, Figure 4.15a and Figure 4.16 , there are only three phases: the dense lamellar phase, and the A- and B-rich disordered phases. They can coexist. Note the very low miscibility of the pure homopolymers in Figure 4.16.

When χN is decreased to a value slightly below that of the unbinding transition on the binary side, $\chi_U N > \chi N > \chi_{pu} N$, as in Figure 4.15b and Figure 4.17, the addition of B homopolymer to the binary AB/A-system not only extends the unbinding transition into the interior of the three-component diagram, but also the preunbinding region in which the symmetric lamellar phase coexists with the asymmetric A-rich lamellar phase. Note that the repeat distance of the L_A phase, coexisting with the dense L phase, increases with the amount of B-homopolymer added. Three-phase coexistence is still between the symmetric lamellar and A-rich and B-rich disordered phases as long as χN is larger than a certain value $\chi^* N$.

At this value $\chi^* N = 11.222$, Figure 4.15c, the nature of the three-phase coexistence changes. For values of χN less than $\chi^* N$, (c.f. Figure 4.15d and Figure 4.18), three-phase coexistence is between a dense lamellar phase L and two asymmetrically

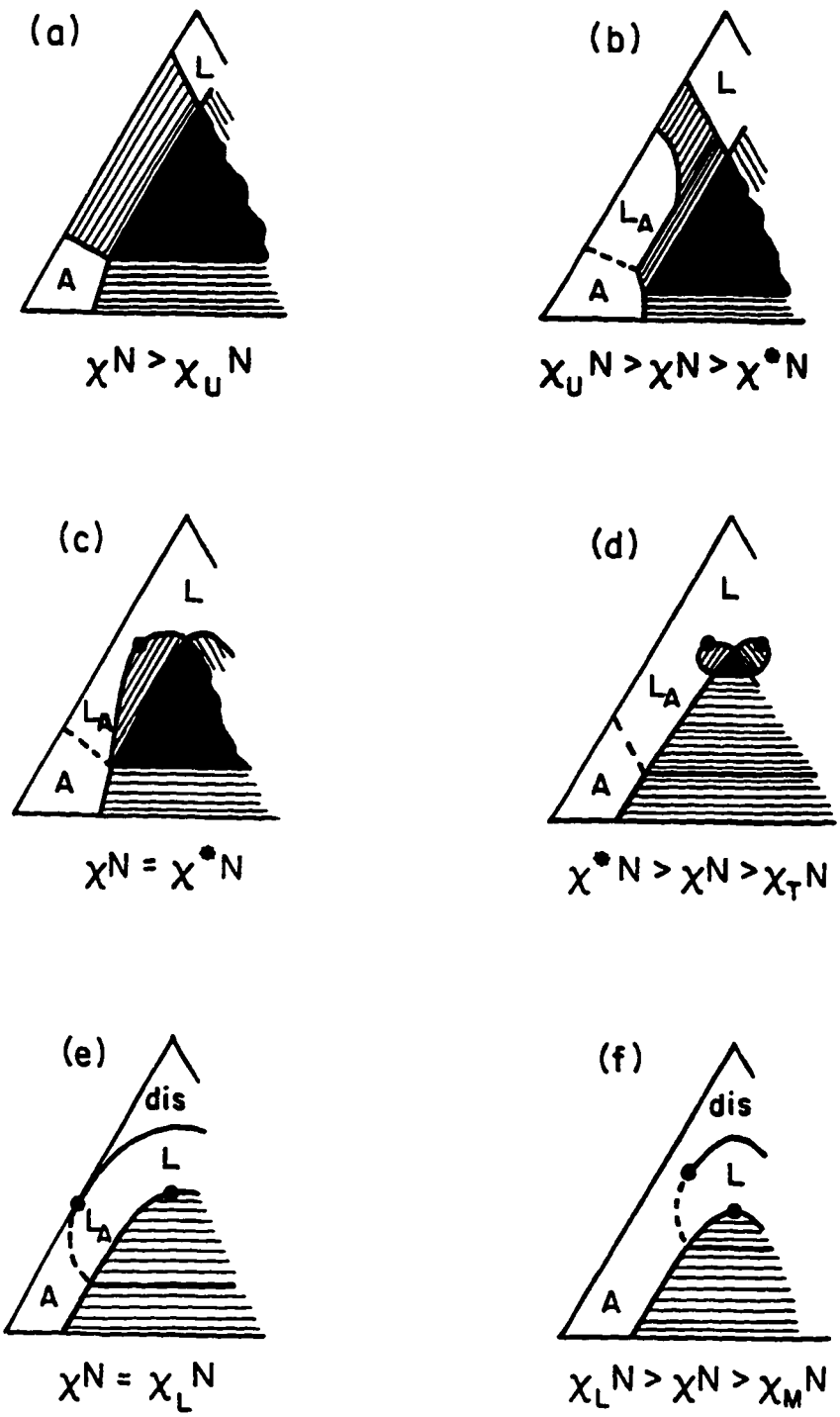

Figure 4.15: Schematic drawings of the left-hand side of the full ternary phase diagram for various values of χN.

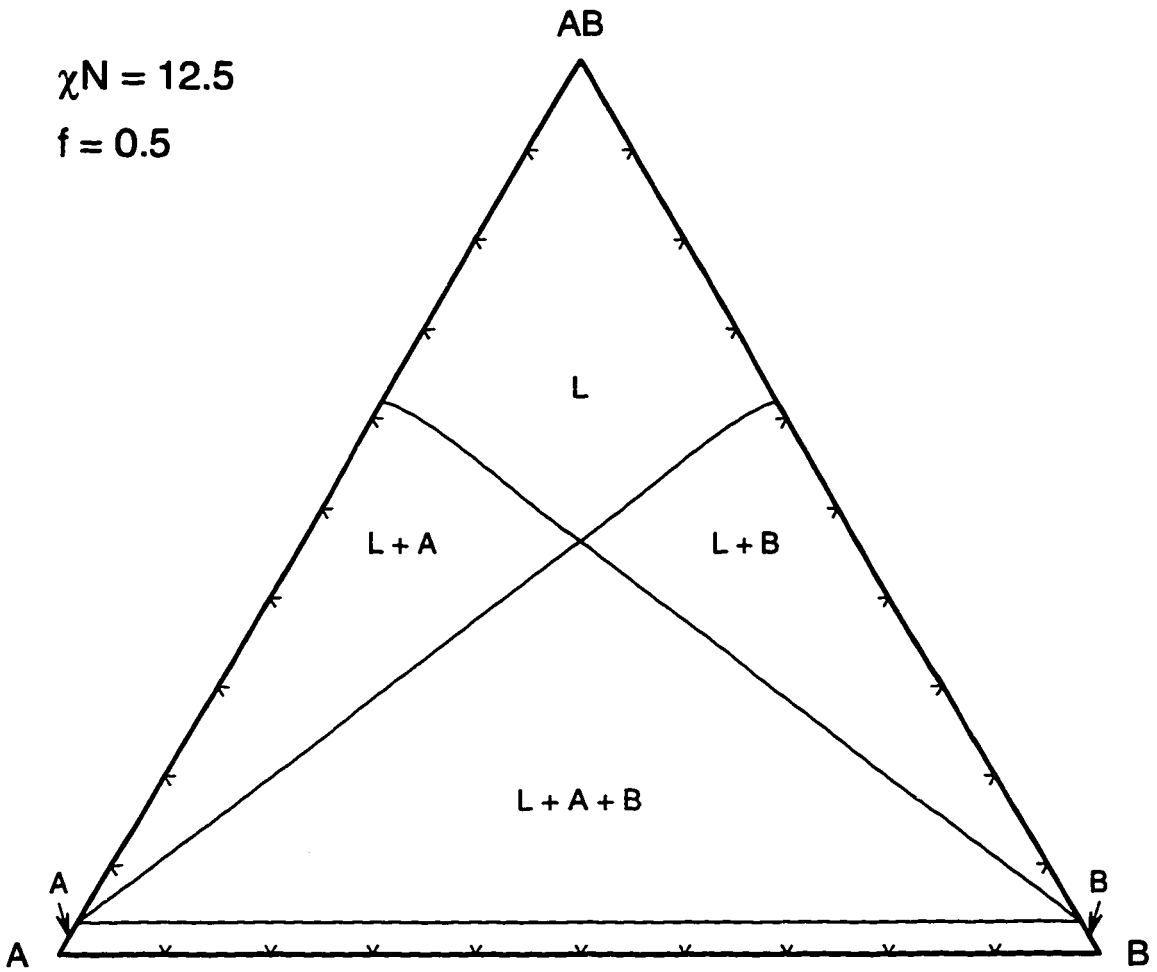

Figure 4.16: Calculated phase diagram for $\chi N = 12.5$, above the unbinding transition on the binary side.

swollen bilayer phases (L_A and L_B). Adjacent to the three-phase triangle are two-phase regions along which different lamellar phases coexist. The regions of $L + L_A$ and $L + L_B$ coexistence are clearly seen to be preunbinding regions. Note in particular the coexistence of two asymmetric, swollen lamellar phases, below the base of the three-phase triangle.

As χN is reduced still further, three-phase coexistence vanishes at a tricritical point at $\chi_T N = 10.629$. At smaller incompatibilities, the two asymmetric lamellar

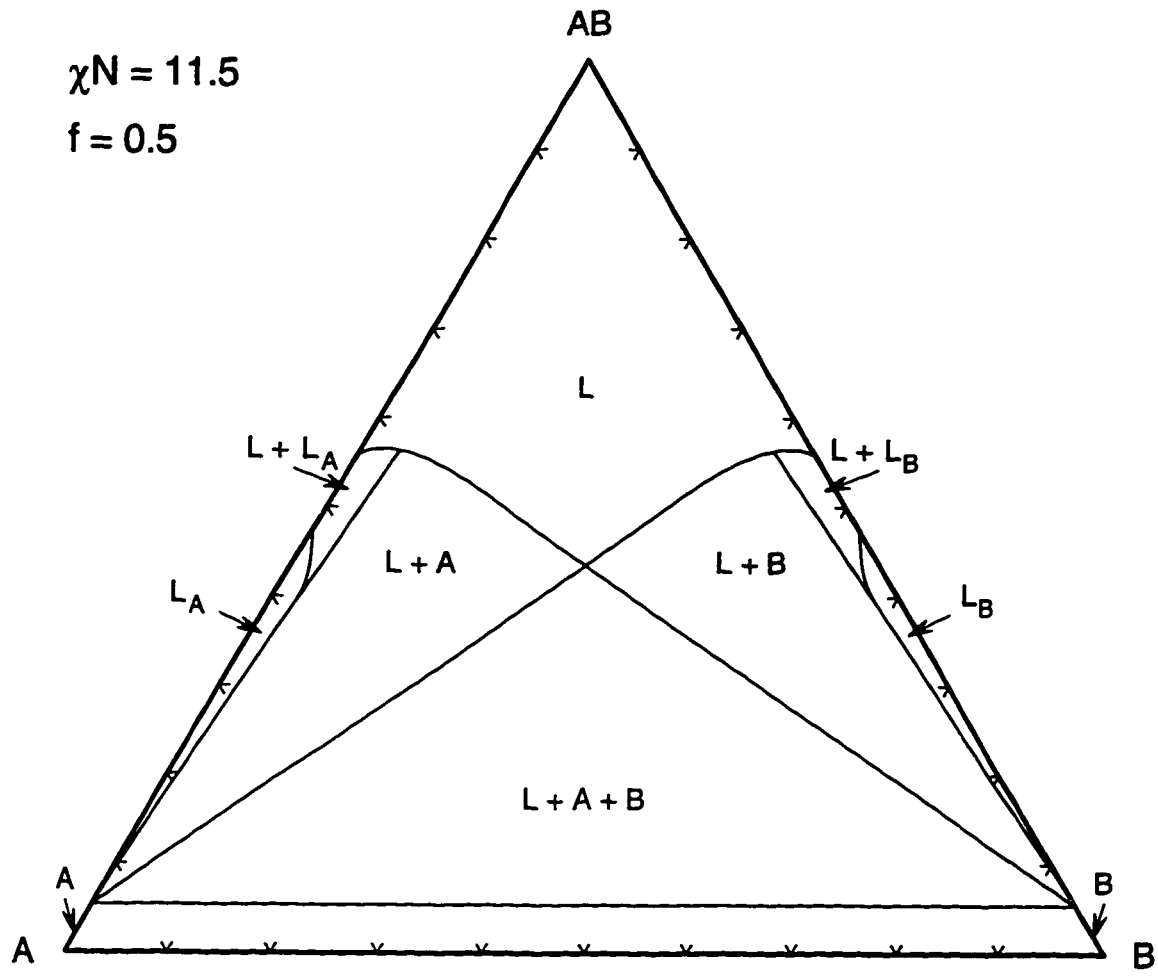

Figure 4.17: Calculated phase diagram for $\chi N = 11.5$. The lamellar phase unbinds along the binary sides, but not on the isopleth.

phases merge continuously at a consolute line. For values of $\chi N < 10.49$, we encounter an order/disorder transition at *high* copolymer concentration. This transition, first described by Leibler [125] for the pure diblock melt, is continuous in mean field theory presumably at all compositions. There is, therefore, an entire sheet of continuous transitions separating the disordered phase from a lamellar phase of non-zero wave vector.

As the incompatibility is reduced even more, the disordered region extends further

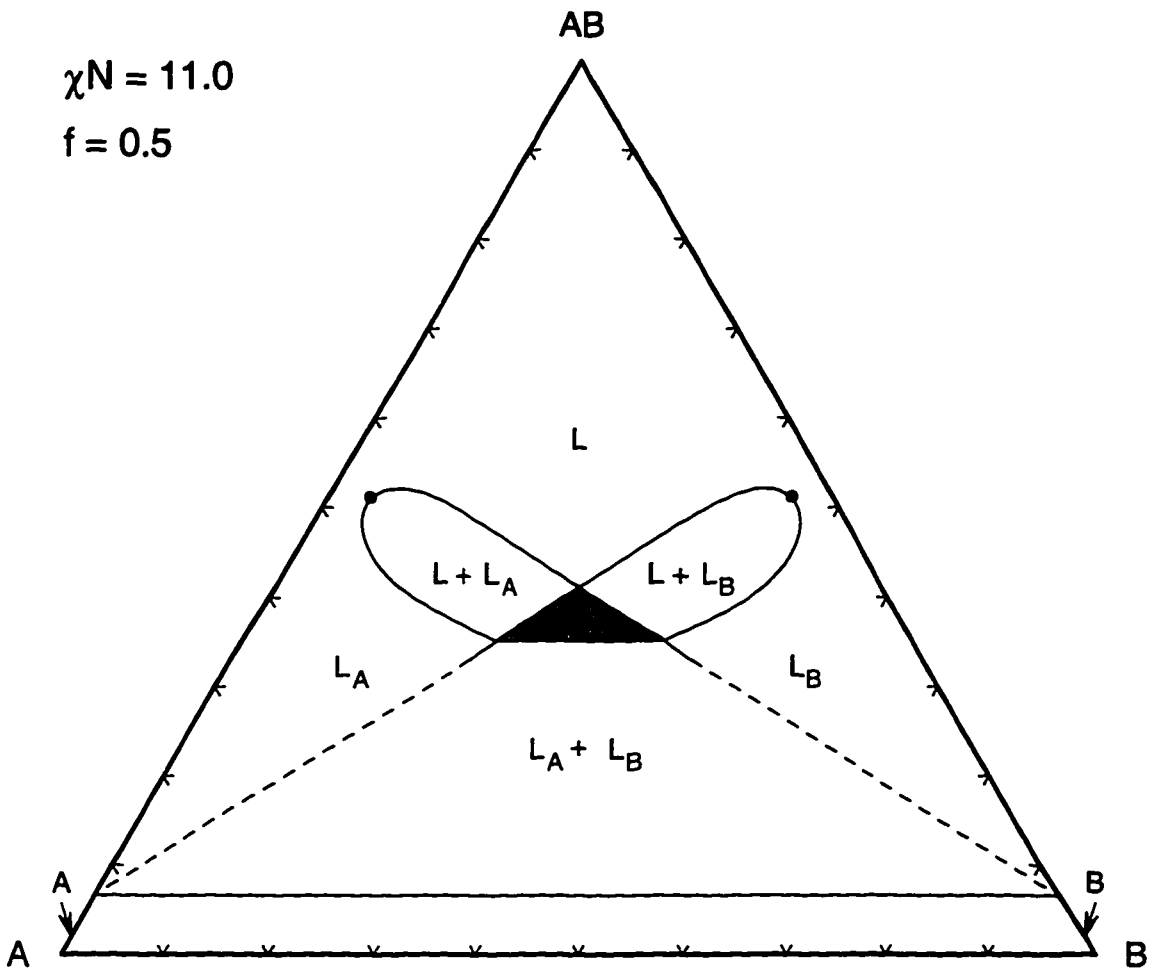

Figure 4.18: Calculated phase diagram for $\chi N = 11.0$. Three-phase coexistence between the symmetric lamellar, L and two disordered phases, A, B, has been replaced by one between the symmetric lamellar and two asymmetric lamellar phases, L_A, L_B. The region of three-phase coexistence is shaded. Extrapolated phase boundaries are shown with dashes.

down the binary sides to lower diblock concentrations. A lamellar phase remains on the binary side and unbinds into the A-rich disordered phase at still lower compositions. At $\chi N = \chi_L N = 8.0$, Figure 4.15e, the lamellar phase just detaches from the binary side, and the sheet of Leibler transitions meets the sheet of complete unbinding transitions there at a Lifshitz point [21].

At still smaller values of χN, the stability region of the lamellar phase detaches completely from the binary sides, forming an island in the center of the phase diagram (Figure 4.15f). At the multicritical Lifshitz point, $\chi_M N = 6.0$, this island vanishes, leaving just the coexistence region of the immiscible, disordered homopolymer phases.

4.2.3 Discussion

To discuss this phase behavior, it is useful to consider the interactions between the internal interfaces in the lamellar phase. The cost of creating an interface increases with the magnitude of the density difference across it. In a lamellar phase, there is an overall attraction between neighboring layers, since the presence of the adjacent interfaces prevents the density difference across each one from attaining the value across an isolated interface. As the density difference across the interfaces increases with the degree of segregation, this attraction grows with χN. At short distances, an elastic repulsion due to the compression of the copolymers forming the layer stabilizes the lamellae at a non-zero separation.

For large values of χN, the attraction is strong enough to outweigh the entropic penalty of phase separation: It is more favorable for added homopolymer to phase separate from a dense lamellar phase than to swell it. The same mechanism prevents the formation of a symmetrically swollen phase on the isopleth for $\chi N \leq \chi^* N$: in a symmetrically swollen lamellar phase, each pair of interfaces is well separated, whereas in the bilayer phases L_A and L_B, only every second pair of interfaces is separated, while the interfaces forming each bilayer are close to each other. The binding energy gained hereby compensates the entropy loss of phase separation.

This instability of the symmetric lamellar phase to the asymmetric ones, clearly seen in Figure 4.18, is in good agreement with experimental observations in ternary systems containing short-chain amphiphiles [236]. The major difference between our Figure 4.18 and experiment is that a disordered microemulsion phase is found to be stable in the region in which mean-field theory predicts a *metastable* ordered phase.

The reason for this discrepancy is that our mean-field calculation ignores fluctuations which favor the disordered microemulsion phase [67].

There are several other effects of fluctuations which will also alter the results obtained by mean-field theory. One knows that they introduce a repulsive interaction between bilayers [87], causing them to unbind more easily than in mean-field theory. However the orientational order of the lamellae cannot be sustained when the lamellar spacing exceeds the persistence length of the bilayer [34], with the consequence that the unbinding transition is expected to be pre-empted by a first order transition to a disordered, but structured, sponge phase [66, 181]. It is also known that the continuous transition from the disordered phase to the lamellar phase of non-zero wavenumber is driven first-order by fluctuations [20, 61]. Finally, fluctuations can eliminate the entire coexistence region between asymmetric lamellar phases because the difference in energy between them and the symmetric lamellar phase is so small (c.f. Section 3.2.2). This is almost certainly the case in the simulation of relatively short-chain polymers [185]. Nonetheless one expects to observe in ternary polymer blends asymmetric lamellar phases which are stable to much smaller diblock concentrations than are symmetric ones.

4.3 Chain Length and Temperature Dependence in the Binary System[3]

4.3.1 Introduction

Systems containing block copolymers are fascinating objects because of the ability of the copolymer to bring about a variety of structured, ordered or partially ordered morphologies. As shown by Leibler [125], in mean field theory the phase diagram is given by the fraction f of the chain being of type A, and χN, the product of the dimensionless interaction parameter χ between A- and B-monomers, and the total number of segments N per chain. For roughly symmetric copolymers, flat

[3] The material in this section has been submitted for possible publication in *Macromolecules*.

lamellae are formed, for more asymmetric diblocks, we find hexagonally arranged cylinders and finally spheres on a body-centered-cubic lattice. Between the lamellar and the hexagonal phases there is at intermediate segregation a narrow region of the bicontinuous gyroid phase (space group $Ia3d$). The order/disorder transition is continuous for $f = 0.5$, first-order otherwise. The mean field phase diagram for this system [157, 151] has been worked out, and is in general agreement with experiments [18]. Fluctuations affect mainly the behavior in the weak segregation limit. The critical point is destroyed, and the order/disorder transition is driven first-order for all f [61].

Blends of AB-diblock with A- or B-copolymer are more complicated. First of all, for each homopolymer blended with the diblock, there are *two* additional independent variables, namely the volume fraction of the homopolymer φ and the chain length ratio $\alpha = N_A/N_{AB}$. Mapping out the entire parameter space for homopolymer/diblock blends is clearly infeasible, one has to make some representative cuts through the parameter space.

A second complication arises in considering blends, since two new features, absent in a one-component system, may occur. On the one hand, the blend may macrophase separate, so that we have two or more coexisting phases, each of which may be microstructured. On the other hand, added homopolymer may swell the microstructure without disordering it or phase separating from it. In the extreme case this swelling can continue indefinitely, giving rise to a complete unbinding transition in which the wave vector of the ordered phase approaches zero continuously with increasing homopolymer concentration.

These transitions are governed by two mechanisms specific to blends, namely the interactions of the interfaces separating microdomains, and the varying ability of homopolymers of different length to swell the brush formed by the copolymers straddling the interfaces. These mechanisms exist in addition to the chain stretching and interfacial contributions to the free energy already present in the pure diblock

system [152]. In the weak to intermediate segregation regime, the balance between these forces is a subtle one, with hard to predict consequences. In particular, it is virtually impossible to predict reliably even the general topology of the phase diagram for a given set of architectural parameters. For these reasons it seemed necessary to compile a representative catalogue of phase diagrams, both to investigate the general trends in the expected behavior and as a guide for experiments.

In a previous section (c.f. Section 4.1), we have studied the chain length dependence of the phase diagram for a symmetric AB-diblock, blended with corresponding A- and B-homopolymers by systematically varying the relative chain lengths at fixed $\chi N = 11.0$. The surprisingly intricate microphase behavior in the "symmetric system", consisting of a symmetric diblock and two corresponding homopolymers, all three components being of equal length was also investigated (c.f. Section 4.2). Up to three different lamellar phases are found in mean field theory. The unbinding behavior, including two lines of Lifshitz critical points, was mapped out at all compositions of the ternary blend, and for several values of χN. In the present section, we complete this study of blends containing *symmetric* copolymer by calculating mean field phase diagrams for blends containing a symmetric AB-diblock blended with A-homopolymer. We vary the chain length of the homopolymer from $\alpha = 0.1$ to $\alpha = 1.5$, and consider values of χN from the order/disorder transition up to $\chi N = 17.5$. We present and discuss our results in the following section. As compared to the ternary system [99, 79, 240, 137], experiments on binary homopolymer/diblock blends are relatively numerous [113, 83, 241, 240, 82, 115, 116, 256, 255, 258, 257, 265, 206, 193, 104, 41]. We are therefore able to compare our phase diagrams with experimental results, and will make some assertions on the outcome of future experiments. Available are also results from Monte Carlo simulations of short chain amphiphiles [121] and a fluctuation calculation [110] based on the Fredrickson-Helfand method [61], with which to compare our results. We conclude by summarizing the general trends we found.

4.3.2 Results

We employ the standard Gaussian chain model [43] and solve the mean field equations in Fourier space [157] in the semi-grand canonical ensemble [146]. We plot our phase diagrams in terms of the volume fraction φ of the copolymer and the effective interaction parameter χN, where $N = N_{AB}$ is the number of segments in the copolymer chain. All our diagrams are for a diblock with A- and B-block of equal length (*i.e.* $f = 0.5$), but we change the relative chain length of the A-homopolymer, $\alpha = N_A/N_{AB}$ from $\alpha = 0.1$ in Figure 4.19 to $\alpha = 1.5$ in Figure 4.32. We consider only the three classical phases: sheetlike lamellae (LAM), hexagonally arranged cylinders (HEX) and spherical micelles on a body-centered-cubic lattice (BCC), besides homogeneous phase (DIS).

In Figure 4.19 and Figure 4.20, showing the phase diagrams for blends containing homopolymers shorter than a quarter the length of the diblock (*i.e.* $\alpha < 0.25$). This was noted previously [21] to be the threshold for which homopolymers have a disordering effect on any microstructure present. We see clearly that the transition to an ordered structure occurs at higher values of χN as more homopolymer is added. This is due to the relatively large entropy of mixing that these short chain molecules gain by distributing themselves randomly. A similar effect was also observed in ternary systems containing homopolymers of this length [102]. Since the homopolymers are shorter than the diblock, they enter the brushes formed by the copolymer at the internal interfaces and bring about transitions to phases characterized by non-vanishing mean curvature of the interfaces.

In Figure 4.21 and Figure 4.22 the homopolymers are now longer than $\alpha = 0.25$. Consequentially the spinodal for microphase separation has positive slope at Leibler's critical point at $\chi N = 10.495$, $\varphi = 1.0$, *i.e.* adding small amounts of homopolymer to the diblock initially lowers the value of χN at which ordered phases become stable. Since for low copolymer concentration any microphase will eventually dissolve, the

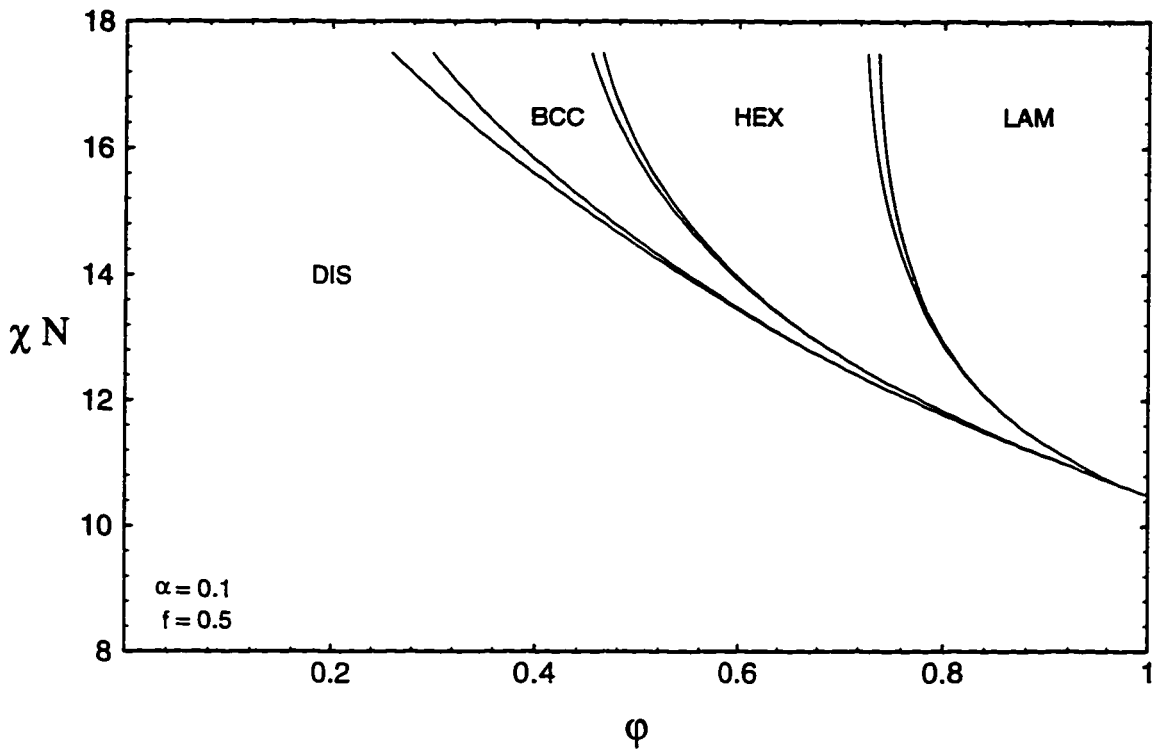

Figure 4.19: Phase diagram for a symmetric AB-diblock of N monomers. The copolymer volume fraction is denoted φ, the Flory-Huggins parameter by χ. The ratio of the chain lengths $\alpha = N_A/N$ is $\alpha = 0.1$. The order/disorder transition for the pure diblock at $\chi N = 10.495$ is continuous, all other transitions are first-order. The lamellar phase is denoted LAM, the phase of hexagonally arranged cylinders HEX, and the phase of spherical micelles on a body-centered-cubic lattice by BCC. The disordered DIS phase is assumed homogeneous. Regions of two phase coexistence are unlabeled. Notice how the order/disorder transition occurs at larger values of χN as homopolymer is added. This disordering effect is due to the large entropy of mixing of such short chains.

regions of phase coexistence must have a lower extremal point at finite homopolymer concentration. In the present, case these points are not critical points, but "points of equal concentration" [119], where the mixture forms an azeotrop.

If we make the homopolymer even longer ($\alpha \geq 0.5$), a new feature occurs: a continuous transition from the ordered to the disordered state at *high* homopolymer

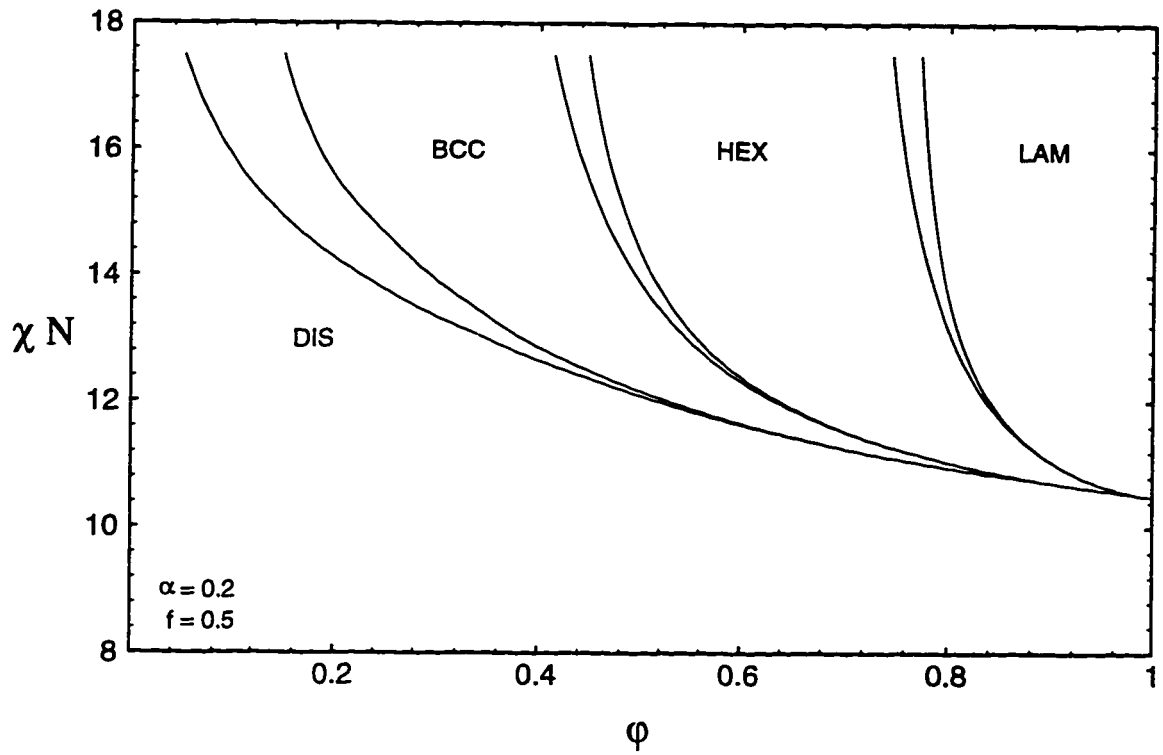

Figure 4.20: As Figure 4.19, but with $\alpha = 0.1$. Notice that the homopolymer still has a disordering effect, but much less so than in Figure 4.19.

concentration. As homopolymer is added, the periodicity of the ordered phase increases without bounds, leading to a complete unbinding of the mesophase into the disordered phase without encountering a region of phase coexistence. Surprisingly, only the lamellar and hexagonal phases undergo an unbinding transition, but not the body-centered-cubic phase. For $\alpha \geq 0.5$, we find the BCC phase stable for weak segregation, being replaced by a hexagonal phase for increasing χN. This can easily be understood: the relatively short homopolymers enter the spherical micelles making up the body-centered-cubic lattice and relieve stretching stress experienced by the symmetric diblocks straddling the curved interface of the spheres. However, this increases the number of unfavorable AB-contacts and becomes more costly as χN is

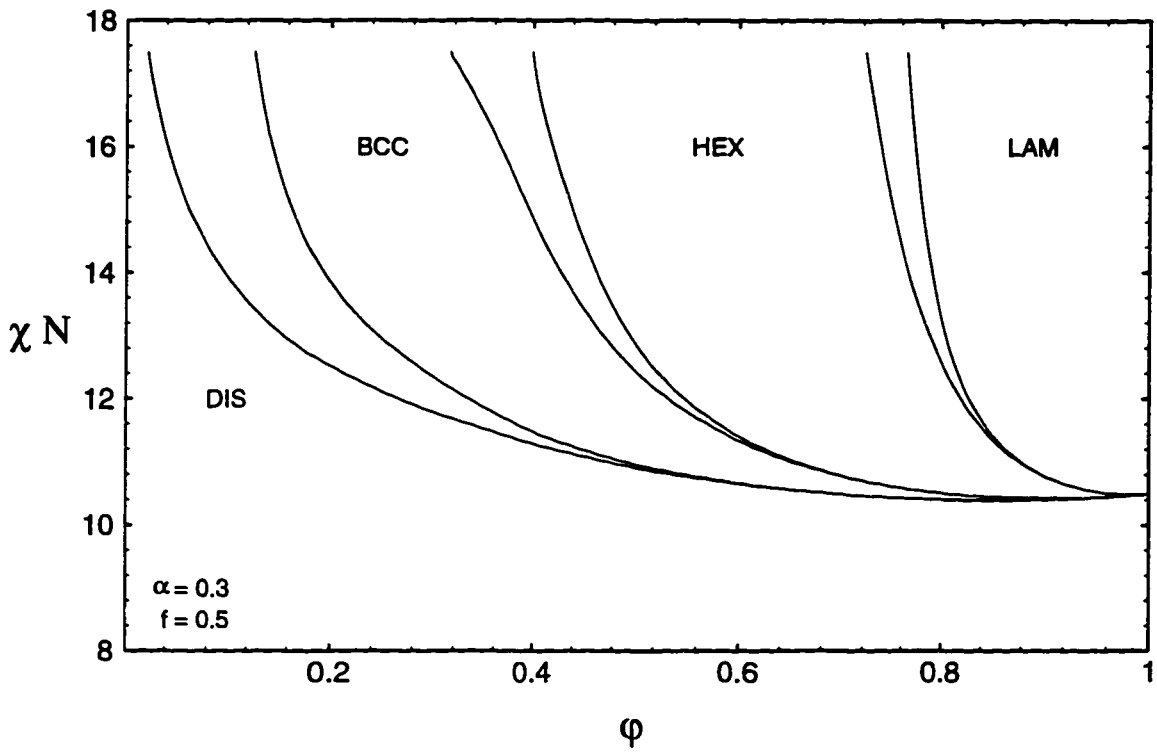

Figure 4.21: As Figure 4.19, but with $\alpha = 0.3$. The order/disorder transition occurs first at $\varphi \approx 0.8$, *i.e.* for lower values of χN than for the pure diblock. This ordering effect of the homopolymer is due to its ability to enter the microstructure and relieve stress. All transitions, except the order/disorder transition for the pure diblock are first-order. The minimum of the coexistence curves are azeotropical points.

increased. The homopolymers become less efficient in reducing stress as they become longer. Consequentially, we find that the transition to the hexagonal phase occurs for lower values of χN as the homopolymers length increases (c.f. Figure 4.23 through Figure 4.27).

For $\alpha = 0.5$ and $\alpha = 0.6$, the phase diagram exhibits another unexpected feature: a region of coexistence between two BCC phases, differing in their homopolymer content. Phase coexistence between ordered phases differing in their repeat distances have been discussed before [101, 103], but only for lamellar phases. In the present

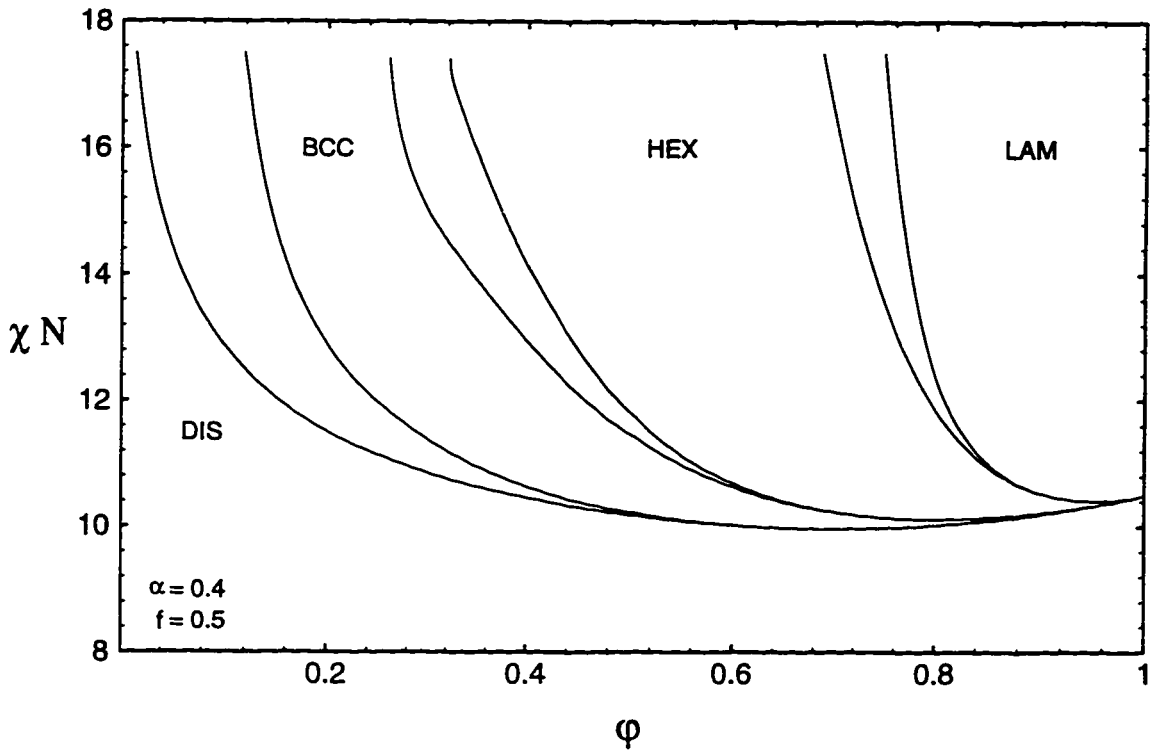

Figure 4.22: Binary phase diagram with $\alpha = 0.4$. Notice the degree by which the order/disorder transition is shifted from the pure copolymer value.

case, these coexistence regions end at critical points, where the two BCC phases become indistinguishable. There is no BCC/BCC phase coexistence for $\alpha < 0.4$ or for $\alpha > 0.9$ (and probably none for $\alpha \geq 0.7$ either, we are currently unable to evaluate the free energy here to the desired degree of accuracy). Consequentially there is a finite line of critical points in the region $0.4 \leq \alpha \leq 0.9(0.7)$. It presumably ends in critical end points, coexisting with a hexagonal phase, although a scenario seems also possible in which the critical end point coexists with both a disordered and a hexagonal phase.

For $\alpha \geq 0.8$ (Figure 4.26) the homopolymers phase separate from the lamellar microphase at high χN, without entering the brushes at the internal interfaces. (The

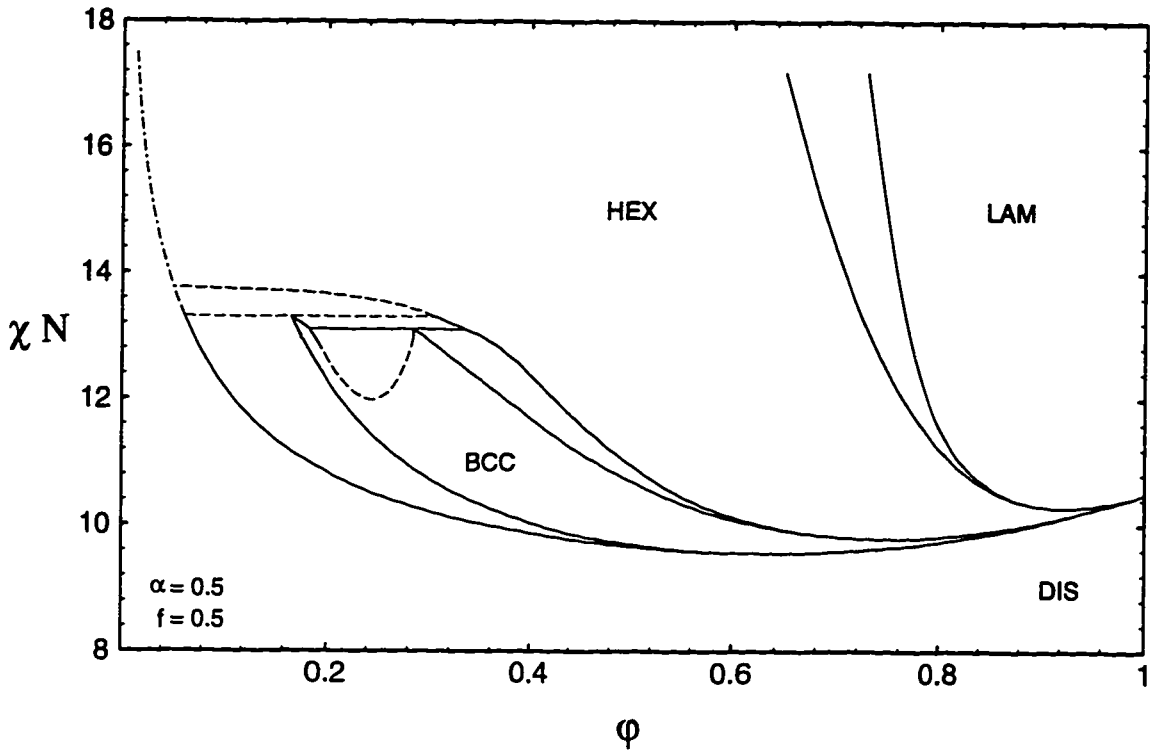

Figure 4.23: Binary phase diagram with $\alpha = 0.5$. The unbinding line, at which the periodicity of the hexagonal phase becomes infinite is indicated by a dot-dashed line. Notice the BCC/BCC phase coexistence for low copolymer content. Dashes indicate extrapolated phase boundaries.

same trend is clearly visible in Figure 4.25.) The lamellar/disordered phase coexistence region ends in a degenerate three phase coexistence between the lamellar and disordered phase, coexisting with an infinitely swollen hexagonal phase. This three phase coexistence marks the maximum value of χN at which microphase unbinding can occur. As α grows, the region of LAM/DIS phase coexistence extends towards smaller values of χN, indicating that the ability of the homopolymer to swell the mesophase decreases as α becomes greater than 0.7, since homopolymer chains comparable in length to the microdomain spacing loose too much configurational entropy when being confined to the microstructure.

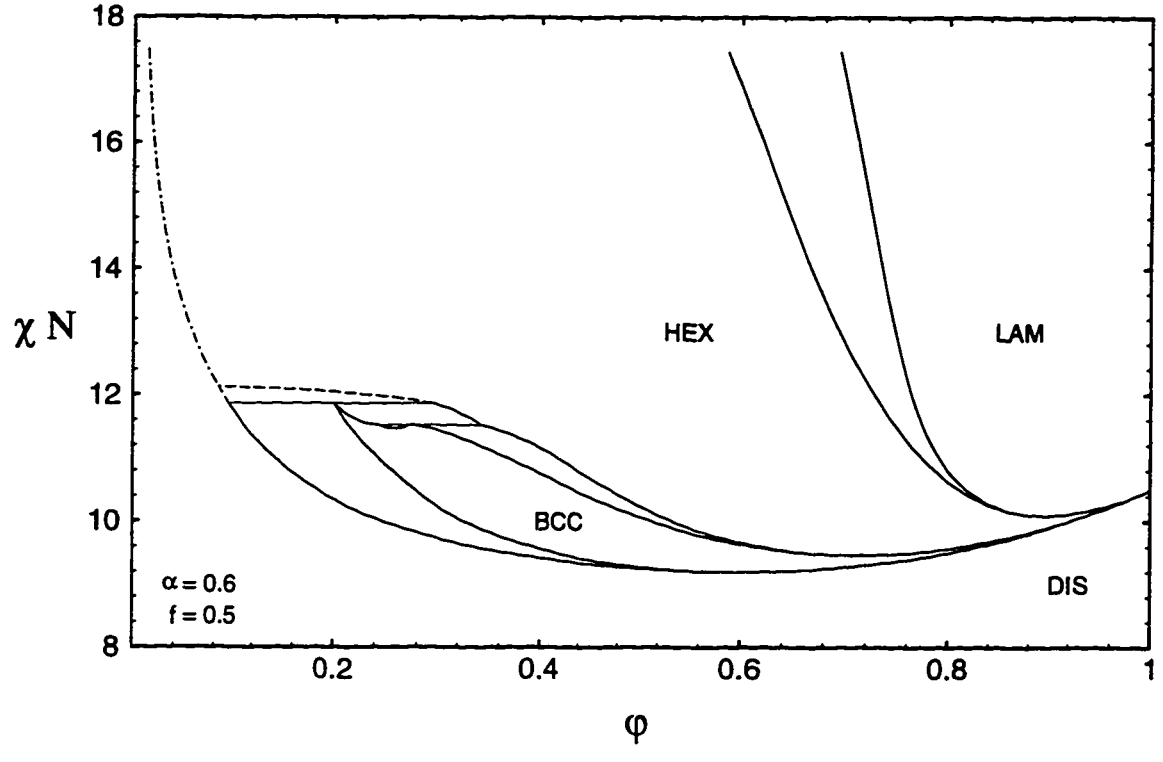

Figure 4.24: Binary phase diagram with $\alpha = 0.6$. Notice that the BCC/BCC phase coexistence region has shrunk as compared to Figure 4.23. The notation is the same as in Figure 4.23.

As the length of the homopolymer approaches the length of the diblock, all ordered phases except the lamellar one disappear. In Figure 4.28, showing the phase diagram for $\alpha = 1.0$, only the lamellar phase remains and the unbinding line, where the lamellar spacing becomes infinite, extends all the way from the LAM/DIS phase coexistence to the Lifshitz point at $\chi N = 8.0$, $\varphi = 0.5$ [21].

As χN is lowered, the lamellar phase undergoes a first-order unbinding transition, as is clearly indicated by the preunbinding region, where two lamellar phases of different spacing coexist. The preunbinding region ends at a critical point [101]. The way the other ordered phases disappear in the narrow region $0.9 < \alpha < 1.0$ is

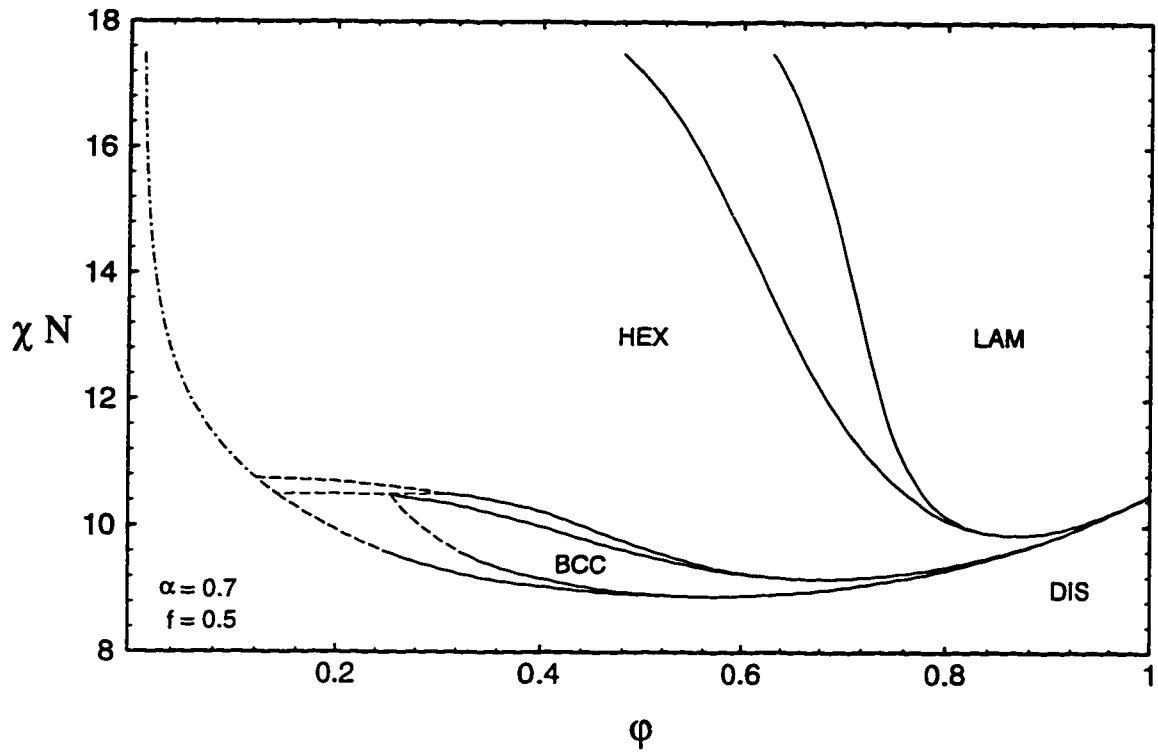

Figure 4.25: Binary phase diagram with $\alpha = 0.7$. The BCC/BCC phase coexistence has vanished. Notation is that of Figure 4.23.

presumably as follows: As α becomes greater that 0.9, a narrow channel of lamellar phase opens up between the lamellar/disordered coexistence and the hexagonal region. This lamellar phase undergoes a complete unbinding as homopolymer is added. As α approaches 1.0, this channel widens, while the region of hexagonal and body-centered-cubic phases shrink and are shifted towards lower values of χN. At $\alpha = 1.0$ they have collapsed completely, and the transition from the disordered to the lamellar state takes continuously place on the spinodal for $\varphi > 0.5$.

As α becomes greater than 1.0, the Lifshitz point is preempted by a disorder/disorder phase coexistence for *low* values of χN, ending in an ordinary (Ising) critical point. The order/disorder transition for high copolymer concentration is

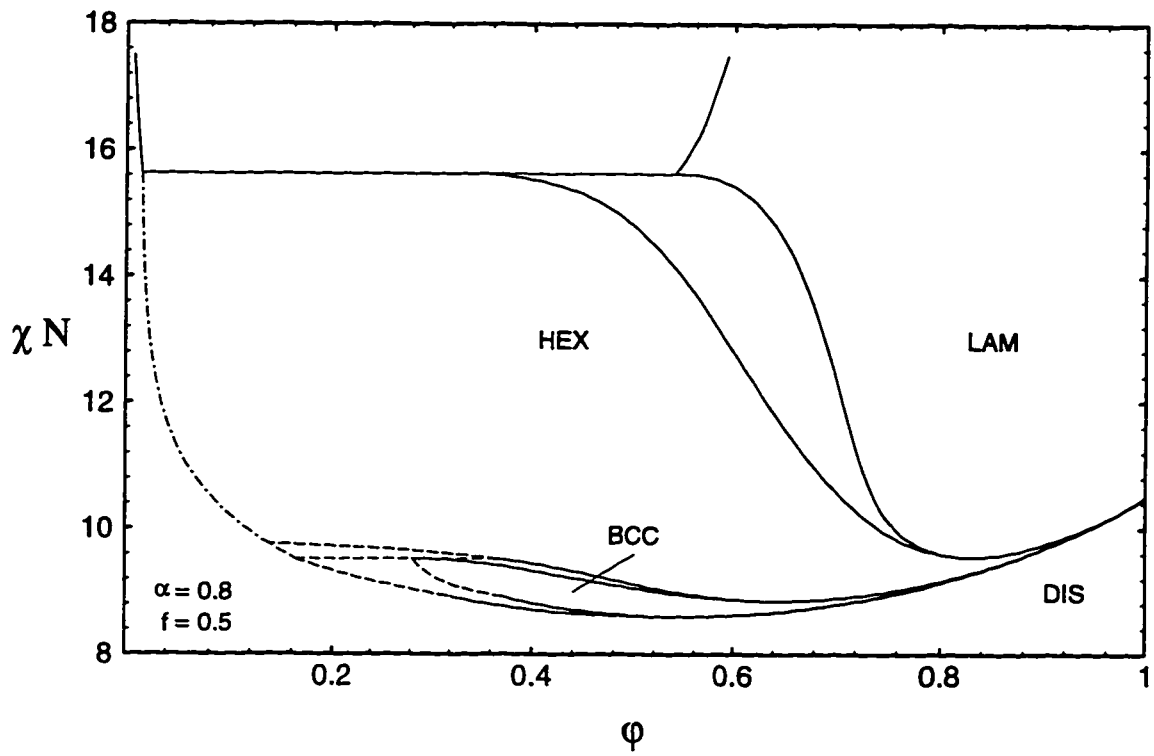

Figure 4.26: Binary phase diagram with $\alpha = 0.8$. Notice the large two phase region between the lamellar phase and an almost pure homopolymer phase. Extrapolated phase boundaries are indicated by dashes. The notation is that of Figure 4.23.

presumably still continuous (c.f. Section 4.2.2.1), and a narrow channel of lamellar unbinding remains for $\alpha = 1.05$ (Figure 4.29), between the disorder/disorder phase coexistence for weak and the lamellar/disorder coexistence for strong segregation. Notice that the unbinding transition is critical for the former, but first-order for the latter.

The channel of complete lamellar unbinding closes rapidly, for $\alpha = 1.1$, the lamellar phase is bound at all temperatures (Figure 4.30), although the signature of the nearby unbinding transition is still visible in the non-monotonic behavior of the composition and periodicity of the lamellar phase in coexistence with the disordered one.

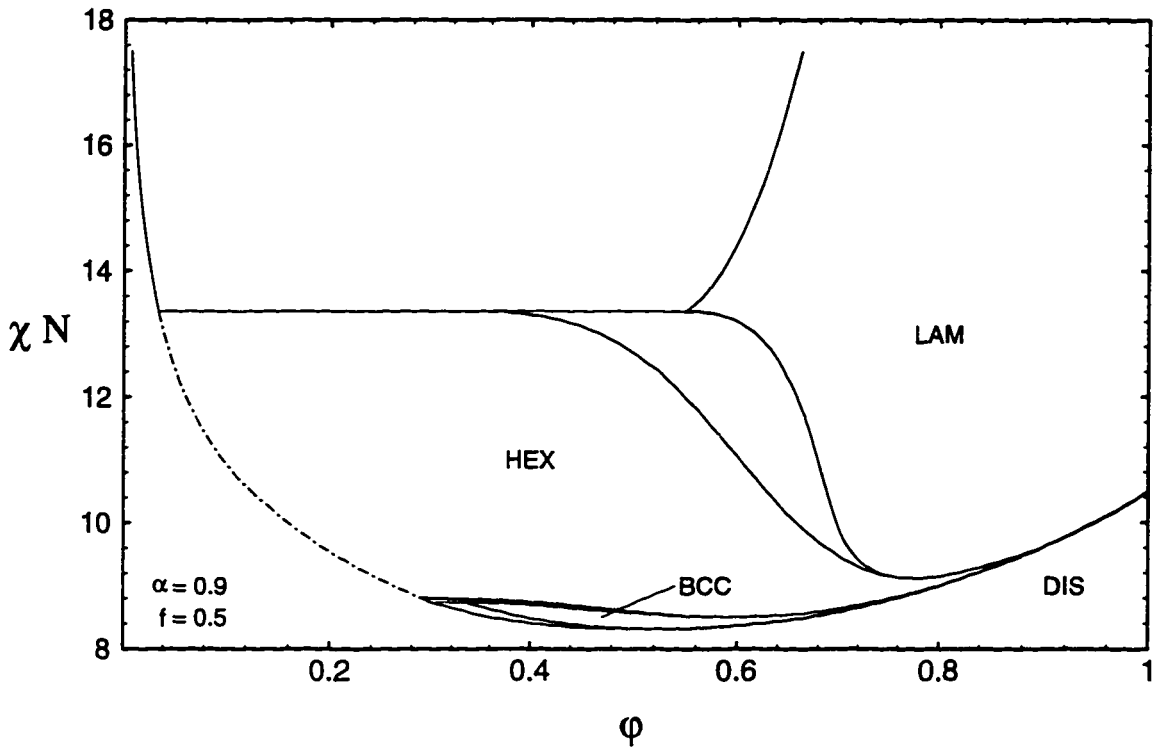

Figure 4.27: Binary phase diagram with $\alpha = 0.9$. Notice how much the lamellar/disordered phase coexistence extends further down, as compared to Figure 4.26.

As α moves further away from 1.0, this effect diminishes (Figure 4.31), and at $\alpha = 1.5$ (Figure 4.32) the periodicity of the lamellar phase on the phase coexistence with the disordered phase is monotonic in χN, although there is still the slightest trace of the unbinding transition in the composition.

4.3.3 Discussion

There has been a large number of experiments on diblocks blended with a homopolymer [113, 83, 241, 240, 82, 115, 116, 256, 255, 258, 257, 265, 206, 193, 104, 41]. Here, we will focus on those [256, 255, 258, 257, 83, 240, 241, 115, 116, 41, 104, 138], that

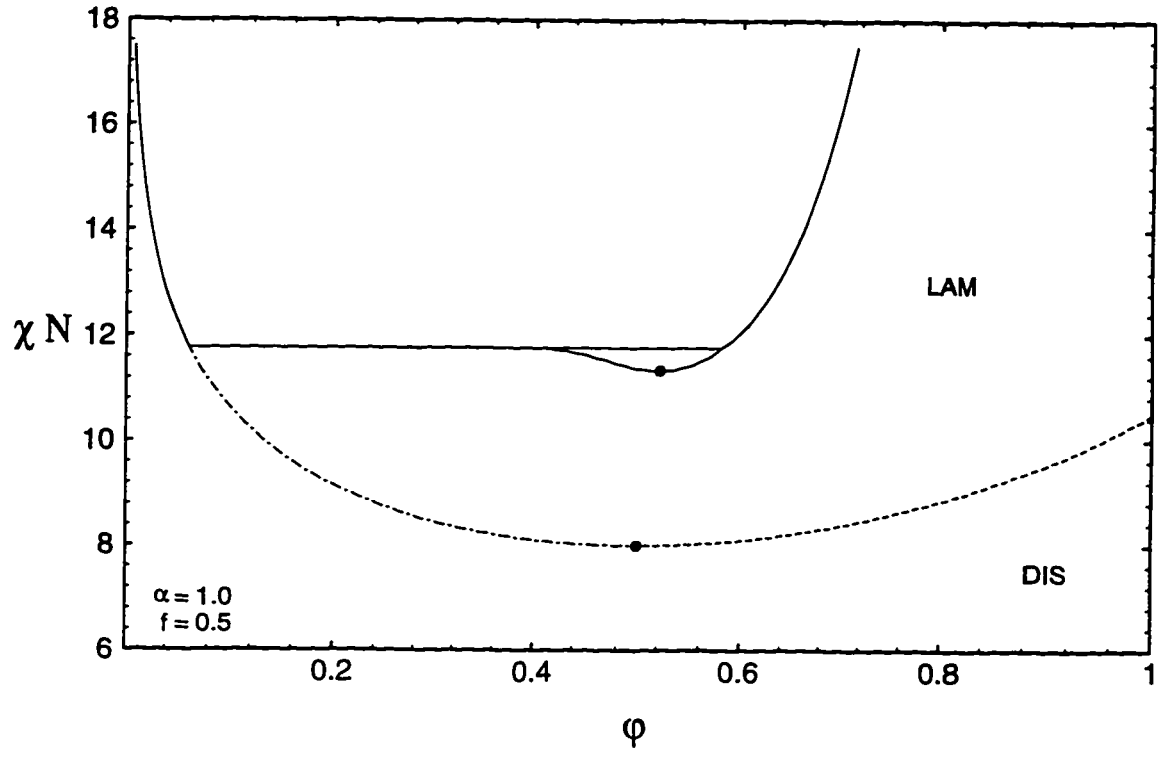

Figure 4.28: Binary phase diagram with $\alpha = 1.0$. The ordered phases, except for the lamellar phase have disappeared, the order/disorder transition is continuous for $\varphi > 0.5$. The Lifshitz point at $\varphi = 0.5$, $\chi N = 8.0$ is indicated by a dot, as is the critical point of the preunbinding region. After [103].

specifically address microphase behavior in systems containing a symmetric ($f = 0.5$) diblock.

One serious difficulty in comparing calculated phase diagrams with experiments is the proper identification of the Flory-Huggins parameter χ. Various values are reported in the literature [242, 9]. Hashimoto and coworkers [242] find for a blend of poly-styrene-*block*-poly-isoprene with poly-styrene homopolymer a very strong dependence not just on temperature, but also on φ *and* on α. Furthermore, the change with α is not even monotonic. We will therefore not try to identify a specific value of χN for a given experiment, but just distinguish between strong, intermediate, and

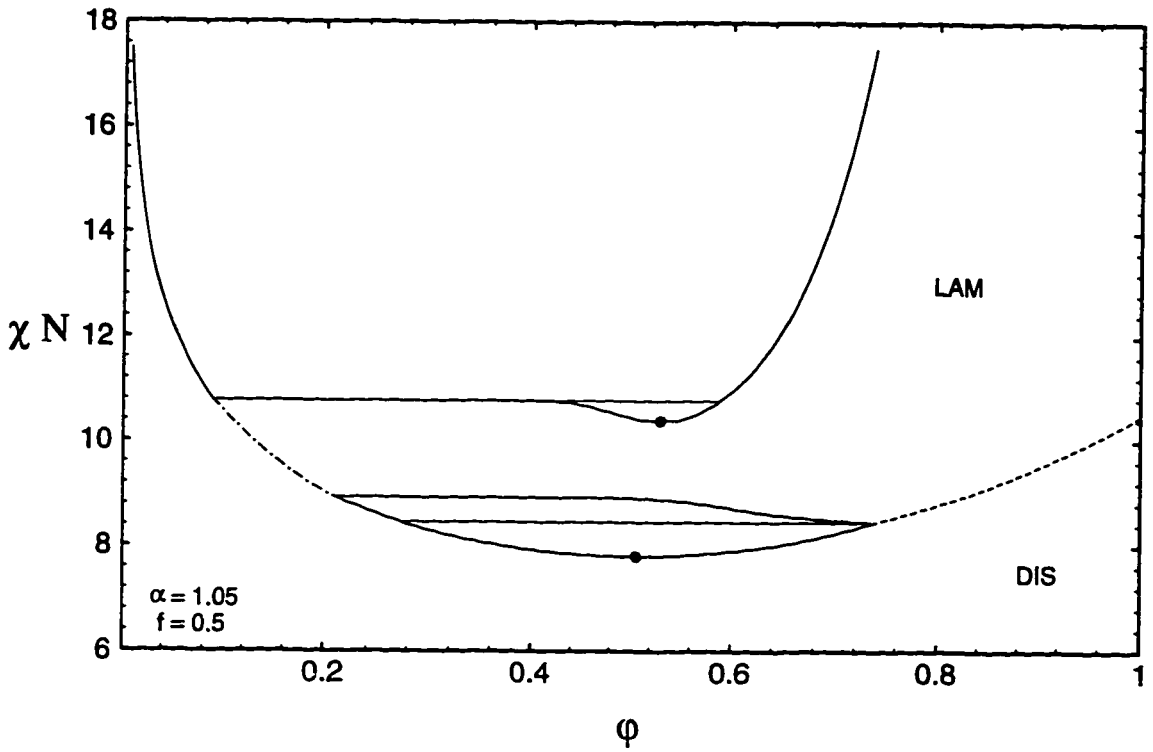

Figure 4.29: Binary phase diagram with $\alpha = 1.05$. The order/disorder transition is still continuous for high copolymer content. In the weak segregation limit, there is a phase coexistence between different disordered phases. Notice the narrow channel of lamellar unbinding.

weak segregation regime.

Experiments for very short homopolymers ($\alpha < 0.25$) usually show good agreement with our calculations. Reports by two different groups [255, 257, 83, 240] on homopolymers with $\alpha \approx 0.07$ and $\alpha \approx 0.125$ find the ordered phases stable at compositions where they are stable in our phase diagrams for intermediate segregation (*i.e.* $\chi N > 15 \ldots 20$). Particular noteworthy is that the order is retained for fairly high dilution (up to $\varphi = 0.2$) [240], while for $\varphi < 0.2$ the body-centered-cubic crystal melts and is replaced by a disordered micellar solution [257]. A recent fluctuation calculation [110], using the Fredrickson-Helfand approach [61], shows a phase diagram

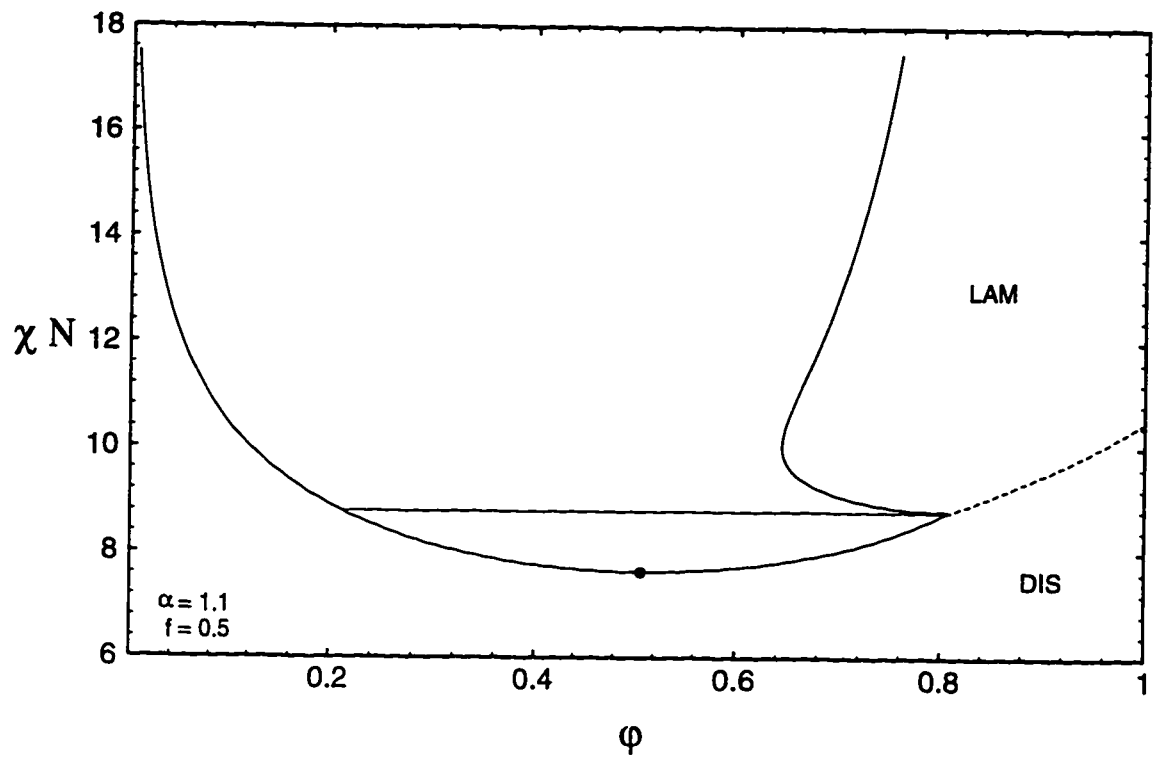

Figure 4.30: Binary phase diagram with $\alpha = 1.1$. The channel of lamellar unbinding has closed, although its signature is still visible in the strongly non-monotonic behavior of the phase boundary.

for $\alpha = 0.1$, which is very similar to our Figure 4.19. Fluctuations destroy Leibler's critical point at $\varphi = 1$ and open up a channel of direct transitions from the lamellar to the disordered phase at high copolymer content. The stability region of the BCC phase is also reduced by fluctuations, so that the BCC phase occurs only at higher segregation and for lower value of φ than in mean field theory.

In the range $0.25 < \alpha < 0.5$, homopolymers with $\alpha \approx 0.25$ and $\alpha \approx 0.3$ have been studied [83, 255, 257]. Again, the ordered phases are observed at those compositions where we find them stable. Winey *et. al.* [258] also report a complex phase, allegedly of ordered bicontinuous double diamond symmetry (OBDD, space group $Pn3m$) in

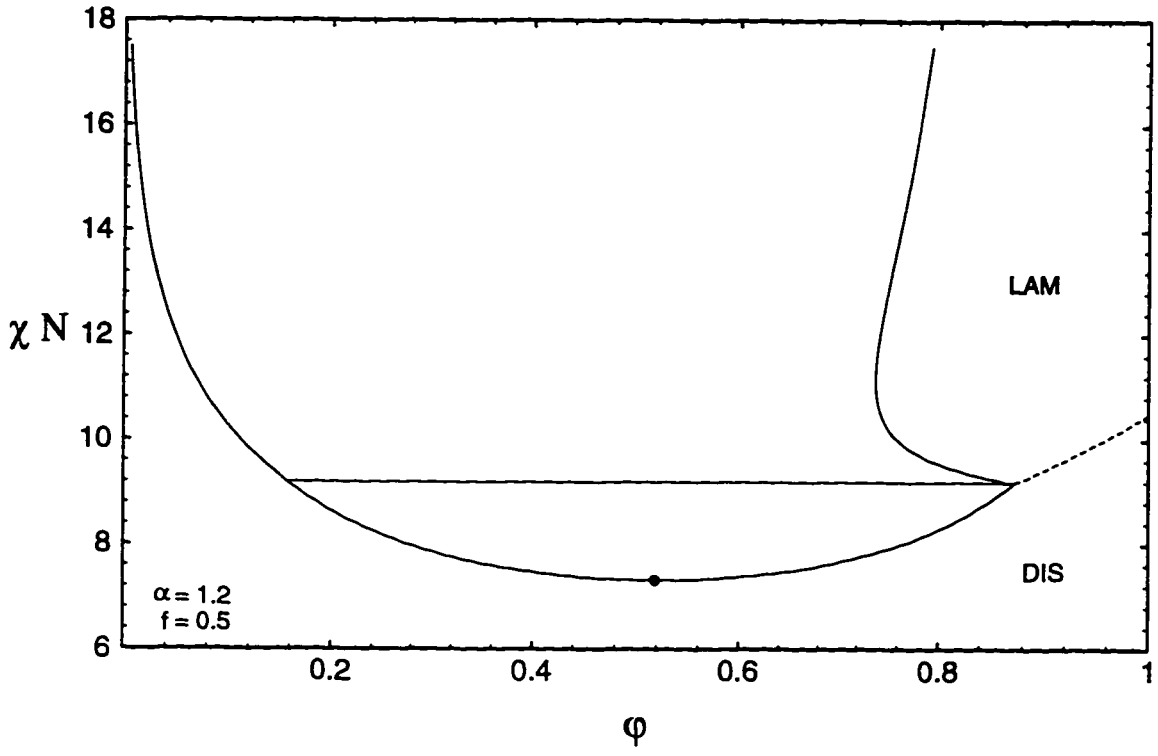

Figure 4.31: Binary phase diagram with $\alpha = 1.2$. The non-monotonic behavior of the lamellar phase boundary is still clearly visible.

the composition range $\varphi = 0.66 \ldots 0.7$. Since we consider only the classical phases in this work, we cannot comment on the stability of the OBDD phase in this region, as compared to the gyroid phase (space group $Ia3d$), which is often found in amphiphilic systems [70, 157, 71, 121]. The stability region of the ordered phases seems to be smaller for $\alpha > 0.25$ than for blends containing shorter homopolymers: for $\varphi < 0.4$, one finds a disordered micellar fluid [257], presumably of spherical micelles. This would mean that the entire region of BCC phase in Figure 4.21 and Figure 4.22 has been destroyed by fluctuations. A similar result was found in a Monte Carlo simulation for short chain surfactants with $\alpha = 0.25$ [121]. The entire region of BCC phase is replaced by a disordered phase while the LAM and HEX phases are found

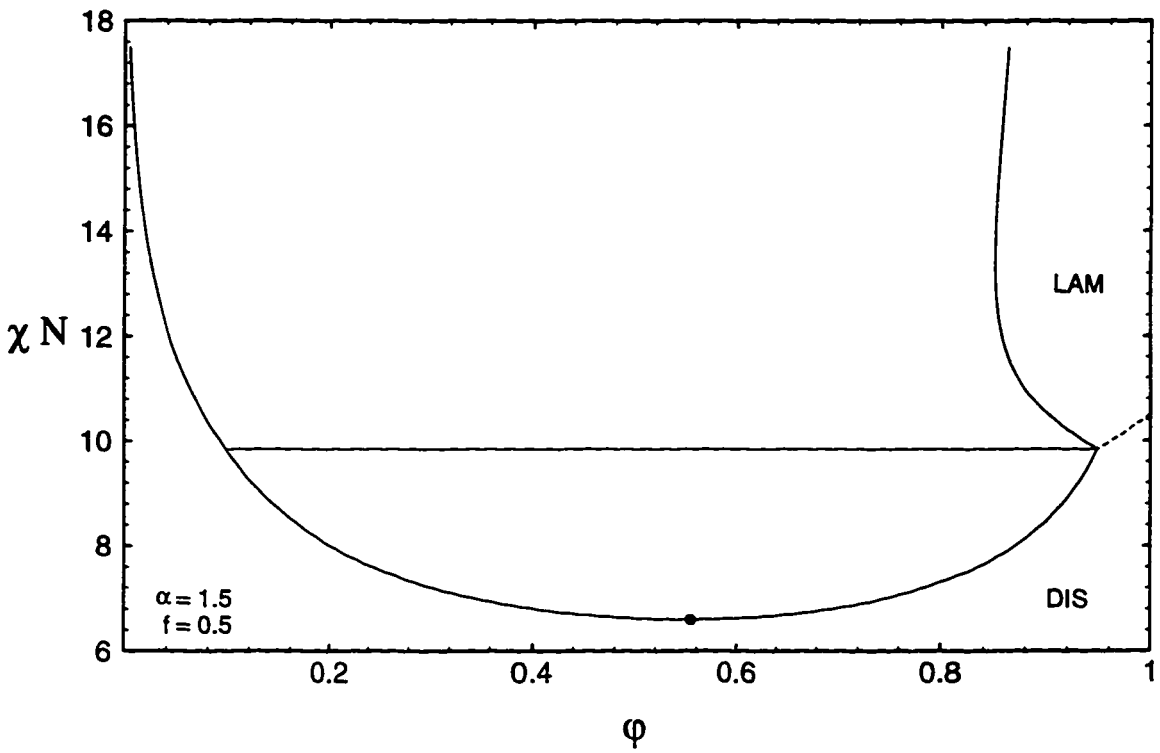

Figure 4.32: Binary phase diagram with $\alpha = 1.5$. Only the slightest trace remains of the unbinding transition in the non-monotonic behavior of the lamellar phase boundary. The maximum wave length to which the lamellar phase can be swollen before macrophase separation occurs increases monotonically with χN.

at essentially the same compositions as in Figure 4.20. Krieghorn and Muthukumar find a large region of HEX/DIS phase coexistence in the weak segregation limit ($\chi N < 13.0$), which is replaced by LAM/DIS coexistence for $\chi N > 13.0$. This result, which is not in accord with neither experiment, nor the full mean field treatment used here, certainly signifies the breakdown of their approach, which is based on a Landau expansion around the uniform state [155]. Additionally, their description of the ordered phase by the first harmonic only, prevents them from finding strongly swollen phases, which are characterized by two very different length scales.

As the length of the homopolymer approaches the length of the diblock (0.5 <

$\alpha < 1.0$), the experimental situation seems less clear. Although ordered phases are observed only for relatively large copolymer concentration in most studies ($\varphi > 0.5$ for $\alpha \approx 0.5$ [83, 255, 41, 104] or $\varphi > 0.7$ for $\alpha \approx 0.7$ [257]), Hashimoto and coworkers [116] report for a system with $\alpha \approx 0.6$ a phase of strongly undulating layers, but clearly with lamellar order, for copolymer concentration as low as $\varphi = 0.2$! This is reminiscent of the situation found in short-chain amphiphiles [237], where undulations *stabilize* the lamellar phase [87] and allow it to be swollen to an extreme degree. In parallel to surfactant systems, other ordered phases do not occupy large regions of the phase diagram [41, 104] and in particular do not exist for high homopolymer concentration. Instead, the blend forms a disordered micellar fluid phase for $\varphi < 0.7$ [257] or $\varphi < 0.5$ [41]. The transition to the regime of strongly swollen layers, as observed by Hashimoto and coworkers [116], may be achieved by changing the temperature in surfactant systems [237], or the effective interaction parameter χN in polymer blends [101]. An experimental temperature/composition diagram would be very interesting to test this prediction.

Comparison of the experimental results with our calculated phase diagrams leads to the conclusion that large-scale form fluctuations, which are ignored in our current approach, are extremely important for blends with $0.5 < \alpha < 1.0$. The body-centered-cubic phase is probably wiped out entirely, as is the strongly swollen hexagonal phase. Both are replaced by disordered micellar phases. For a specific. probably narrow, range of external parameters, an undulation stabilized lamellar phase extends to low copolymer concentrations. (Notice that flat interfaces are stable with respect to capillary waves, while cylindrical interfaces are not [209]).

Finally, for blends with $\alpha \geq 1.0$, experiments find a lamellar phase [104, 115], and phase separation for $\varphi < 0.85$ [104], in general agreement with our calculations. Interesting in particular is the behavior of the lamellar wave length with homopolymer concentration. Initially, the lamellar spacing grows linearly as homopolymer is added, but then levels of and remains constant, signifying that additional homopolymer does

not enter the microstructure, but macrophase separates from it [104].

One publication [138], produces a temperature/composition phase diagram for a system with $\alpha \approx 1.0$. The lamellar phase is stable for $\varphi > 0.8$ at all temperatures, for high temperatures (weak segregation) it goes over into a disordered micellar fluid for $\varphi < 0.8$, for lower temperatures (strong segregation), it is in phase coexistence with an almost pure homopolymer phase. Interestingly, at the transition from one regime to the other, the lamellar phase extends to very low copolymer concentration ($\varphi = 0.3$). Although the identification of the lamellar phase does not seem entirely unambiguous from the micrographs provided in [138], this still seems similar to the behavior shown in Figure 4.28 and Figure 4.29. In the weak segregation limit, the ordered phase is destroyed by fluctuations and replaced by a micellar fluid, but there remains a channel of strongly swollen lamellae at the junction of the weak and the strong segregation regime. A close investigation of this effect, for α very close to one, would be most interesting. Particular care certainly has to be taken to avoid metastability effects: Hashimoto and coworkers [115] report a strong dependence of the domain size on the speed of the solvent casting process.

4.3.4 Summary

We will briefly summarize our results for systems of a symmetric AB-diblock, blended with a homopolymer of any length. The topology of the phase diagram is mainly determined by the ratio of the numbers of segments per chain $\alpha = N_A/N_{AB}$. In particular, we find:

1. $\alpha < 0.25$: Homopolymers shorter than a quarter the size of the copolymer tend to enter the brushes formed by the diblock at the internal interfaces and bring about transitions to phases characterized by curved internal interfaces. Because the homopolymers are short, they gain so much entropy of mixing by distributing themselves uniformly that they tend to disorder any ordered microstructure.

As a consequence, the value of χN at the order/disorder transition rises as the homopolymer volume fraction is increased.

2. $0.25 < \alpha < 0.5$: Homopolymers of this length tend to bring about order, the value of χN at which the system orders, initially *falls* with increasing homopolymer content. The reason is the ability of the short homopolymer to enter the cores of the self-assembled aggregates and relieve stretching stress, despite the fact that this increases the number of AB-contacts. In mean field theory, ordered phases extend to very low diblock content (less than 0.1 volume fraction), even for quite modest values of the interaction parameter.

3. $0.5 < \alpha < 0.75$: For intermediate segregation, the hexagonally ordered phase can be swollen infinitely by adding homopolymer of this length, leading to a complete unbinding transitions of the ordered phase. Consequentially, the transition to the disordered state is continuous at *low* copolymer content. The body-centered-cubic phase does not unbind.

4. $0.75 < \alpha < 1.0$: If the length of the homopolymer approaches the length of the diblock, the ability of the homopolymer to swell the diblock brushes at the internal interfaces is reduced. For intermediate segregation, it is unfavorable for the homopolymer to enter the brushes, instead it is expelled from the lamellar phase, and the blend phase separates into a diblock rich phase with lamellar order and an almost pure homopolymer phase, which is disordered.

5. $1.0 \leq \alpha$: Homopolymers longer than the diblock are unable to swell the diblock brushes at any segregation, the only ordered phase occurring is the lamellar one. Since long homopolymers, confined to microdomains of the lamellar phase would loose configurational entropy, the homopolymer readily phase separates from the diblock. The order/disorder transition for high copolymer content

is continuous in mean field theory. For weak segregation and homopolymers only slightly longer than the copolymer, mean field theory predicts a channel of complete lamellar unbinding, as homopolymer is added. Even for longer homopolymers, the periodicity of the lamellar phase coexisting with the disordered phase displays a non-monotonic behavior with χN. A Lifshitz point is predicted within mean field theory only for the system with $\alpha = 1.0$, and lamellar unbinding occurs only for α very close to 1.0.

With this classification of possible behaviors in mind, we will review the experimental situation, and will point out open questions:

1. $\alpha < 0.25$: In the limit of very short homopolymer chains, there is very good agreement between our calculations and experimental results [255, 257, 83, 240]. It would be interesting to see, however, whether the rise of the order/disorder transitions segregation with homopolymer content can be observed experimentally.

2. $0.25 < \alpha < 0.5$: It does not seem clear at the moment whether the strongly swollen *ordered* phases, containing less than 0.4 volume fraction of copolymer, can be found in experiments. It seems possible that the ordered phase would disorder at high dilution, forming *e.g.* a micellar fluid phase.

3. $0.25 < \alpha < 0.75$: The predominant feature of the mean field phase diagrams in this region is the unbinding of the hexagonal phase. Can it be found in experiments, or do the cylinders break apart when their separation becomes too large?

4. $0.75 < \alpha < 1.0$: Is the strong swelling of ordered morphologies observable in these systems, or is the region of very strongly swollen phases wiped out

by fluctuations affecting the order/disorder transition from below and by the lamellar/disordered phase coexisting from above?

5. $1.0 \leq \alpha$: Extremely swollen *lamellar* phases have been observed in surfactant systems [237, 236], it seems plausible that the should also exist in polymer blends. Even when the predicted unbinding transition cannot be found experimentally, there should be a easily detectable signature of it, namely the non-monotonic behavior with χN of the wave vector of the lamellar phase in coexistence with excess homopolymer. This should be visible despite the effect of fluctuations, since it takes place far away from the order/disorder transition and no extremely swollen phases are involved.

Chapter 5

SUMMARY AND OUTLOOK

Diblock copolymers are fascinating materials, combining the characteristics of amphiphiles and of flexible chain molecules. Systems containing copolymers can display a variety of behaviors: micro- and macrophase separation, ordered and disordered aggregates, simple and complex self-assembled phases, Lifshitz-, Leibler- and unbinding transitions.

Despite some seminal work in the 1980s [125, 222], the general phase behavior of even the *pure* diblock copolymer was only understood within the last few years. A new formulation of the general flexible chain model (Section 2.2.2) in Fourier space [157] allowed the calculation of essentially exact mean field phase diagrams for any desired symmetry, without any arbitrary limitations, except those inherent in the Gaussian model. Fluctuation corrections [61, 200] to the mean field theory can be calculated and are well understood. A series of careful experiments [18, 151, 158] tested the phase behavior of diblock copolymers on a variety of chemically and physically quite different systems. In general, the experimental and theoretical phase diagrams have the same topology, in particular with respect to the symmetry and location of complex phases. The most spectacular test certainly was the reevaluation of samples previously misidentified as OBDD, after mean field theory predicted the gyroid phase to be the stable one [71]. Quantitative comparison (to within 1%, say) of the location of phase boundaries, however, is often difficult, because of the uncertainties in translating theoretical parameters, (*e.g.* effective segment length, number of independent links per chain, effective interaction strength) into physically measurable quantities.

While the phase behavior of pure diblock copolymers is fairly well understood by now, the situation for blends containing block copolymers is far less clear. First of all, additional thermodynamic effects, like macrophase separation, microphase unbinding and Lifshitz critical transitions, which are absent from pure substances, can occur in multi-component systems. Furthermore, added homopolymer interacts with the brushes formed by the diblocks straddling the internal interfaces of the mesophases, leading to non-vanishing spontaneous curvature, even for symmetric copolymers, and to non-trivial interactions between the self-assembled aggregates. Despite numerous experiments on blends of diblocks with corresponding homopolymers [113, 83, 241, 240, 82, 115, 116, 256, 255, 258, 257, 265, 206, 193, 104, 41] no coherent picture of the general phase behavior of these systems has emerged. One reason is the large parameter space of copolymer blends comprising, besides temperature and composition, the architectural parameters of the constituents as well. Without an understanding of the mechanisms governing the behavior, it is virtually impossible to find the right set of parameters for a given purpose. With some insight, however, these additional degrees of freedom can turn polymer blends into flexible and adjustable model systems that can be tailored to fit any particular experimental purpose, *e.g.* the study of specific effects, like the isotropic Lifshitz point or unbinding transitions. The related microemulsion phases have even been proposed as experimental realizations of gauge Higgs systems [98].

Another difficulty in developing an understanding of these compounds from experiments alone is the interplay between various universal and system specific effects. One cannot distinguish what is solely a fluctuation effect and what exists even in mean field theory; what is a generic behavior and what stems from experimental imperfections (such as polydispersity and conformational asymmetry). Another important question in polymer systems concerns possible non-equilibrium effects. The tales of the misidentified HPL and gyroid phases demonstrates that the interpretations of experiments on polymeric systems can be difficult even for experienced

experimentalists, and that they can lead astray those without a solid understanding of the underlying theory.

The present work addressed these questions. I present a *complete* catalogue of mean field phase diagrams for *all* possible binary and ternary blends containing a symmetric AB-diblock and corresponding A- and B-homopolymers. The method utilized is free of arbitrary limitations except for the mean field approximation and the choice of the Gaussian chain model. The latter is generally accepted to be an excellent model for the *universal* behavior of flexible chains, while the former is a very good approximation in polymer systems in the intermediate to strong segregation limit. In particular, the method used here is not limited to phases with simple geometries (compare *e.g.* [10]. Even phases as complex as the gyroid, or as asymmetric as the extremely swollen phases can be treated. The theory is also not limited to the case of weak segregation or small order parameter [125, 131, 38, 37]. Furthermore, no constraint is made on the infinitely many configurations of the polymer chains [222, 175], instead the single chain partition functions for each chain is solved exactly.

The phase diagrams presented in Chapter 4 provide a complete catalogue for blends containing a symmetric diblock copolymer and corresponding homopolymer of any degree of polymerization. In Section 4.1 we studied the effect of adding two different homopolymers to a diblock copolymer at all compositions, for fixed temperature. In Section 4.3, we studied the temperature dependence in a binary system, again for all possible choices of chain length ratios. In Section 4.2, we investigated at all compositions of the ternary blend and for the relevant temperature range, the amazingly complex phase behavior in the "symmetric system", in which all chains are of equal length. From these very complex calculations, a final simple, coherent and intuitive picture emerged.

The main factor influencing the topology of the phase diagram is the chain length of the homopolymer, with very short homopolymers tending to disorder any ordered morphology, while homopolymers shorter than or comparable in length to the copoly-

mer induce order. Homopolymers longer than the diblock finally phase separate from the mixture. In the intermediate segregation regime, and for homopolymers somewhat shorter than the diblock, mean field theory predicts an unbinding of the microphase upon addition of homopolymer: the wavelength of the ordered phase becomes infinite and the system continuously transforms into the the disordered state. All these trends can be understood in terms of the varying ability of the homopolymer to swell the diblock brush formed at the internal interfaces and the changing "grafting density" of this brush as temperature is varied.

This very simple and complete picture of the phase behavior of homopolymer/diblock blends, and the mechanisms that govern it, can be cross checked with existing experimental results. We find that our results agree with experiments for the limit of very short or very long homopolymer chains. As far as experimental parameters can be transcribed into our units, we find agreement is to within about 15 % (c.f. Section 4.3).

For intermediate chain lengths, the situation is less clear, mainly because experimental results on such systems are lacking. We propose a series of future experiments (Section 4.3.4) to investigate in particular the regime of strongly swollen microphases and of the unbinding transition. It is now clear what choice of architectural parameters brings about a specific desired behavior. Moreover, with a clear understanding of the *mean field* phase diagram, we can discern the possible effect of fluctuations.

The most surprising result of this work has certainly been the discovery of the preunbinding behavior in swollen lamellar phases, and the characterization of the sudden swelling with changing temperature of certain blends as first-order unbinding transitions (Section 4.2). Although experimental verification of this result in polymeric systems is still lacking, this discovery has shed new light on the perplexing behavior found in some closely related amphiphilic systems [67, 237, 236]. There, it was found that a minute change in temperature could bring about a swelling of a lamellar phase to a wavelength of about 3000Å, over one hundred times the diam-

eter of an amphiphilic molecule! The experimental phase diagrams obtained there are strikingly similar to some of the figures obtained here (Section 4.2). In fact, the results presented here are (so far) the only microscopic calculations that can account for and explain these extremely swollen, yet ordered, phases. We would expect, that in polymeric systems, where fluctuations are generally better controlled, these phases can also be found.

Some important developments took place while the present work was in progress. Matsen and Bates [150, 152], using essentially the same method as in the present work, considered the various contributions to the free energy, arising from the chain conformations, as well as from the internal interfaces. They were able to show that the presence (or absence) of certain ordered morphologies can be understood as arising from a competition between an enthalpic surface contribution, favoring as little interfacial area as possible, and an entropic stretching penalty favoring interfaces with constant curvature and domains of constant thickness. In particular, it could be shown that the often postulated OBDD phase is inferior to the gyroid phase on both counts.

Two attempts were made to consider more realistic chain models. While one publication [153] considered only different effective segment lengths, while retaining the Gaussian model, Müller and Schick [186, 184] developed an extension of the method used here to *arbitrary* chain models.

Finally, Krieghorn and Muthukumar [110] included fluctuations [61] into a calculation for the ternary and binary blends comparable to systems considered in the present work. Although they find that the phase diagrams are slightly modified near the order/disorder transition, the topology of the phase diagrams is not changed from the mean field result upon inclusion of fluctuations. The phase diagrams presented here should therefore provide a reliable guide for future experimental work.

A further attempt has been made to calculate the influence of fluctuations in pure diblock melts [261, 227, 120], by considering harmonic corrections to the mean field

result. While the consequences for the phase diagram are not clear, these calculations make interesting predictions for the dynamics of transitions between different ordered phases.

One aspect has not been addressed in the present work: the effects of asymmetric diblock copolymers. We can assume that for weakly asymmetric diblocks our results will be changed only slightly (Section 4.1) and that for strong asymmetry the general guiding principles outlined above will apply. However, no attempt has been made to map out the effect of architectural asymmetry comprehensively.

One gap in our general understanding that has become more apparent in this work concerns the behavior of systems close to a Lifshitz point, in particular at an isotropic Lifshitz point. Previous theoretical investigations [166, 167, 168, 95] focused almost exclusively on systems with one preferred direction. Some rigorous calculations, based *e.g.* on a general Landau type analysis, would be helpful to determine the general shape of the phase diagram in the vicinity of such a point. There are also concerns about the reliability of some of the previously published material on this matter [213]. Moreover, the effect of fluctuations on an isotropic Lifshitz point is completely unclear at the moment [110]. More experimental and theoretical work is clearly needed, despite some encouraging effort in the recent past [14, 110].

The greatest challenge, however, will be to extend the present reliable and realistic theory to include form fluctuations on the scale of a single aggregate. For instance, it is known experimentally that lamellae in strongly swollen phases do not remain flat, but undulate [207, 116], and that these undulations are important for the stabilization of such phases [87, 88]. One would also expect a strongly swollen BCC phase to disorder long before the spherical micelles themselves fall apart [129, 47, 48, 163, 161, 162, 217]. Our present formalism does not allow for these possibilities.

Intuitively, one expects these situations to be important in the region of strong swelling and close to the unbinding transition. Their effect on the preunbinding regions is also not clear. It would be desirable to find a way to allow for such partial

disorder within the framework of the present full self-consistent field theory. Closely related is the study of single aggregate properties: an isolated bilayer, a spherical micelle, the interactions between them, etc. It would be exciting to extend our methods, free of ad hoc assumptions and using realistic microscopic chain models, to these cases. In a similar vein, it would be interesting to study the self-assembly of copolymeric systems close to a hard wall or in confined geometries. With few exceptions [229, 147], most of the work done is only reliable in certain limiting cases [59, 244]. One final interesting possibility concerns the combination of self-consistent field methods with Monte Carlo simulations. For instance, one could study the properties of one specific test chain (simulated) in a self-assembled tube or layer (found self-consistently) [202, 192, 132]. The attraction here lies in the efficiency and ease with which slowly varying properties (*i.e.* the self-assembled matrix) can be calculated in mean field theory, while naturally strongly fluctuating single particle properties can only be found realistically from simulations. These ideas provide exciting new material for future work.

BIBLIOGRAPHY

[1] Bruce Alberts, Dennis Bray, Julian Lewis, Martin Raff, Keith Roberts, and James D. Watson. *Molecular Biology of the Cell.* Garland Publishing, Incorporated, 1983.

[2] Paschalis Alexandridis, Ulf Olsson, and Björn Lindman. Self-assembly of amphiphilic block copolymers: The $(EO)_{13}(PO)_{30}(EO)_{13}$–water–p-xylene system. *Macromolecules*, 28(23):7700–7710, 1995.

[3] Daniel Amit. *Field Theory: The Renormalization Group and Critical Phenomena.* The McGraw-Hill Companies, 1978.

[4] Karl Amundson and Eugene Helfand. Quasi-static mechanical properties of lamellar block copolymer microstructure. *Macromolecules*, 26(6):1324–1332, 1993.

[5] C. Aragao de Carvlho and S. Caracciolo. A new Monte-Carlo approach to the critical properties of self-avoiding random walks. *Journal de Physique (France)*, 44(3):323–331, 1983.

[6] Clemens Auschra and Reimund Stadler. New ordered morphologies in ABC triblock copolymers. *Macromolecules*, 26(9):2171–2174, 1993.

[7] Anna C. Balazs and Mark T. DeMeuse. Miscibility in ternary mixtures containing a copolymer and two homopolymers. Effect of sequence distribution. *Macromolecules*, 22(11):4260–4267, 1989.

[8] R. C. Ball, J. F. Marko, S. T. Milner, and T. A. Witten. Polymers grafted to a convex surface. *Macromolecules*, 24(3):693–703, 1991.

[9] N. P. Balsara. Thermodynamics of polymer blends. In Mark [140], chapter 19.

[10] M. Banaszak and M. D. Whitmore. Mean field theory of the phase behavior of ternary block copolymer-homopolymer blends. *Macromolecules*, 25(1):249–260, 1992.

[11] M. Banaszak and M. D. Whitmore. Self-consistent theory of block copolymer blends: Selective solvent. *Macromolecules*, 25(13):3406–3412, 1992.

[12] Jean-Louis Barrat and Glenn H. Fredrickson. Collective and single-chain correlations near the block copolymer order-disorder transition. *Journal of Chemical Physics*, 95(2):1281–1289, 1991.

[13] Jean-Louis Barrat and Jean-François Joanny. Theory of polyelectrolyte solutions. *Advances in Chemical Physics*, 94:1–66, 1996.

[14] Frank S. Bates, Wayne Maurer, Timothy P. Lodge, Mark F. Schulz, Mark W. Matsen, Kristoffer Almdal, and Kell Mortensen. Isotropic Lifshitz behavior in block copolymer-homopolymer blends. *Physical Review Letters*, 75(24):4429–4432, 1995.

[15] Frank S. Bates, Wayne W. Maurer, Paul M. Lipic, Marc A. Hillmyer, Kristoffer Almdal, Kell Mortensen, and Timothy P. Lodge. Polymeric bicontinuous microemulsions. *Science*, preprint, 1997.

[16] Frank S. Bates, Jeffrey H. Rosedale, and Glenn H. Fredrickson. Fluctuation effects in a symmetric diblock copolymer near the order-disorder transition. *Journal of Chemical Physics*, 92(10):6255–6270, 1990.

[17] Frank S. Bates, Jeffrey H. Rosedale, Glenn H. Fredrickson, and Charles J. Glinka. Fluctuation-induced first-order transition of an isotropic system to a periodic state. *Physical Review Letters*, 61(19):2229–2232, 1988.

[18] Frank S. Bates, Mark F. Schulz, Ashish K. Khandpur, Stephan Förster, Jeffrey H. Rosedale, Kristoffer Almdal, and Kell Mortensen. Fluctuations, conformational asymmetry and block copolymer phase behviour. *Faraday Disc.*, 98:7–18, 1994.

[19] Birger Bergersen and Michael Plischke. *Equilibrium Statistical Physics.* World Scientific Publishing Company, Incorporated, 1994.

[20] S. A. Brazovskii. Phase transitions of an isotropic system to a nonuniform state. *Sov. Phys. JETP*, 41(1):85, 1975.

[21] Daniel Broseta and Glenn H. Fredrickson. Phase equilibria in copolymer/homopolymer ternary blends: Molecular weight effects. *Journal of Chemical Physics*, 93(4):2927–2938, 1990.

[22] Andrzej Budkowski, Jacob Klein, and Lewis J. Fetters. Brush formation by symmetric and by highly asymmetric diblock copolymers at homopolymer interfaces. *Macromolecules*, 28(25):8571–8578, 1995.

[23] Andrzej Budkowski, Jacob Klein, Lewis J. Fetters, and Takeji Hashimoto. Competitive adsorption at homopolymer interfaces from a binary mixture of diblock copolymer. *Macromolecules*, 28(25):8579–8586, 1995.

[24] M. A. Carignano and I. Szleifer. Statistical thermodynamic theory of grafted polymeric layers. *Journal of Chemical Physics*, 98(6):5006–5018, 1993.

[25] M. A. Carignano and I. Szleifer. Structure and thermodynamics of grafted three-arm branched polymer layers. *Macromolecules*, 27(3):702–710, 1994.

[26] M. A. Carignano and I. Szleifer. On the structure and pressure of tethered polymer layers in good solvent. *Macromolecules*, 28(9):3197–3204, 1995.

[27] P. M. Chaikin and T. C. Lubensky. *Principles of Condensed Matter Physics.* Cambridge Press, Incorporated, 1995.

[28] Mark Dadmun. Effect of copolymer architecture on the interfacial structure and miscibility of a ternary polymer blend containing a copolymer and two homopolymers. *Macromolecules*, 29(11):2868–3874, 1996.

[29] Chi-An Dai, Klaus D. Jandt, Dhamodharan R. Iyengar, Nelle L. Slack, Kevin H. Dai, William B. Davidson, Edward J. Kramer, and Chung-Yuen Hui. Strengthening polymer interfaces with triblock copolymers. *Macromolecules*, 30(3):549–560, 1997.

[30] Kevin H. Dai, Laura J. Norton, and Edward J. Kramer. Equilibrium segment density distribution of a diblock copolymer segregated to a polymer/polymer interface. *Macromolecules*, 27:1949–1956, 1994.

[31] P. G. de Gennes. Theory of X-ray scattering by liquid macromolecules with heavy atom labels. *Journal de Physique (France)*, 31(2-3):235–238, 1970.

[32] P. G. de Gennes. Qualitative features of polymer demixtion. *Journal de Physique (France)*, 38(21):L441–L443, 1977.

[33] P. G. de Gennes. Conformations of polymers attached to an interface. *Macromolecules*, 13(5):1069–1075, 1980.

[34] P. G. de Gennes and C. Taupin. Microemulsions and the flexibility of oil/water interfaces. *Journal of Physical Chemistry*, 86(13):2294–2304, 1982.

[35] Pierre-Gilles De Gennes. *Scaling Concepts in Polymer Physics.* Cornell University Press, 1979.

[36] Pierre-Gilles De Gennes and J. Prost. *The Physics of Liquid Crystals.* Oxford University Press, Incorporated, 1995.

[37] M. Olvera de la Cruz, A. M. Mayes, and B. W. Swift. Transitions to lamellar-catenoid structures in block copolymer melts. *Macromolecules*, 25(2):944–948, 1992.

[38] Monica Olvera de la Cruz. Transitions to periodic structures in block copolymer melts. *Physical Review Letters*, 67(1):85–88, 1991.

[39] John E. Dennis and Robert B. Schnabel. *Numerical Methods for Unconstrained Optimization and Nonlinear Equations.* Prentice Hall, 1983.

[40] J. Des Cloizeaux and Gerard Jannink. *Polymers in Solution: Their Modelling and Structure.* Oxford University Press, Incorporated, 1991.

[41] M. M. Disko, K. S. Liang, S. K. Behal, R. J. Roe, and K. J. Jeon. Catenoid-lamellar phase in blends of styrene-butadiene diblock copolymer and homopolymer. *Macromolecules*, 26(11):2983–2986, 1993.

[42] M. Doi and S. F. Edwards. *The Theory of Polymer Dynamics.* Oxford University Press, Incorporated, 1986.

[43] S. F. Edwards. The theory of polymer solutions at intermediate concentrations. *Proceedings of the Physical Society*, 88:265–280, 1966.

[44] S. F. Edwards. Functional problems in the theory of polymers. In A. M. Arthurs, editor, *Functional integration and its applications*, pages 51–59. Clarendon Press, Oxford, 1975.

[45] S. F. Edwards. The size of a polymer molecule in a strong solution. *Journal of Physics A: Mathematical and General*, 8(10):1670–1680, 1975.

[46] Per Ekwall. Composition, properties and structure of liquid crystalline phases in systems of amphiphilic compounds. In Glenn H. Brown, editor, *Advances in Liquid Crystals*, volume 1, pages 1–142. Academic Press, Incorporated, 1975.

[47] F. J. Esselink, A. N. Semenov, G. ten Brinke, G. Hadziioannou, and G. T. Oostergetel. Formation and structural ordering of micelles of block copolymers in a thin-film-homopolymer matrix. *Physical Review B*, 48(18):13451–13458, 1993.

[48] F. J. Esselink, A. N. Semenov, G. ten Brinke, G. Hadziioannou, and G. T. Oostergetel. Ordering of block copolymer micelles in confined two-dimensional solutions. *Macromolecules*, 28(9):3479–3481, 1995.

[49] William Feller. *An Introduction to Probability Theory and Its Applications*, volume 1. John Wiley & Sons, Incorporated, 1968.

[50] William Feller. *An Introduction to Probability Theory and Its Applications*, volume 2. John Wiley & Sons, Incorporated, 1971.

[51] Richard P. Feynman and A. Hibbs. *Quantum Mechanics and Path Integrals*. The McGraw-Hill Companies, 1965.

[52] G. J. Fleer. *Polymers at Interfaces*. Chapman and Hall, 1994.

[53] R. J. Fleming. Monte Carlo studies of the configurational properties of freely rotating polymer chains subject to excluded volume conditions. *Proceedings of the Physical Society of London*, 90:1003–1009, 1967.

[54] R. J. Fleming. Monte Carlo studies of the excluded volume problem in freely rotating chains. *Journal of Physics A*, 1:404–406, 1968.

[55] Paul J. Flory. The configuration of real polymer chains. *Journal of Chemical Physics*, 17(3):303–310, 1949.

[56] Paul J. Flory. *Principles of Polymer Chemistry.* Cornell University Press, 1953.

[57] Paul J. Flory. *Statistical Mechanics of Chain Molecules.* Hanser-Gardner Publications, 1989.

[58] Stephan Förster, Ashish K. Khandpur, Jin Zhao, Frank S. Bates, Ian W. Hamley, Anthony J. Ryan, and Wim Bras. Complex phase behavior of polyisoprene-polystyrene diblock copolymers near the order-disorder transition. *Macromolecules*, 27(23):6922–6935, 1994.

[59] Glenn H. Fredrickson. Surface ordering phenomena in block copolymer melts. *Macromolecules*, 20(10):2535–2542, 1987.

[60] Glenn H. Fredrickson and Kurt Binder. Kinetics of metastable states in block copolymer melts. *Journal of Chemical Physics*, 91(11):7265–7275, 1989.

[61] Glenn H. Fredrickson and Eugene Helfand. Fluctuation effects in the theory of microphase separation in block copolymers. *Journal of Chemical Physics*, 87(1):697–705, 1987.

[62] Karl F. Freed. Functional integrals and polymer statistics. *Advances in Chemical Physics*, 22:1–128, 1972.

[63] Karl F. Freed. *Renormalization Group Theory of Macromolecules.* John Wiley & Sons, Incorporated, 1987.

[64] Dilip Gersappe and Anna C. Balazs. Random copolymers as effective compatibilizing agents. *Physical Review E*, 52(5):5061–5064, 1995.

[65] Samuel P. Gido, Dwight W. Schwark, Edwin L. Thomas, and Maria do Carmo Concçalves. Observation of a non-constant mean curvature interface in an ABC triblock copolymer. *Macromolecules*, 26(10):2636–2640, 1993.

[66] Leonardo Golubović. Passages and droplets in lamellar fluid membrane phases. *Physical Review E*, 50(4):R2419–R22422, 1994.

[67] G. Gompper and M. Schick. Self-assembling amphiphilic systems. In Cyril M. Domb and Joel L. Lebowitz, editors, *Phase Transition and Critical Phenomena*, volume 16. Academic Press, Incorporated, 1994.

[68] P. C. M. Grim, I. A. Nyrkova, A. N. Semenov, G. ten Brinke, and G. Hadzioannou. The free surface of thin diblock copolymer films: Experimental and theoretical investigations on the formation and growth of surface relief structures. *Macromolecules*, 28(22):7501–7513, 1995.

[69] Damian Hajduk. Private Communication.

[70] Damian A. Hajduk, Paul E. Harper, Sol M. Gruner, Christian C. Honeker, Gia Kim, Edwin L. Thomas, and Lewis J. Fetters. The gyroid: A new morphology in weakly segregated diblock copolymers. *Macromolecules*, 27(15):4063–4075, 1994.

[71] Damian A. Hajduk, Paul E. Harper, Sol M. Gruner, Christian C. Honeker, Edwin L. Thomas, and Lewis J. Fetters. A reevaluation of bicontinuous cubic phases in starblock copolymers. *Macromolecules*, 28(7):2570–2573, 1995.

[72] A. Halperin. On polymer brushes and blobology: An introduction. In Y. Rabin and R. Bruinsma, editors, *Soft Order in Physical Systems*, volume 323 of *NATO ASI Ser.: Series B, Physics Vol.*, pages 33–56. Plenum Publishing Corporation, 1994.

[73] A. Halperin, M. Tirrell, and T. P. Lodge. Tethered chains in polymer microstructures. *Advances in Polymer Science*, 100:31–71, 1992.

[74] Ian W. Hamley and Frank S. Bates. Harmonic corrections to the mean-field phase diagram for block copolymers. *Journal of Chemical Physics*, 100(9):6813–6817, 1994.

[75] Ian W. Hamley, Mark D. Gehlsen, Ashish Khandpur, Kurt A. Koppi, Jeffrey Rosedale, Mark F. Schulz, Frank S. Bates, Kristoffer Almdal, and Kell Mortensen. Complex layered phases in asymmetric diblock copolymers. *Journal de Physique 2 (France)*, 4(12):2161–2186, 1994.

[76] Ian W. Hamley, Kurt A. Koppi, Jeffrey Rosedale, Frank S. Bates, Kristoffer Almdal, and Kell Mortensen. Hexagonal mesophases between lamellae and cylinders in a diblock copolymer melt. *Macromolecules*, 26(22):5959–5970, 1993.

[77] Chang Dae Han, Deog Man Back, Jinhwan Kim, Kohtaro Kimishima, and Takeji Hashimoto. Viscoelastic behavior, phase equilibira, and microdomain morphology in mixtures of a block copolymer and a homopolymer. *Macromolecules*, 25(12):3052–3067, 1992.

[78] J. P. Hansen and Ian R. McDonald. *The Theory of Simple Liquids.* Academic Press, Incorporated, 1977.

[79] Hiroshi Hashimoto, Mineo Fujimura, Takeji Hashimoto, and Hiromichi Kawai. Domain-boundary structure of styrene-isoprene block copolymer films cast from solutions. 7. Quantitative studies of solubilization of homopolymers in spherical domain systems. *Macromolecules*, 14(3):844–851, 1981.

[80] Takeji Hashimoto, Kohtaro Kimishima, and Hirokazu Hasegawa. Self-assembly and patterns in binary mixtures of SI block copolymer and PPO. *Macromolecules*, 24(20):5704–5712, 1991.

[81] Takeji Hashimoto, Satoshi Koizumi, and Hirokazu Hasegawa. Ordered structure in blends of block copolymers. 2. Self-Assembly for immiscible lamella-forming copolymers. *Macromolecules*, 27(6):1562–1570, 1994.

[82] Takeji Hashimoto, Satoshi Koizumi, Hirokazu Hasegawa, Tatsuo Izumitani, and Stephen T. Hyde. Observation of "mesh" and "strut" structures in block copolymer/homopolymer mixtures. *Macromolecules*, 25:1433–1439, 1992.

[83] Takeji Hashimoto, Hideaki Tanaka, and Hirokazu Hasegawa. Ordered structures in mixtures of block copolymers and homopolymers. 2. Effects of molecular weight of homopolymers. *Macromolecules*, 23(20):4378–4386, 1990.

[84] Takeji Hashimoto, Komei Yamasaki, Satoshi Koizumi, and Hirokazu Hasegawa. Ordered structure found in blends of block copolymers. 1. Miscibility criterion for lamellar block copolymers. *Macromolecules*, 26(11):2895–2904, 1993.

[85] E. Hecht, K. Mortensen, and H. Hoffmann. L_3 phase in a binary block copolymer/water system. *Macromolecules*, 28(16):5465–5476, 1995.

[96] Kalina Hristova and David Needham. Phase behavior of a lipid/polymer–lipid mixture in aqueous medium. *Macromolecules*, 28(4):991–1002, 1995.

[97] Wenchun Hu, Jeffrey T. Koberstein, J. P. Lingelser, and Y. Gallot. Interfacial tension reduction in polystyrene/poly(dimethylsiloxane) blends by the addition of poly(styrene-*b*-dimethylsiloxane). *Macromolecules*, 28(15):5209–5214, 1995.

[98] David A. Huse and Stanislas Leibler. Are sponge phases of membranes experimental gauge-Higgs systems? *Physical Review Letters*, 66(4):437–440, 1991.

[99] Takashi Inoue, Toshiichi Soen, Takeji Hashimoto, and Hiromichi Kawai. Studies on domain formation of the A-B-type block copolymer from its solutions. ternary polymer blend of the styrene-isoprene block copolymer with polystyrene and polyisoprene. *Macromolecules*, 3(1):87–92, 1970.

[100] José R. Isasis, Luis C. Cesteros, and Issa Katime. Poly(4-vinylpyridine)/-poly(vinyl acetate-*co*-vinyl alcohol) blends: effect of sequence distribution on miscibility. *Polymer*, 36(6):1235–1241, 1995.

[101] Philipp K. Janert and Michael Schick. First-order unbinding and preunbinding in amphiphilic systems. *Physical Review E*, 54(1):R33–R35, 1996.

[102] Philipp K. Janert and Michael Schick. Phase behavior of ternary homopolymer/diblock blends: Influence of relative chain lengths. *Macromolecules*, 30(1):137–144, 1997.

[103] Philipp K. Janert and Michael Schick. Phase behavior of ternary homopolymer/diblock blends: Microphase unbinding in the symmetric system. *Macromolecules*, 1997.

[104] Kyung-Jin Jeon and Ryong-Joon Roe. Solubilization of a homopolymer in a block copolymer. *Macromolecules*, 27(9):2439–2447, 1994.

[105] Hiroshi Jinnai, Takeji Hashimoto, Daniel Lee, and Sow-Hsin Chen. Morphological characterization of bicontinuous phase-separated polymer blends and one-phase microemulsions. *Macromolecules*, 30(1):130–136, 1997.

[106] J. F. Joanny. Critical properties of a system of two molten polymers. *J. Phys. A*, 11(5):L117–L120, 1978.

[107] J. L. Jones and M. Olvera de la Cruz. Transitions to periodic structures: Higher harmonic corrections with concentration fluctuations. *Journal of Chemical Physics*, 100(7):5272–5279, 1994.

[108] Mark Kac. *Probability and Related Topics in Physical Sciences.* American Mathematical Society, reprint edition edition, 1972.

[109] A. R. Khoklov and A. Grosberg. *Statistical Physics of Macromolecules.* American Institute of Physics (AIP Press), 1994.

[110] L. Kielhorn and M. Muthukumar. Fluctuation theory of diblock copolymer/homopolymer blends and its effects on the Lifshitz point. *preprint*, 1997.

[111] Jin Kon Kim. Compatibilization effect of a block copolymer in two random copolymer blends. *Polymer*, 36(6):1243–1252, 1995.

[112] Kohtaro Kimishima, Takeji Hashimoto, and Chang Dae Han. Spatial distribution of added homopolymer within the microdomains of a mixture consisting of an ABA-type triblock copolymer and a homopolymer. *Macromolecules*, 28(11):3842–3853, 1995.

[113] Satoshi Koizumi, Hirokazu Hasegawa, and Takeji Hashimoto. Mutual diffusion of block copolymer and homopolymer. Visualization using mirodomain as a probe. *Macromolecules*, 23(11):2955–2962, 1990.

[114] Satoshi Koizumi, Hirokazu Hasegawa, and Takeji Hashimoto. Ordered structure in blends of block copolymers. 3. Self-Assembly in blends of sphere- or cylinder-forming copolymers. *Macromolecules*, 27:4371–4381, 1994.

[115] Satoshi Koizumi, Hirokazu Hasegawa, and Takeji Hashimoto. Ordered structures of block copolymer/homopolymer mixtures. 5. Interplay of macro- and microphase transitions. *Macromolecules*, 27(22):6532–6540, 1994.

[116] Satoshi Koizumi, Hirokazu Hasegawa, and Takeji Hashimoto. Spatial distribution of homopolymers in block copolymer microdomain as observed by a combined SANS and SAXS method. *Macromolecules*, 27:7893–7906, 1994.

[117] Nagraj Koneripalli, Navjot Singh, Rastislav Levicky, Frank S. Bates, Patrick D. Gallagher, and Sushil K. Satija. Confined block copolymer thin films. *Macromolecules*, 28(8):2897–2904, 1995.

[118] K. Kremer and K. Binder. Dynamics of polymer chains confined into tubes: Scaling theory and Monte Carlo simulations. *Journal of Chemical Physics*, 81(12):6381–6394, 1984.

[119] L. D. Landau and E. M. Lifshitz. *Statistical Physics*, volume 5 of *Course of Theoretical Physics*. Pergamon Press, 1969.

[120] Mohamed Laradji, An-Chang Shi, Rashmi C. Desai, and Jaan Noolandi. Stability of ordered phases in weakly segregated diblock copolymer systems. *Physical Review Letters*, 78(13):2577–2580, 1997.

[121] R. G. Larson. Monte Carlo simulations of the phase behavior of surfactant solutions. *Journal de Physique 2 (France)*, 6(10):1441–1463, 1996.

[122] Michel Le Bellac. *Quantum and Statistical Field Theory.* Oxford University Press, Incorporated, 1992.

[123] J. C. Le Guillou and J. Zinn-Justin. Critical exponents for the n-vector model in three dimensions from field theory. *Physical Review Letters*, 39(2):95–98, 1977.

[124] F. A. M. Leermakers, C. M Wijmans, and G. J. Fleer. On the structure of polymeric micelles: Self-consistent-field theory and universal properties for volume fraction profiles. *Macromolecules*, 28(9):3434–3443, 1995.

[125] Ludwik Leibler. Theory of microphase separation in block copolymers. *Macromolecules*, 13(6):1602–1617, 1980.

[126] Ludwik Leibler. Theory of phase equilibria in mixtures of copolymers and homopolymers. 2. Interfaces near the consolute point. *Macromolecules*, 15(5):1283–1290, 1982.

[127] Ludwik Leibler. Emulsifying effects of block copolymers in incompatible polymer blends. *Makromolekulare Chemie, Macromolecular Symposia*, 16:1–17, 1988.

[128] Ludwik Leibler. Block copolymers at interfaces. *Physica A*, 172:258–268, 1991.

[129] Ludwik Leibler and Philip A. Pincus. Ordering transition of copolymer micelles. *Macromolecules*, 17(12):2922–2924, 1984.

[130] Stanislas Leibler and Reinhard Lipowsky. Complete unbinding and quasi-long-range order in lamellar phases. *Physical Review Letters*, 35(13):7004–7009, 1987.

[131] Robert L. Lescanec and M. Muthukumar. Density functional theory of phase transitions in diblock copolymer systems. *Macromolecules*, 26(15):3908–3916, 1993.

[132] C. Ligoure, B. Bouglet, G. Porte, and O. Diat. Smectic compressibility of polymer-containing lyotropic lamellar phases: An experimental tool to study the thermodynamics of polymer confinement. *Journal de Physique 2 (France)*, 7(3):473–491, 1997.

[133] Alexey E. Likhtman and Alexander N. Semenov. Stability of the OBDD structure for diblock copolymer melts in the strong segregation limit. *Macromolecules*, 27(11):3103–3106, 1994.

[134] Eric K. Lin and Alice P. Gast. Self consistent field calculations of interactions between chains tethered to spherical surfaces. *Macromolecules*, 29(1):390–397, 1996.

[135] Reinhard Lipowsky. Discontinuous unbinding transitions of flexible membranes. *Journal de Physique 2 (France)*, 4(10):1755–1762, 1994.

[136] Reinhard Lipowsky. From bunches of membranes to bundles of strings. *Zeitschrift für Physik B*, 97:193–203, 1995.

[137] B. Löwenhaupt and G. P. Hellmann. Interface stabilization and micelle formation in blends with a block copolymer. *Colloid and Interface Science*, 268(10):885–894, 1990.

[138] B. Löwenhaupt, A. Steurer, G. P. Hellmann, and Y. Gallot. Microphases and macrophases in polymer blends with a diblock copolymer. *Macromolecules*, 27(4):908–916, 1994.

[139] M. Malmsten, P. Linse, and K.-W. Zhang. Phase behavior of aqueous poly(ethylene oxide)/poly(propylene oxide) solutions. *Macromolecules*, 26(11):2905–2910, 1993.

[140] James E. Mark, editor. *Physical Properties of Polymers Handbook*. American Institute of Physics (AIP Press), 1996.

[141] J. F. Marko and T. A. Witten. Phase separation in a grafted polymer layer. *Physical Review Letters*, 66(11):1541–1544, 1991.

[142] C. M. Marques and M. E. Cates. Hormonic corrections near the ordering transition. *Europhysics Letters*, 13(3):267–272, 1990.

[143] M. W. Matsen. Bridging and looping in multiblock copolymer melts. *Journal of Chemical Physics*, 102(9):3884–3887, 1995.

[144] M. W. Matsen. Immiscibility of large and small symmetric diblock copolymers. *Journal of Chemical Physics*, 103(8):3268–3271, 1995.

[145] M. W. Matsen. Phase behavior of copolymer/homopolymer blends. *Macromolecules*, 28(17):5765–5773, 1995.

[146] M. W. Matsen. Stabilizing new morphologies by blending homopolymer with copolymer. *Physical Review Letters*, 74(21):4225–4228, 1995.

[147] M. W. Matsen. Thin films of block copolymer. *preprint*, 1997.

[148] M. W. Matsen and F. S. Bates. One-component approximation for binary diblock copolymer blends. *Macromolecules*, 28(21):7298–7300, 1995.

[149] M. W. Matsen and F. S. Bates. Testing the strong-stretching assumption in a block copolymer microstructure. *Macromolecules*, 28(26):8884–8886, 1995.

[150] M. W. Matsen and F. S. Bates. Origins of complex self-assembly in block copolymers. *Macromolecules*, 29(23):7641–7644, 1996.

[151] M. W. Matsen and F. S. Bates. Unifying weak- and strong-segregation block copolymer theories. *Macromolecules*, 29(4):1091–1098, 1996.

[152] M. W. Matsen and F. S. Bates. Block copolymer microstructures in the intermediate-segregation regime. *Journal of Chemical Physics*, 106(6):2436–2448, 1997.

[153] M. W. Matsen and F. S. Bates. Conformationally asymmetric block copolymers. *Journal of Polymer Science B*, pages 945–952, 1997.

[154] M. W. Matsen and M. Schick. Elastic properties of an interface of diblock copolymer. *Macromolecules*, 26(15):3878–3884, 1993.

[155] M. W. Matsen and M. Schick. Elastic properties of an interface of diblock copolymer. 2. *Macromolecules*, 27(8):2316–2318, 1994.

[156] M. W. Matsen and M. Schick. Lamellar phase of a symmetric triblock copolymer. *Macromolecules*, 27(1):187–192, 1994.

[157] M. W. Matsen and M. Schick. Stable and unstable phases of a diblock copolymer melt. *Physical Review Letters*, 72(16):2660–2663, 1994.

[158] Mark W. Matsen and Michael Schick. Self-assembly in block copolymers. *Current Opinion in Colloid and Interface Science*, 1:329–336, 1996.

[159] A. M. Mayes and M. Olvera de la Cruz. Concentration fluctuation effects on disorder-order transitions in block copolymer melts. *Journal of Chemical Physics*, 95(6):4670–4677, 1991.

[160] A. M. Mayes, T. P. Russell, V. R. Deline, S. K Satija, and C. F. Majkrzak. Block copolymer mixtures as revealed by neutron reflectivity. *Macromolecules*, 27(25):7447–7453, 1994.

[161] Glen A. McConnell and Alice P. Gast. Predicting disorder-order phase transitions in polymeric micelles. *Physical Review E*, 54(5):5447–5455, 1996.

[162] Glen A. McConnell and Alice P. Gast. Melting of ordered arrays and shape transitions in highly concentrated diblock copolymer solutions. *Macromolecules*, 30(3):435–444, 1997.

[163] Glen A. McConnell, Alice P. Gast, John S. Huang, and Steven D. Smith. Disorder-order transitions in soft sphere polymer micelles. *Physical Review Letters*, 71(13):2102–2105, 1993.

[164] D. S. McKenzie. Polymers and scaling. *Physics Reports*, 28(2):35–88, 1976.

[165] J. Melenkevitz and M. Muthukumar. Density functional theory of lamellar ordering in diblock copolymers. *Macromolecules*, 24(14):4199–4205, 1991.

[166] A. Michelson. Phase diagrams near the Lifshitz point. I. Uniaxial magnetization. *Physical Review B*, 16(1):577–584, 1977.

[167] A. Michelson. Phase diagrams near the Lifshitz point. II. Systems with cylindrical, hexagonal, and rhombohedral symmetry having an easy plane of magnetization. *Physical Review B*, 16(1):585–592, 1977.

[168] A. Michelson. Phase diagrams near the Lifshitz point. III. Tetragonal crystals with an easy plane of magnetization. *Physical Review B*, 16(11):5121–5124, 1977.

[169] S. T. Milner and D. Roux. Flory theory of the unbinding transition. *Journal de Physique 1 (France)*, 2(9):1741–1754, 1992.

[170] S. T. Milner, Zhen-Gang Wang, and T. A. Witten. End-confined polymers: Corrections to the newtonian limit. *Macromolecules*, 22(1):489–490, 1989.

[171] S. T. Milner and T. A. Witten. Bending moduli of polymeric surfactant systems. *Journal de Physique (France)*, 49(11):1951–1962, 88.

[172] S. T. Milner, T. A. Witten, and M. E. Cates. Theory of the grafted polymer brush. *Macromolecules*, 21(8):2610–2619, 1988.

[173] S. T. Milner, T. A. Witten, and M. E. Cates. Effects of polydispersity in the end-grafted polymer brush. *Macromolecules*, 22(2):853–861, 1989.

[174] Scott T. Milner. Strong-stretching and Scheutjens-Fleer description of grafted polymer brushes. *J. Chem. Soc. Faraday Trans.*, 86(9):1349–1353, 1990.

[175] Scott T. Milner. Strongly stretched polymer brushes. *Journal of Polymer Science B*, 32:2743–2755, 1994.

[176] Scott T. Milner and David C. Morse. Wetting description of block copolymer thin films. *Physical Review E*, 54(4):3793–3810, 1996.

[177] Yasuhiro Mogi, Katsuaki Mori, Hiroyuki Kotsuji Yushu Matsushita, Ichiro Noda, and Charles C. Han. Molecular weight dependence of the lamellar domain spacing of ABC triblock copolymers and their chain confromations in lamellar domains. *Macromolecules*, 26(19):5169–5173, 1993.

[178] Yasuhiro Mogi, Katsuaki Mori, Yushu Matsushita, and Ichiro Noda. Tricontinuous morphology of triblock copolymers of the ABC type. *Macromolecules*, 25(20):5412–5415, 1992.

[179] Yasuhiro Mogi, Mahito Nomura, Hiroyuki Kotsuji, Kouki Ohnishi, Yushu Matsushita, and Ichiro Noda. Superlattice structures in morphologies of the ABC triblock copolymers. *Macromolecules*, 27:6755–6760, 1994.

[180] Keiji Mori, Hideaki Tanaka, Hirokazu Hasegawa, and Takeji Hashimoto. Small-angle X-ray scattering from block copolymers in disordered state: 2. Effect of molecular weight distribution. *Polymer*, 30:1389–1398, 1989.

[181] David C. Morse. Topological instabilities and phase behavior of fluid membranes. *Physical Review E*, 50(4):R2423–R2426, 1994.

[182] Kell Mortensen. Cubic phase in a connected micellar network of poly(propylene oxide)-poly(ethylene oxide)-poly(propylene oxide) triblock copolymers in water. *Macromolecules*, 30(3):503–507, 1997.

[183] Kell Mortensen, Wyn Brown, and Erling Jørgenson. Lamellar mesophase of poly(ethylene oxid)-poly(propylene oxide)-poly(ethylene oxide) melts and water swollen mixtures. *Macromolecules*, 28(5):1458–1463, 1995.

[184] M. Müller and M. Schick. *unpublished.*

[185] M. Müller and M Schick. Bulk and interfacial thermodynamics of a symmetric, ternary homopolymer-copolymer mixture: a Monte Carlo study. *Journal of Chemical Physics*, 105(19):8885–8901, 1996.

[186] M. Müller and M. Schick. Ordered phases in rod-coil diblock copolymers. *Macromolecules*, 29(27):8900–8903, 1996.

[187] Marcus Müller. Private Communication.

[188] M. Muthukumar and Bernie G. Nickel. Perturbation theory for a polymer chain with excluded volume interaction. *Journal of Chemical Physics*, 80(11):5839–5850, 1984.

[189] Hatsumi Nakazawa and Takao Ohta. Micorphase separation of ABC-type triblock copolymers. *Macromolecules*, 26(20):5503–5511, 1993.

[190] R. R. Netz and M. Schick. Classical theory of polymer brushes. *Europhysics Letters*, 38(1):37–42, 1997.

[191] Roland R. Netz and Reinhard Lipowsky. Unbinding of symmetric and asymmetric stacks of membranes. *Physical Review Letters*, 71(21):3596–3599, 1993.

[192] C. Nicot, M. Waks, R. Ober, T. Gulik-Krzywicki, and W. Urbach. Squeezing of oil-swollen surfactant bilayers by a membrane protein. *Physical Review Letters*, 77(16):3485–3488, 1996.

[193] Shuichi Nojima and Ryong-Joon Roe. Effect of molecular weight of added polystyrene on the order-disorder transition of styrene-butadiene diblock copolymer. *Macromolecules*, 20(8):1866–1876, 1987.

[194] Jaan Noolandi and Kin Ming Hong. Effect of block copolymers at a demixed homopolymer interface. *Macromolecules*, 17(8):1531–1537, 1984.

[195] Takao Ohta and Kyozi Kawasaki. Equilibrium morphology of block copolymer melts. *Macromolecules*, 19(10):2621–2632, 1986.

[196] Peter D. Olmsted and Scott T. Milner. Strong-segregation theory of bicontinuous phases in block copolymers. *Physical Review Letters*, 72(6):936–939, 1994.

[197] Peter E. Olmsted and Scott T. Milner. Strong-segregation theory of bicontinuous phases in block copolymers. *Physical Review Letters*, 74(5):829, 1995.

[198] Henri Orland and M. Schick. Simple integral equation for the polymer brush. *Macromolecules*, 29(2):713–717, 1996.

[199] Harry J. Ploehn. Structure of polymer layers: Molecular volume effects. *Macromolecules*, 27(6):1617–1626, 1994.

[200] V. E. Podneks and I. W. Hamley. Landau-Brazovskii theory for the $Ia3d$ structure. *JETP Letters*, 64(8):617–624, 1996.

[201] William H. Press, Brian P. Flannery, Saul A. Teukolsky, and William T. Vetterling. *Numerical Recipies in C.* Cambridge Press, Incorporated, second edition, 1988.

[202] E. Z. Radlinska, T. Gulik-Krzywicki, F. Lafuma, D. Langevin, W. Urbach, C. E. Williams, and R. Ober. Polymer confinement in surfactant bilayers of a lyotropic lamellar phase. *Physical Review Letters*, 74(21):4237–4240, 1995.

[203] E. Raphaël, G. H. Fredrickson, and P. Pincus. One long chain among shorter chains: the Flory approach revisited. *Journal de Physique 2 (France)*, 2(10):1811–1823, 1992.

[204] M. Rawiso, R. Duplessix, and C. Picot. Scattering function of polystyrene. *Macromolecules*, 20(3):630–648, 1987.

[205] R. J. Rivers. *Path Integral Methods in Quantum Field Theory.* Cambridge Press, Incorporated, 1988.

[206] Ryong-Joon Roe and Wang-Cheol Zin. Phase equilibria and transitions in mixtures of homopolymer and a block copolymer. 2. Phase diagram. *Macromolecules*, 17(2):189–194, 1984.

[207] Didier Roux, Cyrus Safinya, and Frederic Nallet. Lyotropic lamellar L_α phases. In W. Gelbart, A. Ben-Shaul, and D. Roux, editors, *Micelles, Membranes, Microemulsions and Monolayers*, chapter 6, pages 303–346. Springer-Verlag New York, Incorporated, 1995.

[208] C. Sadron and B. Gallot. *Makromolekulare Chemie*, 164:301, 1973.

[209] Samuel A. Safran. *Statistical Thermodynamics of Surfaces, Interfaces, and Membranes.* Addison-Wesley Publishing Company, Incorporated, 1994.

[210] J. M. H. M. Scheutjens and G. J. Fleer. Statistical theory of the adsorption of interacting chain molecules. 1. Partition function, segment density distribution, and adsorption isothermes. *Journal of Physical Chemistry*, 83(12):1619–1635, 1979.

[211] J. M. H. M. Scheutjens and G. J. Fleer. Interaction between two adsorbed polymer layers. *Macromolecules*, 18(10):1882–1900, 1985.

[212] M. Schick. Introduction to wetting phenomena. In J. Charvolin, J. F. Joanny, and J. Zinn-Justin, editors, *Liquids at Interfaces: Proceedings of the Les*

Houches Summer School, Session XLVIII, 30 May-24 June, 1988, pages 415–497. Elsevier Science, Incorporated, 1991.

[213] M. Schick and Philipp Janert. Unpublished.

[214] L. S. Schulman. *Techniques and Applications of Path Integration.* John Wiley & Sons, Incorporated, 1981.

[215] Mark F. Schulz and Frank S. Bates. Morphologies of block copolymers. In Mark [140], chapter 32.

[216] Mark F. Schulz, Frank S. Bates, Kristoffer Almdal, and Kell Mortensen. Epitaxial relationship for hexagonal-to-cubic phase transition in a block copolymer mixture. *Physical Review Letters*, 73(1):86–89, 1994.

[217] Mario Schwab and Bernd Stühn. Thermotropic transition from a state of liquid order to a macrolattice in asymmetric diblock copolymers. *Physical Review Letters*, 76(6):924–927, 1996.

[218] U. S. Schwarz, K. Swamy, and G. Gompper. The lamellar-to-isotropic transition in ternary amphiphilic systems. *Europhysics Letters*, 36(2):117–122, 1996.

[219] Kenneth S. Schweizer. Analytic PRISM theory of structurally asymmetric polymer blends and copolymers. *Macromolecules*, 26:6050–6067, 1993.

[220] Kenneth S. Schweizer. Analytic RISM theory of polymer alloys: Molecular closure predictions of structurally symmetric blends. *Macromolecules*, 26:6033–6049, 1993.

[221] Kenneth S. Schweizer and John G. Curro. Integral equation theories of the structure, thermodynamics, and phase transitions of polymer fluids. *Advances in Chemical Physics*, 98:1–142, 1997.

[222] A. N. Semenov. Contribution to the theory of microphase layering in block-copolymer melts. *JETP*, 61(4):733–742, 1985.

[223] A. N. Semenov. Theory of diblock-copolymer segregation to the interface and free surface of a homopolymer layer. *Macromolecules*, 25(19):4967–4977, 1992.

[224] A. N. Semenov. Phase equilibria in block copolymer-homopolymer mixtures. *Macromolecules*, 26(9):2273–2281, 1993.

[225] A. N. Semenov. Theory of block-copolymer interfaces in the strong segregation limit. *Macromolecules*, 26(24):6617–6621, 1993.

[226] An-Chang Shi and Jaan Noolandi. Binary mixtures of diblock copolymers: Phase diagrams with a new twist. *Macromolecules*, 28(9):3103–3109, 1995.

[227] An-Chang Shi, Jaan Noolandi, and Rashmi C. Desai. Theory of anisotropic fluctuations in ordered block copolymer phases. *Macromolecules*, 29(20):6487–6504, 1996.

[228] An-Chang Shi, Jaan Noolandi, and Heinz Hoffmann. Diblock copolymer blends as mixtures of surfactants and cosurfactants. *Macromolecules*, 27(22):6661–6664, 1994.

[229] Kenneth R. Shull. Mean-field theory of block copolymers: Bulk melts, surfaces and thin films. *Macromolecules*, 25(8):2122–2133, 1992.

[230] Kenneth R. Shull. Interfacial phase transitions in block copolymer/homopolymer blends. *Macromolecules*, 26(9):2346–2360, 1993.

[231] Kenneth R. Shull, Edward J. Kramer, Georges Hadziioannou, and Wing Tang. Segregation of block copolymers to interfaces between immiscible homopolymers. *Macromolecules*, 23(22):4780–4787, 1990.

[232] Kenneth R. Shull, Anne N. Mayes, and Thomas P. Russell. Segment distributions in lamellar diblock copolymers. *Macromolecules*, 26(15):3929–3936, 1993.

[233] Navjot Singh, Andrew Kudrle, Mohan Sikka, and Frank S. Bates. Surface topography of symmetric and asymmetric polyolefin block copolymer films. *Journal de Physique 2 (France)*, 5(3):377–396, 1995.

[234] Richard J. Spontak, Jennifer C. Fung, Michael B. Braunfeld, John W. Sedat, David A. Agard, Lisaleigh Kane, Steven D. Smith, Michael M. Satkowski, Arman Ashraf, Damian A. Hajduk, and Sol M. Gruner. Phase behavior of ordered diblock copolymer blends: Effect of compositional heterogeneity. *Macromolecules*, 29(13):4494–4507, 1996.

[235] S. Stepanow. Extension of the theory of microphase separation in block copolymer melts beyond the random phase approximation. *Macromolecules*, 28(24):8233–8241, 1995.

[236] R. Strey. On the stability range of microemulsions: From the tricritical point to the lamellar phase in water/formamide-octane-C_iE_j systems. *Berichte der Bunsengesellschaft, Physik und Chemie*, 97(5):742–746, 1993.

[237] Reinhard Strey, Reinhard Schomäcker, Didier Roux, Frederic Nallet, and Ulf Olsson. Dilute lamellar and L_3 phases in the binary water–$C_{12}E_5$ system. *J. Chem. Soc. Faraday Trans.*, 86(12):2253–2261, 1990.

[238] Mårten Svensson, Per Linse, and Folke Tjerneld. Phase behavior in aqueous two-phase systems containing micelle-forming block copolymers. *Macromolecules*, 28(10):3597–3603, 1995.

[239] Igal Szleifer, Diego Kramer, Avinoam Ben-Shaul, William M. Gelbart, and S. A. Safran. Molecular theory of curvature elasticity in surfactant films. *Journal of Chemical Physics*, 92(11):6800–6817, 1990.

[240] Hideaki Tanaka, Hirokazu Hasegawa, and Takeji Hashimoto. Ordered structure in mixtures of block copolymer and homopolymers. 1. Solubilization of low molecular weight homopolymers. *Macromolecules*, 24(1):240–251, 1991.

[241] Hideaki Tanaka and Takeji Hashimoto. Ordered structures of block polymer/homopolymer mixtures. 3. Temperature dependence. *Macromolecules*, 24(20):5713–5720, 1991.

[242] Hideaki Tanaka and Takeji Hashimoto. Thermal concentration fluctuations of block polymer/homopolymer mixtures in the disordered state. 1. Binary mixtures of SI/HS. *Macromolecules*, 24(19):5398–5407, 1991.

[243] G. J. T. Tiddy. Surfactant-water liquid crystal phases. *Physics Reports*, 57(1):1–46, 1980.

[244] M. S. Turner and J.-F. Joanny. Diblock copolymer lamellae at rough surfaces. *Macromolecules*, 25(24):6681–6689, 1992.

[245] M. S. Turner, M. Maaloum, D. Ausserré, J.-F. Joanny, and M. Kunz. Edge dislocations in copolymer lamellar films. *Journal de Physique 2 (France)*, 4(4):689–702, 1994.

[246] Mathhew S. Turner, Michael Rubinstein, and Carlos M. Marques. Surface-induced lamellar ordering in a hexagonal phase of diblock copolymers. *Macromolecules*, 27(18):4986–4992, 1994.

[247] Matthew S. Turner, A. Johner, and J.-F. Joanny. Wetting behaviour of thin diblock films. *Journal de Physique 1 (France)*, 5(7):917–932, 1995.

[248] M. Wagner and B. A. Wolf. Effect of block copolymers on the interfacial tension between two 'immiscible' homopolymers. *Polymer*, 34(7):1460–1464, 1993.

[249] Heidi E. Warriner, Stefan H. J. Idziak, Nelle L. Slack, Patrick Davidson, and Cyrus Safinya. Lamellar biogels: Fluid-membrane-based hydrogels containing polymer lipids. *Science*, 271:969–973, 1996.

[250] W. Werner, F. Schmid, K. Binder, and M. Müller. Diblock copolymers at a homopolymer-homopolymer interface: A Monte Carlo simulation. *Macromolecules*, 29(25):8241–8248, 1996.

[251] F. W. Wiegel. Path integral methods in statistical mechanics. *Physics Reports*, 16(2):57–114, 1975.

[252] F. W. Wiegel. *Introduction to Path-Integral Methods in Physics and Polymer Science*. World Scientific Publishing Company, Incorporated, 1986.

[253] C. M. Wijmans and E. B. Zhulina. Polymer brushes at curved interfaces. *Macromolecules*, 26(26):7214–7224, 1993.

[254] Karen I. Winey, Maria Luisa Berba, and Mary E. Galvin. Ternary phase diagrams of poly(styrene-*co*-methyl methacrylate), poly(methyl methacrylate), and polystyrene: Monomer sequence distribution effect and encapsulation. *Macromolecules*, 29(8):2868–2877, 1996.

[255] Karen I. Winey, Edwin L. Thomas, and Lewis J. Fetters. Ordered morphologies in binary blends of diblock copolymer and homopolymer and characterization of

their intermaterial dividing surfaces. *Journal of Chemical Physics*, 95(12):9367–9375, 1991.

[256] Karen I. Winey, Edwin L. Thomas, and Lewis J. Fetters. Swelling a lamellar diblock copolymer with homopolymer: Influences of homopolymr concentration and molecular weight. *Macromolecules*, 24(23):6182–6188, 1991.

[257] Karen I. Winey, Edwin L. Thomas, and Lewis J. Fetters. Isothermal morphology diagrams for binary blends of diblock copolymer and homopolymer. *Macromolecules*, 25(10):2645–2650, 1992.

[258] Karen I. Winey, Edwin L. Thomas, and Lewis J. Fetters. The ordered bicontinuous double-diamond morphology in diblock copolymer/homopolymer blends. *Macromolecules*, 25(1):422–428, 1992.

[259] Guangwei Wu, Qicung Ying, and Benjamin Chu. Lamellar structure of block copolymer poly(oxyethylene-oxypropylene-oxyethylene) in xylene/water mixtures. *Macromolecules*, 27(20):5758–5765, 1994.

[260] Haowen Xi and Scott T. Milner. Bicontinuous phase in diblock copolymer melts with added homopolymer. *Macromolecules*, 29(7):2404–2411, 1996.

[261] Chuck Yeung, An-Chang Shi, Jaan Noolandi, and Rashmi C. Desai. Anisotropic fluctuations in ordered copolymer phases. *Macromolecular Theory and Simulation*, 5:291–298, 1996.

[262] Jin Zhao, Biswaroop Majumdar, Mark F. Schulz, Frank S. Bates, Kristoffer Almdal, Kell Mortensen, Damian A. Hajduk, and Sol M.Gruner. Phase behavior of pure diblock and binary diblock blends of poly(ethylene)-poly(ethylethylene). *Macromolecules*, 29(4):1204–1215, 1996.

[263] Wei Zheng and Zhen-Gang Wang. Morphology of ABC triblock copolymers. *Macromolecules*, 28(21):7215–7223, 1995.

[264] E. B. Zhulina and A. Halperin. Lamellar mesogels and mesophases: A self-consistent-field theory. *Macromolecules*, 25(21):5130–5741, 1992.

[265] Wang-Cheol Zin and Ryong-Joon Roe. Phase equilibria and transitions in mixtures of homopolymer and a block copolymer. 1. Small-angle X-ray scattering study. *Macromolecules*, 17(2):183–188, 1984.

VITA

PHILIPP KLAUS JANERT

Personal:

Born: 12. January 1970 in Köln (Cologne), Germany
Citizenship: German

Education:

1992–97 University of Washington, Seattle, USA
Supervisor: Prof. Michael Schick
Thesis Topic: Self-Assembly in Homopolymer/Diblock Blends
M.S. awarded 1994
1991–92 Johannes-Gutenberg Universität, Mainz, Germany
1989–91 B.S. ("Vordiplom") in Physics from Georg-August Universität, Göttingen, Germany
1980–89 High School Diploma ("Abitur") from Hildegard-von-Bingen Gymnasium, Köln, Germany

Conference Presentations:

1996 *Unbinding of Lamellae in Homopolymer/Diblock Blends as a Wetting Transition* presented at the APS March Meeting 1996 in St. Louis, MO, USA

Refereed Publications:

P.K. Janert and M. Schick: *First-Order Unbinding and Preunbinding in Amphiphilic Systems* Phys. Rev. E **54** (1996), R33

P.K. Janert and M. Schick: *Phase Behavior of Ternary Homopolymer/Diblock Blends: Influence of Relative Chain Lengths* Macromolecules **30** (1997), 137

P.K. Janert and M. Schick: *Phase Behavior of Ternary Homopolymer/Diblock Blends: Microphase Unbinding in the Symmetric System* Macromolecules *in press*

P.K. Janert and M. Schick: *Phase Behavior of Binary Homopolymer/Diblock Blends: Chain length and Temperature dependence* Macromolecules *submitted*